University of Southampton

Variability of phytoplankton production rates in the Atlantic Ocean as observed using the Fast Repetition Rate Fluorometer

David John Suggett

This thesis is submitted for
Doctor of Philosophy

Faculty of Science
School of Ocean & Earth Science

May 2000

Abstract

This thesis examines some aspects of *in situ* phytoplankton physiology and subsequent production rates within the Atlantic Ocean, as observed using a novel instrument, the Fast Repetition Rate Fluorometer (FRRF). The underlying theory and use of this instrument is described in detail. High resolution FRRF data collection was performed during three oceanographic cruises: RV *Pelagia*, March 1998, RRS *James Clark Ross*, May-June 1998 and RRS *Challenger*, August 1999. These data observe characteristics of phytoplankton physiology and, therefore, production, over daily (diel), small (turbulent) and broad (seasonal) scales. The sampling sites for all cruises were chosen within a variety of hydrographic regimes to further assess the light-nutrient dependencies of this variability.

Phytoplankton physiology is described by the functional absorption cross section (σ_{PSII}) and the quantum yield of photochemistry (F_v/F_m) which relate to the rate at which photosystem II (PSII) saturates with light and the proportion of functional PSII reaction centres, respectively. Changes in both σ_{PSII} and F_v/F_m are most evident at the diel scale. σ_{PSII} correlates with corresponding changes in PSII pigments indicating non-photochemical quenching of excess solar energy as part of a diel rhythm in cellular constituents. A novel calculation for the number of *in situ* PSII reaction centres (n_{PSII}), based on FRRF measurements, is described and tested and shows similar diel variability. Smaller-scale variations in σ_{PSII} are also observed continually throughout the diel period apparently as an attempt to balance the distribution of energy between PSII and PSI and, therefore, maintain high rates of photosynthesis. Such smaller-scale processes are most obvious in low nutrient (oligotrophic) waters where hydrographic variability and consequently new nutrient input, remains relatively low. FRRF estimates of production were most related to nutrient conditions in these oligotrophic waters. Conversely, production correlated with light in waters where nutrients were in abundance. FRRF production estimates compared well with corresponding *in situ* gross O_2 measurements but were typically a factor of 3-4 higher than ^{14}C production estimates. This difference can be accounted as the stochiometry between O_2 evolution and carbon uptake for photosynthesis but may also represent the limitations associated with the calculation of production from one or both techniques. These limitations are discussed as a premise for further work.

Acknowledgements

I would like to thank the following for their assistance and support throughout this work: Patrick Holligan and Jim Aiken for giving me unequalled guidance and supervision. Richard Geider, Margaret Davey, Mark Moore and Ed Abraham for aiding in data collection (RV *Pelagia*, RRS *Challenger*) and providing insight and discussion into phytoplankton physiology. Thanks also to Gerald Moore, Nigel Rees, Malcolm Woodward, Guy Westbrook, Matt Pinkerton and Hester Wilson at CCMS (Plymouth) and Klaas Timmermanns at NIOZ for providing additional data and discussion. The Captains and crew of RV *Pelagia*, March 1998, RRS *James Clark Ross*, May-June 1998 and RRS *Challenger*, August 1999.

This work was largely funded by NERC (grant no. GR3/11829) and would not have been possible without the support of Justin Dunning and John Atkins, Chelsea Instruments, for FRRF support and development.

I would also like to thank Rebecca Whitfield for helping with the preparation of the thesis and keeping me well looked after in times of need.

Contents

List of figures

List of tables

1. Introduction

Phytoplankton comes from the Greek *phyton* (plant) and *planktos* (that which passively drifts) and applies to the vagrant communities of aquatic photoautotrophs, or organisms which use light to grow and reproduce, whose dynamics are strongly dependent upon the physical motions of their environment (*sensu* Margalef 1997). Thousands of [unicellular] species, organised into 12 algal divisions, comprise the marine component of phytoplankton. One of these divisions is composed of the earliest oxygenic photosynthetic organisms (prokaryotes) whilst the rest are formed from more recently evolved, eukaryotes. Most marine phytoplankton are microscopic and are described as micro- (20-200μm), nano- (2-20μm) or pico- (0.2-2μm) phytoplankton. Some individual species achieve large sizes (1-2mm), or form chains and aggregates using mucilaginous threads or spines, but still remain at the mercy of ocean hydrodynamics for the continual provision of favourable irradiance and nutrients for production and growth.

The largest and most robust marine phytoplankton are represented by Bacillariophyceae (diatoms), Dinophyceae (dinoflagellates) and Prymnesiophyceae (coccolithophores) Jeffrey and Vesk 1997). Diatoms are typically large and opportunistic but are dependent upon a supply of silicate for the production of a 'glassy' exoskeleton, or frustule. Dinoflagellates have paired whip-like flagella and are able to maintain themselves in optimal light-nutrient conditions where physical mixing of the water column may be relatively weak. Coccolithophores are characterised by an armour of calcium carbonate plates and proliferate in warmer waters. The smaller picoplankton are predominantly composed of prokaryotic Cyanophyceae (cyanobacteria) and Prochlorophyceae (prochlorophytes), and of some eukaryotic divisions. Ultimately, members of the marine phytoplankton are adapted to different light, nutrient and temperature conditions and, therefore, display global patterns of standing crop and production according to the global circulation of their marine environment, for example, the Atlantic Ocean (*fig 1.1.*):

The Atlantic Ocean has a range that spans nearly the entire latitude of the globe. It is bounded to the north by the Arctic polar basin and to the south by the Southern Ocean. As a result, the ocean plays host to a range of sub-polar, temperate, sub-tropical and tropical climates, each of which is governed by characteristic wind regimes. The east and west Atlantic are bordered by continents where an abundance of nutrients can support

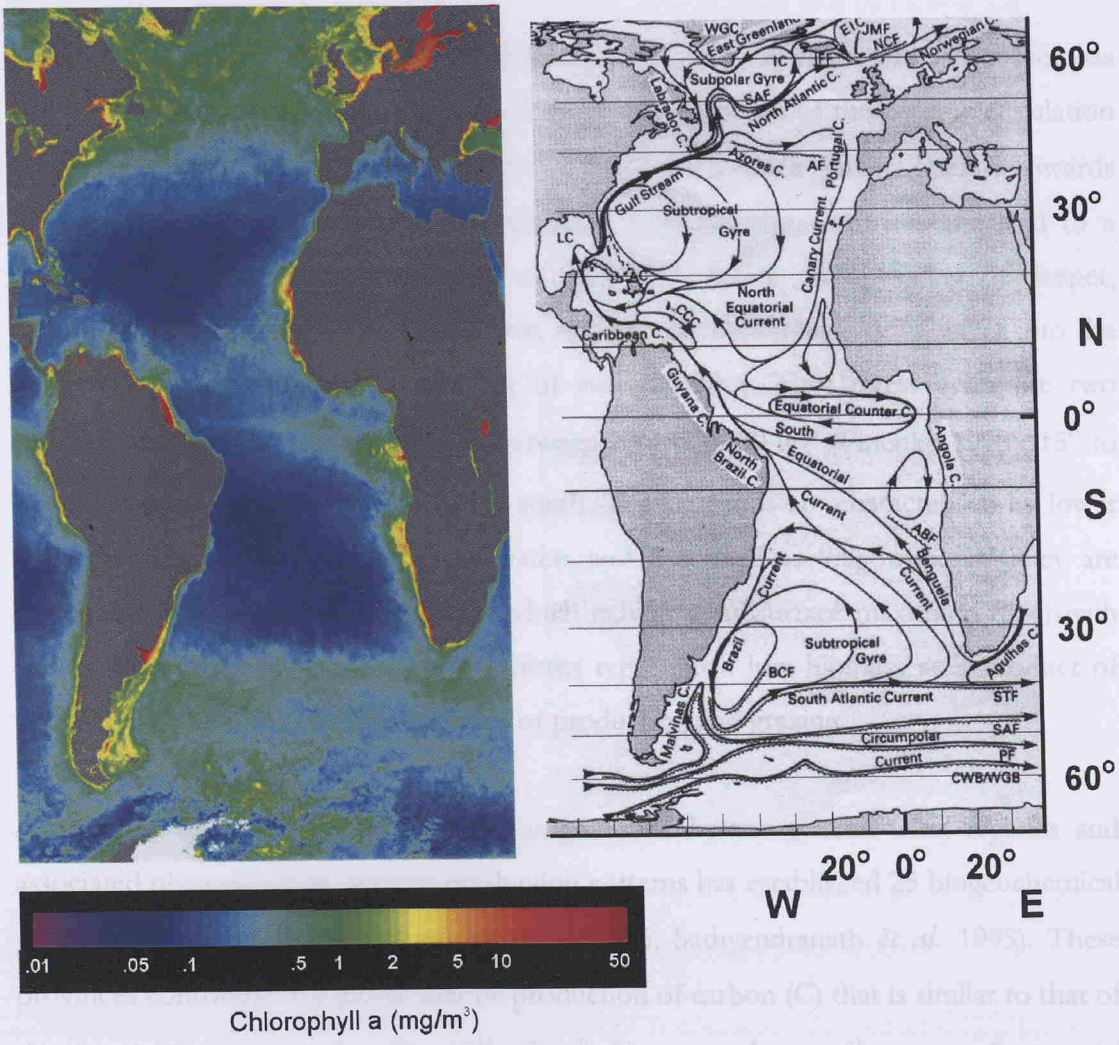

Figure 1.1.— (left) SeaWiFs image of sea surface chlorophyll *a* concentration in the Atlantic Ocean. Chlorophyll *a* is found in all marine phytoplankton and the concentration [of chl *a*] is a useful indicator of the phytoplankton standing crop (or biomass). Image represents a composite of data observed between September 1997 and August 1998; (right) Surface currents of the Atlantic Ocean (modified from Tomczak and Godfrey 1994). Abbreviations are used for: East Iceland (EIC), Irminger (IC), West Greenland (WGC), Loop (LC) and Antilles (AC) currents and Caribbean counter-current (CCC). Other abbreviations refer to fronts: Jan Meyen (JMF), Norwegian current (NCF), Iceland-Faroe (IFF), Subarctic (SAF), Azores (AF), Angola-Benguela (ABF), Brazilian current (BCF), Sub-tropical (STF), Subantarctic (SAF), Polar (PF), Continental water boundary/ Weddell gyre boundary (CWB/WGB). **Note** the projections for the 2 images are different.

the highest levels of phytoplankton growth, for example, upwelling activity (e.g. Shannon and Nelson 1996) driven by offshore winds, and shelf seas and shelf margins influenced by dynamic mixing regimes (e.g. Simpson and Pingree 1978, Holligan 1981, Longhurst *et al.* 1995). Such systems are dominated by large opportunistic, fast growing, diatoms and dinoflagellates that are able to accumulate a large biomass against the pressures of grazing. This biomass typically accumulates at or near the sea surface where light energy for growth is highest.

Much of the Atlantic Ocean is represented as vast expanses of waters with lower biomass and productivity. These waters, known as gyres, are a product of the oceanic circulation (*fig. 1.1.*). Two tropical cyclonic gyres, the Angola and Guinea domes, operate towards the east of the ocean (Tomczak and Godfrey 1994). Cyclonic movements lead to a divergence of water from the centre of the gyre creating an upwelling of deeper, (relatively) nutrient-rich water. Conversely, anticyclonic movements drive water into the centre of a gyre creating downwelling of surface water. The largest gyres are two anticyclonic subtropical gyres situated between 10-15° to 50-60° (Finenko 1978); 15° to 45° (Mann and Lazier 1996) north and south. These regions are characterised by lower nutrient concentrations than inshore waters and described as 'oligotrophic'. They are dominated by the pico-phytoplankton which exhibit a subsurface maximum of growth and biomass accumulation. These organisms represent a low biomass as a product of their small cell size and the relative rates of production and grazing.

A synthesis of such physical features, as governed by the general wind regimes and associated phytoplankton primary production patterns has established 25 biogeochemical provinces for the Atlantic (Longhurst *et al.* 1995, Sathyendranath *et al.* 1995). These provinces contribute to a global marine production of carbon (C) that is similar to that of the terrestrial system (each $\approx 50 \times 10^{15}$ gC yr^{-1}). However, the standing crop of terrestrial plants is 500-600 times more than that of marine plants (IPCC 1995, Falkowski and Raven 1997). Therefore, our ability to accurately quantify marine primary production is essential when considering the dynamics of the marine contribution to global processes.

Remote sensing of ocean colour currently provides the most intensive level of temporal and spatial sampling from which one can derive estimates of marine primary production. These derivations are driven by established relationships between production rates and

environmental parameters, such as nutrients and light. Unfortunately, 'classical' methods used to observe phytoplankton production, for example, following ^{14}C-uptake (Steeman Nielsen 1952) or O_2 evolution (eg. Bryan *et al.* 1976) in incubated water samples, neglect the actual environment of phytoplankton. Such methods are also costly and time-consuming thereby leaving gaps in the temporal and spatial resolution of our understanding of *in situ* primary production. Improvements and alternatives to these techniques were, perhaps, only a matter of time. Indeed, a functional method now exists, the Fast Repetition Rate Fluorometer (developed by Z. Kolber and P. Falkowski), which is capable of rapidly sampling phytoplankton physiology and production in the context of the 'real' environment. Such improvements have important consequences for accurate estimates of marine primary production and atmospheric carbon assimilation with regards to global carbon budgets (Longhurst 1991). However, the capabilities of this instrument are largely undocumented and must be carefully validated before any output can be considered conclusive.

1.1. Photosynthesis of marine phytoplankton

Photosynthesis describes the process by which solar energy is used to bond molecules into carbohydrate and is often summarised as the simplistic equation: $6CO_2 + 12H_2O = C_6H_{12}O_2 + 6O_2 + 6H_2O$. However, this process is actually composed of several complex reactions and interactions which function in response to the environment of the plant. A brief description of photosynthesis relevant to marine phytoplankton is provided below and follows the more detailed accounts of Prézelin (1981), Kremer *et al.* (1981), Wallace *et al.* (1991), Geider (1992), Kirk (1994) and Falkowski and Raven (1997):

Two main reactions, termed the light and dark (or light-dependent and light-independent) reactions (*fig 1.2.*) actually comprise the simplistic model of photosynthesis. The apparatus and molecules required for these reactions are located within structures in the cytoplasm. In eukaryotic organisms, organelles known as chloroplasts (*fig 1.3.*) contain stacks of membrane-bounded sacks (thylakoids). An aqueous matrix fills both the intrathylakoid space (the lumen) and the chloroplast (the stroma surrounds the thylakoids). This arrangement appears markedly different in the

Light reaction:

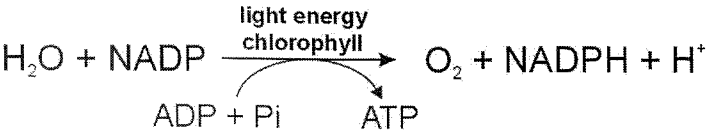

Dark reaction:

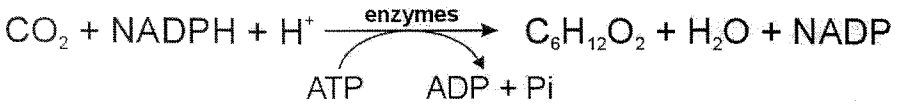

Figure 1.2.— Schematic description of the light and dark reactions of photosynthesis. The **light reaction** is dependent upon the capture of photons to convert adenosine diphosphate (ADP) and inorganic phosphate (Pi) into adenosine triphosphate (ATP) and convert oxidised nicotine adenine dinucleotide phosphate ($NADP^+$) into the reduced form NADPH. The **dark reaction** converts fixed carbon dioxide (CO_2) into carbohydrate using the energy from the products derived in the light reaction.

prokaryotic cyanobacteria and anaerobic photosynthetic bacteria (*fig 1.3.*) in which thylakoid membranes are arranged into sheets and placed free within the cytoplasm rather than bundled into organelles. Irrespective of the different morphologies, the apparatus for the light reactions are always housed within the membrane of the thylakoids whilst the soluble enzymatic components of the dark reactions are contained in the stroma, *fig 1.4.*

There are two components to the light reaction, termed photosystems I and II (PSI and PSII). Each photosystem is composed of an antennae which is energetically coupled to a reaction centre (RCI and RCII). The antennae contain a combination of distinctive pigments (chlorophylls, carotenoids and/or biliproteins) complexed to proteins which absorb light. Each taxa of phytoplankton contain a unique combination of pigments to harness energy from specific wavelengths of the light spectrum. The absorbed light is subsequently passed to a specialised chlorophyll-protein complex housed within each reaction centre, P680 (RCII) and P700 (RCI).

When P680 has received sufficient energy, an electron becomes excited and escapes its orbital. The electron is quickly captured by a closely associated electron transfer system (ETS) preventing it falling to a lower energy level and re-associating with the chlorophyll

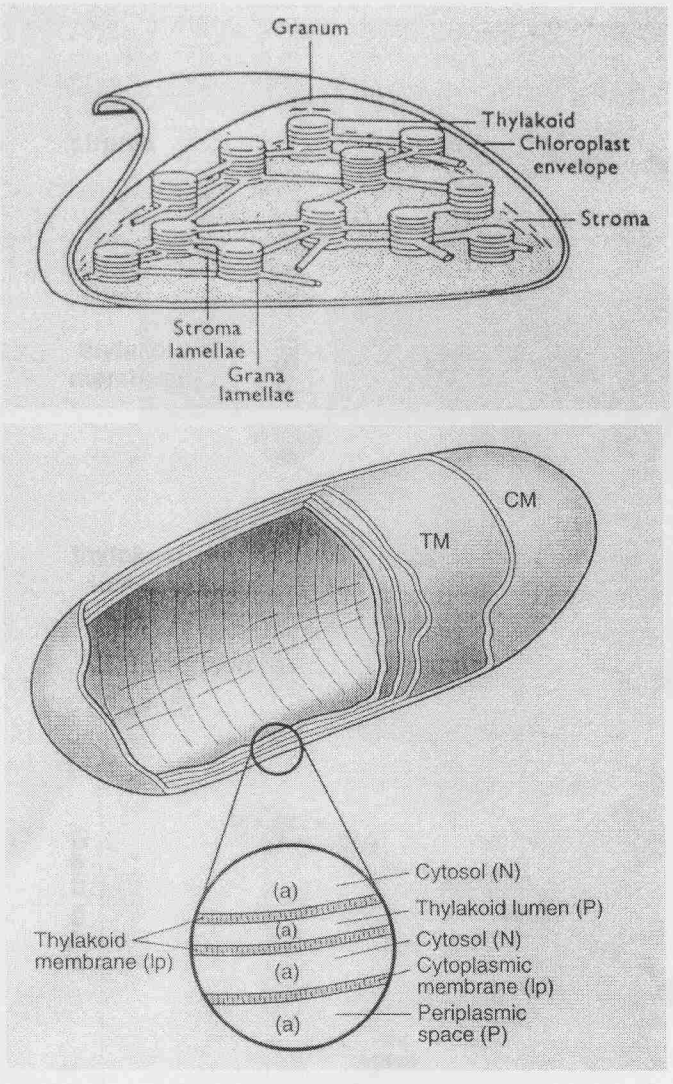

Figure 1.3.— (upper panel) Cut away section of a chloroplast from a eukaryotic cell (taken from Prèzelin 1981). Each thylakoid is a membrane surrounding an aqueous lumen. The thylakoids are stacked into granum Surrounding these stacks is the aqueous matrix of the stroma. The chloroplasts are found within the cytoplasm of the cell; (lower panel) Cut away section of the photosynthetic membrane structure in a cyanobacterium (taken from Falkowski and Raven 1997). The thylakoids are arranged into sheets of membranes (each representing a pair of opposing membranes). The cytoplasm (surrounded by the cytoplasmic membrane, CM) houses the thylakoid membrane (TM). A periplasmic space separates the cell outer wall from the plasma membrane. **Note:** both diagrams are representative of eukaryotes and cyanobacterium but are phenotypically and genotypically plastic at finer taxonomic divisions.

complex. The electron is transported following the 'z-scheme' (*fig. 1.4.*) to cytochrome b-$_6$/f whilst the 'electron hungry' P680 pulls an electron from H_2O via a water-splitting manganese-protein complex. An electron is also excited in PSI (P700) and passed by several electron carriers to ferrodoxin where an enzyme reduces $NADP^+$ to NADPH (see *fig 1.2.*). This leaves the 'electron hungry' P700 to pull the electron from cytochrome b-$_6$/f. The transport of electrons results in proton-pumping from the stroma into the lumen, *fig. 1.4.*, and establishes an electrical and chemical (pH) gradient. The proton gradient is dissipated by the ATP-synthase and leads to the formation of ATP in the stroma. The linear electron flow of the z-scheme may become disrupted where PSI cannot obtain an electron from PSII (essentially where plastoquinone is the slowest to oxidise and cytochrome b-$_6$/f can be oxidised whilst PQ remains reduced) resulting in electron cycling around PSI. This compensation leads to proton pumping and ATP formation but not $NADP^+$ reduction.

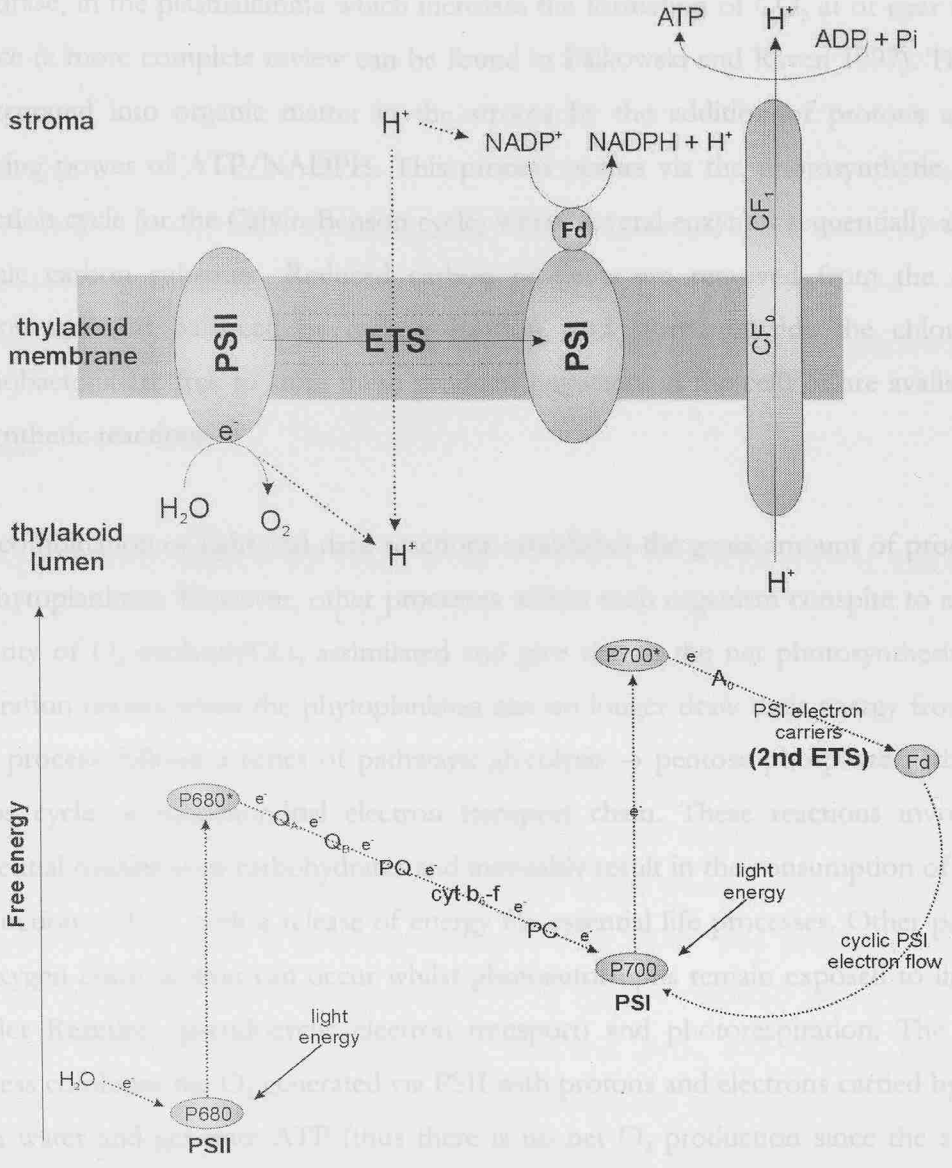

Figure 1.4.— (upper) Schematic of PSII, PSI and ATPase (coupling factor $[CF]_1$ is a peripheral protein attached to CF_0 on the stromal side) within the thylakoid membrane. Proton pumping between the stroma and lumen is also indicated but is not balanced; (lower) The Z-scheme depicts the change in free energy from solar excitation of electrons (e^-) and subsequent passage through the PSII and PSI electron transfer system (ETS). First ETS = phaeophytin → quinone Q_A → quinone Q_B → plastoquinone (PQ) → cytochrome b_6/f (cyt b_6/f) → plastocyanin (PC). Phaeophytin is not indicated in the figure since it only represents an intermediary electron acceptor. Second ETS = chlorophyll monomer A_0 → phylloquinone (A_1) → iron-sulphur cluster F_X → either of iron containing proteins F_A/F_B → ferrodoxin (Fd). Cyclic electron transfer around PSI is indicated and results in a loss of free energy to the electron for each cyclic event.

The products from the light reactions provide the energy and reducing power required for the incorporation of CO_2 in the dark reactions (*fig 1.2.*). The majority of carbon in the ocean is in the form of bicarbonate as a result of the slightly alkaline nature of seawater. However, phytoplankton contain a very catalytically active enzyme, carbonic

anhydrase, in the plasmalemma which increases the formation of CO_2 at or near the cell surface (a more complete review can be found in Falkowski and Raven 1997). The CO_2 is integrated into organic matter in the stroma by the addition of protons and the reducing power of ATP/NADPH. This process occurs via the photosynthetic carbon reduction cycle (or the Calvin-Benson cycle) where several enzymes sequentially alter the organic carbon substrate. Reduced carbon products are removed from the Calvin-Benson cycle, if balanced by carbon fixation, and stored outside the chloroplasts (cyanobacteria are free to store these products anywhere in the cell) or are available for biosynthetic reactions.

The combination of light and dark reactions establishes the gross amount of production by phytoplankton. However, other processes within each organism conspire to alter the quantity of O_2 evolved/CO_2 assimilated and give rise to the net photosynthesis. Dark respiration occurs when the phytoplankton can no longer draw their energy from light. This process follows a series of pathways: glycolysis → pentose phosphate pathway → Krebs cycle → mitochondrial electron transport chain. These reactions involve the sequential oxidation of carbohydrates and inevitably result in the consumption of O_2 and production of CO_2 with a release of energy for essential life processes. Other pathways of oxygen consumption can occur whilst photoautotrophs remain exposed to light: the Mehler Reaction (pseudocyclic electron transport) and photorespiration. The former process combines the O_2 generated via PSII with protons and electrons carried by PSI to form water and generate ATP (thus there is no net O_2 production since the same O_2 molecules are 'consumed'). The latter process describes the light-dependent reduction of CO_2 via the Calvin-Benson cycle for the purpose of energy dissipation. Photorespiration often appears suppressed in microalgae but can account as much as 15% of gross O_2 evolution (Geider 1992).

The response of photosynthesis to environmental variability

Several key environmental factors are responsible for the ability of marine phytoplankton to photosynthesise, grow and reproduce. Following Falkowski and La Roche (1991), Falkowski and Raven (1997), each cell is genetically suited to utilise a specific environmental regime through a selection of phenotypic traits (**adaptation**); this environment is not static within the lifetime of phytoplankton and each cell must further

appropriately respond over a variety of time scales in order to successfully compete (**acclimation**). Similar definitions have been recently employed when describing the response of phytoplankton to light, for example, photoadaptation from genetic transformations of marine diatoms (Cassoti *et al.* 1997), photoacclimation of Chlorophyceae in response to vertical water column mixing (Flameling and Kromkamp 1997). This distinction between processes operating within the evolution and within the lifespan of phytoplankton will be maintained throughout this thesis.

Light

The light environment of the ocean is the product of the solar photon flux density, atmospheric transmission and light attenuation by water (see Kirk 1992, 1994). Clouds and atmospheric particles are responsible for the quality of light that reaches the surface of the ocean. Light is reflected by surface waves and absorbed/scattered by both biologically active and inactive particles in the water resulting in a change in the quantity and spectral composition of light throughout the water column. The term 'euphotic zone' is used to characterise the upper (lit) region of the water column that can be used for photosynthesis and is generally shallower than 200m. The amount of this light available for photosynthesis is determined by the suite of pigments in the photosystem antennae: the Photosynthetically Available Radiation (PAR, 400-700nm). The specific pigment composition of a phytoplankton community will dictate the actual amount of PAR that can be absorbed between 400 and 700nm: the Photosynthetically Usable Radiation (PUR) (Morel 1978). Much of the light absorption by phytoplankton is by accessory pigments, such as accessory chlorophylls *b*, *c* and *d*, carotenoids and biliproteins, which absorb light in the blue and green region (~400-550nm) of the PAR spectrum. This capitalises on the corresponding weak absorption by water in this region of the spectrum.

Photoacclimation— Several mechanisms exist by which phytoplankton attempt to optimise the capture and utilisation of available light. Routine exposure to low light levels results in increase of photosynthetic light harvesting pigments into the photosystem antennae. This promotes the overall light harvesting capability by the phytoplankton; however, an increase in the density of pigments results in self-shading by the overlying thylakoid membranes and actually produces a decrease in the amount of absorption per

pigment and is described as the 'package effect' (eg. Berner *et al.* 1989). Increases to the number of chloroplasts per cell number and in thylakoid stacking also act to boost the light harvesting potential of a phytoplankton cell under low light (eg. Falkowski and La Roche 1991). The opposite pattern is evident under high light.

Alterations to the ratios of accessory pigments to chlorophyll *a* are also evident at different light intensities (eg. Falkowski and La Roche 1991). Some carotenoids, such as diadinoxanthin, diatoxanthin, zeaxanthin and β-carotene, do not transfer any energy to chlorophyll *a* and have been classed as non-photosynthetic pigments (Bidigare *et al.* 1990). These latter pigments are found in high light-acclimated phytoplankton and act to absorb excess light energy that would otherwise damage the reaction centres (Falkowski and Raven 1997). Transformation of certain xanthophylls can also increase the amount of energy that is dissipated non-photochemically. This process of xanthophyll cycling (*fig. 1.5.*) has been correlated with non-photochemical quenching (Demmig-Adams 1990) via thermal deactivation (eg. Olaizola and Yamamoto 1994) or the aggregation of light harvesting chlorophyll protein complexes (Horton 1992).

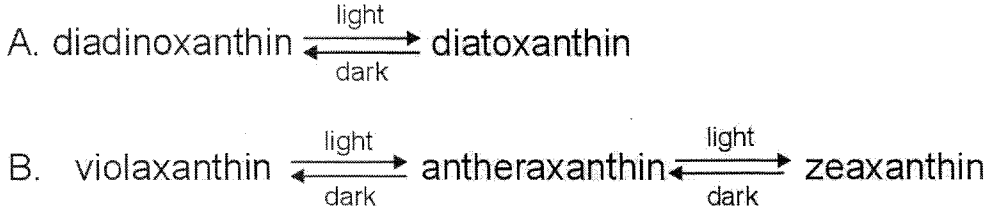

Figure 1.5.— The xanthophyll cycles. A light driven reaction transforms the epoxy containing xanthophyll into an epoxy-free pigment. Enzymes catalyse the back reaction under dark conditions. The 2 cycles are taxa-specific. A. The diadinoxanthin-diatoxanthin (DD-DT) cycle is characteristic to diatoms, dinoflagellates and prymnesiophytes (Liaaen-Jensen 1978). B. The violaxanthin-zeaxanthin (V-Z) cycle is characteristic of chlorophytes [higher plants] and possibly phaeophytes (Sierfermann-Harms 1985). A xanthophyll cycle has, as yet, not been identified in cyanobacteria and pro-chlorophytes (Falkowski *et al.* 1994).

The amount and spectral composition of light distributed between photosystems I and II can affect the flow of electrons from H_2O to NADPH (*fig 1.4.*) (Falkowski and Raven 1997). Under conditions of high light, the pool of the electron carrier plastoquinone (PQ) becomes markedly reduced. The altered redox state of the PQ pool encourages phosphorylation of the light harvesting pigment proteins serving PSII and results in a migration of some of the pigment protein to PSI. This acts to address the deficit of PSI

electron flow and is termed a state-I transition. The opposite occurs under low light conditions to balance relatively lower electron flow through PSII and is termed a state-II transition (Falkowski 1981, 1992, Falkowski *et al.* 1994). This phosphorylation of the photosystems appears almost universal amongst phytoplankton but may only produce relatively small changes to the absorption cross section of PSII (Falkowski *et al.* 1994). State transitions can also occur where light at wavelengths greater than 680nm preferentially excite PSI (and vice versa); however, this explanation does not appear to account for the observed variations of PSI and PSII with depth in the oceanic environment (Falkowski and Raven 1997).

Increases in the number of PSII reaction centres (eg. Berges *et al.* 1996), the ratio of PSII to PSI (eg. Barlow and Alberte 1985), and electron cycling around PSI (Falkowski and Raven 1997) are also observed under low light conditions and may similarly attempt to maintain a steady flow of electrons between and throughout the two photosystems. Electron cycling around PSII has also been observed by Falkowski *et al.* (1986). This mechanism acts to dissipate some of the excess energy absorbed by PSII and limits the amount/onset of high light damage to RCIIs (see below). As such, electron cycling around PSII appears to be a more indirect method by which the photosystem sustains a steady flow of electrons and, therefore, maintain a relatively high rate of photosynthesis.

Photoinhibition— Phytoplankton invariably encounter light levels that are beyond the capabilities of the mechanisms that act to maintain the highest levels of photosynthesis to which the organism is photoacclimated. These circumstances result in a reduction in the number of reaction centres and a subsequent increase in electron turnover time coupled with a decrease in the maximal rate of photosynthesis (eg. Falkowski *et al.* 1994). The exact process by which RCIIs are lost remains unclear; however, Aro *et al.* (1993) suggest that high light levels can create rates of electron turnover from RCII which exceed the rate of electron 'donation' from water. Holes can become established in the molecules that transfer electrons from water to RCII and lead to the generation of free radicals which could oxidise or destroy pigments and proteins in the reaction centres. This retardation of the photosynthetic rate is slowly reversible (eg. Long *et al.* 1994) and is dependent upon the length and degree of high light exposure. Recovery from photoinhibition occurs over a time scale of hours (eg. Vassiliev *et al.* 1994) once the light intensity experienced by the phytoplankton has relaxed below super-optimal levels.

Nutrients

Species of nitrogen, phosphorus, silicon, sulphur and of trace metals (eg. iron, zinc, manganese and copper) are all found in seawater and, in one form or another, are required by phytoplankton for growth. These elements are, in part, used to form proteins/compounds for the photosystems, reactions centres, transport of electrons and regeneration of substrates in the Calvin-Benson cycle and, therefore, provide the nutrition for phytoplankton cells. Nitrogen and phosphorous represent the 'major nutrients' and, in addition to providing the basis of many substrates involved in photosynthesis, are also incorporated into cellular tissue for phytoplankton growth and reproduction. Each one of these elements represents a limiting factor where concentrations fall below a level to which phytoplankton are acclimated (eg. Margalef 1997). The ratio of the major elements in phytoplankton cellular material is remarkably close to that found in seawater. The 'Redfield ratio' describes this ratio as 106C:16N:1P by atoms and represents a mean since the proportions may alter according to the nutritional status and taxanomic composition of the phytoplankton (eg. Falkowski and Raven 1997).

The distribution of nutrients throughout the water column is the product of import and export processes (*fig. 1.6.*). As a result, the lowest concentrations of nutrients are typically found in surface waters where phytoplankton uptake exceeds replenishment. The replenishment of nutrients into the marine system can occur via two pathways, new and regenerated (Eppley and Peterson 1979). New nutrients are supplied to phytoplankton in the euphotic zone from deep water, as a result of upwelling, deep wind induced mixing, eddy activity and diffusion, from advection between bodies of water and from atmospheric supply to the sea surface. The term 'nutricline' defines the zone of sharp change in nutrient concentrations between the surface layer and deeper waters and reflects the product of nutrient flux between deeper waters and the euphotic zone. The amount of new nutrient supplied to a system is used to define its trophic status (Dugdale and Wilkerson 1992). Oligotrophic systems are characterised by very little new nutrient input where phytoplankton must rely on the regeneration of nutrients for photosynthesis and growth. A so-called 'microbial loop' (eg. Azam *et al.* 1983) recycles the nutrients required for photosynthesis resulting in relatively little (biological) export of these elements from the euphotic zone. This provides a tightly coupled system akin to a

spinning wheel (Goldman 1988), the speed of which turns at a speed controlled by the maximum growth rate of the organisms involved. Some cyanobacteria contain an alternative mechanism for obtaining nitrogen whereby they directly fix dissolved molecular nitrogen and avoid either of these two pathways (eg. Mulholland and Capone 1999).

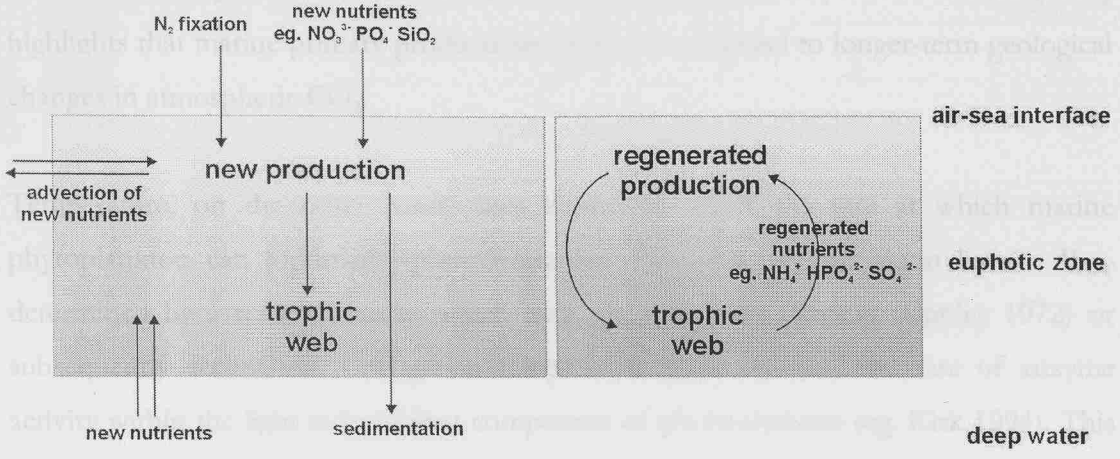

Figure 1.6.— Pathways of nutrients supplied into the euphotic zone of the oceanic ecosystem. New nutrients enter at the air-seas interface, from deep water and advection from neighbouring waters and is used by marine phytoplankton and the associated trophic web for 'new production'. Regenerated nutrients are a result of trophic interactions in the euphotic zone and give 'regenerated production'.

Phytoplankton associated with the different trophic regimes appear to have alternate strategies for acquiring nutrients (Eppley *et al.* 1969). In general, large influxes of new nutrients stimulate the growth of large diatoms since they show rapid rates of nutrient uptake. The phytoplankton of the nutrient poor oligotrophic regions are dominated by small celled cyanobacteria and prochlorophytes (Veldhuis and Kraay 1993, Olson *et al.* 1990a, b) which display slower nutrient-uptake rates but exhibit a much greater affinity for low nutrient concentrations. In addition, these picoplankton require less nutrients to saturate the cell as a result of their smaller cell-size (Agawin *et al.* 2000). Small variations to the nutrient status of a water-body may be reflected by changes in the photosynthetic performance of the dominant species. However, larger variations will eventually favour species with alternate strategies of nutrient acquisition and result in a shift of the phytoplankton community composition according to the new trophic regime.

Other variables

CO_2 is the primary substrate for photosynthesis. As such, the ability of an organism to uptake CO_2 should affect the rate at which photosynthesis can proceed. Whilst this is true for phytoplankton from some aquatic systems, for example, lakes (Kirk 1994), investigations reveal that most marine phytoplankton are not limited by short-term variations in CO_2 (Falkowski and Raven 1997). An investigation by Riebesell *et al.* (1993) highlights that marine primary productivity appears to respond to longer-term geological changes in atmospheric CO_2.

Temperature, on the other hand, does appear to affect the rate at which marine phytoplankton can [optimally] photosynthesise, P_{OPT}. All phytoplankton have a P_{OPT} determined by a temperature to which they are genetically adapted (Eppley 1972) or subsequently acclimated. Changes in temperature primarily alter the rate of enzyme activity within the light independent component of photosynthesis (eg. Kirk 1994). This subsequently determines the maximal rate at which electrons can be transferred through the ETS when the photosystem becomes saturated with light. As such, phytoplankton exposed to low temperatures typically become photoinhibited at lower irradiances (Falkowski and Raven 1997) and phytoplankton production becomes limited even though all other resources are replete. A limitation of nutrients will impede the ability of the photosystem to achieve P_{OPT} where temperature is at, or approaching, the optimal value (Li 1980). However, these effects of temperature upon *in situ* phytoplankton production are difficult to assess since this variable is closely linked with the distribution of nutrients in the marine environment. A comprehensive review of this subject is given by Raven and Geider (1988).

The combined effects of all these environmental parameters give rise to a characteristic profile of phytoplankton production throughout the water column (*fig 1.7.*). The actual shape and magnitude of this profile will be dependent upon the instantaneous quantity of each parameter and will, therefore, be highly variable in time and space (ie. as a function of latitude, season and depth). This, in turn, dictates the amount of phytoplankton biomass available to higher trophic levels.

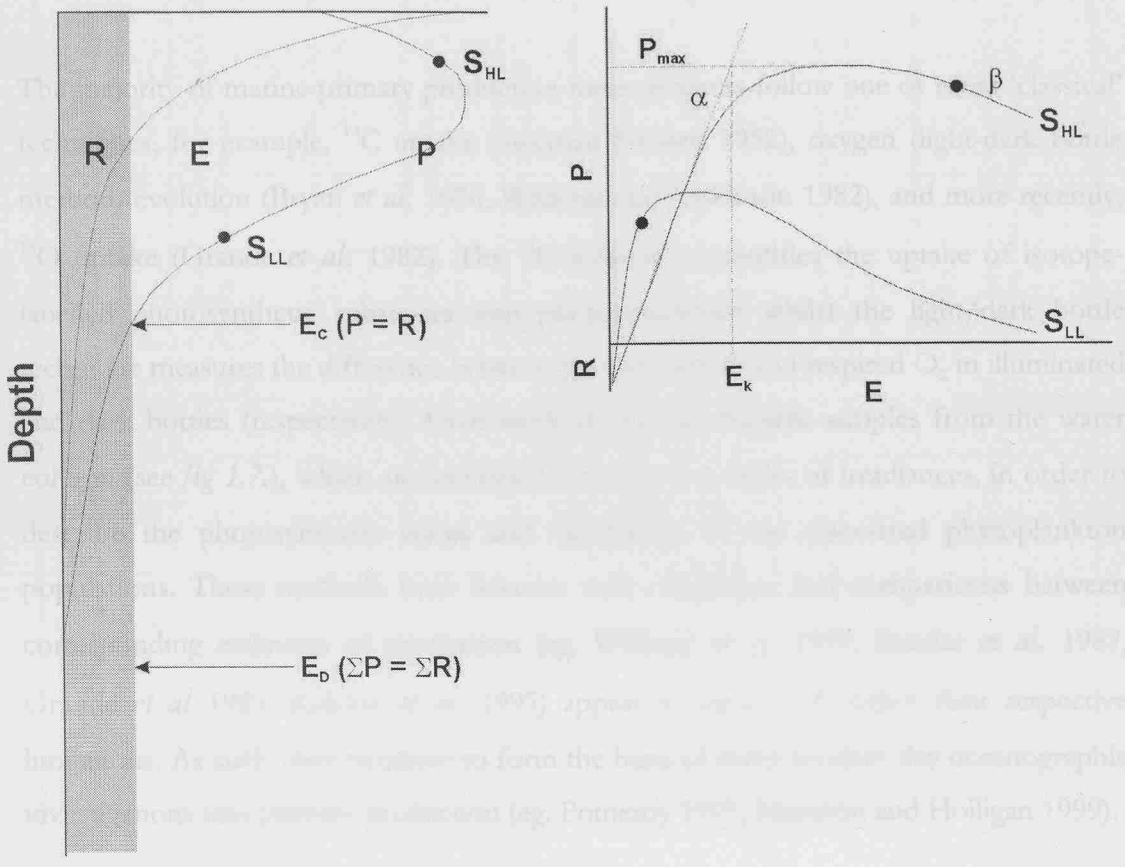

Figure 1.7.— (**left**) Schematic (typical) vertical profile of net primary production (P), irradiance (E) and daily integrated photoautotrophic respiration (R) throughout the water column. When total net P (ΣP: area to left of curve) exceeds that of R (ΣR) there is net growth of phytoplankton biomass. The light intensity at which ΣP=ΣR corresponds to the critical depth (E_D) and is a function of the degree of water column mixing and the solar radiance (Sverdrup 1958). If ΣP < ΣR there is no net phytoplankton growth, for example, increased water column mixing and/or less E and E_D effectively moves closer to the surface. E_C describes the compensation light intensity and represents the depth at which the rate of production = rate of respiration (and signifies the depth of the euphotic zone); (**right**) Schematic Photosynthesis (P) - Irradiance (E) response curves measured using the ^{14}C-uptake technique. Water samples taken from high light (S_{HL}) and low light (S_{LL}) conditions in the water column described by the left panel are each labelled with the isotope and exposed to a range of potential irradiances. The amount of ^{14}C-uptake represents the production (P) at each E. Several parameters of the P-E curve describe the photosynthetic characteristics of the phytoplankton population: light limited initial slopes (α) where the rate of light absorption is < the maximal rate of electron transport; the maximum rate of light saturated photosynthesis (P_{max}) where the rate of light absorption is > the maximal rate of electron transport; the degree of photoinhibition (β); the light intensity at which P_{max} occurs ($E_K = P_{max}/\alpha$). The filled circle on each of the P-E curves signifies the *in situ* E at which the water samples were taken. Therefore, the corresponding P represents the true (instantaneous) production for the respective sample. The FRRF is profiled throughout the water column and provides an instantaneous production profile akin to that described in the left panel.

1.2. Estimates of phytoplankton production

The majority of marine primary production measurements follow one or more 'classical' techniques, for example, ^{14}C uptake (Steeman Nielsen 1952), oxygen (light-dark bottle method) evolution (Bryan *et al.* 1976, Williams and Jenkinson 1982), and more recently, ^{18}O uptake (Grande *et al.* 1982). The ^{14}C technique quantifies the uptake of isotope-labelled photosynthetic substrates into photoautotrophs whilst the light/dark bottle technique measures the difference between photosynthetic and respired O_2 in illuminated and dark bottles (respectively). Each method requires discrete samples from the water column (see *fig 1.7.*), which are incubated throughout a series of irradiances, in order to describe the photosynthetic status and capabilities of the associated phytoplankton populations. These methods have become well established and comparisons between corresponding estimates of production (eg. Williams *et al.* 1979, Bender *et al.* 1987, Grande *et al* 1989, Kiddon *et al.* 1995) appear to agree well within their respective limitations. As such, they continue to form the basis of many modern day oceanographic investigations into primary production (eg. Pomeroy 1997, Marañón and Holligan 1999).

Some of the earliest estimates of production (following the ^{14}C and light/dark methods) were synthesised into global [primary] productivity maps (see Berger *et al.* 1989). The most accurate (and well known) was the map by Koblentz-Mishke *et al.* (1970) which combined over 7000 production estimates taken from the global ocean environment throughout the 1960's. Estimates of production from the Koblentz-Mishke map have been summarised for some of the key Atlantic provinces (described by Longhurst *et al.* 1995) and compared with more modern estimates (*table 1.1.*). The pattern of production in the Atlantic remains throughout 30 years of study whereby values are highest towards the European north-west continental shelf and lowest in the oceanic gyre regions. The quantitative descriptions of production appear markedly different and presumably reflect the variability inherent to the system, however, the evolution of the respective techniques (eg. accuracy and methodology) throughout time may add confusion to this interpretation. The most recent study by Marañón and Holligan 1999 (see also Marañón *et al.* 2000) further underlines the inherent temporal and spatial variability of production that exists within the Atlantic which would be difficult to determine from discrete or synthesised data sets.

Source Material	Time & Date of data collection	NECS (55-45N; E of 10W)	NADR (65-45N)	NAST (45-25N; E of 40W)	NATR (25N-10N)	WTRA (10N-10S; W of 20W)	ETRA (10N-10S; E of 20W)	SATL (10-40S)	Method of Determination
Marañon and Holligan (1999)†	Sept 1995 April 1996 Sept 1996		268 (75) 1083 (304) 481 (113)	77 (28) 436 (98) 287 (56)	240 (190) 229 (52) 737 (420)	111 (25) 179 (72) 564 (49)		301 (149) 190 (58) 393 (91)	^{14}C uptake 6-7 hr incubations on deck. All data rep. integral of euphotic in mgC/m^2/d.
Rees *et al.* (1999)	April-May 1994		498-1458						^{14}C uptake 24 hr incubations on deck / *in situ*. Data rep. integral of euphotic in mgC/m^2/d.
Oschilles and Garçon (1998) *		274-822	274-685	0-410	0-274	0-54	82-410		Simulation using classical NPZD nitrogen based biological model and eddy activity. All data in mgC/m^2/d.
Claustre and Marty (1995)	Sept-Oct 1991& May-Jun 1992			21N31W (267-352)					^{14}C uptake as Morel *et al.* (1996) except data rep integral of 0-250m in mgC/m^2/d.
Longhurst *et al* (1995)	1978-1986 CZCS data	2000	660	330	290	360	430	210	Algorithm based on CZCS climatological data and chlorophyll a, and P-I relationships. All data in mgC/m^2/d.
Savidge *et al.* (1995)	May-June 1990		46N20W (1900-3000)						^{14}C uptake 24 hr incubations *in situ*. All data rep. integral of 0-35m in mgC/m^2/d.
Jochem and Zeitschel (1993)	March-Apr 1989			33N30W (85-350)	18N30W (440-1100)				^{14}C uptake 12 hr incubations *in situ*. All surface data in mgC/m^2/d.
Joint *et al.* (1993)	May 1989 June-July 1989		236-1120 344-1152						^{14}C uptake 24 hr incubations on deck / *in situ*. Data rep. integral of euphotic in mgC/m^2/d.
Bauerfeind (1987)	Feb-June 1979						78-741		^{14}C uptake 6 hr incubations *in situ*. Data in mgC/m^2/d.
Koblentz-Mishke *et al.* (1970)		247-493	148-247	45-35N (148-247) 25-35N (99-149)	148-247	99-249	148-493	<99	Amalgamation of all data to 1970 using Steeman-Nielen or oxygen techniques.All data in mgC/m^2/d.

Table 1.1.— Examples of recent published quantitative estimates of phytoplankton production for provinces of the Atlantic Ocean (according to Longhurst *et al.* 1995): NECS (north-eastern continental shelf), NADR (north Atlantic drift), NAST (northern subtropical gyre), NATR (tropical gyre), WTRA (western tropical Atlantic), ETRA (eastern tropical Atlantic) and SATL (south Atlantic subtropical gyre)). Also provided is comparative data from Koblentz-Mishke *et al.* (1970). Rates of production are given as a mean or a range for each province except where specific locations are indicated. † data for Marañon and Holligan (1999, but also Marañon pers.comm.) indicate the mean (standard error); * These authors note an error associated with the lower limits of estimates for NAST, NATR and WTRA

The major draw-backs of these 'classical' techniques stem from the need to incubate water samples for a period of time. So-called 'bottle effects' can drastically change the nature of the light field from that experienced *in situ* (Grande *et al.* 1989) and create an artificial ecosystem where small scale food webs are able to exchange the tracer molecules between numerous possible pathways (Falkowski and Raven 1997). Discrepancies between light and dark bottles may also confuse the interpretation of photoautotrophic photosynthesis (eg. Banse 1993). Furthermore, considerable time and effort is required to measure production using these 'classical' methods and only provide limited temporal and spatial resolution for the environment under consideration. As a result, interest is increasing in the use of rapid *in situ* profiling instruments (such as the Fast Repetition Rate Fluorometer, Kolber *et al.* 1998), and of algorithms which can be applied to remotely sensed data (eg. Longhurst *et al.* 1995, Behrenfeld and Falkowski 1997a, b), for the analysis of the nature and variability of primary production.

1.3. The Fast Repetition Rate Fluorometer (FRRF) for measuring *in situ* primary production

The pigments contained within photosystems I and II (PSI and PSII) serve to deactivate excitation energy through photochemical and alternative non-photochemical pathways. One of these latter pathways is the photosynthetic emission of fluorescence (Kraus and Weis 1991) which, at ambient temperatures, is emitted predominantly from PSII (Barber *et al.* 1989). The measurement of phytoplankton fluorescence emission (yield) was originally achieved by Lorenzen (1963, 1966) and subsequently provided a rapid assay for the non-destructive measurement of chlorophyll *a*. A great deal of effort has since been invested in understanding the relationship between chlorophyll *a* and fluorescence and has meant that fluorescence measurements have become routine and fundamental to oceanographic studies.

Fluorometers are designed to measure the peak emission of chlorophyll *a* fluorescence (approximately 685nm) from phytoplankton cells stimulated with easily absorbed blue light. The routine use of traditional fluorometers has provided a wealth of information concerning the total fluorescence yield per unit volume of sample. However, to further assess the photosynthetic performance of such a sample requires a more detailed

assessment of the total fluorescence yield. This was initially achieved through the development of 'Fluorescence Induction Techniques' which measure transient fluorescence yields from rapid exposure to continuous light. The earliest attempts to assess fluorescence yields from such techniques were complicated by multiple photochemical turnovers (Kolber 1997) which add confusion to the interpretation of the kinetics of light harvesting and electron transfer. Under a multiple turnover, some reaction centres may remain briefly photochemically inactive upon light saturation (see below) and plastoquinone pool (PQ) reduction is not wholly confined to a single turnover event. Advancing technology led to the development of Pump and Probe (PP) and Fast Repetition Rate Fluorometer (FRRF) techniques which can induce only a single turnover of PSII (Falkowski and Kolber 1995).

The PP technique measures the fluorescence yield (from a probing signal) prior to, and following, a pump of saturating actinic light. This technique was first applied to the analysis of variable chlorophyll *a* fluorescence by Mauzerall (1972), but was not significantly developed until Falkowski *et al.* (1984) began to implement the PP to determine quantitatively the absolute rate of photosynthetic electron transport *in situ*. This use of PP *in situ* was concentrated throughout the late 1980s and early 1990s, e.g. Kolber *et al.* (1990), Falkowski and Kolber (1993), Kolber and Falkowski (1993), Olaizola *et al.* (1996). However, this method proved too slow to follow the dynamic changes in PSII photosynthetic parameters occurring on time scales of less than minutes (Kolber 1997). A need to make on-deck measurements of dark adapted water samples and of more detailed physiological parameters, such as the functional absorption cross section (Kolber and Falkowski 1993, Boyd *et al.* 1997), further decreased the value of this instrument.

The FRRF technique is based on the same photosynthesis-fluorescence relationships as PP (eg. Geider *et al.* 1993) but was developed to overcome the problems associated with the PP technique (Kolber 1997) and has, as such, superseded its use. The FRRF provides a rapid chain of excitation flashlets. The intensity of each flashlet is much less than saturating, but the time between flashlets is so short that cumulative excitation saturates PSII (Falkowski and Kolber 1995) over a time scale of microseconds. This represents the gradual contribution of PSII reaction centres to photochemistry. The ½-time for Q_a^- re-oxidation takes 160-400 μs (Green *et al.* 1994), therefore, the FRRF is typically

programmed to saturate PSII over 50-100 μs (Green *et al.* 1994, Kolber 1997) which is within the time period of a single photochemical turnover. The FRRF also has two data collection chambers incorporated into the instrument to allow *in situ* simultaneous measurement of samples under ambient light and dark conditions (Kolber and Falkowski 1992) and is further described in *Chapter 2.* The FRRF has been designed as a highly flexible sampling tool; for example, it is a relatively small instrument which can be operated directly or remotely to collect data over a range of spatial scales. It can also be packaged with a variety of oceanographic instruments to provide detailed physical-biological accounts of the environment.

The biophysical theory underlying the FRRF technique

The FRR fluorometer has the capability to estimate the absolute rate of *in situ* photosynthetic electron transport (Falkowski *et al.* 1984) and, therefore, the gross oxygen evolution from the photosystems. The robustness of the biophysical theory concerning the measured fluorescence properties of a sample are fundamental towards the application and use of the instrument, as well as the interpretation of the observed fluorescence signal. The following provides a brief summary of this theory which is described in more detail by Falkowski and Kolber (1993), Kolber and Falkowski (1993), Flameling (1997), Kolber (1997), and Falkowski and Raven (1997):

An electron (e^-) is donated from PSII to the first stable acceptor, the quinone Q_A, in the electron transfer chain (*figs 1.4.* and *1.8.*) once the specialised chlorophyll *a*-protein complex of RCII (P680) has received sufficient energy (see pages 6-8). Prior to this, Q_A is oxidised, and the reaction centre is said to be open. When Q_A becomes reduced, the reaction centre is closed. The relationship between the rates of e^- addition-to and subsequent e^- removal-from Q_A determines whether photosynthesis is light-limited or light-saturated: when the removal rate greatly exceeds the addition rate, Q_A is largely oxidised and the rate limiting step in photosynthesis is light absorption by the antennae. This is equivalent to the light-dependent section of a photosynthesis-irradiance (P-E) curve (α) (*fig 1.7*); when the rate of e^- addition to Q_A greatly exceeds the removal rate, Q_A is largely reduced, and the rate-limiting step in photosynthesis is electron transfer away from Q_A by downstream reactions ie. the light-independent section of a P-E curve.

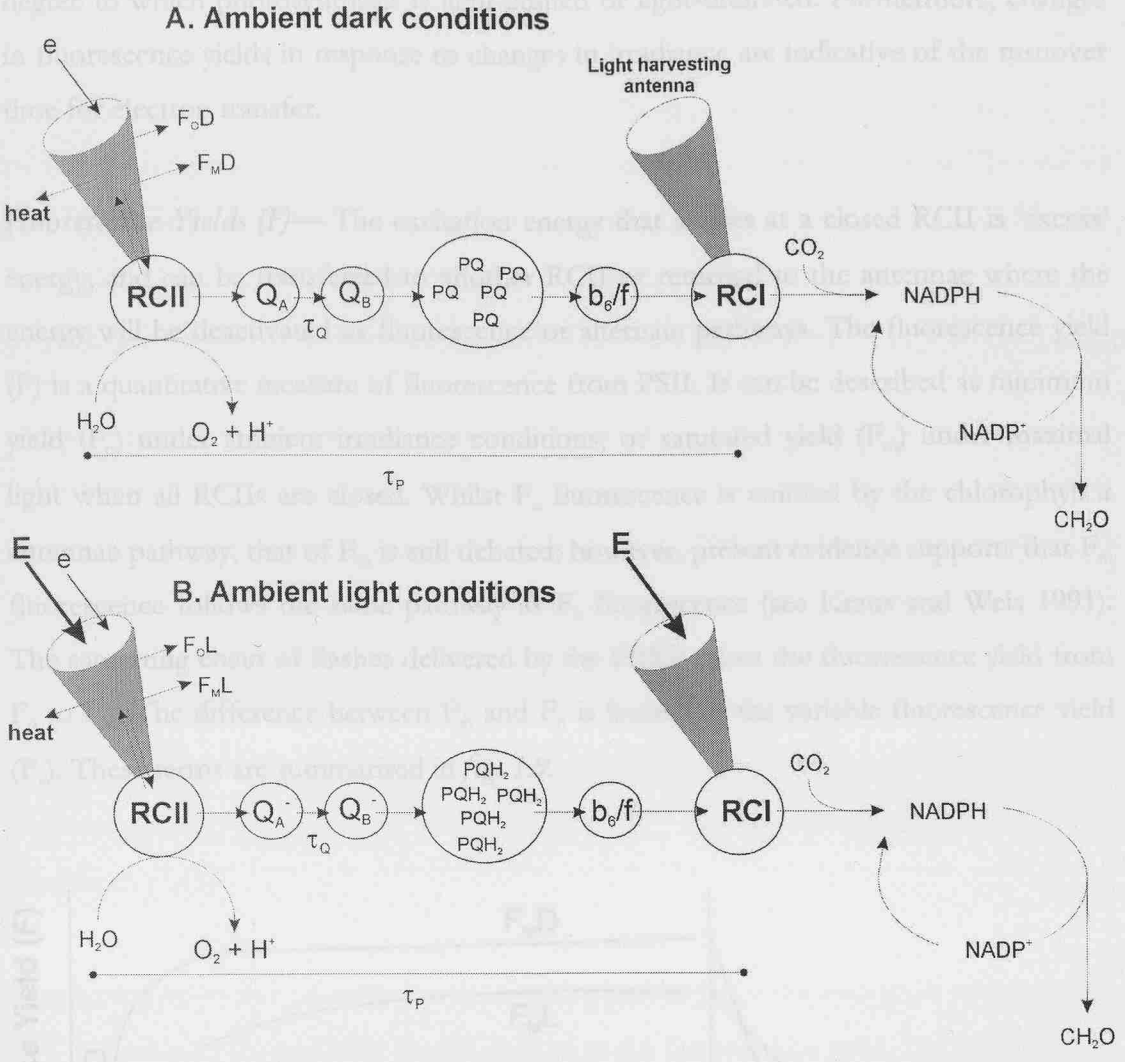

Figure 1.8.— (Adapted from Kolber and Falkowski 1993) Schematic representations of the relationship between reaction centres I and II with respect to light excitation under ambient dark and light conditions. Excitation energy from the FRRF (e) or from the sun (E) is absorbed by pigmented antennae and delivered to the energetically coupled reaction centres. This energy is subsequently de-excited by one of several pathways: conversion to chemical energy via photochemical charge separation, re-emission as fluorescence, or non-radiative emission via thermal deactivation. In the dark, levels of excitation energy are minimal, there is no photochemical reaction, and the fluorescence yield (F_oD) is minimal. As such, the photosystem remains open, and the components of the electron transport chain remain in an oxidised state. Once a degree of solar excitation energy is provided, the oxidation of water and the transfer of electrons from RCII to RCI starts, the RCII closes and the initial electron acceptor (Q_A) becomes reduced The RCII does not re-open until Q_A^- is re-oxidised, and the time taken (τ_P) for Q_A^- re-oxidation represents the rate of electron transfer between RCII and RCI. The time constant for the oxidation of Q_A^- by Q_B is described by τ_Q. The change in the background fluorescence yield (F_o) between ambient light and dark conditions indicates the proportion of RCIIs employed for photochemistry.

The relative number of RCIIs that are able to donate e$^-$s to Q_A reflect the proportion of light energy that is re-emitted as fluorescence. Therefore, yields of fluorescence can determine at any particular time the relative amount of reduced (or oxidised) Q_A and the

degree to which photosynthesis is light-limited or light-saturated. Furthermore, changes in fluorescence yields in response to changes in irradiance are indicative of the turnover time for electron transfer.

Fluorescence Yields (F)— The excitation energy that arrives at a closed RCII is 'excess' energy, and can be transferred to another RCII or returned to the antennae where the energy will be deactivated as fluorescence or alternate pathways. The fluorescence yield (F) is a quantitative measure of fluorescence from PSII. It can be described as minimum yield (F_o) under ambient irradiance conditions, or saturated yield (F_m) under maximal light when all RCIIs are closed. Whilst F_o fluorescence is emitted by the chlorophyll *a* antennae pathway, that of F_m is still debated; however, present evidence supports that F_m fluorescence follows the same pathway as F_o fluorescence (see Kraus and Weis 1991). The saturating chain of flashes delivered by the FRRF raises the fluorescence yield from F_o to F_m. The difference between F_m and F_o is known as the variable fluorescence yield (F_v). These terms are summarised in *fig. 1.9.*

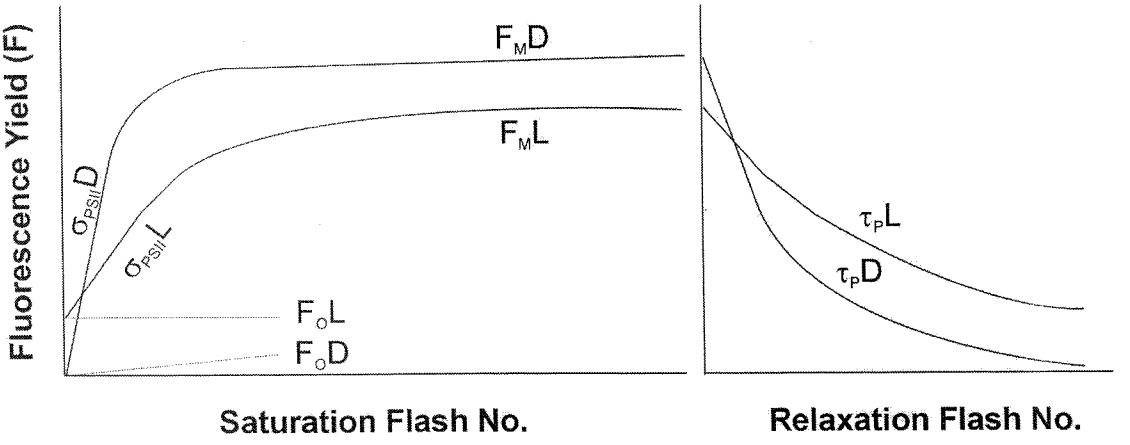

Figure 1.9.— Schematic representation of the saturation and relaxation of photosystem II (PSII) in terms of fluorescence yields (F) detected by the FRRF in response to excitation flashes. The initial fluorescence yields represent background fluorescence levels (F_o) whilst saturation fluorescence yields (F_m) are induced once all reaction centres (RCIIs) are closed. The effective absorption cross section for PSII, σ_{PSII}, is given by the rate at which RCIIs are closed. The saturation sequence typically consists of 100 flashes whilst the relaxation sequence is composed of flashes of lower energy. The relaxation fluorescence yield defines the timescale for electron transfer, τ, that leads to the re-opening of RCIIs. The saturation and relaxation sequences are shown for both the dark (D) and light (L) chambers operated under the same FRRF protocol (flash duration and time between flashes), see *Chapter 2.*

Quantum Efficiency of Photochemistry (F_v/F_m)— A quantum yield is the ratio of energy received to that which is emitted. Quantum yields for photosynthesis can be determined in terms of the fluorescence properties of RCIIs that are fully open (probability of excitation escape is low: F_o) and fully closed (excitation energy cannot be directed to photochemistry: F_m). The dimensionless parameter F_v/F_m (where $F_v = F_m-F_o$) is the maximum change in the quantum yield of fluorescence [normalised to the F_m] and reflects the proportion of energy received by RCII to that which is emitted, ie. the maximum change in the quantum yield of photochemistry or the efficiency of photochemistry. Based on laboratory studies of phytoplankton cultures, the maximum value for F_v/F_m is 0.65, and is <1.0 because of back reactions between donor chlorophyll molecules and the acceptor molecules (Schatz *et al* 1988). Deviations in the observed value of F_v/F_m from the maximum value of 0.65 are seen under different environmental conditions (eg., Falkowski and Kolber 1995) and are considered to be indicative of variations in the fraction of RCIIs capable of converting absorbed light energy to photochemical energy (Geider *et al.* 1993). As such, the proportion of functional PSII reaction centres, *f*, is defined as measured F_v/F_m divided by the theoretical F_v/F_m maximum (0.65).

Quenching (q)— The occurrence of competing pathways for the excitation energy results in a reduction in the potential energy emitted as the fluorescence yield. Excitation energy that proceeds along photochemical pathways will reduce the fluorescence yield and is termed photochemical quenching (qP). Additionally, there are non-photochemical pathways which are competing for the excitation energy, for example, as heat, or as a loss of excitation energy from reactions within the pigment bed, and are termed non-photochemical quenching (qN).

The photochemical quenching coefficient, qP, describes the proportion of RCIIs closed under ambient light, and is calculated from fluorescence yields obtained from the FRRF light and dark chambers: $qP = (F_mL - F_oL)/(F_mL - F_oD)$. Estimation of the non-photochemical quenching coefficient, qN, where $qN = (F_mD^{\infty} - F_mL)/(F_mD^{\infty} - F_oD^{\infty})$, requires a knowledge of the fluorescence yields of fully relaxed photosystems; D^{∞} indicates a measurement on cells that have been kept in darkness for long enough to allow complete relaxation of energy dependent quenching (usually >30 minutes). This parameter can be measured with a bench-top FRRF on discrete samples (eg. Kolber and

Falkowski 1993). qN represents the remainder of fluorescence quenched by sources other than photochemistry. Instantaneous physiological measurements (*in situ*) of the pigment bed and RCII are believed to quantitatively account for the majority of energy that is non-photochemically quenched (Kolber and Falkowski 1993).

PSII effective absorption cross-section (σ_{PSII})— The rate at which PSII is saturated from F_o to F_m (*fig 1.9.*) provides an indication of the area available for light interception, ie. the area of the antennae, relative to the number of reaction centres (Vassiliev *et al.* 1994, Falkowski and Kolber 1995). As such, this term is not an actual size measurement but is a measure of the probability that photon absorption will result in a photochemical event (Falkowski and Raven 1997), and has units of Angstroms^2 (Å^2) quanta^{-1}. For a given excitation energy, a high σ_{PSII} indicates a high efficiency of light interception, and therefore a relatively fast rate of available RCII closure; a lower σ_{PSII} would result in a longer time for light interception and hence RCII closure saturation. Any changes to processes within the pigment bed (relative to the number of RCIIs) are likely to be reflected in these measurements.

Minimum turnover time of electrons (τ)— The decay in the yields of variable fluorescence (*fig. 1.9.*), F_v, in response to a series of relaxation flashlets can be used to obtain the turnover time for photosynthetic electron transfer. Upon the removal of saturating light, the fluorescence yield falls at a rate corresponding to that of RCII opening. This signifies the time taken for electron transfer from PSII to PSI (the maximum rate of electron turnover, $1/\tau$), the rate at which electrons (e^-) can be pulled from water to evolve an oxygen molecule and, therefore, the sequestering of a single photochemical event. The PQ pool can remain highly reduced when the rate of photon absorption by PSII is greater than the rate of PQ re-oxidation (τ_p). Subsequently, PQ becomes highly reduced and PQ re-oxidation is the rate limiting step for re-oxidation of the intermediate electron acceptors (Q_A and Q_B) and ultimately, of the P680 molecule. This condition may occur at high irradiances or during a prolonged FRRF saturation sequence (Kolber and Falkowski 1992).

Several time constants contribute to the turnover of electrons (*figures 1.8.* and *1.9.*), for example, τ_{Q_A} describes the time taken for Q_A^- (the primary electron acceptor from PSII)

re-oxidation and τ_p describes the rate of plastoquinone pool (PQ) re-oxidation (Kolber and Falkowski 1993). The FRRF can resolve up to 4 components of the kinetics of electron transport. However, this can only presently be achieved using an extended protocol which, for *in situ* observations, would last longer than the flushing time for the sample chamber (Kolber 1997). Shorter protocols can provide estimates of τ_{Q_A}, but may only resolve 1 or 2 components of PQ re-oxidation which is insufficient to fully describe the actual electron transfer process (*sensu* Kolber 1997). Therefore, accurate determinations of the *in situ* turnover time for PSII (τ_p) can, at present, only be achieved through indirect methods such as those employed for the Pump and Probe fluorescence technique (Falkowski and Kolber 1993, Kolber and Falkowski 1993).

Some of the *in vivo* fluorescence properties of PSII used to estimate rates of photosynthesis (see *equation 1.1.*) cannot presently be directly resolved without making certain assumptions:

Concentration of PSII reaction centres (n_{PSII})— A knowledge of the number of reaction centres is also required for the calculation of photosynthesis using the FRRF, but is not easily measured by fluorescence techniques alone (Kolber and Falkowski 1993). A value of n_{PSII} (mol RCII mol chl a^{-1}) must be assumed and represents the greatest ambiguity in the use of the FRRF to calculate photosynthesis since this parameter can vary both with phytoplankton taxonomy and environmental conditions (eg. Dubinsky *et al.* 1986). Previously used values of n_{PSII} for the estimation of production using the PP or FRRF (eg. Kolber and Falkowski 1993, Boyd *et al.* 1997) come from several laboratory studies: 1/500 (0.002 mol RCII mol chl a^{-1}) for chlorophytes and diatoms, and 1/300 (0.003 mol RCII mol chl a^{-1}) for cyanobacteria (Falkowski and Kolber 1995).

The quantum yield of electron transport (ϕ_e)— The ratio of oxygen evolved per quanta of energy absorbed sets a limit to the overall quantum yield of photosynthesis. At maximum efficiency, four electrons are transferred for each molecule of O_2 evolved, giving a value for ϕ_e of 0.25 O_2 molecules/quanta. However, ϕ_e is not a constant. At high levels of irradiance, the relationship between irradiance and oxygen yield becomes uncoupled (Falkowski *et al.* 1988). This uncoupling has been attributed to cyclic electron flow around PSII (Falkowski *et al.* 1988, Prasil *et al.* 1996), although other processes, for

example, mitochondrial respiration, Mehler-peroxidase reactions, photorespiration and PSII heterogeneity are also likely to be important (Flameling and Kromkamp 1998), see *section 1.1.* Irrespective of the causes, energy loss occurs when the rate of primary photochemistry exceeds the maximal rate of electron transfer, (τ_p), from PSII to PSI (Kolber and Falkowski 1993), and ϕ_e declines. As such, the degree to which the rate of primary photochemistry exceeds τ_p at saturating irradiance levels represents a measure of ϕ_e and relies on the accuracy with which τ_p is estimated.

1.4. Estimates of oxygenic primary production using the FRRF

The kinetics of photosystem closure can be observed by following the responses in fluorescence or oxygen evolution. Fluorescence yield is defined as the ratio of photons emitted from PSII to photons absorbed by PSII, whilst oxygen yield is the ratio of O_2 evolved to photons absorbed by PSII. However, the action spectra for these 2 factors are remarkably similar (Neori *et al* 1988) and suggest that they share a common photochemical reaction (Falkowski and Raven 1997). Like fluorescence, oxygen generation essentially stems from reactions that occur within PSII. Therefore, the FRR fluorometer can provide a convenient assay for estimating photosynthetic oxygen evolution. The relationship between these two factors can be used to describe an empirical photosynthetic rate model (Kolber and Falkowski 1993) using the fluorescence parameters that the FRRF measures:

$$PO_2^B(E) = E \cdot \sigma_{PSII} \cdot qP(E) \cdot \phi_e(E) \cdot (f \cdot n_{PSII}) \qquad \textbf{[1.1.]}$$

This equation combines derivations of the concentration of photosystem II reaction centres (n_{PSII}), the proportion of these reaction centres that are capable of photochemistry (f), the rate of photon absorption per reaction centre ($\sigma_{PSII} \cdot E$), and the quantum efficiency of photosynthetic oxygen evolution ($qP.\phi_e = \phi O_2$) to calculate gross photosynthesis in terms of oxygen produced. A quantum yield of photochemistry within PSII is also considered by Kolber and Falkowski (1993) but is constant and unity and, therefore, is not necessary in *equation 1.1.* Modification of *equation 1.1.*, to take account

of the relationship between oxygen produced and carbon fixed, gives photosynthetic carbon fixation per unit volume:

$$P_z = E_z \cdot \sigma_{PSII} \cdot \phi O_2 \cdot (f.n_{PSII}). 1/PQ \cdot 3600 \cdot 10^{-6} \qquad \textbf{[1.2.]}$$

Where P_z = photosynthetic carbon fixation per unit volume of seawater at depth z (mol CO_2 m^{-3} h^{-1}); *PQ* is the photosynthetic quotient (the observed efficiency of O_2 evolved per CO_2 assimilated or mol O_2 evolved: mol CO_2 assimilated); and 3600 . 10^{-6} is a numerical factor to account the conversion of seconds to hours and μmol photons to mol photons. All other parameters are defined as *equation 1.1.* but with reference to depth z. As for n_{PSII}, values for *PQ* must be assumed or estimated by other methods.

Summary of the calculation of photosynthetic rate via the FRRF

The following parameters are provided via the output of the FRRF (see *Chapter 2* for more details) but require further manipulation before application to *equation 1.2*:

The absorption cross sectional area of the antennae of RCII (σ_{PSII})—is measured and output through the FRRF in units of $Å^2$ $quanta^{-1}$. This can be converted to more conventional units to compare and associate with other biophysical parameters:

$$\frac{\sigma_{PSII} \cdot Å^2}{quanta} \frac{1m^2}{10^{20}Å^2} \frac{6.0231^{23}quanta}{1 \text{ mol photons}} = \frac{\sigma_{PSII} \cdot 6.0231^{23} (m^2/\text{mol photons})}{10^{20}}$$

The number of functional RCIIs (n_{PSII})—Is a product of the value of the number of RCIIs and the F_v/F_m dark chamber value (dimensionless) relative to the 0.65 maximum:

$$\mathbf{n_{PSII}} \cdot (\mathbf{F_vD/F_mD})/0.65 = n_{PSII} \cdot f \text{ (mol RCII mol chl } a^{-1})$$

Fluorescence yields—F_o, F_m and F_v (F_m-F_o) values from both the light (L) and dark (D) chambers are output through the FRRF (instrument units)and can be used in isolation and provide the calculations for both photochemical (qP) and non-photochemical (qN) quenching:

$(F_mL-F_oL) / (F_mL-F_oD) =$ **qP** (dimensionless number between 0 and 1)

$(F_mD-F_mL) / (F_mD-F_oD) =$ **qN** (dimensionless number between 0 and 1)

Quantum yield of electron transport (ϕ_e)—Is calculated from the rate of light absorption relative to the turnover time of electrons such that:

$$\frac{E\ \mu mol\ photons}{m^2\ s} \frac{1\ mol\ photons}{10^6 \mu mol\ photons} \frac{\sigma_{PSII}\ m^2}{mol\ photons} qP \frac{1\ s}{10^6 \mu s} \leq \frac{1}{\tau_p\ \mu s} \qquad \phi_e = 0.25$$

This quantum yield is at its maximal value (0.25 mol O_2 mol $RCII^{-1}$). However, where there is excessive excitation energy, the process of electron transport becomes less efficient and is accounted for:

$$\frac{E\ \mu mol\ photons}{m^2\ s} \frac{1\ mol\ photons}{10^6 \mu mol\ photons} \frac{\sigma_{PSII}\ m^2}{mol\ photons} qP \frac{1\ s}{10^6 \mu s} \leq \frac{1}{\tau_p\ \mu s} \qquad \phi_e =$$

$$0.25 * \frac{m^2\ s}{E\ \mu mol\ photons} \frac{10^6 \mu mol\ photons}{1\ mol\ photons} \frac{mol\ photons}{\sigma_{PSII}\ m^2} \frac{1}{qP} \frac{10^6 \mu s}{1\ s} \frac{1}{\tau_p\ \mu s}$$

Calculation of τ_p—Can be obtained directly through FRRF relaxation period where one can be confident that $\tau = \tau_p$. Under these conditions estimates of τ_p, E_k and P_{max} can be derived for each FRRF measurement. Following Kolber and Falkowski (1993) for PP estimates of production, and Sakshaug *et al.* (1997), τ_p is unknown but can be determined from the product of the turnover time of electrons and the light intensity at which the rate of photosynthesis changes from light dependant to light independent (E_k):

$$\tau_p\ (\mu s) = \frac{m^2\ s}{E_k\ \mu mol\ photons} \frac{10^6 \mu mol\ photons}{1\ mol\ photons} \frac{mol\ photons}{\sigma_{PSII}\ m^2} \frac{10^6 \mu s}{1\ s}$$

An estimate of E_k can be obtained by plotting a figure of q_p versus E: the sudden decline at high light intensities corresponds to the E_k. This derivation of E_k, and therefore τ_p, means that only one estimate can be derived for a series of q_p versus E data. This single value represents an integration of otherwise discrete depth signatures for the whole water column, as would be expected for a mixed population. From the product of one or more of the above factors, we are now able to calculate:

The instantaneous rate of photosynthesis (P(E): mol O_2 mg chl a^{-1} h^{-1})

$$\frac{f.n_{PSII}\ \text{mol RCII}}{\text{mol chl } a} \quad \frac{\sigma_{PSII}\ \text{m}^2}{\text{mol photons}} \quad \frac{\phi_e\ \text{mol}O_2}{\text{mol RCII}} \quad qP \quad \frac{\text{I mol chl } a}{892\text{g chl } a} \quad \frac{1\text{g chl } a}{10^3\ \text{mg chl } a} \quad \frac{\text{E } \mu\text{mol photons}}{\text{m}^2\ \text{s}} \quad \frac{3600}{\text{h}}$$

Subsequent modifications to the value derived through this equation, for example, mols to mg O_2 or the application of a photosynthetic quotient to observe the amount of carbon uptake can be performed (see *equation 1.2.*). A summary of the major terms and symbols used throughout this thesis are given in the following table (*table 1.2.*).

Term	Definition	Units	Method obtained	Formula (for derived parameters)
F	Fluorescence yield	I.U.	M	-
F_o	Minimum value of F	I.U.	M	-
F_m	Maximum value of F	I.U.	M	-
F_v	Variable fluorescence	Dimensionless	M	$F_m - F_o$
F_v/F_m	Ratio of variable to maximum fluorescence	Dimensionless	M	-
qP	Coefficient for photochemical quenching (quenching of FmL attributable to PSII photochemistry)*	Dimensionless	DE	$(F_vL)/(F_mL - F_oD)$
qN	Coefficient of non-photochemical quenching (quenching of FmL that is independent of PSII photochemistry)*	Dimensionless	DE	$(F_mD - F_mL)/(F_vD)$
σ_{PSII}	Functional cross-section of photosystem II	($Å^2$ quanta^{-1}) (electrons photon^{-1})	M	-
f	Proportion of photosystem II reaction centers that are capable of charge separation.	Dimensionless	DE	(FvD/FmD)/0.65
n_{PSII}	concentration of PSII reaction centres per chlorophyll *a*	mol RCII mol chl *a*$^{-1}$	Λ	-
	concentration of PSII reaction centres per unit volume.	mol RCII m^{-3}	DE	mol RCII mol chl *a*$^{-1}$. [chl *a*]
ϕ_{PSII}	Quantum yield of photochemistry	electrons photon^{-1}	DE	1 electron photon^{-1} (ϕ_e . qP); (α_{chl}/a^*)
ϕ_e	Quantum yield of electron transport	electrons photon^{-1}	DE	E . σ_{PSII} . qP relative to τ_P‡
ϕ_P	Quantum yield of photosynthesis	electrons photon^{-1}	DE	ϕ_e . qP
τ_P	Turnover time of Q_A re-oxidation	μs	M	-
			DE	σ_{PSII}/E_k
E	Irradiance	mol photons m^{-2} s^{-1}	M	
α^{chl}	Light utilisation coefficient	mg C mg chl *a*$^{-1}$ mol photons^{-1} m^{-2} s^{-1}	DE	P-E curves
P_m^{chl}	Light saturated (max) photosynthesis	mg C mg chl*a*$^{-1}$ hr^{-1}	DE	P-E curves
E_k	Light saturation parameter	mol photons m^{-2} s^{-1} $^{-1}$	DE	P_m^{chl}/α^{chl}
P_{O2}^{Chl}	Photosynthetic oxygen evolution Rate per unit chlorophyll	mol O_2 mg chl *a*$^{-1}$ hr^{-1}	DE	see text
PO_2	Photosynthetic oxygen evolution Rate per unit volume	mol O_2 m^{-3} s^{-1}	DE	see text
a*	Chlorophyll *a*-specific light absorption coefficient (This applies to pigments associated with PSI, PSII, as well as nonphotosynthetic pigments)	m^2 mg chl *a*$^{-1}$	M	-

Table 1.2.— (upper section) Definitions of measured and derived fluorescence variables; (middle section) definitions of variables used in calculating primary productivity using the FRRF method; (lower section) definitions of variables used in calculating primary productivity using hybrid Bio-optical/FRRF method. All terms are (M) measured directly through the FRRF and subsequent processing software, for both the dark (D) and light chambers (L); or (A) assumed based on estimates used in alternative studies using different approaches; or (DE) derived using a combination of measured or assumed terms. nb. * qN and qP are normally applied to interpretation of fluorescence yields measured using pulse amplitude modulated (PAM) techniques. The fluorescence yields obtained from FRRF and PAM techniques may vary due to differences in methodology (Kolber *et al.* 1998). None-the-less, these coefficients are applied without modification to interpretation of FRRF data; ‡ this relationship (eg. Kolber and Falkowski 1993) as $\phi_e = 0.25$ *if* E . σ_{PSII}. qP ≤ τ_P *or* $\phi_e = 0.25/(E . \sigma_{PSII} . qP . \tau_P)$ *if* E . σ_{PSII}. qP > τ_P.

1.5. Objectives

This thesis has the broad objective of 'identifying the factors responsible for variability of phytoplankton primary production observed within the Atlantic Ocean' using data collected from Fast Repetition Rate Fluorometers (FRRFs) throughout a series of cruises. Several specific aims will be sought in order to achieve this goal:

1. To provide a better understanding of the application of the Fast Repetition Rate Fluorometer (FRRF) to the measurement of phytoplankton production (*Chapter 3*). Following the theoretical consideration (*sections 1.3.* and *1.4.*), photosystem II (PSII) activity and subsequent primary production estimates are analysed throughout a diel cycle at 3 sample sites of differing nutrient status.

2. To evaluate the physiological processes which control the nature and, therefore, variability of primary production (*Chapter 4*). High resolution (temporal) data collected at two stations over 24 hour sampling periods will build on the observations of PSII activity in relation to environmental variability (*Chapter 3*). A method for calculating the number of reaction centres (n_{PSII}), based on *in situ* (FRRF) data, is also presented in an attempt to identify factors responsible for the variability of PSII based production.

3. To describe the factors responsible for phytoplankton production variability across a range of environmental conditions (*Chapter 5*). Previous chapters consider physiological data from different light-nutrient environments; however, *Chapter 5* will analyse FRRF data in relation to corresponding measurements of light, nutrients and temperature collected throughout different biogeographic provinces of the Atlantic. Further treatment of continuous surface (FRRF and hydrographic) data will be used to describe patterns (scales) of biological and physical variability significant to the process of primary production.

4. To validate the FRRF as a tool for measuring marine phytoplankton production (*Chapter 6*). Corresponding estimates of production from the FRRF and 'classical' techniques (eg. ^{14}C-uptake). Data from all previous chapters will be drawn into the analysis and discussed within their respective limitations.

2. Common Methodology

A common sampling regime was employed throughout a series of cruises to collect the data presented in this thesis. These cruises traversed a range of biogeographical provinces and hydrographic conditions within the Atlantic Ocean and are described in more detail in the relevant chapters (see also *table 2.1.*). The following account describes the routine procedures employed for *in situ* data collection using the FRRF. In addition, methods employed for the collection and measurement of parameters (hydrographic, nutrient and optical measurements; estimates of productivity using conventional methods of carbon-14 (^{14}C)-uptake and oxygen (light/dark) evolution; measurements of chlorophyll *a*-specific absorption) which support those determined by the FRRF are also described.

2.1. Routine FRRF data collection

Preparing the FRRF for in situ data collection— The FRRF primarily collects data under 2 alternate modes of operation: automatically (remotely pre-programmed) or discretely (attached to a p.c.), both of which were employed during each cruise. The automatic mode was employed when the FRRF was attached to a CTD frame or housed within an undulator, and requires that the instrument is 'woken up' immediately before deployment. The FRRF can also be sent to sleep and pre-programmed to acquire data at specific times; however, this option was not required throughout the cruises. The discrete mode is more directly controllable and allows the user to continually interact with the data acquisition. This mode was used when sampling the ship's continuous seawater supply. Two FRRFs were present on all cruises: One (ser.no. 182010) was reserved for continuous sampling of the underway non-toxic ship's seawater supply, whilst the other (ser.no. 182018) was routinely employed for remote operations. A diagram of an FRRF is given in *fig 2.1.*

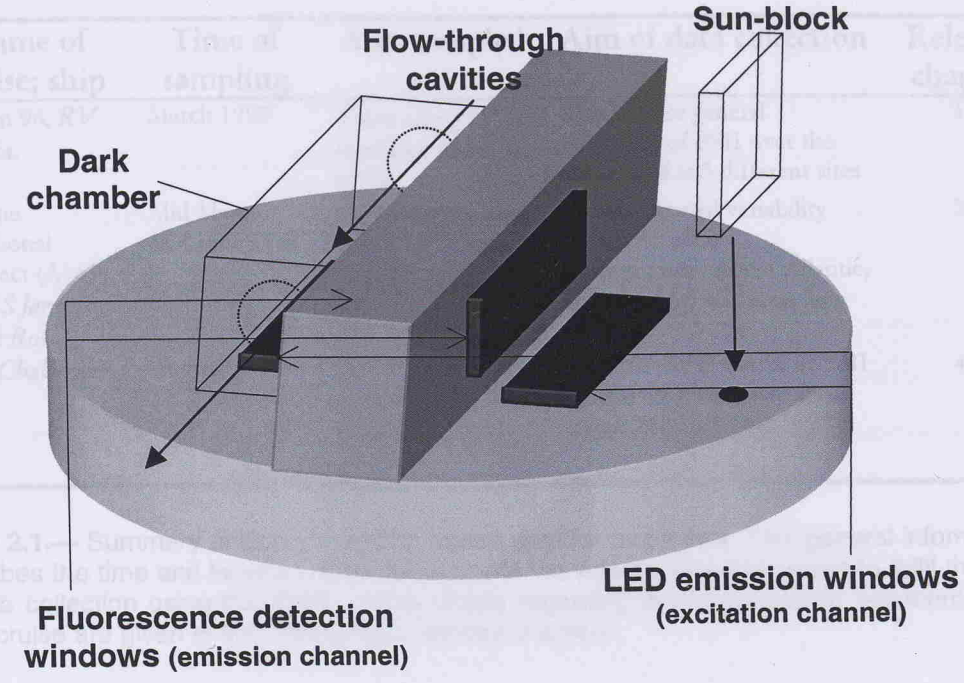

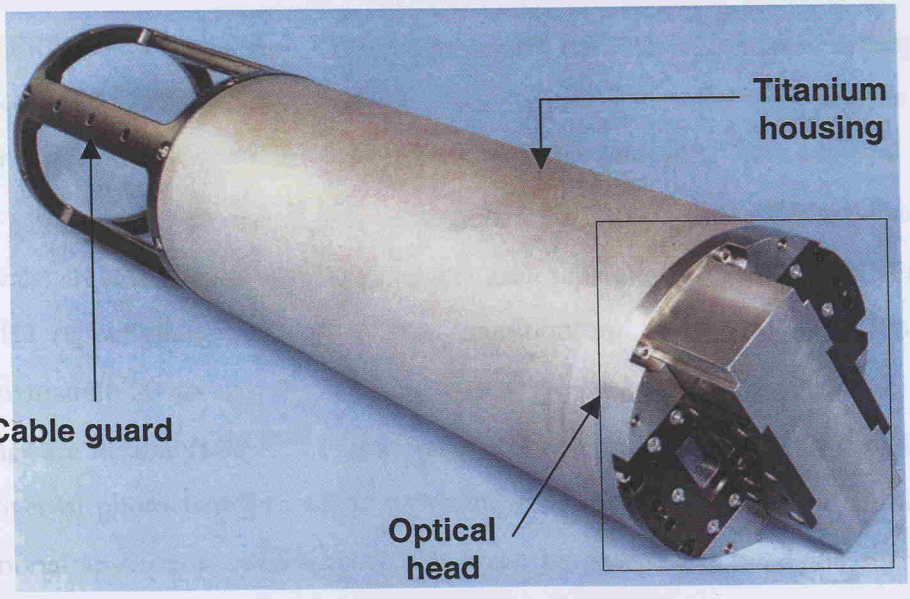

Figure 2.1.— The Fast Repetition Rate Fluorometer (FRRF). Lower figure shows the full instrument (cable guard, titanium housing for the electronics and the optical head) but without the battery pack which is attached to the open end of the cable guard. Upper figure shows a schematic of the optical head. The 4 cable ports are not shown but consist of PAR, pressure sensor, communications (to deck cell or CTD) and battery connectors. The light emission windows (excitation channels) are situated on the base of the optical head and house the LEDs whilst the fluorescence detection channels (emission channels) are situated on opposite sides of the vertical centre-block and house the photomultiplier tubes (PMTs). The grooved sun block is placed opposite the emission channel (see text) of the light chamber. A housing [with specific attachments to allow flow-through or retention of water samples] is placed over the other set of optical windows to provide the dark chamber. The sun-block and dark chamber are black but are represented here as transparent for practical purposes.

Name of cruise; ship	Time of sampling	Area sampled	Aim of data collection	Relevant chapters
Merlim 98; *RV Pelagia.*	March 1998	3 sites along 23°W meridian: 43, 40 & 37°N	Characterise general responses of PSII over the diel period at 3 different sites	3, 6
Atlantic Meridional Transect (AMT) 6; *RRS James Clark Ross.*	Mid May – Mid June 1998	Cruise track Cape Town (37°S 18°E) to U.K. (50°N 2°W).	Observe spatial variability across different hydrographies of the Atlantic, including African upwelling systems.	5, 6
RRS Challenger.	August 1999	2 stations: mixed (48°N 04°W), stratified (49 °N 06 °W).	Observe the response of PSII to light over relatively small scales (of variability).	4, 6

Table 2.1.— Summary of cruises used to collect data for this thesis. This general information describes the time and location of sampling within the Atlantic Ocean in order to fulfil the aim of data collection using the FRRF. More details regarding the hydrographic environment of each cruise are given in the (respective) relevant chapters.

Each FRRF must be (appropriately) programmed before it is used. The settings used for data collection generally remained the same for the 2 instruments and were employed under slight modification of the 'boot protocol', see *table 2.2.*. This protocol provides a flash sequence consisting of 100 saturation (100: 1μs flashes each separated by 1μs intervals) and 20 relaxation (20: 1μs flashes each separated by 50μs intervals) flashes at a 200kHz repetition rate. Therefore, the saturation and relaxation of PSII occurs over approximately 200μs and 970μs, respectively (Kolber 1997). Most of the instrument settings are flexible (*table 2.2.*); however, the boot protocol assesses PSII within a single turnover of photochemistry whilst providing a steady rate of saturation from which the functional absorption cross section (σ_{PSII}) can be precisely derived. As such, the boot protocol is a highly suitable mode of operation for observing PSII activity *in situ*. Any significant modification to these settings should be first scrutinised under a range of conditions in a controlled (laboratory) environment (see Kolber *et al.* 1998).

The speed of data acquisition is, to some extent, controlled by the rate at which the array of light emitting diodes (LEDs) can operate. A bank of LEDs provides the light source for PSII excitation and is housed under the emission window, *fig. 2.1.* The fluorescence response from each saturation and relaxation flashlet were logged to an internal memory card as 1 acquisition averaged from several flash sequences. This was performed in order

to increase the signal to noise ratio, in addition to conserving data storage capacity of the instrument. As such, this internal averaging was set at different rates depending upon the mode of operation. The discrete mode stored 1 (averaged) acquisition per 16 sequences. The remote instrument was operated at 1 acquisition per 3-4 sequences. These modes resulted in a data collection rate of 1 acquisition recorded per 22 seconds per channel, and 1 acquisition recorded per 3-5 seconds per channel, respectively. Technological changes to the FRRF immediately prior to the *RRS Challenger* cruise, August 1999, meant that these data collection rates were improved so that both instrument modes were operated at 1 (averaged) acquisition per 16 sequences providing 1 acquisition/1-2s/channel.

A photomultiplier tube (PMT) is housed under the detection window and intercepts the elicited fluorescence signal, *fig. 2.1.* The gain of the PMT determines the sensitivity of the instrument to the fluorescence signal. The instrument gain setting was pre-determined for each cast/underway run using the fluorescence characteristics of previous acquisitions. This estimation of the gain also required some degree of leeway to account for any unexpected variability and subsurface maxima. However, this incorporation of leeway presented additional restraints when collecting data from more oligotrophic regions since the fluorescence signals would become noisier. Regular observation of real-time data supplied from the ship's underway fluorometer provided some means to avoid the recurrent use of an insensitive gain. The modifications to the FRRF prior to the *RRS Challenger* cruise included an autogaining function. This mechanism changes the gain up (down) when the running average fluorescence signal, as a % of the running average maximum, is less than (exceeds) a lower (upper) threshold value, see *table 2.2.* However, this modification proved too insensitive for the profiling protocols, resulting in saturated or noisy fluorescence signals, and was seldom used.

Data were downloaded from the FRRF to a p.c. in binary format (serial communication parameters: 9600 N 8 1). Binary format was chosen over ASCII format since the former comprises smaller file sizes and is faster to download. The changes to the FRRF hardware prior to *RRS Challenger* cruise also incorporated a faster rate of download (57600 N 8 1); however, this feature appeared more stable when data were downloaded in ASCII format. These data were subsequently analysed by a programme supplied by Z.S. Kolber, to provide values of background (F_o), maximum (F_m), and variable (F_v)

fluorescence yields, photochemical quantum efficiency (F_v/F_m), functional absorption cross section of PSII (σ_{PSII}) and minimum turnover time for electron transport (τ), for both the light and dark chambers. All fluorescence yields are given as instrument units (I.U.).

	Parameter	'boot' setting	Settings used	FRRF range
1	Number of acquisitions	0	64000	0 - 64000
2	Flash sequences per acquisition	1	16	1 - 16
3	Saturation flashes per sequence	100	100	1 - 100
4	Saturation flash duration ‡	4	4	4 - 100
5	Saturation inter-flash delay ‡	0	0	0 - 65535
6	Decay flashes	enabled	enabled	enabled/disabled
7	Decay flashes per sequence	20	20	1 - 20
8	Decay flash duration ‡	4	4	4 - 100
9	Decay inter-flash delay ‡	61	61	0 - 100
10	Sleeptime between acquisitions	1000	10 - 500	10 - 60000
11	PMT gain [**autogain**] lower signal limit PMT gain [**normal mode**]	3 0	3 x4 - x64	autogain (0-9) normal (x1 x4 x16 x64 x256)
12	Analogue output	disabled	disabled	enabled/disabled
13	Desktop verbose mode	disabled	disabled	enabled/disabled
14	Light chamber (A)	active	active	active/inactive
15	Dark chamber (B)	inactive	active	active/inactive
16	Logging mode to internal flashcard	disabled	enabled	enabled/disabled
17	Upper limit autoranging threshold value	90	85	55 - 99
18	Lower limit autoranging threshold value	15	15	5 - 45

Table 2.2.— FRRF settings employed for data collection throughout the 3 cruises: boot protocol, the typical settings used throughout the cruises and the potential range of settings (ie. the flexibility of the instrument). All parameter settings are in numbers of flashes/ sequences/acquisitions, except sleeptime between acquisitions (ms), PMT gain (sensitivity to fluorescence, see also main text, read as increasing/decreasing factors of 4) and the upper/lower limit for the fluorescence threshold value (see main text). ‡ indicates that numbers for these parameters are in instrument units: These units correspond to clock cycles in the field programmable gate array (FGPA which emulates the logic circuitry for generating flash protocols) whereby (a) saturation: 4 = 1.1µs and each additional integer increases the duration by 60ns ie. 14 = 1.9µs (b) relaxation: 0 = 125ns and each additional integer increases the duration by 700ns ie. 14 = 9.2 µs

FRRF data collection—The FRRFs were operated routinely on each cruise. The instrument, which was attached to the CTD frame or in place of one of the CTD sample bottles, was configured with a CI (Chelsea Instruments) 'dark chamber', designed to retain phytoplankton in the dark long enough to induce relaxation of F_v (Kolber 1997). Also a CI grooved sunblock, designed to prevent ambient sunlight from degrading the quality of the fluorescence response of phytoplankton in the 'light chamber' (Kolber 1997) was mounted facing the emission window of the FRRF light chamber [assigned channel A], see *fig. 2.1.* The internal clock of the FRRF was synchronised with that of the CTD logger prior to each deployment.

The FRRF automatically acquired data during each CTD cast. The CTD was stopped for 3-5 minutes at selected depths during the up-cast. These depths were selected based on the hydrographic profile observed from the down-cast. The stops allowed for the collection of water and/or the collection of extended signals for the FRRF. These extended signals provided larger signal sample sizes (typically 20-30 data acquisitions) needed to obtain an 'averaged' signal. These extended stops also gave the FRRF data a definite depth-stamp. A pressure sensor was not incorporated into the FRRF until the

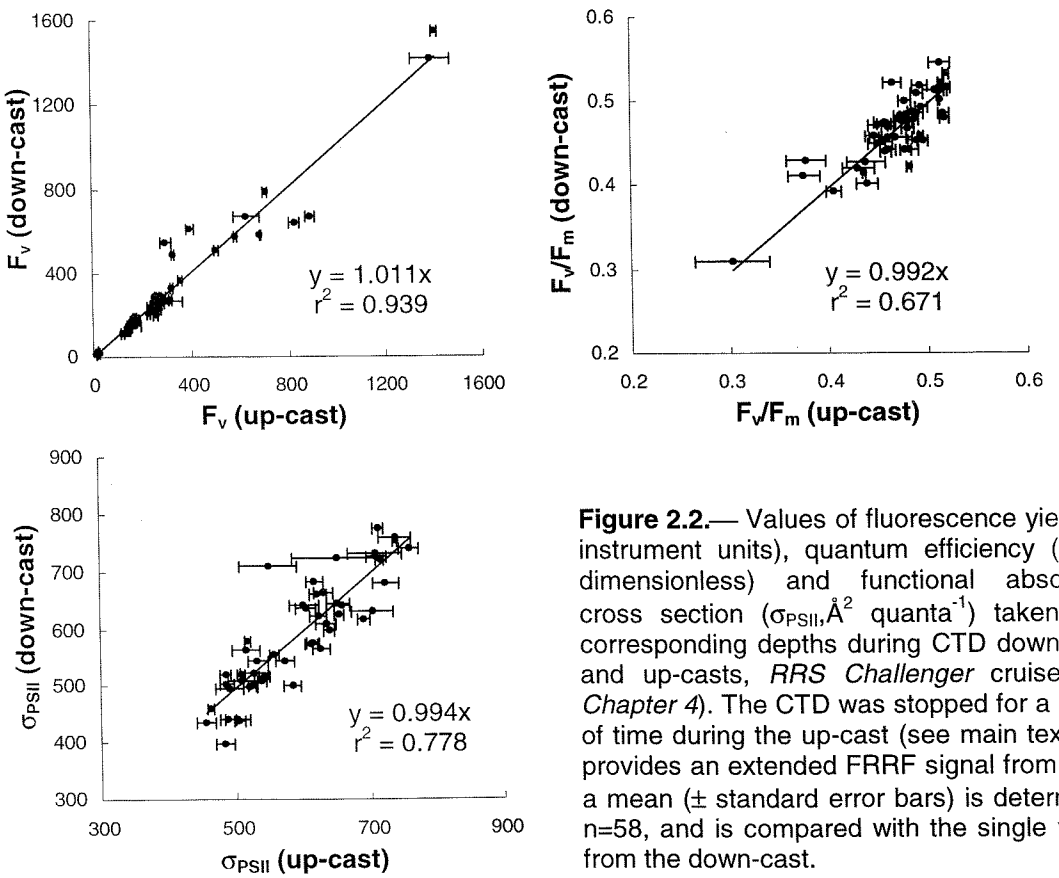

Figure 2.2.— Values of fluorescence yield (F_v, instrument units), quantum efficiency (F_v/F_m, dimensionless) and functional absorption cross section (σ_{PSII},Å^2 quanta^{-1}) taken from corresponding depths during CTD down-casts and up-casts, *RRS Challenger* cruise (see *Chapter 4*). The CTD was stopped for a period of time during the up-cast (see main text) and provides an extended FRRF signal from which a mean (± standard error bars) is determined, n=58, and is compared with the single values from the down-cast.

RRS Challenger cruise. The value of the FRRF as a profiling tool was further enhanced by the faster sampling rate available for the *RRS Challenger* cruise, which generated data of greater resolution during direct profiling. A comparison between data collected from corresponding depths during the down cast (direct profiling) and the up-cast (extended signals from CTD stops), *fig 2.2.*, shows good agreement between both sets of data. A degree of noise still remains in these data but should be considered as encouraging given hydrogaphic variability between the up- and down-cast, and also during the extended data collection period during the up-cast.

The CTD frame was typically fitted with a 25cm path length transmissometer (at 660nm), a cosine PAR (400-700 nm) sensor, water samplers (bottles), and a CTD equipped with pressure, conductivity, and temperature sensors. The data from these CTD instruments was sent up the wire and logged to a p.c. The FRRF also had its own separate PAR sensor attached. As such, the 2 PAR sensors on the CTD were mounted to the CTD frame at the same height and gave comparable outputs, e.g. *RV Pelagia*: $r^2 = 0.985$. The FRRF PAR sensor failed during the AMT 6 cruise and, therefore, all PAR measurements were obtained directly from the CTD PAR sensor. All FRRF and PAR sensor optical heads, and the FRRF dark chamber, were cleaned between immersions to prevent fouling. Water was collected at each appropriate depth to routinely sample for phytoplankton pigments, nutrients and rates of productivity by the conventional methods of ^{14}C-uptake and oxygen (light/dark) evolution.

Additional remote operations were employed for the FRRF during the AMT6 cruise, in which the FRRF was housed within an undulating oceanographic recorder (UOR). These undulators are designed to remotely collect data, free from the constraints imposed from making casts directly from platforms such as ships (eg. Aiken and Bellan 1990). The UOR was towed from the ship at approximately 11 knots for periods of 2 to 7 hours. The altitude of the UOR is controlled by means of a programmable servo, and undulates the instrument between 5m and 75m (every 9 minutes) throughout the water column. A Plymouth Marine Laboratory CTDF (conductivity, temperature, depth, fluorometer), a downwelling radiance and upwelling irradiance sensor were also housed within the UOR to provide corresponding hydrographic data. These instruments logged their data to a PML designs logger (refer to *section 2.2.*) at a sampling interval of 2.0 seconds. More comprehensive details of the UOR vehicle are given in Aiken (1985).

The discrete sampling of the non-toxic seawater supply was also routine. The CI 'dark chamber' was fixed over the optical cells of the FRRF assigned channel B. Blackened silicon tubing was fitted to connect the opening of the dark chamber to the outlet hose of the ship's non-toxic seawater supply. This supply (outlet) flowed through the ship's underway instrumentation, for example, fluorometer, temperature and conductivity sensors, before arrival at the FRRF. This passage typically retained the seawater supply in dark conditions for a period of 2-3 minutes following collection. The data from the ship's underway instrumentation was automatically logged to a p.c. Additional data, such as time (G.M.T.), latitude, longitude, wind speed and irradiance was also collected from the ship's instrumentation and passed through additional channels and logged to the same p.c.

Routine hydrographic measurements— The following account (and *section 2.2.*) summarises the methods used in the measurement of parameters useful to the interpretation of FRRF data. Learning to use the FRRF (and interpret the data) was a time consuming process and meant that I could not be directly involved in a significant proportion of the accessory data collection (see *Appendix 1*). Water was collected at regular intervals from the ship's non-toxic seawater system to analyse for phytoplankton pigments and nutrients. The methods for these analyses are the same as those for water collected from CTD casts. Nitrate was measured as part of a suite of nutrients (nitrate, nitrite, phosphorous, silicate). Nutrients were analysed from water samples using a 4 channel Technicon® Autoanalyser, and subsequently determined colorimetrically following standard methodologies. A mixed nutrient standard was run through the instrumentation daily to check the performance of the analysis and validate the concurrent measurements.

Triplicate volumes of sample water were vacuum filtered through Whatman 25mm GF/Fs. Two of these filters were subsequently stored at -80°C to await analysis for pigments using spectrophotometric (RV *Pelagia; RRS Challenger* only) and HPLC techniques. The third filter was placed in 90% acetone solution and stored at -4°C for extraction of chlorophylls. The extracted solution was analysed for chlorophyll *a* using a Turner Designs digital Fluorometer according to Welschmeyer (1994). This methodology uses a combination of optical filters and lamps, and is thought to reduce interference from chlorophyll *b* (Mantoura *et al.* 1997). Chlorophylls and accessory pigments were

determined at sea using reverse phase High Performance Liquid Chromatography (HPLC) techniques:

GF/F filters were extracted in 2ml of 90% acetone, containing a known concentration of an internal standard canthaxanthin. Extraction was performed with 20s of ultrasonication and centrifugation. Pigment extracts were loaded into a thermoseperation autosampler and mixed with 1mol ammonium acetate (50:50) prior to injection. The pigments were analysed according to Barlow *et al.* (1997), and identified by retention times and absorption spectra using SPECTRA software. The HPLC system was calibrated for each pigment with authentic standards (chl *a*, *b*: sigma; carotenoid, chl *c*: VKI Water Quality Institute, Denmark; dvchl *a*: Bidigare, Hawaii). Calculating the relative response factors of each standard with respect to canthaxanthin provided quantification for each pigment.

2.2. Additional (cruise specific) methodologies

Optical profiling and chlorophyll a-specific light absorption—The optical cross section of photosystem light harvesting antennae ($\sigma_{(\lambda)}$) is calculated as the product of light absorption over a range of wavelengths. The calculation of this cross section, therefore, requires knowledge of this absorption, in addition to the *in situ* light intensities for the range of wavelengths concerned. This parameter is not required when typically using the FRRF since the functional absorption cross-section of PSII (σ_{PSII}) can describe the rate of light absorption by PSII; however, the light absorption by phytoplankton [pigment] samples can still provide useful information concerning their photophysiological status (see *Chapter 4*). Optical data was routinely collected during each cruise. Measurements of light absorption by phytoplankton pigments were only performed for *RV Pelagia* and *RRS Challenger* cruises.

An optical profiling rig, consisting of a CTDF (conductivity, temperature, depth, fluorometer), transmissometer, and 2 *Satlantic* light cells, was lowered throughout the water column to correspond with the CTD profiles. Prior to deployment, the clock of the logger was set to correspond with that of the ship [and therefore the FRRF] for subsequent data merging. The 2 light cells measure upwelling radiance (Ed) and

downwelling irradiance (Lu) light for 7 wavelength bands: 412, 443, 490, 510, 555, 670, and 685nm and correspond to SeaWiFS satellite bands. Data from all instruments was logged (per 0.5s) into a PML data logger. This logger consisted of a microcomputer controlled 16 channel bit oversampled analogue to digital converted with 2MB of solid state storage. The logged data was downloaded to a p.c. upon retrieval. The data were converted into a readable tab separated ASCII file using software provided by Gerald Moore (PML).

Absorption spectra were measured on samples filtered onto Whatman GF/F filters and stored at -80°C until analysis using a Hitachi U-3000 spectrophotometer fitted with a ϕ60 integrating sphere following the protocol of Tassan and Ferrari (1995). Appropriate corrections were made for multiple scattering within the glass-fibre filter using a wavelength independent pathlength amplification factor (β-correction, Kirk 1994), determined from axenic cultures of *Synechoccocus* (strains WH7803 and WH8103) or of a mixed eukaryotic assemblage, supplied by Matt Pinkerton, pers.comm.

Phytoplankton productivity—^{14}C uptake measurements were made during all cruises on 30 ml samples taken at selected depths from the CTD casts. Photosynthesis-irradiance (P-E) curves were determined by uptake of ^{14}C in a temperature-controlled photosynthetron (Lewis & Smith, 1983), essentially as described by MacIntyre *et al.* (1996). Illumination of 10-1700 μmol photons m^{-2} s^{-1} was provided by quartz-halogen lamps, filtered through a 2.5 cm layer of water. Irradiance in the manifold was measured with a Biospherical Instruments QSL-101 4π sensor. The cells were held in darkness for up to 30 minutes between sampling and incubation. The sample was inoculated with 50 μCi ml^{-1} of $NaH^{14}CO_3$ (58 Ci $mole^{-1}$, Amersham CFA.3) and incubated. The incubations were made in the photosynthetron and terminated after 60 min (*RV Pelagia*) or 1-2 hours (*RRS Challenger*) by adding 50 μl of glutaraldehyde to each aliquot. Additional ^{14}C-uptake experiments were performed during AMT6 and *RRS Challenger* cruises in which incubations were made on deck under simulated *in situ* conditions using neutral density filters. Each experiment was conducted at 6 light intensities, 0%, 10% 20%, 33%, 60% and 100% of the incident irradiance, and was performed for a period of 5-6 hours before termination.

Residual inorganic carbon was driven off by addition of 250 µl of 6 N HCl and shaking for 60 min, and then the incorporation of ^{14}C was determined by liquid scintillation counting. Total activity of $NaH^{14}CO_3$ was determined on 20 µl aliquots of sample taken directly into scintillation cocktail with 50 µl ml^{-1} b-phenylethylamine. Data were fit by least-squares, non-linear regression to the following model (MacIntyre *et al.* 1996):

$$P^{Chl} = (P_m^{Chl} (1 - \exp(-\alpha^{Chl} E / P_m^{Chl}))(\exp(-\beta^{Chl} E / P_m^{Chl}))) - P_o^{Chl} \qquad \textbf{[2.1.]}$$

where P^{Chl} (g C [g Chl *a*]$^{-1}$ h^{-1}) is the Chl *a*-specific photosynthetic rate at irradiance E (µmol photons m^{-2} s^{-1}); P_m^{Chl} is the light-saturated rate of photosynthesis that would be observed in the absence of photoinhibition; α^{Chl} (g C [g Chl *a*]$^{-1}$ h^{-1}) (µmol photons m^{-2} s^{-1})$^{-1}$ is the initial slope of the P-E curve; β^{Chl} (g C [g Chl *a*]$^{-1}$ h^{-1}) (µmol photons m^{-2} s^{-1})$^{-1}$ is a photoinhibition parameter; and P_o^{Chl} (g C [g Chl *a*]$^{-1}$ h^{-1}) is an intercept parameter included to improve the distribution of residuals at low irradiances.

Measurements of *in situ* oxygen content for the estimation of primary production using the light-dark technique were made during the *RV Pelagia* cruise (see *Appendix 1*). Water samples (25dm^3) were collected into BOD bottles following each CTD cast. Dissolved oxygen was determined using the 'Shibala' Winkler spectrophotometric method (Pai *et al.* 1993). Winkler chemicals (1ml $MnCl_2$. 4 H_2O 600 gl^{-1} and 1ml NaOH 250g and KI 350gl^{-1}) were added within minutes after sampling the bottles by means of dispensers. 0.8 ml 20N H_2SO_4 was then added after which the samples were shaken and stored under water for at least one hour. The mixture was stirred with a magnetic stirring bar until the precipitate had dissolved completely. The brown yellow solution was siphoned to a Hitachi U1000 spectrophotometer equipped with a 1 cm flow-cell (aperture 11mm x 4mm). Absorption was measured at 456 nm on the analogue output of the spectrophotometer connecting a 4 digit voltmeter (Metex M4650). Corrections were made for the seawater color by subtracting the absorption value for untreated seawater, and for the effects of the volume of Winkler reagents on measured oxygen concentration.

3. Diel variability of phytoplankton physiology and production at three contrasting sites in the North Atlantic

3.1. Introduction

Day-night variability of phytoplankton activity has been well documented in data obtained from a number of observational approaches, for example, fluorescence yield (Lorenzen 1963; Prézelin and Ley 1980, Vincent *et al.* 1984), cellular pigment content (Owens *et al.* 1980) and productivity rates (Harding *et al.* 1982a, b; Neale and Richerson 1987; Prézelin *et al.* 1987). This variability may be produced through circadian rhythms (Sournia 1974; Brand 1982) or represent a tightly coupled light-dark effect that is independent of, but can exhibit a modifying influence, on phased cell division (Owens *et al.* 1980). The corresponding regulation of photosynthesis throughout the day, diurnal variation, occurs through modulation of the photosynthetic light reaction, in particular within PSII (Prézelin 1992).

Active fluorescence techniques allow the observation of photosystem II (PSII) dynamics, in addition to providing a rate estimate for photosynthetic productivity. As such, the FRRF lends itself to the study of processes that occur through the modulation of PSII. Laboratory investigations have shown that variations in photosynthetic physiological parameters, as measured using Pulse Amplified Modulation (PAM), are coupled to simulated light regimes under both nutrient replete (Kroon 1994, Flameling 1998, Flameling and Kromkamp 1997, 1998) and nutrient deplete (Flameling 1998) conditions. *In situ* observations of diel/diurnal variability have been made using both the Pump and Probe (PP) and FRRF but have focused on the efficiency of PSII (Falkowski and Kolber 1993, Greene *et al.* 1994), or have been restricted to surface water samples (Vassiliev *et al.* 1994, Behrenfeld and Kolber 1999). All these studies reveal a decrease in photochemical conversion efficiency with an increase in irradiance as a result of

photoinhibition/quenching processes.

This investigation introduces FRRF [field] measurements and provides an analysis of the *in situ* diel variability of the light harvesting capability, photochemical efficiencies and production by phytoplankton throughout the water column. In addition, the diel response of these parameters will be compared between three sites of differing nutrient status in the north-east Atlantic. A knowledge of diel PSII (and, therefore, photosynthetic) activity under contrasting growth conditions will provide a context for subsequent observations of *in situ* phytoplankton physiology that are removed from an inherent daily irradiance cycle.

General Hydrography

Three sample sites were chosen along the 23°W meridian: 43°N (13-14.3.98), 40°N (16-17.3.98), 37°N (18-19.3.98), *fig. 3.1.*, and are referred to as sites 1, 2 and 3 (respectively) for the remainder of this chapter. The sites are situated within the north Atlantic subtropical gyre close to its boundary with the North Atlantic Drift towards the north (Sathyendranath *et al* 1995). Both hydrographic regimes lie within the westerly wind domain where wind mixing plays a critical role in determining the pattern of seasonal water column stratification and the development of the spring phytoplankton bloom (Longhurst *et al* 1995). As such, the sites were initially chosen in order to observe successive stages of phytoplankton dynamics during the spring. To date, there appears little available published material regarding phytoplankton within this area, with the majority of observations coming from large scale programmes, such as, the Joint Global Ocean Flux Studies and North Atlantic Bloom Experiment (eg. Ducklow and Harris 1993), the CANIGO (Canary Islands Azores Gibralter observations) project (eg. Fernández and Pingree 1996) and the Atlantic Meridional Transect (eg. Marañón *et al.* 2000, Aiken *et al subm.*).

At each of the three sites, a series of CTD casts (a minimum of 7/site) were performed throughout a 24 hour (08:00-08:00 GMT, 07:00-07:00 local time) period. All times are given in GMT unless otherwise indicated. The respective protocols, sampling strategy and the instrumentation employed are described in *Chapter 2.* A more detailed

explanation and derivation of terms used throughout is also given in *Section 1.4.*

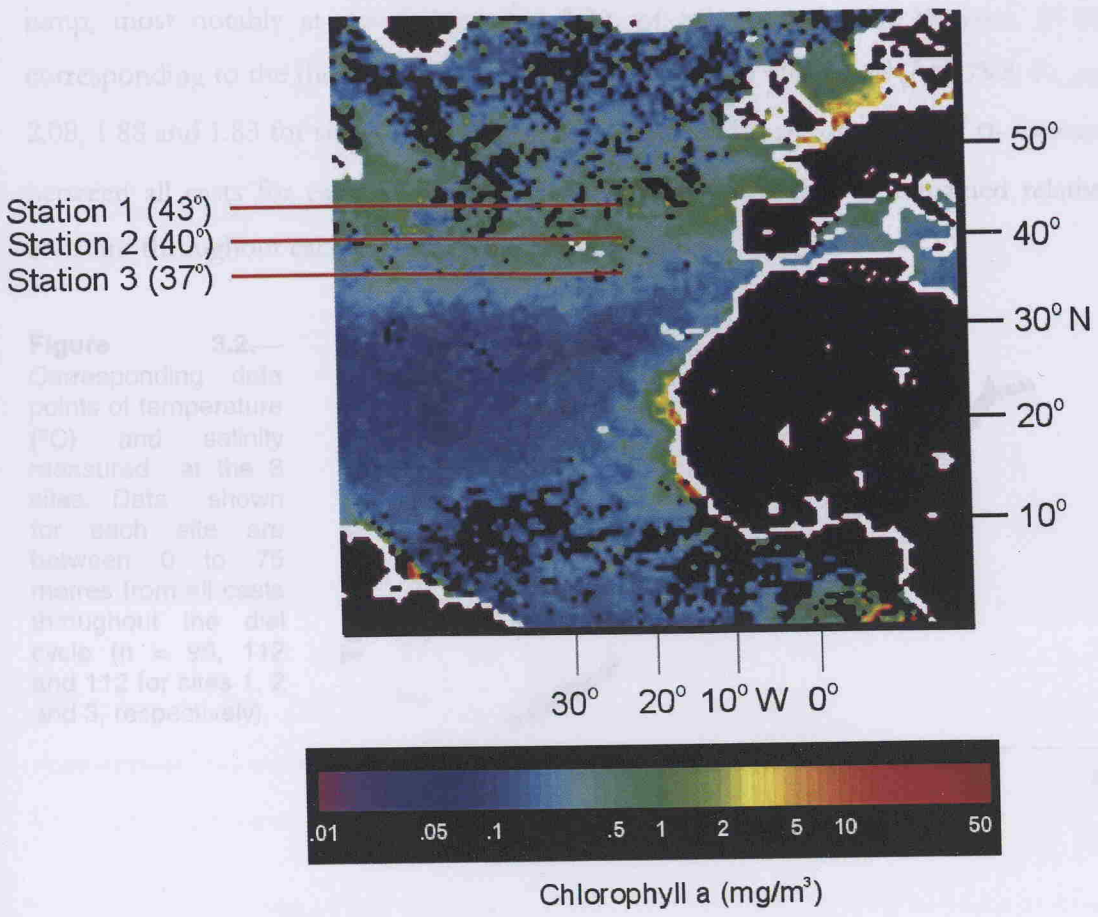

Figure 3.1.— The approximate positions of the three diel sites along 23°W (see text) indicated on a composite SeaWiFs image of chlorophyll *a* distribution in the northern Atlantic Ocean, March 1998. All sites were dominated by the cyanobacteria, *Synechococcus* (Marcel Veldhuis, pers.comm.)

3.2. Specific hydrographic environment and climate at the 3 sites

Values of temperature and salinity measured between 0 and 75 metres appear uniform over the 24-hour period at sites 2 and 3. These sites display similar values of temperature and salinity, 15.34-15.66°C /36.022-36.054 and 15.75-36.48 °C/36.050-36.477 respectively (*fig. 3.2.*). Site 1 shows lower values of temperature and salinity, 13.24-13.67 °C / 35.748-35.811. Values of water density, expressed as σ_τ, were derived from tables of salinity and temperature values at depth. The water masses at sites 2 and 3 have a density

band signal of 26.7-26.75 and 26.45-26.75 $10^3 kgm^{-3}$ respectively whilst σ_τ at site 1 is relatively higher (27.0-27.1 $10^3 kgm^{-3}$). The σ_τ relationship with depth indicates a distinct jump, most notably at site 3 (also *fig. 3.2.*), of increased density between 55-60m corresponding to the thermocline. No significant statistical difference (ANOVA $F_{6, 105}$ = 2.08, 1.88 and 1.83 for sites 1, 2 and 3, respectively) was found for values of σ_τ measured between all casts for each of the three sites, and indicates that σ_τ remained relatively constant throughout each diel series.

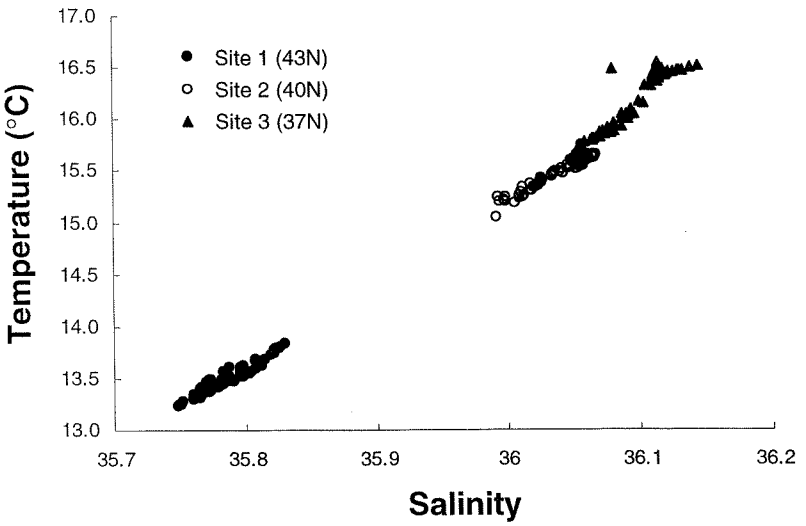

Figure 3.2.— Corresponding data points of temperature (°C) and salinity measured at the 3 sites. Data shown for each site are between 0 to 75 metres from all casts throughout the diel cycle (n = 96, 112 and 112 for sites 1, 2 and 3, respectively).

The profiles of mean nitrate concentration measured throughout the diel period at the three 3 sites are shown in *fig. 3.3.* Nitrate concentration [NO_3] increases from the surface to deeper water with the zone of maximum increase (the nutricline, p.12) at 40-50m at site 1, and 50-60m at sites 2 and 3. [NO_3] were highest at site 1 (3-4 mmol m^{-3}) and lowest at sites 2 and 3 (0-0.3 mmol m^{-3} in the surface 50m increasing to 1-3 mmol m^{-3} below 50m). *Fig. 3.4.* shows the diel variability of water temperature for the three sites. A permanent thermocline is most evident at site 3, as reflected by the strong density discontinuity in *fig. 3.2.*, and remains throughout the 24 hour period. A similar feature appears evident at site 2, however, the temperature difference between 10 and 75 metres is less (0.6°C) than at site 3 (0.8°C). Conversely, water temperature at site 1 is more variable throughout the upper 75 metres but does not correspond with any significant changes in water mass density over the 24 hour period (see above). The mean of the surface wind speeds measured throughout the diel cycle increased with decreasing latitude: 3.55, 5.56, and 5.48 at sites 1, 2 and 3, respectively.

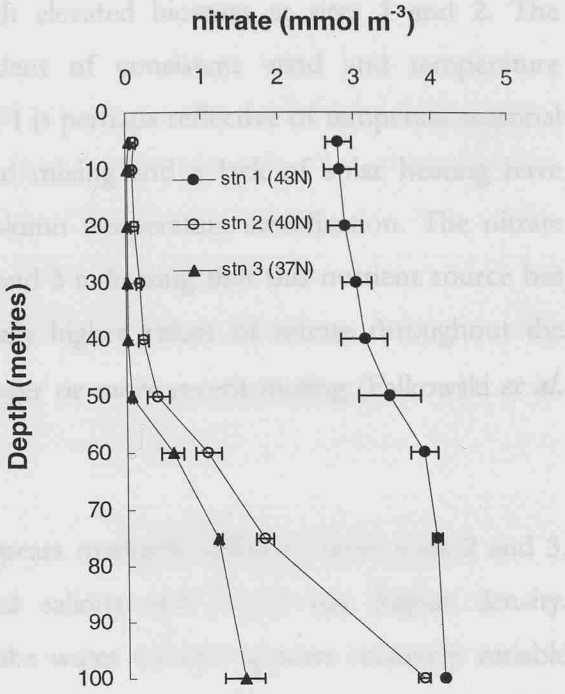

Figure 3.3.— Depth profiles of mean nitrate concentration (mmol m^{-3}) for each of the 3 sample sites (sites 1, 2 and 3) along 23 W. The mean NO_3 concentration is taken from all diel (nutrient) casts performed (site 1, n=3; 2, n=6; 3, n=5). The corresponding standard error bars are also given.

Variations in the strength and stability of the thermocline, which is a function of temperature and wind regimes (e.g., Herbland and Voiturez 1979; Doney *et al.* 1995), are related to the presence of a stable, deeper subsurface chlorophyll maximum at site 3, and

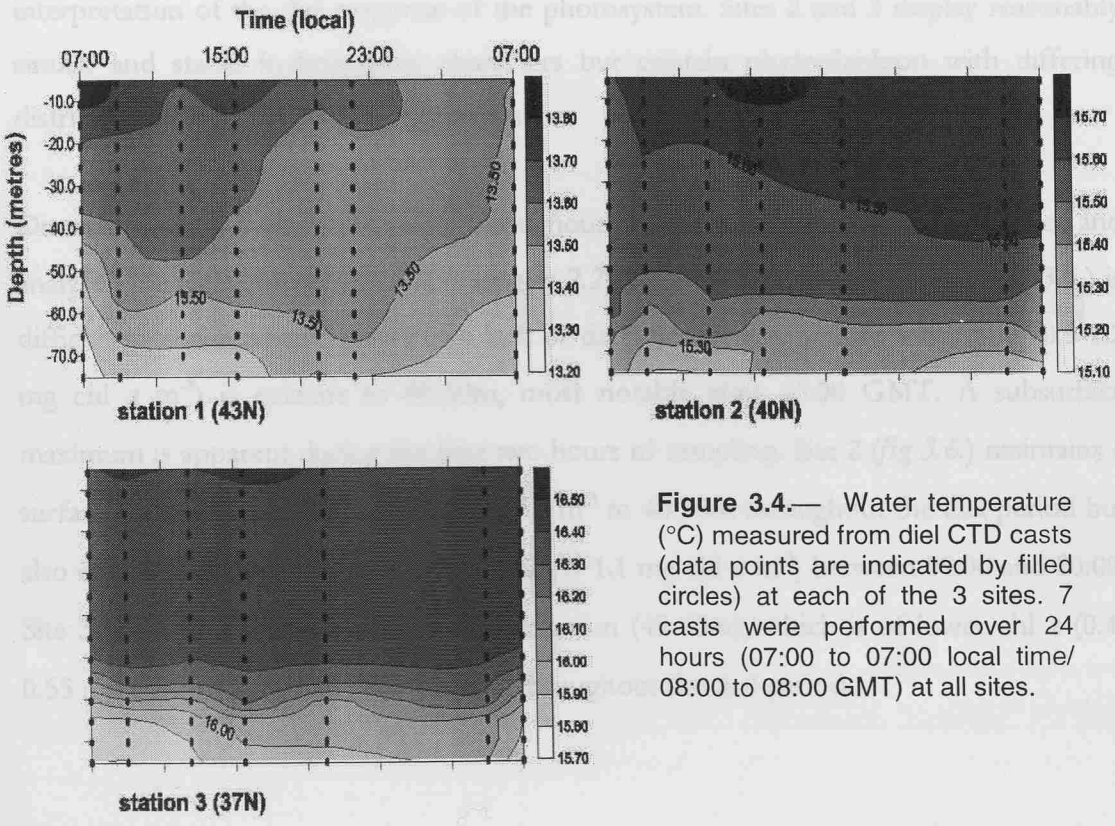

Figure 3.4.— Water temperature (°C) measured from diel CTD casts (data points are indicated by filled circles) at each of the 3 sites. 7 casts were performed over 24 hours (07:00 to 07:00 local time/ 08:00 to 08:00 GMT) at all sites.

of a well mixed upper water column with elevated biomass at sites 1 and 2. The permanent thermocline at site 3 is evident of consistent wind and temperature conditions (eg. Pond and Pickard 1983); site 1 is perhaps reflective of temperate seasonal conditions where, presumably, strong wind mixing and a lack of solar heating have retarded the formation of strong water column temperature stratification. The nitrate concentrations are relatively low at sites 2 and 3 indicating that this nutrient source has become exhausted. Conversely, the generally higher values of nitrate throughout the water column at site 1 would suggest stronger or more recent mixing (Falkowski *et al.* 1994).

The stability and hydrography at site 1 appears markedly different from sites 2 and 3. The water is of lower temperature and salinity and hence has higher density. Furthermore, the temperature profile of the water column appears relatively variable throughout the diel period. The proximity of site 1 to the northern-most section of the Azores Current (Gould 1985) might suggest that site 1 could be significantly affected by another water mass compared to that of the other 2 sites. Although changes in water mass density were not apparent throughout the diel period at site 1, the apparent variability in hydrography throughout the diel period could still add confusion to the interpretation of the diel response of the photosystem. Sites 2 and 3 display reasonably similar and stable hydrographic characters but contain phytoplankton with differing distributions and physiological signatures.

Discrete water samples were taken throughout the diel series at each of the 3 sites and analysed for total chlorophyll *a* (see *section 2.2*), *figs. 3.5-3.7* (panel b). Site 1 (*fig 3.5.*) is difficult to characterise because of a lack of data; however, a surface maximum (0.9-1.2 mg chl *a* m^{-3}) is evident to 40-50m, most notably after 15:00 GMT. A subsurface maximum is apparent during the first two hours of sampling. Site 2 (*fig 3.6.*) maintains a surface chl *a* maximum of 0.8-1.0 mg chl *a* m^{-3} to 40-50m throughout the diel period but also displays a strong subsurface maximum (>1.1 mg chl *a* m^{-3}) between 09:00 and 20:00. Site 3 (*fig 3.7.*) displays a subsurface maximum (45-65m), which is of lower chl *a* (0.4-0.55 mg chl *a* m^{-3}) than at sites 1 and 2, throughout the diel period.

3.3. FRRF variables observed at the 3 sites.

Diel variability of phytoplankton physiology— The *in situ* PAR and FRRF-derived values of the variable fluorescence yield (F_v), quantum efficiency (F_v/F_m), photochemical quenching (qP), non-photochemical quenching (qN), functional absorption cross section (σ_{PSII}) and instantaneous production (P^{chl}) from throughout the sampling period are given in *figs 3.5.* (site 1), *3.6.* (site 2) and *3.7.* (site 3). All FRRF derived parameters display a clear diurnal trend that follows that of the measured PAR at each site. As such, a general account of phytoplankton physiology can be described throughout the diurnal period:

The variable fluorescence yield (F_v) exhibited uniform values in the upper layer in the early morning and a subsurface maximum developing by midday when irradiance is highest. A subsurface F_v-maximum also appears to develop during the night at sites 1 and 3. In surface waters (10m), F_v declines between morning (08:00) and midday (13:30), and recovered thereafter. Casts throughout the night (21:00-08:00, inclusive) show relatively consistent profiles for F_v but may reflect the limited sampling resolution during this period of the diel cycle. The fluorescence profiles can have contributions from photochemical (qP) and non-photochemical (qN) quenching. Most quenching occurs at 13:30; least at 08:00 and is intermediary at 10:00 and 16:30. Quenching increases dramatically from deeper to shallower water. The distribution of the values of qP and qN indicate that photochemical quenching occurs over a higher portion of the water column than non-photochemical quenching.

Chl *a* exhibits a similar distribution pattern as F_v (see above). A regression between these two parameters using data amalgamated from all 3 sites is given in *fig. 3.8.* The relationships are strongly significant (see figure heading) despite the lack of chl *a* data collected throughout the diel period. The highest covariance occurs for samples taken in waters where there is virtually no light and at night. Conversely, the lowest covariance is observed in samples taken during the day in the lit upper euphotic zone. The most scattered points are from the shallowest (10-20m) depths. Where estimates of qN are removed from the corresponding values of F_v, the relationship between F_v and chlorophyll *a* increases.

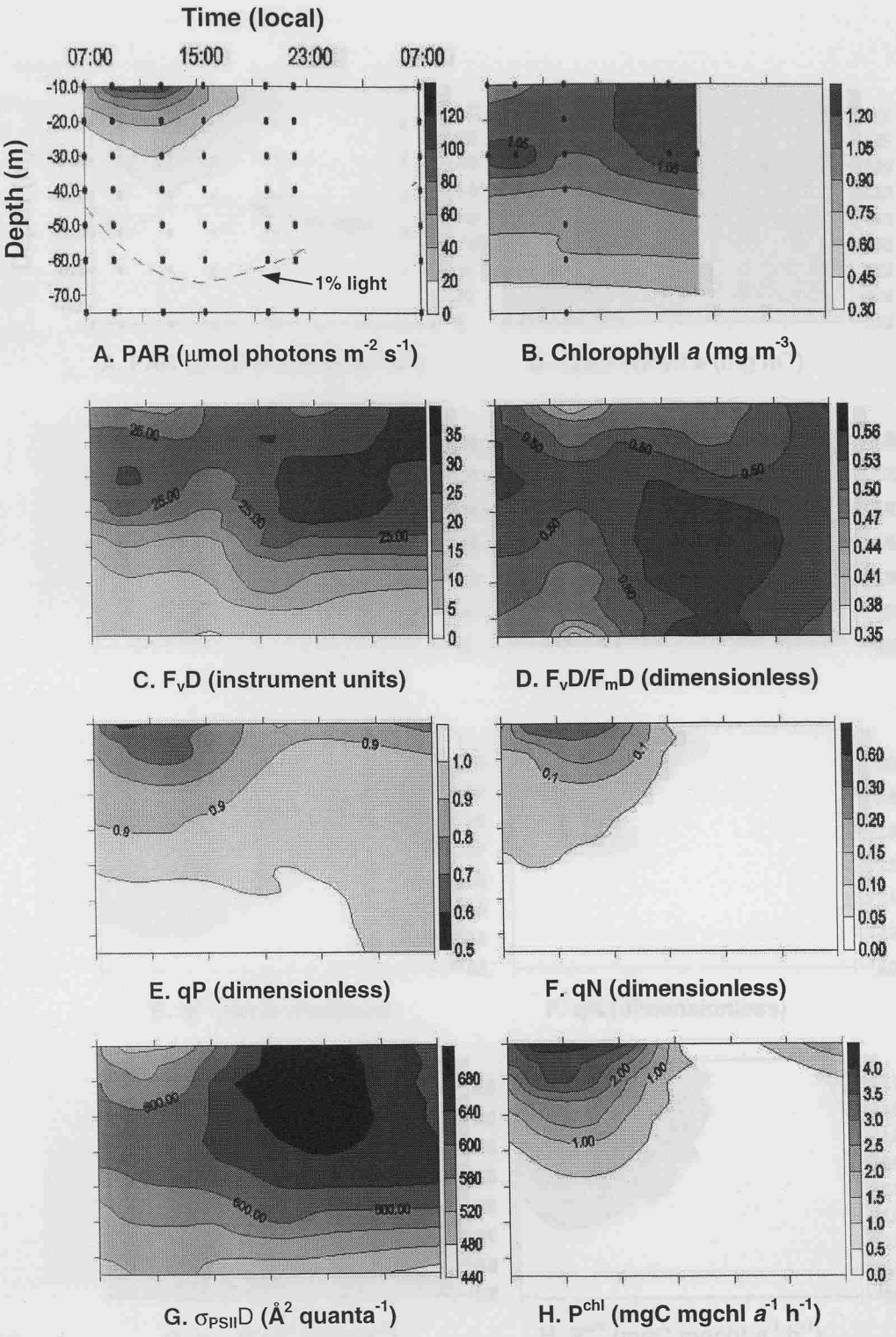

Figure 3.5.— Changes in parameters observed with the FRRF throughout the water column at site 1 (43°N 23°W). Filled circles in upper 2 panels represent sample points for the FRRF via CTD casts: (A) PAR (µmol photons m^{-2} s^{-1}) (C) Variable fluorescence (F_vD: instrument units) (D) Quantum efficiency of photochemistry (F_vD/F_mD: dimensionless) (E) Photochemical quenching (qP: dimensionless) (F) non-photochemical quenching (qN: dimensionless) (G) Functional absorption cross section ($\sigma_{PSII}D$: $Å^2$ $quanta^{-1}$) (H) Photosynthetic rate (P^{chl}: mgC mgchl a^{-1} h^{-1}). Panel (B) shows corresponding chlorophyll a concentration, as measured by filtration and extraction (*Chapter 2*). (C), (D) and (G) were measured in FRRF dark chamber.

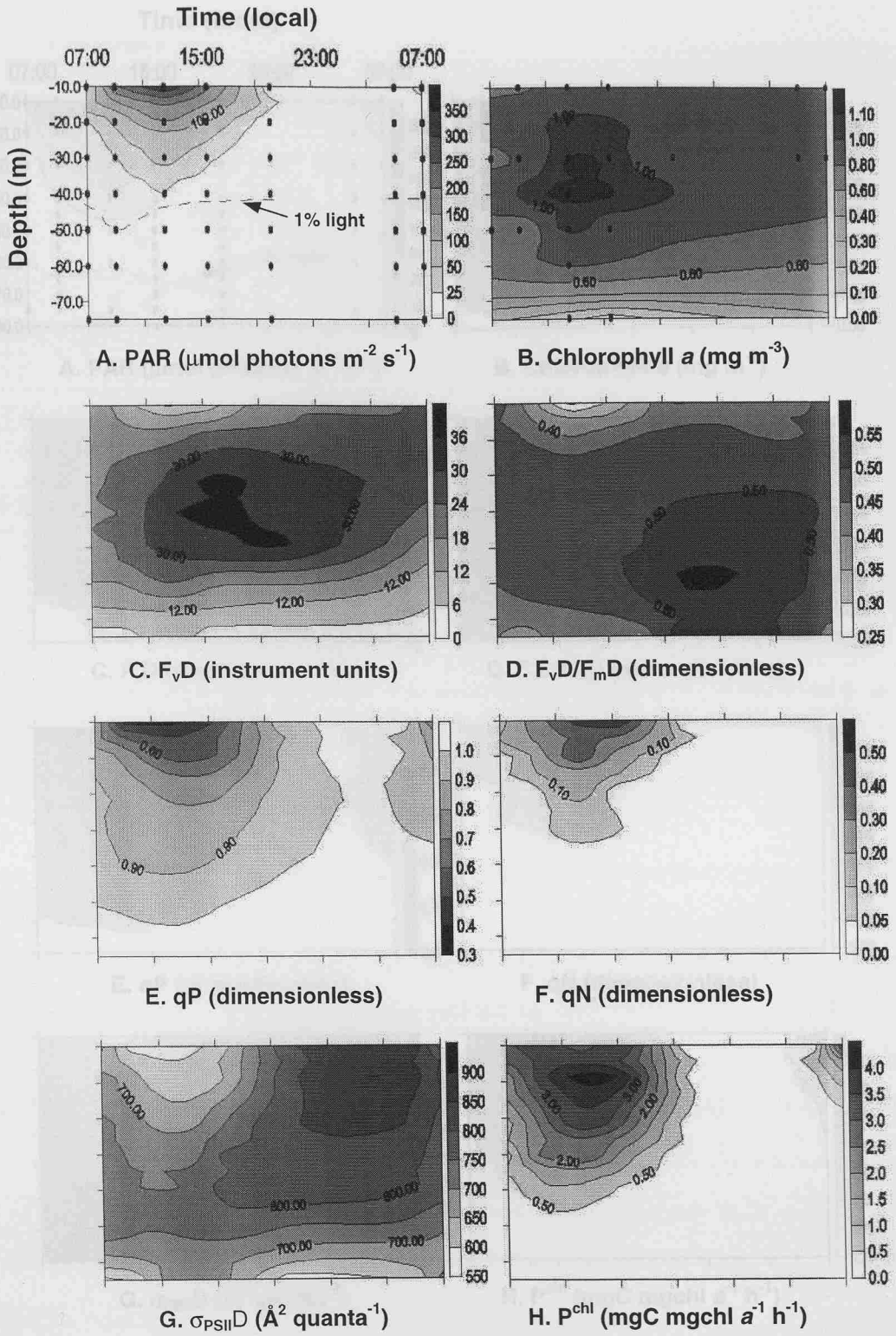

Figure 3.6.— Changes in parameters observed with the FRRF throughout the water column at site 2 (40°N 23°W). Filled circles in upper 2 panels represent sample points for the FRRF via CTD casts: (A) PAR (µmol photons m^{-2} s^{-1}) (C) Variable fluorescence (F_vD: instrument units) (D) Quantum efficiency of photochemistry (F_vD/F_mD: dimensionless) (E) Photochemical quenching (qP: dimensionless) (F) non-photochemical quenching (qN: dimensionless) (G) Functional absorption cross section ($\sigma_{PSII}D$: $Å^2$ $quanta^{-1}$) (H) Photosynthetic rate (P^{chl}: mgC mgchl a^{-1} h^{-1}). Panel (B) shows corresponding chlorophyll *a* concentration, as measured by filtration and extraction (*Chapter 2*). (C), (D) and (G) were measured in FRRF dark chamber.

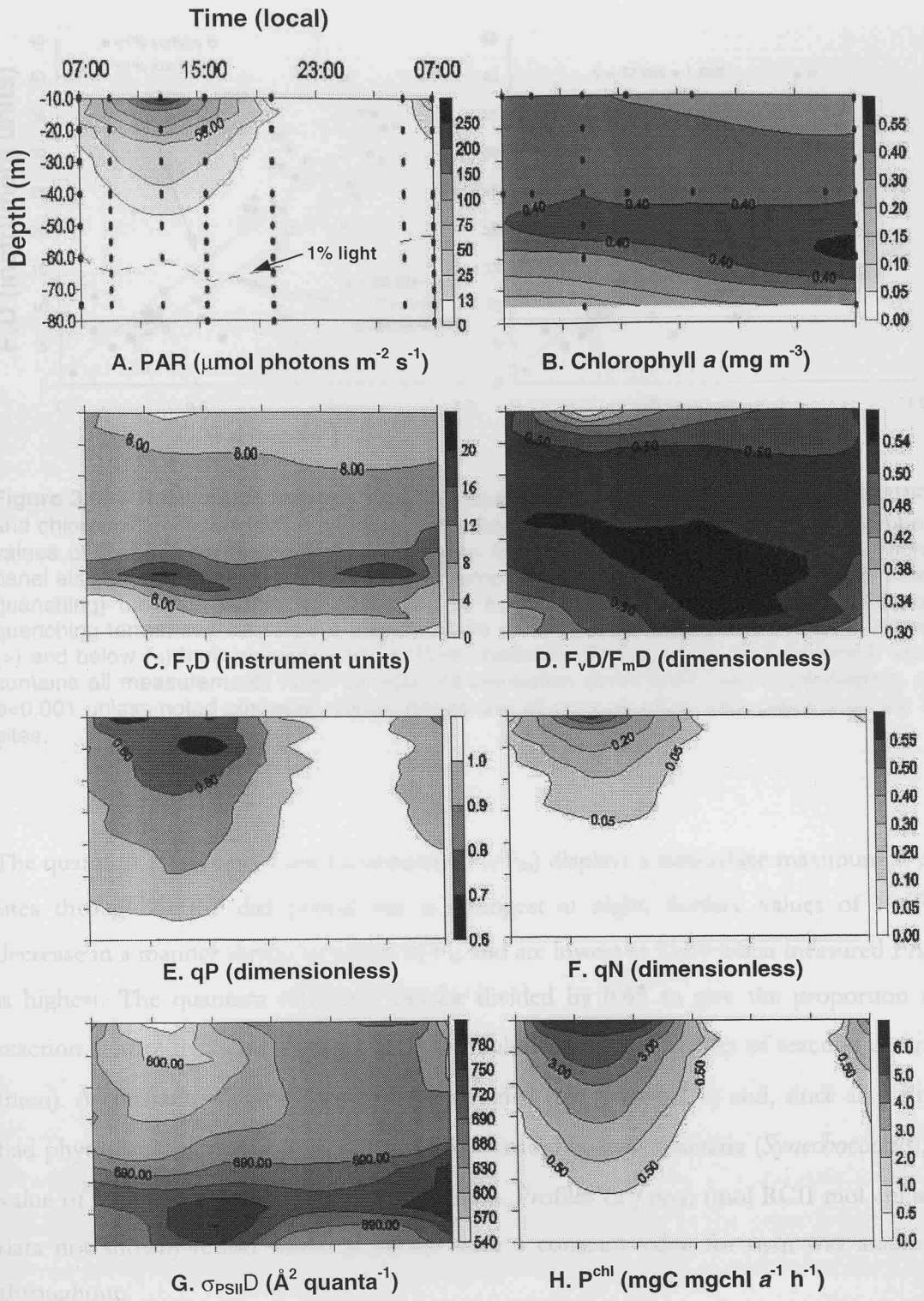

Figure 3.7.— Changes in parameters observed with the FRRF throughout the water column at site 3 (37°N 23°W). Filled circles in upper 2 panels represent sample points for the FRRF via CTD casts: (A) PAR (μmol photons m^{-2} s^{-1}) (C) Variable fluorescence (F_vD: instrument units) (D) Quantum efficiency of photochemistry (F_vD/F_mD: dimensionless) (E) Photochemical quenching (qP: dimensionless) (F) non-photochemical quenching (qN: dimensionless) (G) Functional absorption cross section ($\sigma_{PSII}D$: $Å^2$ $quanta^{-1}$) (H) Photosynthetic rate (P^{chl}: mgC mgchl a^{-1} h^{-1}). Panel (B) shows corresponding chlorophyll *a* concentration, as measured by filtration and extraction (*Chapter 2*). (C), (D) and (G) were measured in FRRF dark chamber.

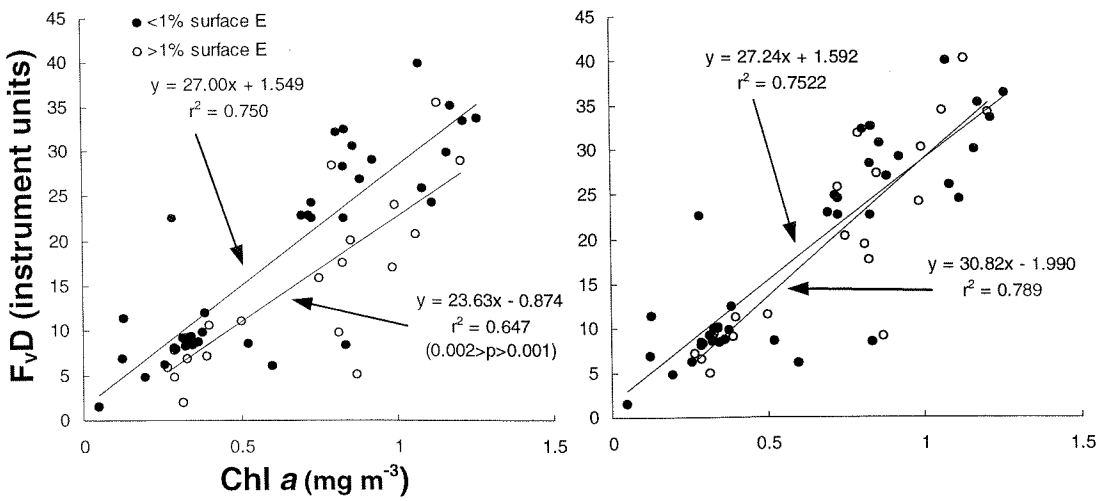

Figure 3.8.— Relationship between variable fluorescence (F_v), as measured with the FRRF, and chlorophyll *a* concentration (extraction and fluorescence). Left panel uses dark chamber values of F_v (F_vD) to minimise the contribution from qP (photochemical quenching). Right panel also shows this relationship but further removes an estimate of qN (non-photochemical quenching) for each respective data point (= $F_v/(1\text{-}qN)$. For definition and calculation of quenching terms, see *section 1.4.* Relationships are shown for data points collected above (>) and below (<) their respective 1% incident irradiance (E). Data from <1% surface E also contains all measurements taken at night. All correlation coefficients have a significance of $p<0.001$ unless noted otherwise. Relationships use all corresponding data points from the 3 sites.

The quantum efficiency of photochemistry (F_v/F_m) displays a subsurface maximum at all sites throughout the diel period but is strongest at night. Surface values of F_v/F_m decrease in a manner similar to values of F_v, and are lowest at 13:30 when measured PAR is highest. The quantum efficiency can be divided by 0.65 to give the proportion of reaction centres that are functional (*f*) when multiplied by the number of reaction centres (n_{PSII}). A constant value of n_{PSII} must be assumed (see *section 1.3.*) and, since all 3 sites had phytoplankton populations that were dominated by cyanobacteria (*Synechococcus*), a value of 1/300 mol RCII mol chl a^{-1} was used. Profiles of $f.n_{PSII}$ (mol RCII mol chl a^{-1}, data not shown) reflect those of F_v/F_m since a constant value for n_{PSII} was assumed throughout.

The functional absorption cross section (σ_{PSII}) exhibits diel variability that is similar to that of F_v at sites 1 and 3. There is a decline in the surface (10m) σ_{PSII} from 08:00 until 13:30 and an increase back between 13:30 and 21:00. A subsurface maximum of σ_{PSII} is evident at all sites, but is most intense at site 3 where it remains throughout the diel period. The night casts (21:00 and 06:00) at all sites have values that are relatively

uniform throughout the surface 50m, after which there is a rapid decline with increasing depth. The decrease of σ_{PSII}, F_v/F_m and F_v in the deeper water samples corresponds with a decrease in chl *a* and presumably reflects the sensitivity of the FRRF rather than a true physiological response, for example, of highly stressed phytoplankton that have escaped the mixed layer, given the hydrographic characteristics of the three sites.

The quantum yield of electron transfer (ϕ_e) is a key parameter when determining the rate of chlorophyll *a*-specific instantaneous production (P^{chl}), and is obtained using the value of E_k, the light saturation parameter. E_k is derived as the inflection point in a plot of qP versus irradiance (Kolber and Falkowski 1993; *section 1.3*); however, the low spatial sampling resolution throughout this investigation resulted in few high light/near surface FRRF measurements and E_k could not be determined from the qP-E relationships of each individual cast. Instead, all diurnal data was amalgamated to produce a single qP versus E response representative of the respective phytoplankton population from each site; for example, site 2, *fig, 3.9.* P^{chl} displays clear diurnal variability at the three sites and again reflects the change in the light field. The magnitude of P^{chl} throughout the water column is greatest where light intensity is highest.

Comparison between the 3 sites— The incident light fields (measured as PAR irradiance attached to the FRRF) were similar at the three sites. Absolute values show that irradiance at 10m was highest (approximately 280-350 μmol photons m^{-2} s^{-1}) at sites 2 and 3, but only reaching 120 μmol photons m^{-2} s^{-1} at site 1, at the peak of the light period (13:30). Fluorescence yield profiles at site 1 were similar to those observed at site 2, where fluorescence is high at the surface and reaches a maximum at 35-45m. Fluorescence values below this depth were significantly reduced. Fluorescence values at site 3 were generally lower (0-20 instrument units) than those at the other 2 sites (0-40 instrument units). In addition, there is a subsurface fluorescence maximum at site 3 at a deeper depth of 60m evident throughout the diel period. Surface fluorescence values at site 3 remain low throughout the 24 hours but become slightly elevated during the dark period.

Surface (10m) values of F_v/F_m range from 0.35-0.5, 0.25-0.45 and 0.3-0.5 (dimensionless) at sites 1, 2 and 3, respectively, with the lowest values reflecting the peak of the light period and the highest values occurring at night. The subsurface values show less diel

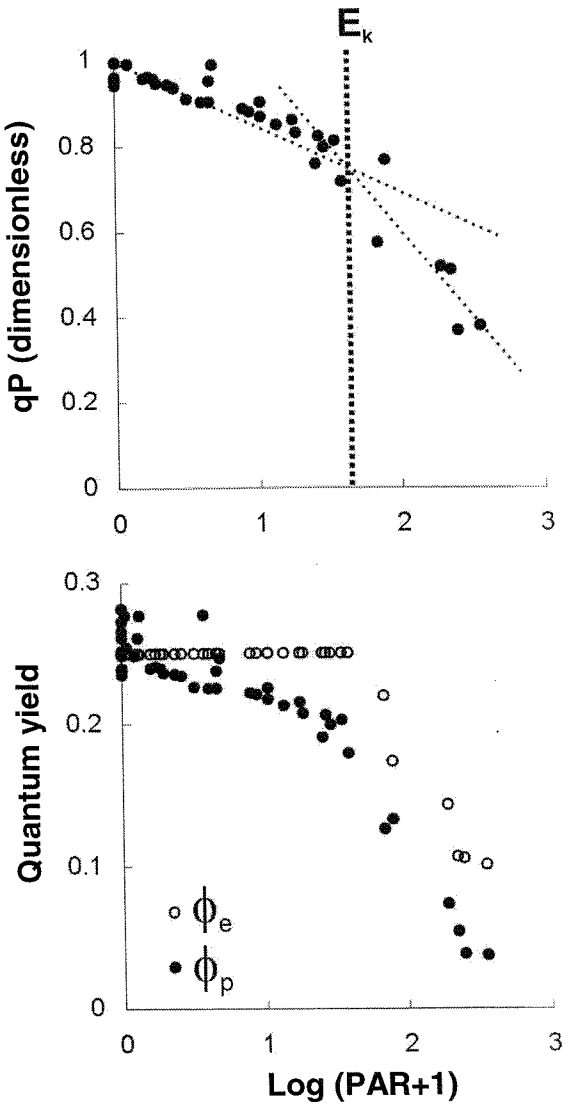

Figure 3.9.— (upper) photochemical quenching (qP) versus log (irradiance (E)+1) for all data collected from site 2 (40°N) throughout the diurnal (daylight) period of diel casting. The inflection point corresponds to the light intensity at which maximal light saturated photosynthesis (E_k) occurs (Kolber and Falkowski 1993), and is determined by 'eye'; (lower panel) E_k is then used in the calculation of the quantum yield of electron transfer (ϕ_e) , see *sections 1.3* and *1.4*. Where phytoplankton physiology is measured under irradiances exceeding E_k, ϕ_e will decrease accordingly. The quantum yield of photosynthesis ϕ_p (which is calculated as ϕ_e * qP) is then used in the calculation of photosynthesis, P^{chl}. ϕ_e and ϕ_p have units of molO_2 mol electrons^{-1} (or mol photons^{-1}).

variation. The range of σ_{PSII} at 10m is 560-700 Å^2 quanta^{-1} at site 1, but is greatest at sites 2 and 3 (540-880 and 380-780 Å^2 quanta^{-1}, respectively). σ_{PSII} values at depth (40-60m) over the 24-hour period remain at a relatively constant intermediary value (540-620 Å^2 quanta^{-1}) at sites 1 and 3 but are higher (720-800 Å^2 quanta^{-1}) at site 2. Finally, values of P^{chl} decrease from 10m to 60m and reduce to values of zero throughout the water column during the dark period at all 3 sites. P^{chl} reaches a maximum of 3.62 (site 1), 4.35 (site 2) and 6.31 (site 3) mgC mg chl a^{-1} h^{-1} between 13:30 and 16:30. At both sites 1 and 2, the P^{chl}-maximum is situated at, or just above, the depth of the biomass-maximum (F_v, chl *a*). Interestingly, the P^{chl}-maximum at site 3 appears at the surface 10m whilst the biomass-maximum exists much deeper at approximately 60m

3.4. Accounting for diel activity of PSII and production at the 3 sites

All photosynthetic parameters displayed a strong diel trend, which could be observed at the sampling resolution of 2-3 hours, at all three sites. Minimum values of σ_{PSII}, F_v/F_m and associated maximum values of P^{chl} and quenching coefficients coincide with solar noon (13:00-13:30 GMT) and reflect changes to both the background (F_o) and maximal (F_m) fluorescence yields (see below). Similar diurnal relationships between *in situ* PSII activity (eg. Falkowski and Kolber 1993, Greene *et al.* 1994) or production rates (for *Synechoccocus*, Prézelin et al. 1986) with irradiance have been previously observed.

The diel variability of fluorescence is produced by several forcing factors including changes in chl *a*/cell (Owens *et al.* 1980), changes in biomass (Marra 1997), and changes in quenching of F_o and F_m (Demers *et al.* 1991). The variable fluorescence yield (F_vD) correlated with chl *a* concentration (*fig. 3.8.*, left panel), most noticeably for the lower (<1% surface irradiance) depths. The lack of correspondence in the surface data is attributed to quenching (Falkowski and Kolber 1990, 1993, 1995). As such, accounting for non-photochemical quenching (qN) improved the correlation between F_v and [chl *a*] for samples taken in the upper (>1% surface irradiance) depths (r^2 increased from 0.647 to 0.789). Overall, this effect of qN is a function of the diurnal irradiance and contributes to the change in the vertical gradient of fluorescence with depth. Quenching of fluorescence in the pigment bed reduces both F_o and F_m and subsequently the rate of PSII light saturation (σ_{PSII}) whilst quenching in, or loss of, reaction centres reduces F_m and, therefore F_v/F_m, without affecting σ_{PSII} (Falkowski *et al.* 1994, Vassiliev *et al.* 1994). As such, qN, fluorescence yields and σ_{PSII} all describe the ability of phytoplankton to respond to diurnal variations in E.

Diurnal photoinhibition of P^{chl} at the surface/near-surface (10-20m) was only evident at site 2. This reflects reduced values of F_v/F_m (photochemistry inhibition), σ_{PSII} (quenching) and also of ϕ_e (and hence ϕ_p) and corresponding *in situ* irradiances which exceed the ability of this phytoplankton population to maintain maximal light-saturated photosynthesis. Reduced values of F_v/F_m and σ_{PSII} are also observed in surface waters of

sites 1 and 3 but do not correspond with an apparent photoinhibition of P^{chl} and remains difficult to explain. Surface (10m) values of F_v/F_m are reduced (between 08:00 and 13:30 GMT) by a factor of 2.02 at site 2 but only by 1.22 and 1.77 at sites 1 and 3, respectively. This relatively small physiological change at site 1 corresponds with a lack of high irradiances. A closer look at the P-E characteristics of the individual diurnal casts from site 3 (*fig 3.10.*) shows a limited amount of photoinhibtion present during the 13:30 GMT cast which was not described by the resolution of the contouring in *fig 3.7.* However, the limited amount of F_v/F_m and P^{chl} inhibtion observed at site 3 is perhaps circumstantial given the lack of samples taken under high light and without considering the photoacclimation strategies of the alternate phytoplankton populations.

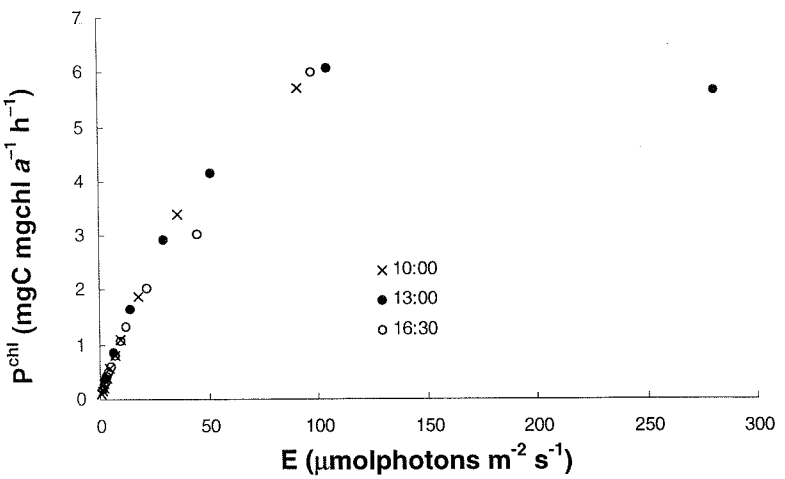

Figure 3.10.— FRRF derived chl a-specific instantaneous production (P^{chl}) against corresponding values of *in situ* irradiance (E) from site 3. Data is shown for water column casts made at 10:00, 13:30 and 16:30 GMT.

Accounting for physiological differences between the 3 sites— σ_{PSII} is essentially considered to be indicative of a photoacclimatory response to growth irradiance levels (eg. Falkowski 1980) and phytoplankton will endeavour to increase their ability to harvest light and saturate σ_{PSII} when grown for extended periods under low light conditions (Dubinsky *et al.* 1986). Values of σ_{PSII} measured at the three sites are all significantly different from one another (ANOVA, $F_{2,167} = 48.235$; Tukey test, $q_{3,167} = 5.309$, $p<0.001$). The mean (± standard deviation) of all σ_{PSII} values measured above the thermocline (at night, to exclude any differential effects of quenching) at each of sites 1, 2 and 3 are 703.7 ± 18.6, 849.6 ± 31.6, 670.2 ± 13.0. The lower mean σ_{PSII} at sites 1 and 3 suggests phytoplankton are photoacclimated to higher irradiances than those at site 2 since saturation of PSII would take longer and require more light. Lower values of σ_{PSII}

would account for the corresponding low values of P^{chl} estimated at site 1 given that the irradiance levels remained relatively low throughout the day.

Phytoplankton at site 2 appear acclimated to relatively lower mean irradiances but are exposed to the highest light levels. However, high values of σ_{PSII} are also produced under nutrient limiting conditions (eg. Kolber *et al.* 1988, Falkowski and Kolber 1995). Values of F_v/F_m were generally lower throughout the diurnal period at site 2 (see above). Similarly the mean of all night values of F_v/F_m from above the thermocline are relatively lower at site 2 (0.482) when compared with those from sites 1 and 3 (0.503 and 0.523, respectively) but is not statistically significant (ANOVA $F_{2, 36} = 2.93$). It might be considered that the site 2 phytoplankton population display characteristics that are more indicative of physiological stress.

Site 3 is characterised by relatively low values of σ_{PSII} above the thermocline, but by high values (mean ± standard deviation 10-50m: 734 ± 40.4 $Å^2$ $quanta^{-1}$) at the F_v and chl *a* maximum, corresponding to the depth of the thermocline. F_v/F_m values above the thermocline are slightly lower (mean 10-50m: 0.502), but still remain relatively high, throughout the diel period when compared with those found at the thermocline (mean 55-70m: 0.516). In addition, the maintenance of high P^{chl} values in surface waters might suggest the presence of separate phytoplankton populations which are acclimated to high irradiances in the surface waters and to lower irradiances deeper in the water column. These photoacclimated phytoplankton populations would require stable hydrographic conditions for a significant period of time (eg. Olson *et al.* 1990a, b), as reflected by a well established thermocline (site 3).

Conclusions— The consideration of phytoplankton physiology and water column hydrography has, in part, accounted for differences between the 3 sites. Site 1 is described by phytoplankton that are typically adapted to conditions of higher light but were measured under conditions of mixing that are apparently more recent than the time required for the population to photoadapt. This condition and the occurrence of elevated nutrient concentrations might be described as pre-bloom, however, the instability of the water column throughout the diel period could confound this interpretation. Site 2 appears to have been under conditions of mixing for a longer period of time, however, the corresponding phytoplankton physiological status and lower nutrient concentrations

might imply that this population is beginning to decline. Site 3 is generally characterised by a stable hydrography and an efficient phytoplankton population, most notably at the nutricline.

The FRRF has, therefore, provided a quantitative *in situ* assessment of PSII and photosynthetic variability throughout a 24 hour (diel) period. Furthermore, the biophysical characteristics associated with PSII emulate the dynamics of the system under observation where corresponding hydrographic signals are available. The phytoplankton populations at the three sites behaved in a similar manner despite the alternate nutrient (trophic) regimes that were chosen for sampling, and may reflect the stress tolerant nature of the dominant (prokaryotic) phytoplankton. The importance of PSI variability within cultured cyanobacterial populations has been highlighted (eg. Barlow and Alberte (1985), and may need to be further considered to help explain differences in physiological response between populations. Finally, this study also exemplifies the problems associated with a limited sampling resolution where a lack of surface and near-surface samples has confounded the interpretation of the phytoplankton response to high light, and therefore, the photoacclimatory status of the populations.

4. The response of phytoplankton physiology to light under different conditions of vertical water column mixing

4.1. Introduction

Phytoplankton are genetically photoadapted to particular types of light environment. These environments are dynamic and individual cells must further adjust their physiology and morphology within their genetic constraints (Falkowski *et al.* 1994), or photoacclimate within their lifetime, to variations in light (see *section 1.1.*). Photoacclimation can occur on a time scale of hours (eg. Falkowski and La Roche 1991) and phytoplankton generally photoacclimate to the mean irradiance at which they are exposed to during the day (Falkowski and Raven 1997). However, continual variations in cloud cover and of vertical water column mixing (Vincent *et al.* 1984) expose phytoplankton to high and low irradiances to which they are not best acclimated. As a result, a number of physiological mechanisms, for example, state transitions (Falkowski *et al.* 1994), non-photochemical thermal deactivation in both the antenna and reaction centre (eg. Aro *et al.* 1993, Olaizola and Yamamoto 1994), fluorescence (eg. Krause and Weis 1991), and electron cycling (eg. Falkowski *et al.* 1986), act to protect the photosystem, on scales of seconds to 10's of minutes, in an attempt to maintain efficient photochemistry.

Processes of photoacclimation can be directly measured from the FRRF. Smaller-scale responses of σ_{PSII} to light are thought to be indicative of antennae quenching of excess energy/fluorescence (eg. Vasilliev *et al.* 1994, Falkowski 1992) and signify the ability with which a cell can photoprotect the reaction centres. Photoacclimation can be characterised from significant changes in the 'size' (σ) or number (n) of either or both photosytems (ie. PSII and/or PSI), Falkowski and La Roche (1991). FRRF

measurements are concerned with PSII, however, whilst the FRRF is able to directly measure σ_{PSII}, the assessment of n_{PSII} is more problematic. This chapter describes, and subsequently tests, a novel method for calculating n_{PSII} based on FRRF measurements. These data, in addition to a consideration of pigment content and light absorption, which can also reveal valuable information regarding the photoacclimative status of cells (see *section 1.1.*), will be further used to assess the response of the phytoplankton photosystem to light under different conditions of vertical water column mixing. Following Cullen and Lewis (1988), it is expected that characteristics relating to photoacclimation will reflect the turnover times of the different water columns.

4.2. A method for calculating the number of reaction centres, n_{PSII}

A knowledge of n_{PSII} (mol RCII mol chl a^{-1}) is fundamental for the estimation of primary production via FRRF measurements (see *section 1.3*). This parameter also yields valuable information regarding the photoacclimative condition of phytoplankton. However, n_{PSII} measurements cannot be measured non-destructively by fluorescence techniques alone and have been confined to laboratory studies. An approximation of $1/n_{PSII}$ for both eukaryotes (500 molchl *a* molRCII^{-1}) and prokaryotes (300 molchl *a* molRCII^{-1}) has been determined from these laboratory measurements (eg. Falkowski and Kolber 1995) but is clearly recognised as a potential source of error in the calculation of production (Falkowski and Kolber 1993, Kolber and Falkowski 1993). A search of the literature (*table 4.1.*) reveals that $1/n_{PSII}$ is a highly variable parameter when considering both different taxa and growth conditions and, therefore, various states of acclimation. The nature of n_{PSII} has yet to be described for *in situ* phytoplankton populations

Taxa/Species	Growth irradiance (μmol photons m^{-2} s^{-1})	$1/n_{PSII}$ (mol chl *a* mol $RCII^{-1}$)	Reference
Bacillariophyceae			
Skeletonema costatum	30, 200, 600	605, 600, 590	Falkowski *et al.* 1981
Thalassiosira weissflogii	30, 70, 150, 320, 600	723, 613, 585, 638, 553	Dubinsky *et al.* 1986
Phaeodactylum tricornutum	250 (Fe replete, straved)	298, 512	Greene *et al.* 1991
Thalassiosira weissflogii	150 (nutrient replete, starved)	280, 770	Berges *et al.* 1996
Chlorophyceae			
Dunadiella tertiolecta	45, 600	830, 710	Falkowski *et al.* 1981
	70, 700	734, 520	Sukenik *et al.* 1990
	150 (nutrient replete, starved)	350, 570	Berges *et al.* 1996
Chlorella pyrenoidesa	Not stated	380, 220	Jursinic & Dennenberg 1985
Chlamydomonas reinhardtii	47, 400	672, 380	Neale & Melis 1986
Chlamydomonas reinhardtii	Not stated	830, 440	Jursinic & Dennenberg 1985
Dinophyceae			
Prorocentrum micans	70, 150, 320, 600	725, 588, 526, 514	Dubinsky *et al.* 1986
Haptophyceae			
Isochrysis galbana	30, 70, 150, 320, 600	637, 463, 389, 366, 624	Dubinsky *et al.* 1986
Cyanobacteria			
Anabaena variabilis	500-1500 lx, 4000-6000 lx*	293, 178	Kawamura *et al.* 1979
Synechococcus 6301	5800 lx*	384	Monodori *et al.* 1984
Synechococcus 7803 (DC-2 type)	Grown at 40-50, exposed to 10, 25, 50, 100, 250	133, 172, 192, 275, 311	Barlow & Alberte 1985
Synechococcus 7803 (1600 type)	Grown at 40-50, exposed to 10, 25, 50, 100, 250	154, 153, 168, 199, 307	Barlow & Alberte 1985

Table 4.1.— Summary of literature which describe values for the number of PSII reaction centres, $1/n_{PSII}$ (mol chl *a* mol $RCII^{-1}$). These estimates are based on laboratory calculations of total chlorophyll*a*: oxygen evolved per flash (ie. the Emerson-Arnold PSU size) which are then divided by 4 since each PSU_{O2} contains the equivalent of 4 PSII reaction centres, see text; Mauzerall and Greenbaum (1989). All species were grown under nutrient replete (except Greene *et al.* 1991, Berges *et al.* 1996, as indicated) conditions over a range of irradiances (expressed in μmolphotons m^{-2} s^{-1}, except *).

The following describes an empirical method for calculating n_{PSII} based on *in situ* measurements made using the FRRF and additional data on chlorophyll *a*-specific absorption (see *Chapter 2* for a full description of the methodologies employed):

Following Mauzerall and Greenbaum (1989), photosynthetic unit size (PSU) is related to the functional absorption cross section (σ_{PSII}), chlorophyll *a*-specific light absorption coefficient (a*) and the maximum quantum efficiency of photosynthesis (ϕ_P) through the relation $PSU_{O2} = \sigma_{O2}/(a^* \cdot \phi_P)$. σ_{O2} is the functional absorption cross section of the oxygen evolving PSII and can, therefore, be described by σ_{PSII}. ϕ_P is given as 0.125 $molO_2$ mol photons^{-1} (Kok 1960). To summarise:

$$\mathbf{PSU_{O2}}\ \frac{\text{mol chl } a}{\text{mol } O_2} = \frac{\sigma_{PSII}\ m^2}{\text{mol photons}} \cdot \frac{\text{mg chl } a}{\mathbf{a^*}\ m^2} \cdot \frac{8\ \text{mol photons}}{\phi_P\ \text{mol } O_2} \cdot \frac{1\ \text{mol chl } a}{892 \times 10^3\ \text{mg chl } a} \qquad [4.1.]$$

PSU_{O2}, or the Emerson-Arnold unit size (eg. Falkowski and Raven 1997), is the ratio of chlorophyll *a*: O_2 evolved in a single saturating turnover flash. PSU_{O2} can be divided by 4, since each PSU_{O2} contains the equivalent of 4 PSII reaction centres, to give PSU_{RCII} or $1/n_{PSII}$ (eg. Kawamura *et al.* 1979, Falkowski *et al.* 1981):

$$\mathbf{PSU_{RCII}}\ \frac{\text{mol chl } a}{\text{mol RCII}} = \frac{PSUO_2}{4} \qquad [4.2.]$$

The value of PSU_{RCII} in *equation 4.2.* actually represents the *functional* size of PSII reaction centres as measured in the water column by the FRRF and should, therefore, be denoted as *f*. PSU_{RCII} (see *section 1.3.*). To obtain the actual number of reaction centres, *equation 4.2.* should be divided by *f*, the proportion of functional reaction centres (Kolber and Falkowski 1993), a parameter which can be derived as the measured *in situ* quantum efficiency of photochemistry relative to the theoretical maximum, ie. $[F_v/F_m]/0.65$:

$$\frac{\mathbf{1}}{\mathbf{n_{PSII}}}\ \frac{\text{mol chl } a}{\text{mol RCII}} = PSU_{RCII} \cdot \frac{0.65}{[F_vD/F_mD]} \qquad [4.3.]$$

This method of using the FRRF to calculate n_{PSII} is indirect and contains several potential sources of error that must be considered when interpreting the results. The peak emission of the FRRF and subsequent measurement of σ_{PSII} occurs at 475nm with a half band-width of 30nm. The band-width can be accounted for following Dubinsky *et al.* (1986, pp.1338) to produce a mean (appropriately weighted) value of σ_{PSII} (475nm). Both the σ_{PSII} and a* at 475 nm are then used in *equation 4.1.* The emission spectrum of

the FRRF corresponds to the region of blue-green absorption of light by phytoplankton. Most phytoplankton taxa show peak absorption on or near to this wave-band but will vary according to species (Babin *et al.* 1996). However, the apparent [antennae] absorption (σ_{PSII}) is increased by the presence of wavelength-specific accessory pigments which exist to promote energy harvesting and transfer to PSII reaction centres (see Falkowski and Raven 1997). As such, σ_{PSII} is wavelength dependent, and therefore, this method of calculating n_{PSII} may prove unsatisfactory when considering populations with large taxanomic differences. In addition, *equation 4.1.* assumes that ϕ_P is constant. The removal of the proportion of functional reaction centres from the equation could account for any reduction in ϕ_P from the inactivation of reaction centres. Irrespective of these potential problems, this method does begin to satisfy the need for refining a technique of measuring n_{PSII} based on *in situ* measurements. Here it is examined using data collected in the English Channel in August 1999.

4.3. General hydrography and phytoplankton physiology

Two sites were visited by *RRS Challenger* in the western English Channel, August 1999 (*fig. 4.1.*). The western English Channel is situated on the north-western European Continental Shelf within the westerly wind domain. The vertical distribution of phytoplankton on continental shelves is dictated by heat exchange, wind and tides throughout the year (eg. Holligan 1987); however, it is the mixing by tides that determines the degree of mixing during summer months (Pingree 1980). Consideration of these physical processes can be used to predict areas of stratified and well-mixed waters on the shelf (Pingree *et al.* 1978) and ultimately, the potential physiological and photosynthetic responses of phytoplankton. Whilst observations of phytoplankton physiology and productivity have been made from these contrasting mixing regimes in the Celtic Sea (eg. Joint and Pomeroy 1986), the North Sea (eg. Tett *et al.* 1993) and the eastern English Channel (Pingree *et al.* 1986, Lizon *et al.* 1995), smaller-scale changes in PSII activity have yet to be described under similar conditions.

A well-mixed site (**M**, 48°45′N 04°44′W) was occupied around neap tide (August 6th) between 06:30 GMT August 6th and 11:20 GMT August 7th, whilst a stratified site (**U**,

49°14'N 06°10'W) was occupied between 13:45 GMT August 8th and 15:10 GMT August 9th. CTD casts were performed every 1-1.5 hours at both sites and FRRF measurements were made (at least) every metre (see *Chapter 2*). This intense sampling resolution allows for the characterisation of smaller-scale PSII variability that could not be described from the broad-scale diel sampling regime of the RV *Pelagia* cruise, *Chapter 3*. The respective protocols and sampling strategy employed with the instrumentation are described in *Chapter 2*. In addition, a more detailed explanation and derivation of terms used throughout is given in *Section 1.6*. All times are given in GMT throughout this Chapter unless stated otherwise.

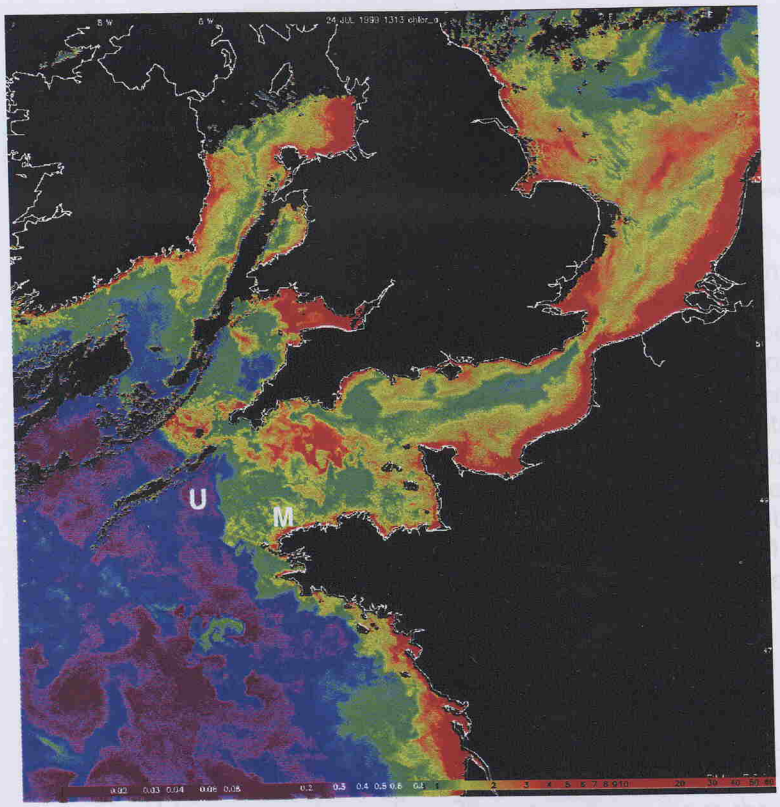

Figure 4.1.— SeaWiFS satellite image of surface chlorophyll *a* concentration (for key see *figure 3.1.*) from waters around the U.K and northern France. Image taken 24th July 1999, 1 week before the cruise commenced, but is representative of the conditions experienced throughout. The approximate positions of the mixed (**M**) and stratified (**U**) sampling sites are indicated in high and low areas of [chl *a*], respectively.

Hydrographic and physiological characteristics— Site M was characterised by relatively high rates of vertical water column turnover (diffusivity and shear, *table 4.2.*). Mean surface water temperatures were low and there was little evidence of a thermocline throughout the sampling period. Nitrate concentrations ($[NO_3]$) were low in surface (stratified) waters when compared to values from deeper in the water column. Values of PAR (*fig. 4.2.*) were significantly affected by cloud during the first day of sampling and are relatively low (and variable). PAR was much higher on the second day of sampling.

Photochemical quenching (qP, *fig. 4.2*) follows the trends in PAR where quenching was highest [= qP values are lowest] on the second day of sampling.

Parameter	Site M	Site U
Mean water temp (°C)	1-2m: 14.50 (±0.154) 90-95m: 13.72 (±0.019)	1-2m: 18.69 (±0.095) 103-110m: 11.10 (±0.045)
thermocline depth (m)	-	30 - 32
[NO_3] (mmol m^{-3})	1-2m: 1.0 > 30m 2.8	1-2m: <0.01 below thermocline: 5.47
[chl *a*] (mgchl *a* m^{-3})	1-5m: 5.08 > 30m 0.97	1-5m: 0.31 thermocline: 61.32
Mean turbulence dissipation (m^2s^{-3})	1.14×10^{-6}	1.60×10^{-7}
Mean diffusivity (m^2s^{-1})	2.08×10^{-3}	1.097×10^{-5}
σ_{PSII} ($Å^2quanta^{-1}$)	454 - 771	282 - 913
F_v/F_m (dimensionless)	0.33 – 0.57	0.19 - 0.52

Table 4.2.— Values of hydrographic and physiological parameters recorded at the 2 sites. The range (lowest-highest) of all parameter values measured throughout the 25 hour casting period are given for the depth of the thermocline (m), nitrate concentration ([NO_3], mmol m^{-3}), chlorophyll *a* concentration [chl *a*], as measured from filtration and extraction methodology, see *section 2.2.*], the functional absorption cross section (σ_{PSII}, $Å^2quanta^{-1}$) and the photochemical efficiency (F_v/F_m, dimensionless) measured with an FRRF. The depths where the highest and lowest [chl *a*] and [NO_3] were observed is indicated. The mean temperature (°C) ± standard error at each respective station is also given for all measurements made (throughout the sampling period) at the surface (1-2m at both stations) and at the deepest depth of the CTD cast ('bottom' water: 90-95m site M; 103-110m site U). Mean vertical eddy diffusivity (m^2s^{-1}) and turbulence dissipation rates (m^2s^{-3}) were measured using a FLY (Free-fall Light Yo-yo) shear profiler, c/o M.Moore.

The chlorophyll *a* concentration and variable fluorescence yields ([chl *a*] and F_v, *fig. 4.2.*) remained highest in the surface 20 metres throughout the sampling period, in particular, between 00:00 and 06:00 GMT. The functional absorption cross section (σ_{PSII}, *fig. 4.2.*) was lowest during daylight hours in the surface 20m. A subsurface σ_{PSII}-maximum can be identified between 40 and 60m despite the more variable nature of σ_{PSII} signals deeper in the water column. The quantum efficiency (F_v/F_m, *fig. 4.2.*) appears less variable. The lowest values of F_v/F_m were found in the surface 10m, and coincided with periods of highest PAR (16:00 first day and 11:00 second day), whilst a maximum of F_v/F_m was maintained between the surface and 20m throughout the sampling period. Water column [chlorophyll *a*-specific] instantaneous production (P^{chl}, *fig 4.2.*) was calculated using a

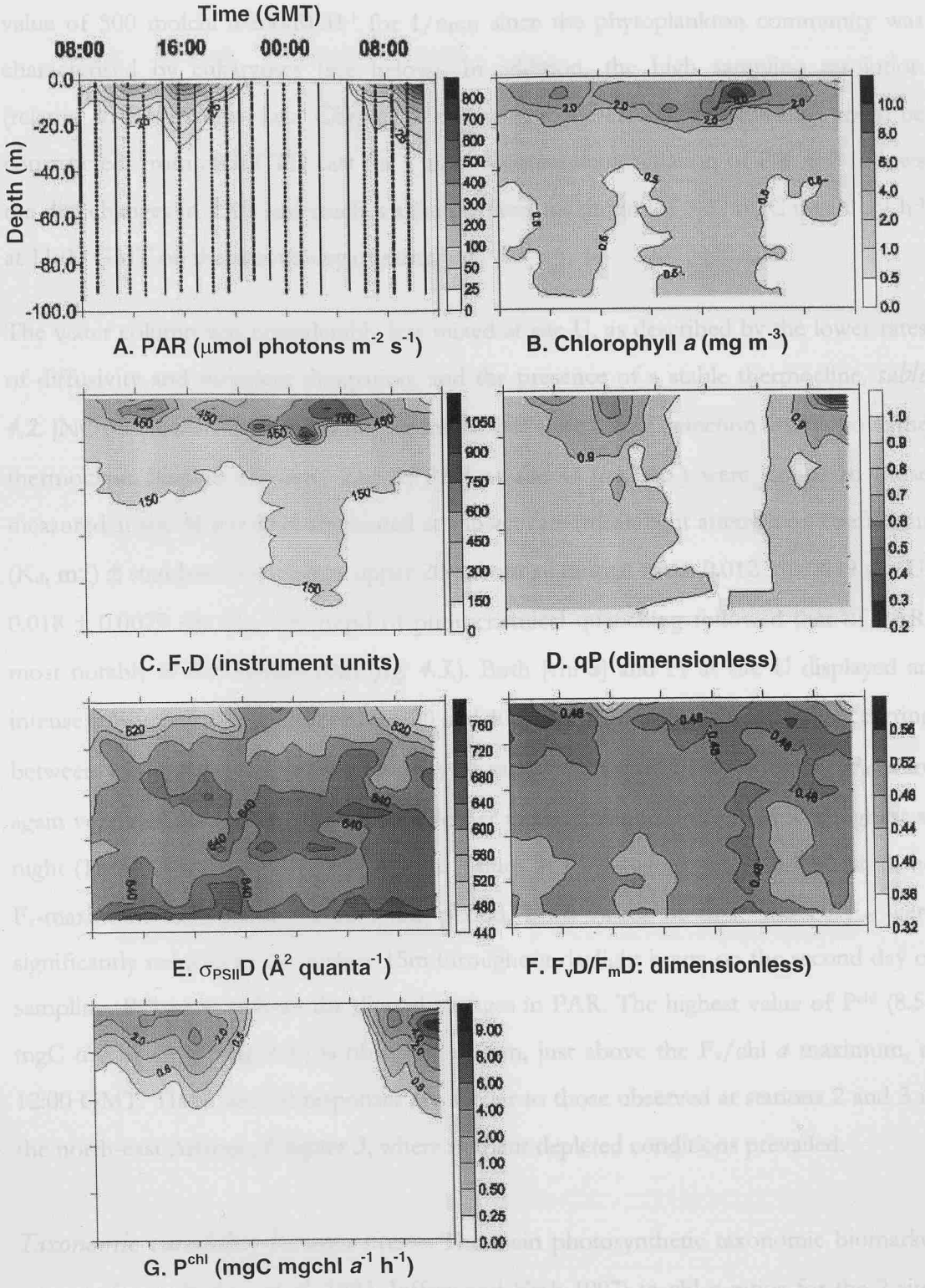

Figure 4.2.— Changes in parameters observed with the FRRF throughout the water column at site M (48°45'N 04°44'W). Filled circles in upper panel represent sample points for the FRRF via CTD casts: (A) PAR (µmol photons m^{-2} s^{-1}) (C) Variable fluorescence (F_vD: instrument units) (D) Photochemical quenching (qP: dimensionless) (E) Functional absorption cross section ($\sigma_{PSII}D$: $Å^2$ $quanta^{-1}$) (F) Quantum efficiency of photochemistry (F_vD/F_mD: dimensionless) (G) Photosynthetic rate (P^{chl}: mgC mgchl a^{-1} h^{-1}). Panel (B) shows corresponding chlorophyll *a* concentration at the same resolution as panels (A), (D) – (G) using the relationship established between discrete chl *a* measurements and CTD measured (not FRRF) fluorescence. (C), (E) and (F) were measured in FRRF dark chamber.

value of 500 molchl *a* molRCII^{-1} for $1/n_{PSII}$ since the phytoplankton community was characterised by eukaryotes (see below). In addition, the high sampling resolution (relative to *RV Pelagia* data, *Chapter 3*) meant that qP versus E relationships could be constructed from each CTD cast for a more accurate determination of P^{chl}. P^{chl} follows the diel changes in PAR and reaches a [subsurface] maximum of 9.32 mgC mgchl a^{-1} h^{-1} at 11:00 GMT on the second day of sampling.

The water column was considerably less mixed at site U, as described by the lower rates of diffusivity and turbulent dissipation, and the presence of a stable thermocline, *table 4.2.* [NO_3] remained high in the deeper waters but were below detection limits above the thermocline. Surface values (1-2m) of PAR at site U (*fig. 4.3.*) were similar to those measured at site M but were attenuated at a lower rate (mean light attenuation coefficient (K_d, m^{-1}) ± standard deviation in upper 20m from all diurnal casts: 0.012 ± 0.0049 site U, 0.018 ± 0.0025 site M). The trend of photochemical quenching followed that of PAR, most notably in the surface 20m (*fig. 4.3.*). Both [chl *a*] and F_v at site U displayed an intense subsurface maximum between 20 and 40m (*fig. 4.3.*) with highest levels occurring between 16:00 and 20:00 on the first day of sampling. Values of σ_{PSII} and F_v/F_m were again very variable (*fig. 4.3.*), especially deeper in the water column. σ_{PSII} was highest at night (18:00 - 06:00) between 0 and 35m. Values of F_v/F_m were generally highest at the F_v-maximum throughout the sampling period. Both values of σ_{PSII} and F_v/F_m were significantly reduced in the surface 15m throughout daylight hours on the second day of sampling. P^{chl} again follows the diurnal changes in PAR. The highest value of P^{chl} (8.56 mgC mgchl a^{-1} h^{-1}, *fig 4.3.*) is observed at 20m, just above the F_v/chl *a* maximum, at 12:00 GMT. These diurnal responses are similar to those observed at stations 2 and 3 in the north-east Atlantic, *Chapter 3*, where nutrient depleted conditions prevailed.

Taxonomic variability between sites— The main photosynthetic taxonomic biomarker piments (*sensu* Barlow *et al.* 1993, Jeffrey and Vesk 1997) to chl *a* ratios for the 2 sites are given in *fig. 4.4.* Both the deep and shallow HPLC samples (see legend text) from site M are dominated by phytoplankton containing chlorophyll *b* ('green' algae, ie. chlorophyceae, prasinophyceae and euglenophyceae) and, to a lesser extent, fucoxanthin (diatoms and prymnesiophytes). Site U is characterised by the strong presence of 19'hexanoyloxyfucoxanthin (prymnesiophytes) and fucoxanthin. Significantly smaller

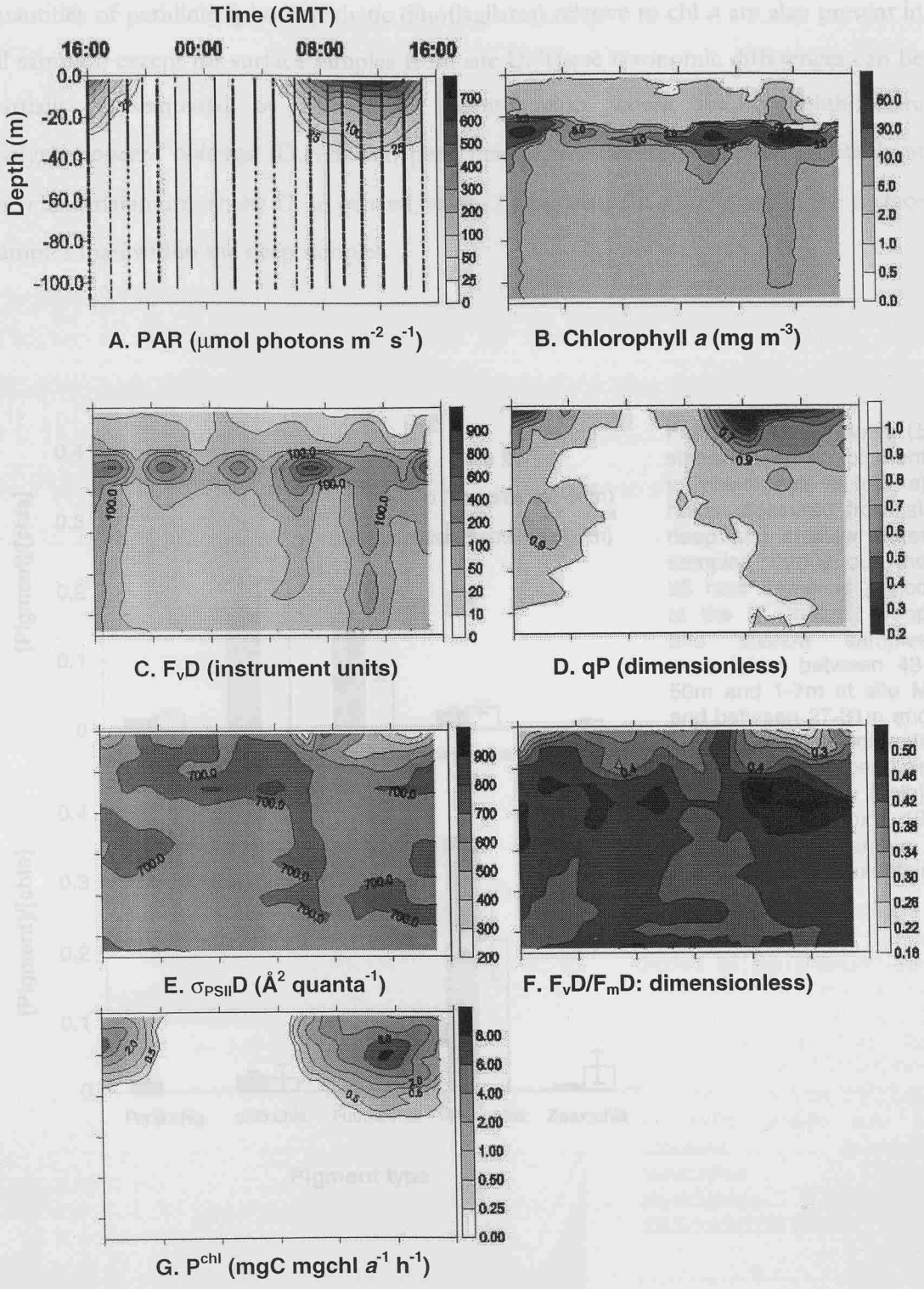

Figure 4.3.— Changes in parameters observed with the FRRF throughout the water column at site U (49°14'N 06°10'W). Filled circles in upper panel represent sample points for the FRRF via CTD casts: (A) PAR (µmol photons m^{-2} s^{-1}) (C) Variable fluorescence (F_vD: instrument units) (D) Photochemical quenching (qP: dimensionless) (E) Functional absorption cross section ($\sigma_{PSII}D$: $Å^2$ $quanta^{-1}$) (F) Quantum efficiency of photochemistry (F_vD/F_mD: dimensionless) (G) Photosynthetic rate (P^{chl}: mgC mgchl a^{-1} h^{-1}). Panel (B) shows corresponding chlorophyll *a* concentration at the same resolution as panels (A), (D) – (G) using the relationship established between discrete chl *a* measurements and CTD measured (not FRRF) fluorescence. (C), (E) and (F) were measured in FRRF dark chamber.

quantities of peridinin (photosynthetic dinoflagllates) relative to chl *a* are also present in all samples, except for surface samples from site U. These taxonomic differences can be partially substantiated by microscopic identification where the coccolithophore *Calyptrosphaera oblonga* (D.Harbour, pers.comm.) was predominant, most notably at the chl *a* maximum, at site U. In general, values of pigment:chl *a* are lower in the surface samples than within the deep samples.

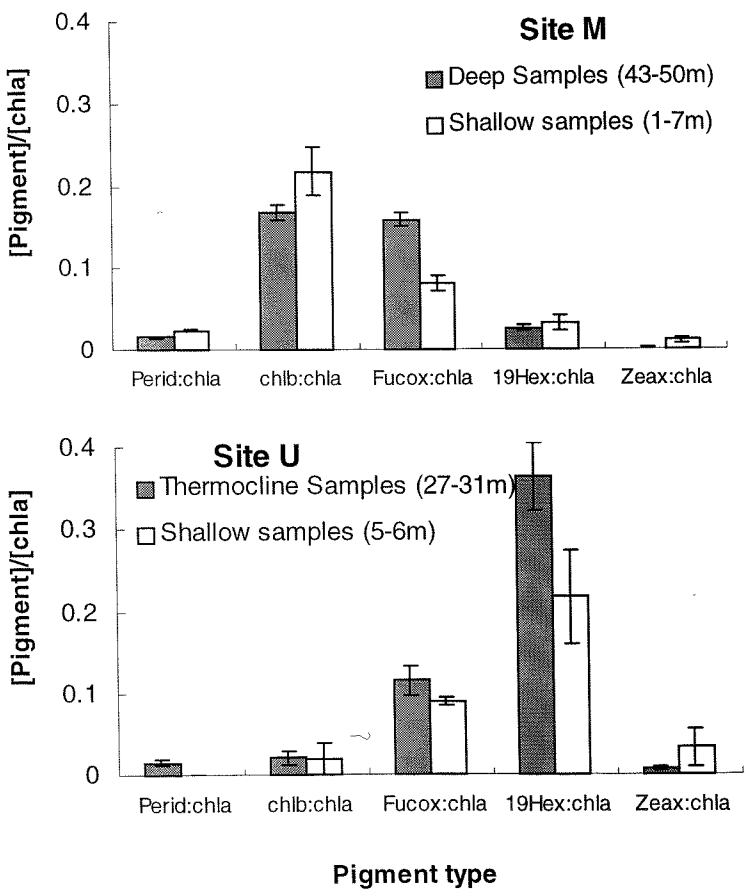

Figure 4.4.— Mean (± standard error) pigment to chlorophyll *a* (chl *a*) ratios measured from all deep and shallow water samples throughout the 25 hour sampling period at the 2 stations. Deep and shallow samples were taken between 43-50m and 1-7m at site M and between 27-31m and 5-6m at site U. Pigments included are: peridinin (Per), chlorophyll*b* (chlb), fucoxanthin (Fucox), 19' hexanoyloxyfucoxanthin (19'hex) and zeaxanthin (Zeax).

4.4. Observations of photoacclimation and photoprotection at the 2 sites

Non-photosynthetic pigment composition and PSII activity— Phytoplankton pigments can be divided into those which contribute significantly towards photosynthesis (chlorophylls and photosynthetic carotenoids) and those which are non-photosynthetic or photoprotectant, ie. diadinoxanthin, diatoxanthin, β-carotene and zeaxanthin (Bidigare *et al.* 1990). The magnitude of the ratios of each of these main non-photosynthetic pigments (NPP) relative to chlorophyll *a* at sites M and U are given in *fig. 4.5*. The sum of the total NPP:chl *a* ratios is largely comprised of diadinoxanthin:chl *a* at both sites, although a significant contribution from β-carotene:chl *a* is also apparent at site M. A significant positive relationship is found between corresponding values of the total[NPP] and light (*fig. 4.6.*).

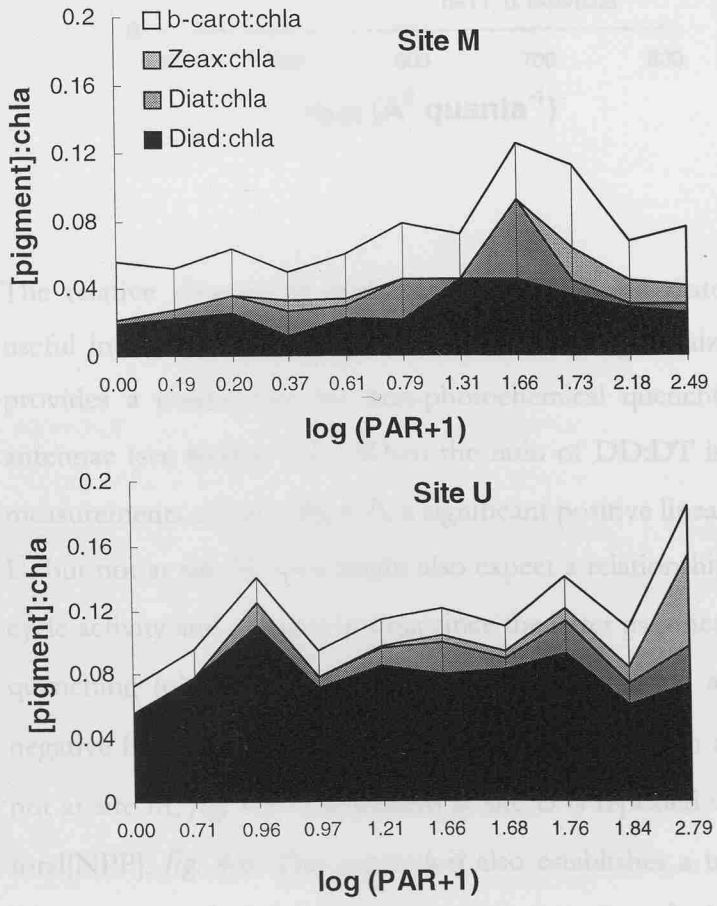

Figure 4.5.— Pigment to chl *a* ratios of the main non-photosynthetic pigments (Bidigare *et al.* 1990) at the respective irradiances measured at the 2 sites. A mean pigment:chl *a* is given for all samples where PAR = 0. As such, irradiance is plotted as log (PAR+1) and not log (PAR). Each of the pigment: chl *a* are plotted cumulatively so that the upper limit at each irradiance represents the total [NPP]:chl *a*. NPPs plotted are: β-carotene (b-carot), zeaxanthin (Zeax), diatoxanthin (Diat) and diadinoxanthin (Diad).

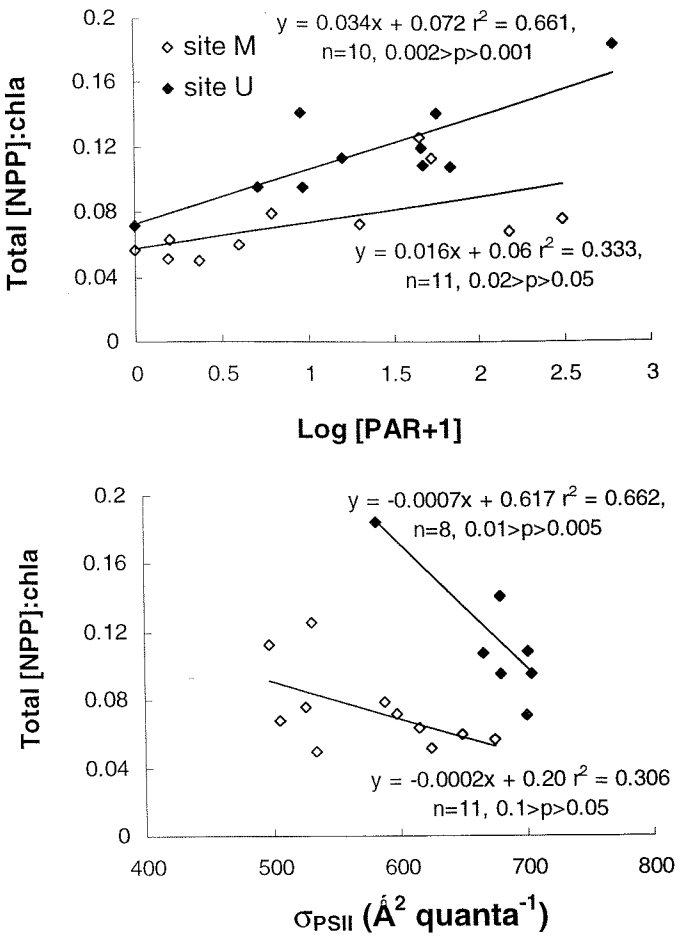

Figure 4.6.— (upper panel) Regression between total non-photosynthetic pigment concentration (total[NPP]):chl *a* and irradiance (log[PAR+1]), presented in *figure 4.5.*, from the 2 sites; (lower panel) Regression between Total [NPP]:chl *a* and corresponding values of the effective absorption cross section, σ_{PSII}, at sites M and U. Two data points from site U have very similar values (0.1413, 679.98 and 0.1408, 679.83 from 26m 16:00 GMT and 27m 17:30GMT, respectively) and cannot be individually identified in the figure. All relationships are significant as indicated.

The relative changes in diadinoxanthin (DD) and diatoxanthin (DT) pigments are a useful indication of xanthophyll-cycle activity (eg. Olaizola and Yamamoto 1994) and provides a mechanism for non-photochemical quenching excess light energy in the antennae (see *section 1.1.*). When the ratio of DD:DT is plotted against corresponding measurements of light (*fig 4.7*), a significant positive linear relationship is observed at site U, but not at site M. One might also expect a relationship to exist between xanthophyll-cycle activity and changes in σ_{PSII} since the latter parameter is also indicative of antennae quenching (qN), eg. Vassiliev *et al.* 1994, Falkowski and Kolber 1995. A significant negative linear relationship is established between σ_{PSII} and DD:DT again at site U but not at site M, *fig. 4.7.* The pattern at site U is repeated when σ_{PSII} is plotted against the total[NPP], *fig. 4.6.* This regression also establishes a trend, albeit of low significance, between non-photosynthetic pigment content and the functional absorption cross section of PSII (σ_{PSII}) at the well mixed site, M.

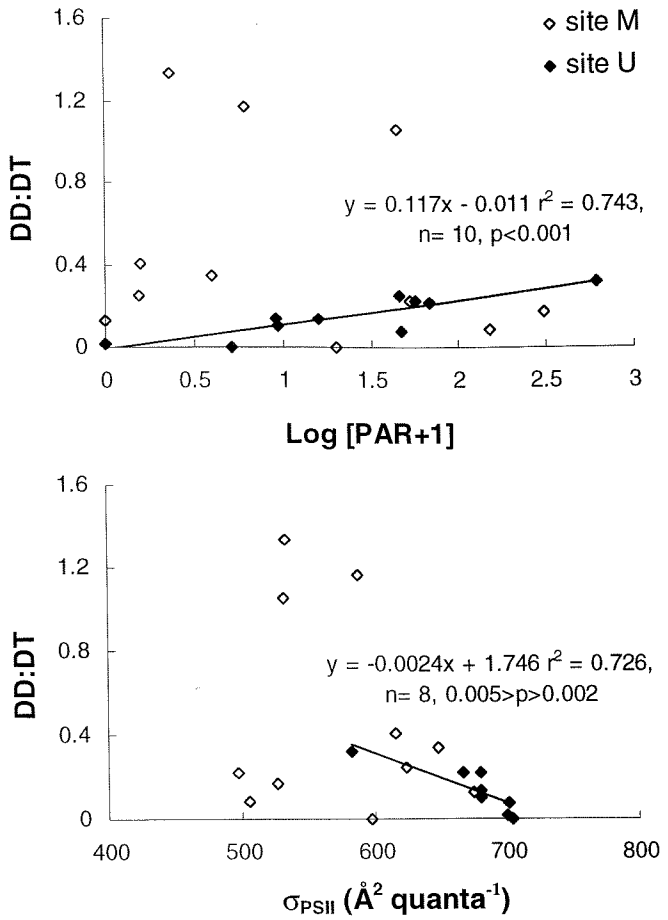

Figure 4.7.— (upper panel) Regression between DD:DT (ratio of non photosynthetic pigments diadinoxanthin (DD) to diatoxanthin (DT)) and corresponding values of irradiance (log[PAR+1]) from the 2 sites; (lower panel) Regression between DD:DT and corresponding values of the functional absorption cross section, σ_{PSII}, at sites M and U. All relationships are significant as indicated. No relationship could be identified from the data of site M.

Light absorption by pigments— Examples of chlorophyll *a*-specific absorption ($a^*_{(\lambda)}$) measurements between 380 and 840nm are given in *fig. 4.8.* (raw data plots are presented in *Appendix* 2). The data must be expressed as m^2 mg chl a^{-1} for the calculation of n_{PSII} (*equation 4.1.*). Chlorophyll *a* measurements made using spectrophotometric or fluorometric acidification techniques do not necessarily discriminate against all species of phaeopigment (chlorophyll degradation products), Jeffrey and Welschmeyer (1997). The application of such techniques would result in measurements of $a^*_{(\lambda)}$ expressed as m^2 (mg chl *a* + phaeopigments)$^{-1}$, for example, Babin *et al.* (1996), Bisset *et al.* (1997). Instead, chl *a* should be determined, as in this study, using the Welschmeyer (1994) method or HPLC techniques.

Both sites M and U show strong absorption peaks at 435 and 675 nm corresponding to absorption by chlorophyll *a*, and a secondary absorption shoulder between 410 and

470nm indicating absorption by chlorophyll *b*, photoprotectant and photosynthetic carotenoids (Bidigare *et al.* 1990). The absorption shoulder at 470nm (corresponding to chl *b*) and the absorption peaks of chl *a* appear less prominent at site U. As such, one might consider that chromatic differences could, in part, account for variations in σ_{PSII} between the 2 sites. There is little evidence of strong absorption by phycobiliproteins (see Kirk 1994), for example, phycoerythrin (490-565nm) to indicate the significant presence of cyanobacteria in any of the samples.

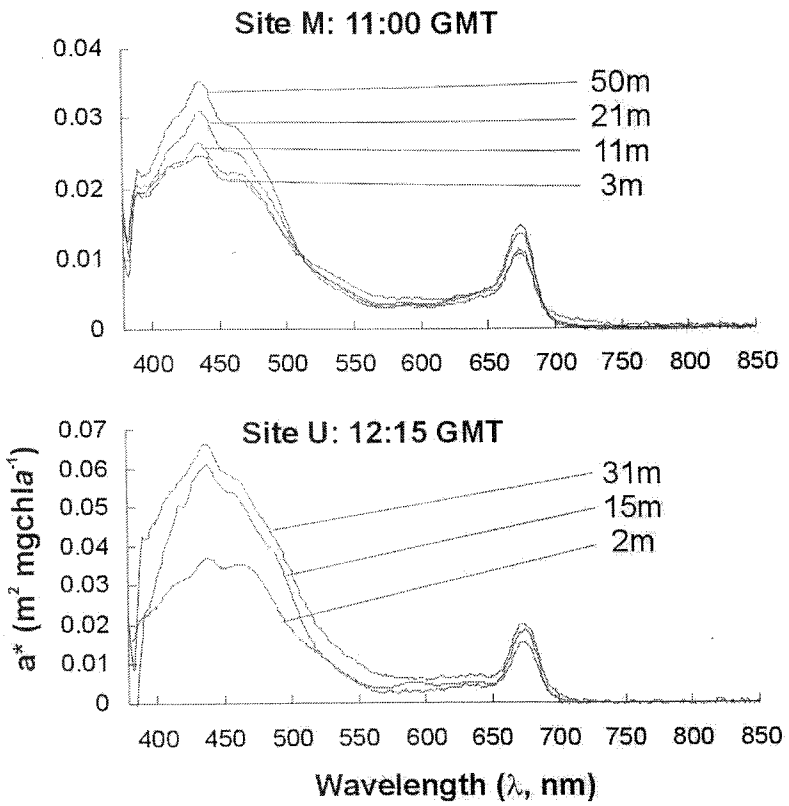

Figure 4.8.— Examples of chl *a*-specific absorption spectra (a*) from 11:00 and 12:15 (GMT) at sites M and U, respectively. Spectra are shown between wavelengths (380-850nm), as measured by the spectrophotometer, for all depths sampled at that sample time. All spectra measured at the two sites can be found in *appendix 2.* **Note** the different scales for the y-axis of the 2 panels.

Measurements of $a^*_{(\lambda)}$ between 400 and 500 nm, where absorption is most apparent, were significantly lower in surface samples (2-5m) than from corresponding deeper (thermocline) samples ($t\text{-test}_{1,\ 612} = 3.192$, $0.002>p>0.001$) at site U. A similar analysis observes no significant differences between surface and deep samples at site M. Mean values of $a^*_{(\lambda)}$ were further calculated from all samples for the wavelengths 412, 443, 490, 510, 555, 670 and 685 nm corresponding to SeaWiFS satellite bands for both sites and compared (*table 4.3.*). Mean absorption was highest at site U for all wavelengths, except 555nm.

λ (nm)	a* (λ) (m^2 mgchl a^{-1})	
	Site M	Site U
412	0.0233	0.0368
443	0.0266	0.0442
490	0.0169	0.0277
510	0.0105	0.0158
555	0.0046	0.0041
670	0.0113	0.0141
685	0.0074	0.0086

Table 4.3.— Summary of mean values of the chlorophyll *a*-specific absorption (a*, m^2 mgchl a^{-1}) at wavelengths corresponding to SeaWiFS satellite bands (412, 443, 490, 510, 555, 670 and 685nm) from the 2 sample sites. The mean is derived from all samples taken at each respective sample site, irrespective of time of day or depth.

Changes in n_{PSII}— The number of PSII reaction centres ($1/n_{PSII}$, molchl *a* molRCII^{-1}, *equation 4.3.*) calculated for both sites throughout the sampling period are given in *fig.*

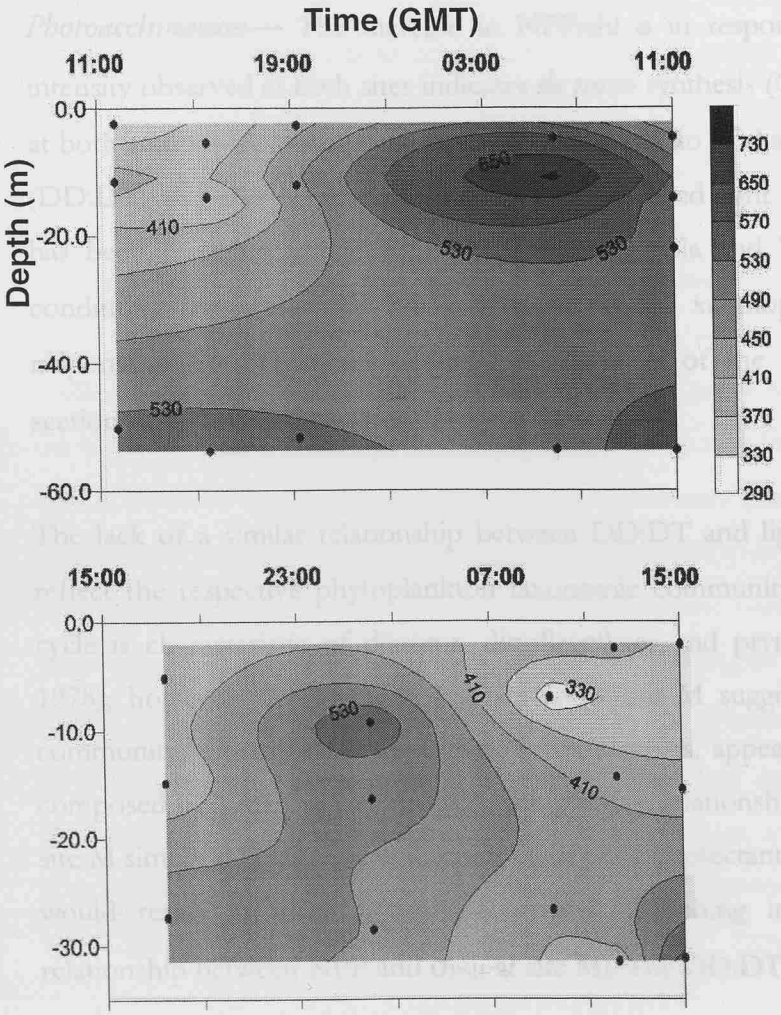

Figure 4.9.— number of reaction centres ($1/n_{PSII}$), molchl *a* molRCII^{-1} as determined from *equation 4.2.* for sites M (upper panel) and U (lower panel). Times are given in GMT for both sites and are on different scales following the respective sampling series. The key applies to both panels. Filled circles represent the points at which samples were taken.

4.9. The highest overall values are observed at site M (356-745 molchl *a* molRCII^{-1}, mean ± standard error, 493 ± 23) whilst the lowest are seen at site U (310-560 molchl *a* molRCII^{-1}, 428 ± 18). In general, $1/n_{PSII}$ from samples taken during the day increase with depth and hence decrease with irradiance at both sites (a regression of $1/n_{PSII}$ and irradiance showed significant negative correlations for both sites, M: $1/n_{PSII}$ = -68.4[Log PAR+1] +577.6, n=12 r^2=0.593 0.005>p>0.002; U: $1/n_{PSII}$ = -86.8 [Log PAR+1] +581.4, n=12 r^2=0.573 0.005>p>0.002). A high surface $1/n_{PSII}$ is observed in the 05:50 (GMT) sample from site M and corresponds with a large increase in F_v (*fig. 4.2.*). A higher value of $1/n_{PSII}$ is also observed in the surface waters (than in deeper waters) of site U during the night, however, this increase appears to remain independent of any changes in chlorophyll *a* or fluorescence yield.

4.5 Discussion and conclusions

Photoacclimation— The increase in NPP:chl *a* in response to an increase in light intensity observed at both sites indicates *de novo* synthesis (Olaizola and Yamaoto 1994) at both stations. A corresponding increase in the ratio of diadinoxanthin to diatoxanthin (DD:DT) was also observed in response to increased light at site U. This trend, which has been recorded under both laboratory (Olaizola and Yamamoto 1994) and field conditions (Brunet *et al.* 1993), is indicative of xanthophyll activity and is partly responsibly for the corresponding loss observed of the functional absorption cross section of PSII antennae, σ_{PSII}.

The lack of a similar relationship between DD:DT and light (or σ_{PSII}) at site M may reflect the respective phytoplankton taxonomic community. The DD-DT xanthophyll cycle is characteristic of diatoms, dinoflagellates and prymnesiophytes (Liaaen-Jensen 1978); however, the pigment analyses from site M suggests that this phytoplankton community, most notably in surface, 1-7m, samples, appears to have been significantly composed of 'green' algae. As such, the positive relationship between NPP and light at site M simply reflects a general synthesis of photoprotectant xanthophyll pigments which would result in more non-photochemical quenching in the antennae (hence the relationship between NPP and σ_{PSII} at site M). The DD:DT relationships of site M (from

fig 4.7.) become significant, and more consistent with those observed at site U, when all surface data points (1-7m) are removed from the analysis (DD:DT = -0.0065*σ_{PSII} + 4.45, r^2= 0.921, n= 4, 0.01> p>0.005; DD:DT = 0.523*log[PAR+1] + 0.158, r^2 = 0.924, n= 4, 0.01> p>0.005). This is suggested to correspond to a significant increase in the concentration of fucoxanthin, and hence diatoms and prymnesiophytes (eg. Jeffrey and Vesk 1997), in the deeper waters of site M

The changes in NPP were observed from a broad sampling resolution and are not, therefore, strict evidence of a short term response of photoacclimation to fluctuating irradiance. Values of σ_{PSII} from the continuous FRRF surface water record reveals further differences between stratified and mixed waters, *fig 4.10.* Small-scale variations (minutes-10's minutes) can be observed and signifies the ability with which phytoplankton can regulate light harvesting of PSII (Dubinsky *et al.* 1986, Falkowski *et al.* 1986). Incident irradiance correlates with σ_{PSII} at site U (σ_{PSII} = -0.162*light + 599, n=35, r^2 = 0.323, p<0.001) but not at site M. The significant response of phytoplankton with light may reflect the lower water column mixing rates at site U. Conversely, it could be considered that the higher mixing rates at site M appear to exceed the time scale of short-term physiological responses that are reflected by variations in σ_{PSII}. However, the lack of data from site U (and hence variations in light-σ_{PSII}) limit these interpretations.

Phytoplankton appear to display strong photoacclimative strategies, at greater time scales, under the contrasting water column mixing regimes at the two sites. The well mixed site (M) is characterised by values of n_{PSII} that are generally higher than those from the stratified site (U). These different characteristics can be considered to reflect mean light conditions that the respective communities receive (Falkowski 1980) and should be expected, if it could be assumed that phytoplankton in well mixed waters receive, on average, less light than those in less dynamic waters. Laboratory studies indicate that phytoplankton grown at lower light intensities have higher values of $1/n_{PSII}$ (mol chl *a* molRCII^{-1}) (*table 4.1.*) since relative increases in chl *a*/cell are greater than those of mol RCII/cell (Sukenik *et al.* 1990). A greater $1/n_{PSII}$ will result in faster 'processing' of available light energy and is hence an acclimation strategy to lower irradiances. However, n_{PSII} represents a limited interpretation of photoacclimation based on photosynthetic unit size (n_{PSU}) (Falkowski and La Roche 1991), since corresponding alterations to the

number of PSI photosynthetic units (n_{PSI}) also occur (eg. Dubinsky et al. 1986). Furthermore, the apparent taxonomic differences between the phytoplankton communities of the two sites could, in part, account for actual divergence in values of $1/n_{PSII}$ (see *table 4.1.*).

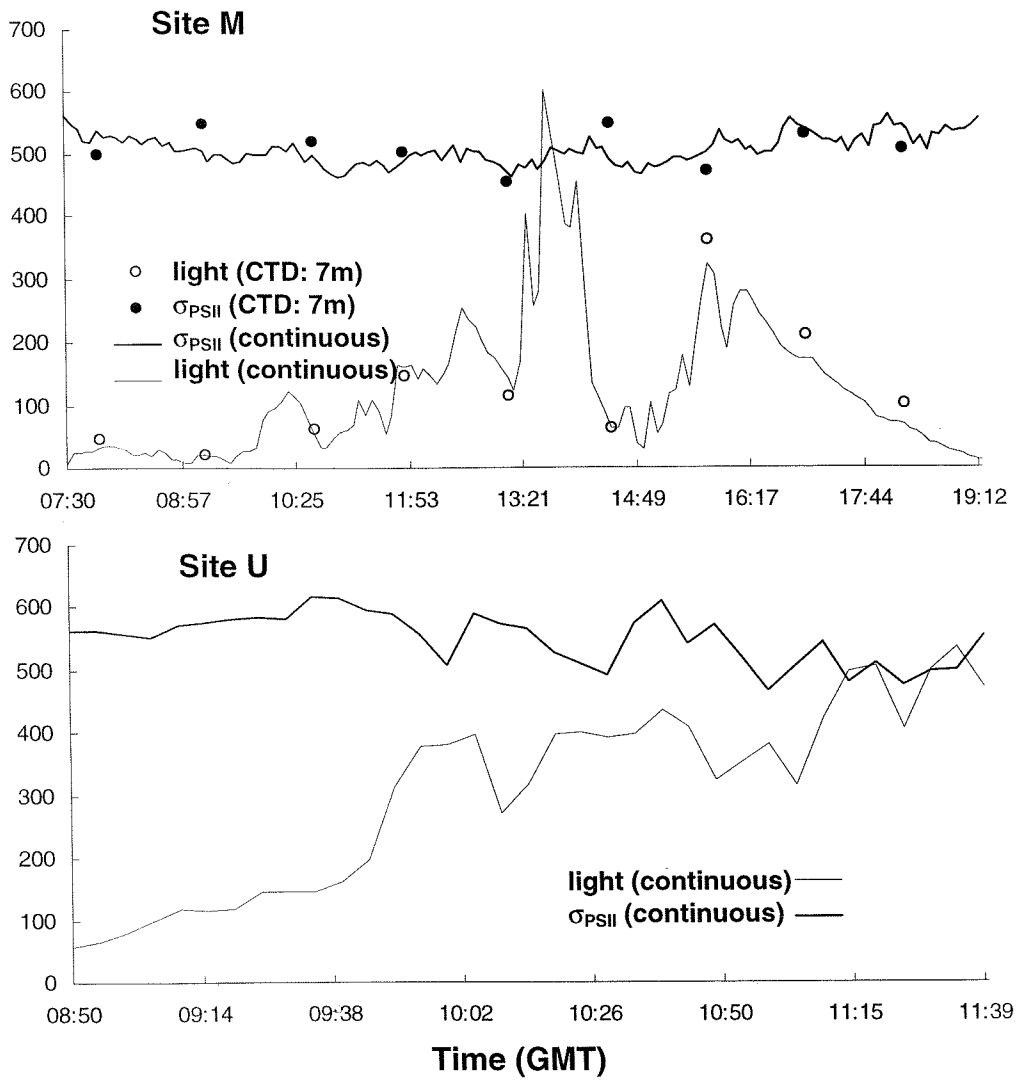

Figure 4.10.— Continuous record of the functional absorption cross section (σ_{PSII}, $Å^2$ $quanta^{-1}$) from the surface seawater supply (7m) and of incident irradiance (µmolphotons m^{-2} s^{-1}) from the ship-mounted PAR sensor. Data were measured whilst at site M. The σ_{PSII} data measured whilst at site U was corrupted. Therefore, the run of data measured in stratified waters immediately prior to the station is presented as a means of comparison. Also shown are the corresponding discrete measurements of σ_{PSII} and PAR from the CTD profiles which were used in *figures 4.5.* to *4.7.* This high resolution FRRF surface data (1 stored acquisition per 2-3s, dark chamber) were 'binned' into 5 minute averages.

Phytoplankton will also attempt to photoacclimate by altering their ability to saturate the number of PSII reaction centres. Different amounts of light harvesting and

photoprotectant pigments relative to $1/n_{PSII}$ will result in changes to σ_{PSII} and to the chl *a*-specific absorption (a*). The mean of all σ_{PSII} values measured at night (to minimise any differences associated with fluorescence quenching) are significantly higher (t-test$_{1, 827}$ = 3.804, $p<0.001$) at station U (694.34 Å^2 quanta^{-1}) than at site M (629.37 Å^2 quanta^{-1}). This indicates that the PSIIs of phytoplankton at site U become saturated at relatively lower light energy levels but does not conform with the suggestion that these phytoplankton are acclimated to higher light intensities. Phytoplankton cells in surface waters at site U experience very low nutrient concentrations (see *table 4.2.*). Nutrient limitation produces elevated values of σ_{PSII} since the functional antennae typically serves fewer PSII reaction centres and can, therefore, saturate them faster (eg. Falkowski 1992). The higher values of σ_{PSII} observed in the surface waters of site U coincide with reduced values of F_v/F_m which are also indicative of nutrient limitation (Kolber *et al.* 1988). Nutrient limited cells are more susceptible to the effects of light (eg. photoinhibition, Falkowski *et al.* 1994) and this may have contributed to the daytime reduction of both F_v/F_m and σ_{PSII} in the surface waters at both sites. Values of σ_{PSII} at site U remain elevated at and below the thermocline perhaps indicating a separate lower-light acclimated phytoplankton population which can successfully maintain the high levels of production and biomass.

All values of a*, except at 555nm, are higher at site U than at site M. In addition, values of a* at site M remain constant from the depths at which samples were taken. Conversely, a* from site U are significantly lower at the thermocline than in surface samples. These differences can occur through changes in pigment composition and the 'package effect' (Falkowski and La Roche 1991, Bricaud *et al.* 1995), *see section 1.1.* The highest concentrations of photosynthetic pigments:chl *a* (*fig. 4.4.*) and chl *a* (*fig. 4.3.*) were found at site M and in the thermocline samples of site U. This results in more light absorption (m^2, data not shown) but reduced values of chlorophyll *a*-specific absorption (m^2 mgchl a^{-1}) and is evidence of pigment packaging (eg. Allali *et al.* 1997). This further suggests that the phytoplankton populations at site M and in the thermocline region at site U were both acclimated to relatively low light conditions. Phytoplankton cells reduce the amount of chl *a*/cell and increase their cell volume, thereby reducing the degree of pigment packaging, in response to nutrient starvation (Berges *et al.* 1996) and high light (Berner *et al.* 1989). As such, the relatively high values of a* observed in the surface

[strongly stratified, high light] waters of site U may be considered as a combination of forcing factors. Alternate mechanisms contributing to this apparent pigment packaging, for example, number of chloroplasts per cell number and thylakoid stacking (eg. Berner *et al.* 1989, Sukenik *et al.* 1990) were not considered and subsequently investigated at the time of sampling but could provide a more detailed explanation regarding the changes to σ_{PSII}, F_v/F_m and a*.

Validation of n_{PSII} estimations— The range of $1/n_{PSII}$ (molchl *a* molRCII^{-1}) calculated for both sites M and U fall within previously cited values (see *table 4.1.*). Acclimation to relatively low light levels (eg. Falkowski *et al.* 1981, Dubinsky *et al.* 1986) correspond with higher values of $1/n_{PSII}$ at site M compared to site U. At site U, conditions of nutrient starvation (eg. Berges *et al.* 1996) may have contributed to the higher $1/n_{PSII}$ in [dark adapted, 02:00 GMT] surface samples. These acclimations reflect the balance of reductions in chl *a*/cell versus those of RCII/cell (Falkowski *et al.* 1981, Berges *et al.* 1996). Barlow and Alberte (1985) measured an increase of $1/n_{PSII}$ when phytoplankton (*Synechococcus*) were subjected to photoinhibition. A decrease in values of both F_v/F_m and P^{chl} was observed in the surface stratified layers of both sites U (30-32m) and M (0-10m) when irradiance was highest and is indicative of photoinhibition (eg. Falkowski *et al.* 1994); however, $1/n_{PSII}$ did not correspondingly increase. Previous estimations of n_{PSII} (*table 4.1.*) have been confined to phytoplankton cultures in the laboratory, presumably as a consequence of the sensitivity of oxygen electrodes used for the technique (eg. Mauzerall and Greenbaum 1989). In addition, no other field data of FRRF and corresponding a* values appears evident in current literature for the derivation of n_{PSII} following *equation 4.1.* Therefore, there is a lack of data with which to compare variations of n_{PSII} observed in this field investigation. A consideration of the kinetics of PSII activity under laboratory and *in situ* conditions may, in part, account for the n_{PSII} variations at sites M and U:

Laboratory investigations relevant to n_{PSII} typically allow cultures of single species to acclimate over a period of several days. Throughout this period, changes in mol chl *a*/cell occur at nearly twice the rate of corresponding changes in mol RCII/cell when acclimating to low light (Sukenik *et al.* 1990). Only after a period of approximately 72 hours are new steady state values reached. If it is assumed that this is also true for

phytoplankton cells exposed to prolonged increases in light throughout the day then it is possible that the observed surface values of $1/n_{PSII}$ remain low because the rate of chl *a*/cell reduction exceeds that of RCII/cell loss at this scale. As such, phytoplankton cells *in situ* would not have the same time period of acclimation as those in the laboratory.

Chlorophyll *a*-specific absorption describes the mean target for the absorption of photons within a cell (Falkowski *et al.* 1994) and can, therefore, reflect the [chl *a*] per cell volume. A closer look at changes of a* shows that this parameter responds to increases in light at a faster rate than corresponding changes of σ_{PSII} and *f*, *fig 4.11.*, at both sites (although data from site M is not statistically significant, see figure legend). The parameter *f* represents the number of functional reaction centres whilst σ_{PSII} is related to the average size of the antennae composed of light harvesting proteins (Falkowski 1992)

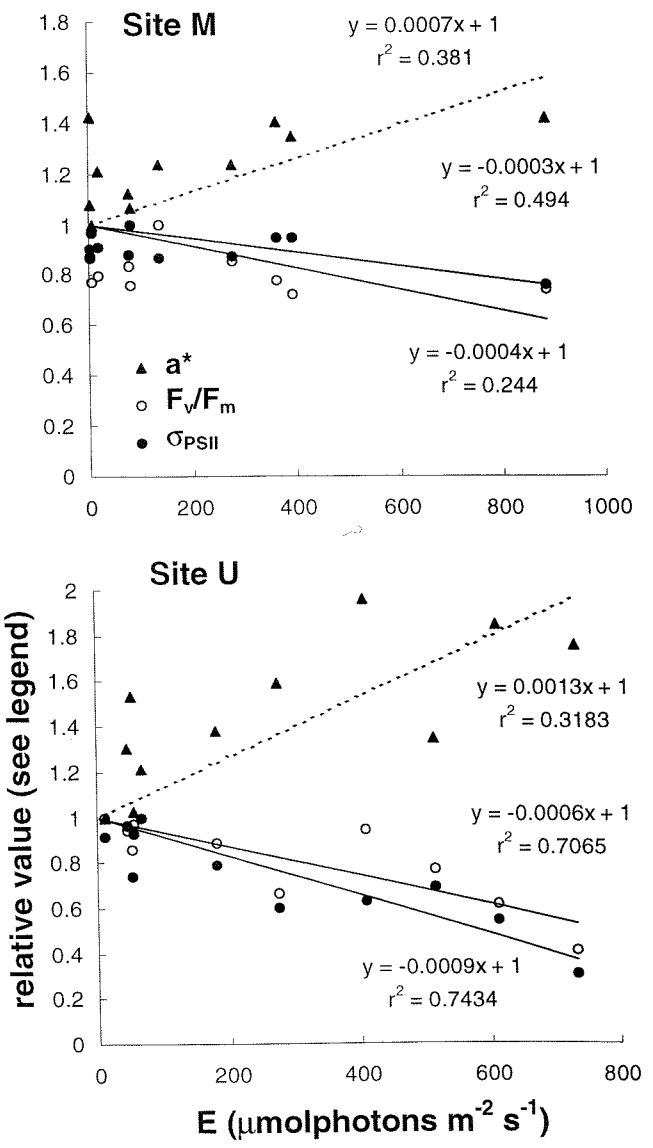

Figure 4.11.— Regression between PAR and relative values of chlorophyll *a*-specific absorption (a*), effective absorption cross section (σ_{PSII}) and the quantum efficiency (F_v/F_m). All values of a* were divided by the lowest determined value to observe the relative increase in this parameter. Conversely, all corresponding values of σ_{PSII} and F_v/F_m were divided by the highest determined value to observe the relative decrease of these parameters. The relative change of each parameter, with respect to irradiance, is indicated by the gradient of the relationship. n= 11 for each parameter at both sites. $P<0.001$ except site M: a* ($0.05>p>0.02$), σ_{PSII} ($0.01>p>0.005$), F_v/F_m ($0.2>p>0.1$) and site U: a* ($0.1>p>0.05$).

and is influenced by both changes in antennae quenching and f (see above). The relative rate of a* increase (chl *a*/cell volume reduction) exceeds the loss of RCII (f), hence relatively less chl *a* serves the number of RCII thereby reducing the rate at which RCII saturation can occur (combined with non-photochemical quenching processes in the antennae) to produce lower values of σ_{PSII}. In terms of *equation 4.3.*, (essentially $\sigma_{PSII}/[a^* . f]$) the product of the a* increase and σ_{PSII} decrease exceeds the corresponding decrease in f, and $1/n_{PSII}$ will decrease. Therefore, it would appear that the decrease in $1/n_{PSII}$ with increasing light [at this diurnal time scale] is a function of the greater relative changes in pigment than of functional reaction centres.

Similar data concerning a*, σ_{PSII} and f for *Synechococcus* from the strongly stratified site of the *RV Pelagia* cruise (site 3, 37°N 23°W, *Chapter 3*) can also be considered as a

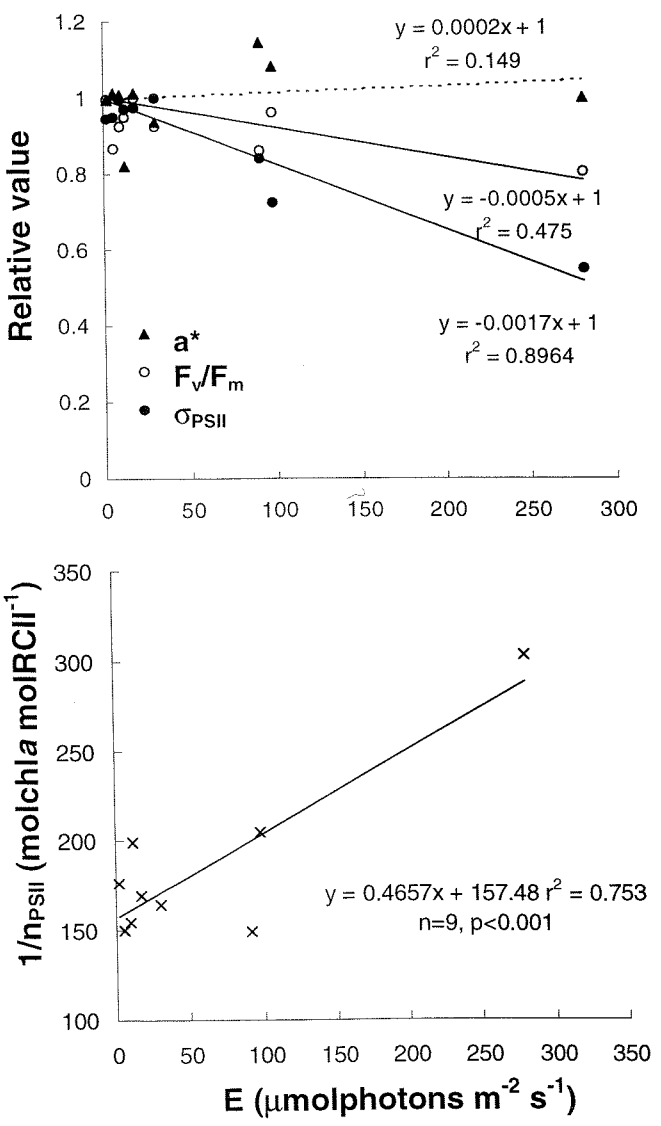

Figure 4.12.— (upper panel) regressions between PAR and relative changes in a*, σ_{PSII} and F_v/F_m (see *figure 4.10.* legend for a more detailed description following calculations of these parameters); (lower panel) regression between corresponding data of the number of reaction centres ($1/n_{PSII}$) and PAR using the data from the upper panel and following *equation 4.3.* This data is taken from the strongly stratified site 37°N 23°W from the RV *Pelagia* cruise and is described in more detail in *Chapter 3.* This site was dominated by populations of *Synechococcus.* n=9, a* (0.5> p>0.2), σ_{PSII} (0.05>p>0.02), F_v/F_m (p<0.001).

means of comparison (*fig 4.12.*). With an increase in light, a* shows no significant change whilst σ_{PSII} decreases at a similar rate to that seen above. *f* (the proportion of functional reaction centres) decreases at a relatively greater rate. As such, the rate of RCII loss exceeds corresponding losses of chl *a*/cell volume. This should result in an increase in σ_{PSII} since the available chl *a* serves fewer RCIIs and PSII saturation can occur relatively faster. However, it is clear from *fig. 4.12.* that σ_{PSII} decreases, presumably as a result of additional quenching processes. In terms of *equation 4.3.*, the reduction in *f* exceeds the product of changes to a* and σ_{PSII}. The lack of change in a* presumably reflects the already small cell size and the low cellular chl *a* content of *Synechococcus*. The product of these changes is an increase of $1/n_{PSII}$ with an increase in light (*fig. 4.12.*) and is in agreement with the results of Barlow and Alberte (1985).

Conclusions— Phytoplankton display general photoacclimation differences in n_{PSII}, σ_{PSII} and a* and pigment content under the different light climates at the 2 sites. However, the use of n_{PSII} and σ_{PSII} may confound this interpretation where taxonomic and trophic differences (respectively) also exist between the sites. The significant differences in a* and σ_{PSII} throughout the water column at site U compared to site M indicates that mixing rates are, in general, lower than the time scale required for acclimation. Changes in a* are also observed at different depths of the water column at site U and correlate with corresponding values of light (*fig. 4.11.*). This suggests that phytoplankton display significant acclimation *in situ* or, more likely, reflects a diel rhythm in cellular chlorophyll *a* (Owens *et al.* 1980). Evidence of smaller-scale changes of σ_{PSII} also appears to reflect the time scale of water column mixing but remains uncertain given the lack of data.

The novel calculation of n_{PSII} (using *in situ* data) described here appears to give absolute values which conform within the limits of values obtained from the oxygen flash yield technique upon phytoplankton cultures in the laboratory (*table 4.1.*), given the respective limitations. It is clear that the environmental dynamics experienced by phytoplankton under natural conditions are vastly different to those applied in the laboratory. As such, these initial results appear promising given an absence of existing n_{PSII} *in situ* observations and the limited understanding of the kinetics of cellular components under combined light-nutrient regimes both *in situ* and in the laboratory. However, a, proper validation of this technique is required before these results can be considered firmly

conclusive. The significant *in situ* n_{PSII} variability throughout a variety of temporal and spatial scales is likely to be of considerable consequence to the calculation of production using the FRRF (see *section 1.4.*), and is pursued in *Chapter 6.*

5. Variability of phytoplankton physiology and production throughout the Atlantic Ocean

5.1. Introduction

The variability of primary production rates is predominantly a function of light (Kirk 1994), nutrients (Marañón and Holligan 1999, Marañón *et al.* 2000) and temperature (Behrenfeld and Falkowski 1997a, b). The most recent observations within the Atlantic using both ^{14}C-uptake (Marañón and Holligan 1999) and fluorescence induction techniques (Geider *et al.* 1993, Babin *et al.* 1996, Behrenfeld *et al.* 1996, Olaizola *et al.* 1996, Behrenfeld and Kolber 1999) underline that nutrients are the most significant variables to drive the variability of photosystem performance, and ultimately, production. However, this does not preclude the importance and predominance of the effects of light and temperature under certain conditions.

This investigation aims to assess the variability of phytoplankton physiology and production throughout biogeographic provinces of the Atlantic. Broad-scale sampling was accomplished by performing CTD casts at regular intervals (10:00-11:00 local time each day). As a result, diurnal effects upon fluorescence signal variability (*Chapters 3* and *4*) between samples should be minimal. An analysis of the broad-scale relationships between taxonomy (using HPLC data) and physiology (FRRF) will provide a general description of photoadaptive characteristics, and will be considered in terms of the light-nutrient environment. Furthermore, a continuous FRRF assessment of the surface water will be used to describe the spatial scales at which PSII physiological variability occurs (in relation to corresponding scales of hydrographical variability) throughout the Atlantic Ocean. Following the relationships that have been observed between PSII variability and environmental variability (*Chapters 3* and *4*), it is expected that biological variability should reflect the nature of the predominant physical processes in the respective

biogeographic provinces.

General Hydrography

The cruise transect followed a course from Cape Town (34°S 18°E) to the U.K. (50°N 1°W) and traversed a number of biogeographic provinces (*fig. 5.1.*). These provinces are summarised from descriptions by Longhurst (1993), Longhurst *et al.* (1995), Sathyendranath *et al.* (1995):

The open ocean provinces fall within 2 domains: The most northerly open ocean provinces of the transect are within the westerlies wind domain which sets up conditions for algal spring blooming (see *section 3.2.*). These provinces are the north Atlantic drift (NADR: 40°N to 60°N) and the north Atlantic subtropical gyre (NAST: 25°N to 40°N). This gives way to the trade winds domain at approximately 30°N which encompasses the rest of the open ocean provinces traversed by this cruise. These provinces are characterised by a shallow permanent pycnocline of very high stability and an excess of precipitation over evaporation. The mixed layer depth, the column of well mixed surface water above the thermocline, changes seasonally as a geostrophic response to the wind field, whilst breakdown of the pycnocline and nutrient renewal into the mixed layer only occurs at strong divergences. Provinces within this domain are the north Atlantic tropical gyre (NATR: 25°N to 10°N) and the eastern tropical Atlantic (ETRA: 10° N to 15° S, eastwards of the 20°W hingeline of seasonal basin scale tilt). Such boundaries are not static and consistent features associated with the nutrient-field and phytoplankton activity of ETRA (described later) were observed to change north of approximately 6-7°N. As such, the boundary between NATR and ETRA is defined as this transition (6-7°N) for the purposes of this study.

The NATR province can be further sub-divided into 2 distinct hydrographic regions. The northern leg of the NATR crossing (17°N to 25°N) is characterised by waters of relatively high chl *a* concentration (*fig. 5.1.*) as a result of upwelling activity originating from the Canary Current coastal province (CNRY: 15°N to 43°N). However, the area 17°N to 25°N will be referred to as the northwest African upwelling (NWA) province

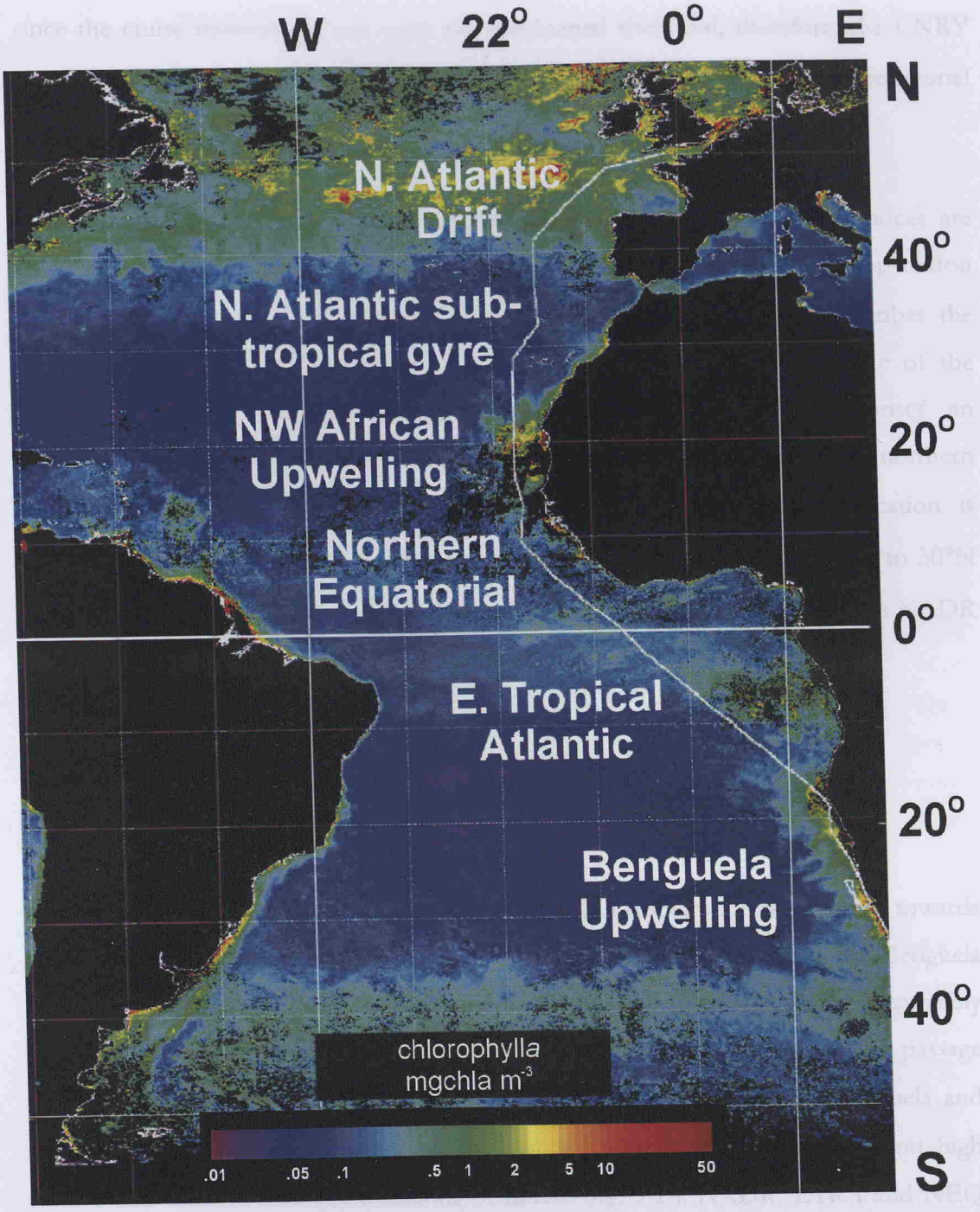

Figure 5.1.— AMT 6: Cruise track of RRV James Clark Ross, Cape Town (34°S 18°E) to the U.K. (50°N 1°W), 15th May to 16th June 1998. Track is superimposed onto SeaWiFS composite image of chl*a* concentration taken throughout May and June 1998. The track traversed a number of biogeographic provinces (described by Longhurst *et al.* 1995, Sathyendranath *et al.* 1995): Benguela upwelling (southern Benguela: **SB**: 33-27°S; northern Benguela: **NB**, 27-18°S°), Eastern tropical Atlantic (**ETRA**: 15°S-6°N), Northern equatorial (**NEQ**: 6-17°N), North-west African upwelling (**NWA**: 17-25°N), North Atlantic subtropical gyre (**NAST**: 25-40°N), North Atlantic drift (**NADR**: 40-60°N). Note that for the purposes of data presentation, the NADR province also encompasses the north-east Atlantic continental shelf (**NECS**) when the cruise-track finished at the U.K. (50°N).

since the cruise transect did not enter the continental shelf and, therefore, the CNRY province. The remainder of NATR (6°N to 17°N) encompasses the northern equatorial and hence will be referred to as the NEQ province.

Several coastal provinces were also sampled along this transect. These provinces are characterised by dynamic hydrographies which promote high levels of phytoplankton biomass and production. The Benguela system (BENG: 18°S to 40°S) describes the upwelling off the south west coast of Africa. The principal upwelling centre of the Benguela system is located around Lüderitz (27°N 15°E), and comprises an environmental barrier so that the Benguela system is effectively divided into northern (NB) and southern (SB) components (Pitcher *et al.* 1992). This classification is maintained for this study. The north Atlantic drift region (NADR: 40°N 18°E to 50°N 1°W) will be used to describe the final leg of the transect which traversed both NADR but also NECS (the north-east Atlantic continental shelf).

5.2. Province characteristics based on broad-scale sampling

CTD profiling— Surface water temperature (*fig. 5.2.*) displays a clear increase towards the equatorial provinces but the gradient is more abrupt moving from the Benguela (southern hemisphere) than from northern hemisphere provinces. This presumably reflects the cruise track which sampled the Benguela close to the coast whilst the passage through north-west African waters was further offshore (*fig. 5.1.*). The Benguela and NWA provinces are characterised by shallow mixed layer depths (15-30m) and high surface and near-surface concentrations of nitrate (*fig, 5.2.*). NADR, ETRA and NEQ provinces display deeper mixed layers and nutriclines (50-60m). The NAST province is characterised by a deep thermocline (100-140m) and low concentrations of nitrate throughout the upper 150m of the water column. The nutricline and thermocline are defined as the zone of sharp change in nutrients and temperature, respectively, from surface to deep waters (see also p.12).

Nitrate concentrations (*fig. 5.2.*) closely follow those of phosphate ($[NO_3] = 14.281 [PO_4] - 0.0377$, $r^2 = 0.91$, $n = 161$). Nitrite concentrations (*fig. 5.2.*) display surface and

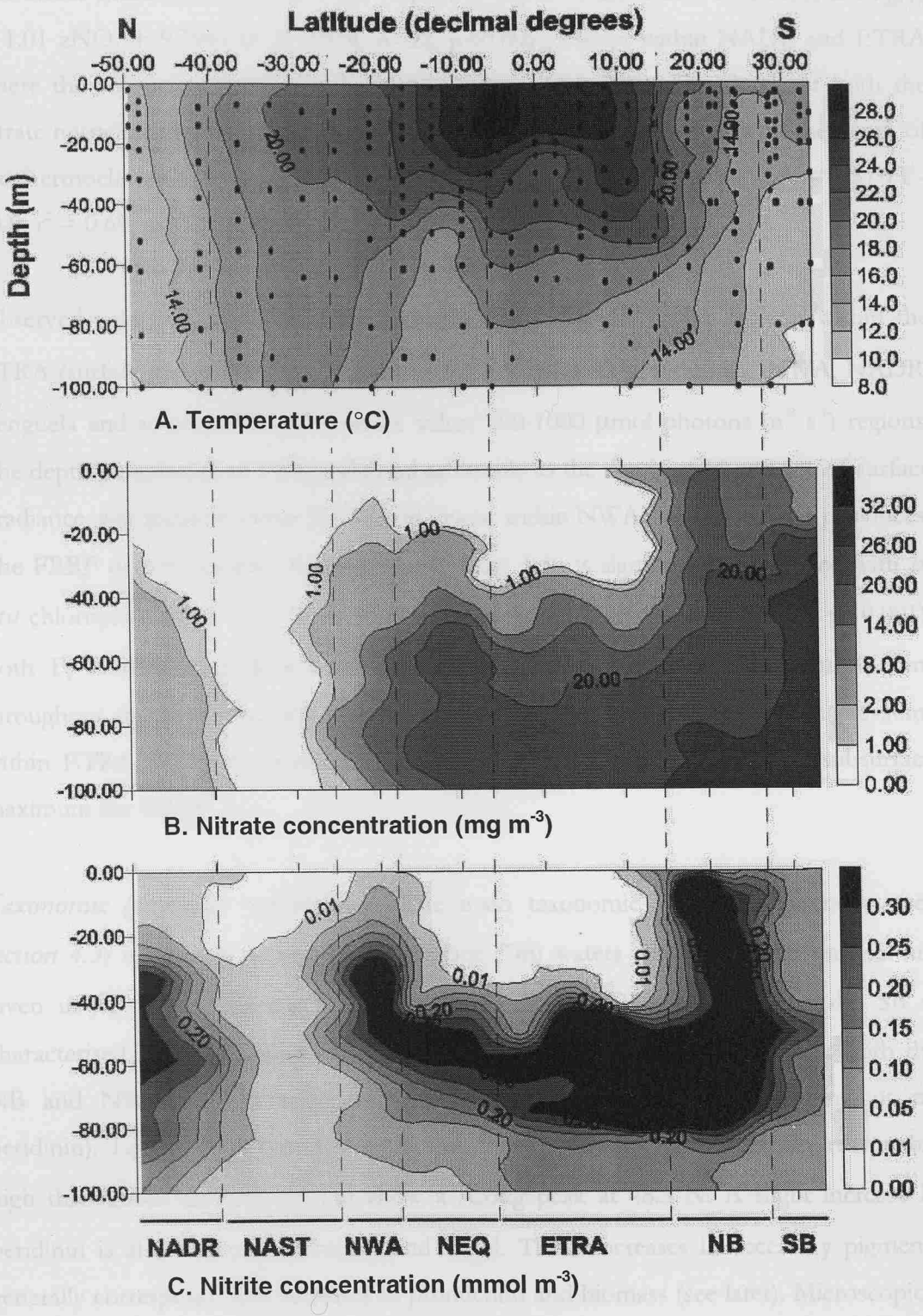

Figure 5.2.— Changes in parameters within the upper 100m of the water column, as collected from CTD casts throughout the AMT 6 transect. Black circles in upper panel represent sample points for (A) Temperature (°C) (B) Nitrate concentration [NO_3] (mmol m^{-3}) (C) Nitrite concentration [NO_2] (mg m^{-3}). Time of each CTD cast was approximately 10:00-11:00 local time. Transect has been divided into respective biogeochemical provinces (Longhurst *et al.* 1995) and are described in more detail in *section 5.2.*

subsurface maximum and follow the respective depth of the nitrate nutricline, zNO_{2MAX} = 1.01 zNO_3 + 9.7943 (r^2 = 0.914, n=22, p<0.001), except within NADR and ETRA where the subsurface maximum becomes shallower (10-20m). The depth of both the nitrate nutricline and the nitrite maximum display a strong relationship with the depth of the thermocline, zNO_3 = 1.52 zT - 21.8, r^2= 0.81, n = 23, p<0.001; zNO_{2MAX} = 1.57 zT - 13.9, r^2 = 0.69, n = 23, p<0.001.

Observed values of water column irradiance (PAR: *fig. 5.3.*) were highest within the ETRA (surface value: 2400 µmol photons m^{-2} s^{-1}) and lowest within the NWA, NADR, Benguela and southern NAST (surface value: 800-1000 µmol photons m^{-2} s^{-1}) regions. The depth penetration of PAR, indicated arbitrarily as the depth of 10 and 1% of surface irradiance, was greatest within NAST and lowest within NWA, SB and NADR provinces. The FRRF derived variable fluorescence (F_v: *fig. 5.3.*) is significantly correlated with *in situ* chlorophyll *a* (*fig 5.3.*), (F_v = 9.9818 [chl *a*] + 7.0022; r^2 = 0.401, n=207, p<0.001). Both F_v and chlorophyll *a* have high surface and near-surface maximum (0-25m) throughout the Benguela, NWA and northern NADR, subsurface maximum (40-50m) within ETRA, NEQ and southern NADR provinces, and deep (80-120m) subsurface maximum the NAST.

Taxonomic (pigment) variability— The main taxonomic biomarker pigments (see *section 4.3*) in relation to chl *a* from surface (7m) waters throughout the transect are given in *fig. 5.4.* Following R.Barlow (pers.comm; AMT6 Cruise Rept.), the SB is characterised by dinoflagellates (high peridinin and some fucoxanthin), whilst both the NB and NWA are generally characterised by diatoms (high fucoxanthin but no peridinin). Levels of 19'hexanoyloxyfucoxanthin (prymnesiophytes) remain reasonably high throughout the transect but show a strong peak at 48.3°N. A slight increase in peridinin is also evident between 9 and 16°N. These increases in accessory pigments generally correspond with increases in production and biomass (see later). Microscopical analysis of water samples confirmed that the SB phytoplankton community was dominated by *Ceratium* spp. (Dinophyceaea) whilst that of the NWA was predominantly composed of centric diatoms and *Rhizosolenia* spp. (Bacillariophyceae) together with small flagellates. The increase in phytoplankton pigments and production at 48.3°N was identified as a bloom of *Phaeocystis* spp. (Prymnesiophyceae). The provinces ETRA,

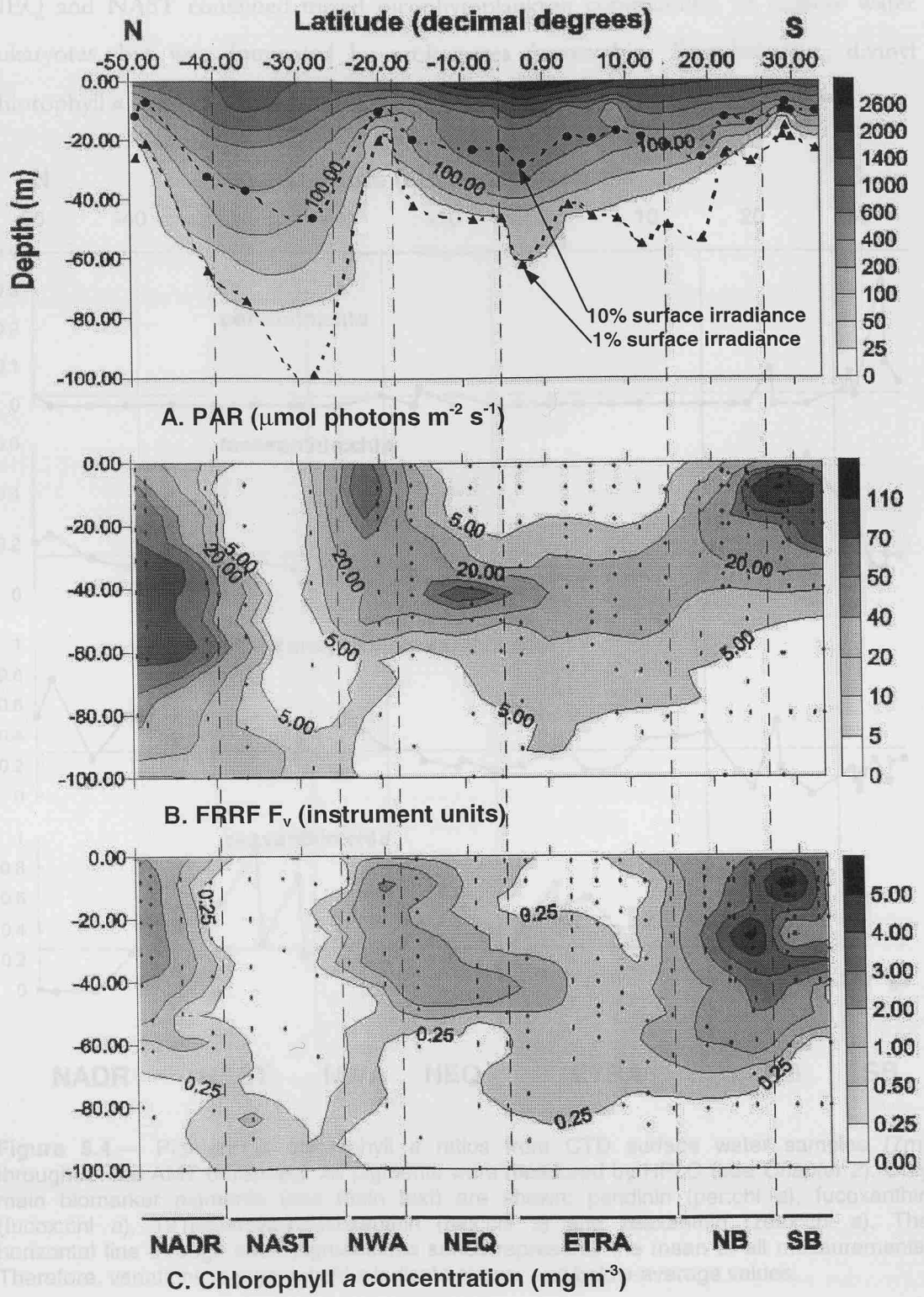

Figure 5.3.— Changes in parameters within the upper 100m of the water column throughout the AMT 6 transect. Panels (A) PAR (μmol photons m^{-2} s^{-1}) and (C) chlorophyll *a* concentration (mg m^{-3}) are taken from CTD casts/ water samples. The depths of 10 and 1% of surface irradiance from each cast are also indicated in panel (A). Data in panel (B) Fluorescence yield (F_v: instrument units) are taken from FRRF measurements. Filled circles in lower 2 panels represent sample points for the 2 forms of data collection. Time of each CTD cast was approximately 10:00-11:00 local time. Transect has been divided into respective biogeochemical provinces as in *figure 5.2.*

NEQ and NAST contained mixed picophytoplankton communities of shallow water eukaryotes, but was dominated by prokaryotes (zeaxanthin- *Synechococcus*,; divinyl chlorophyll *a* (dvchl *a*)- *Prochlorococcus*).

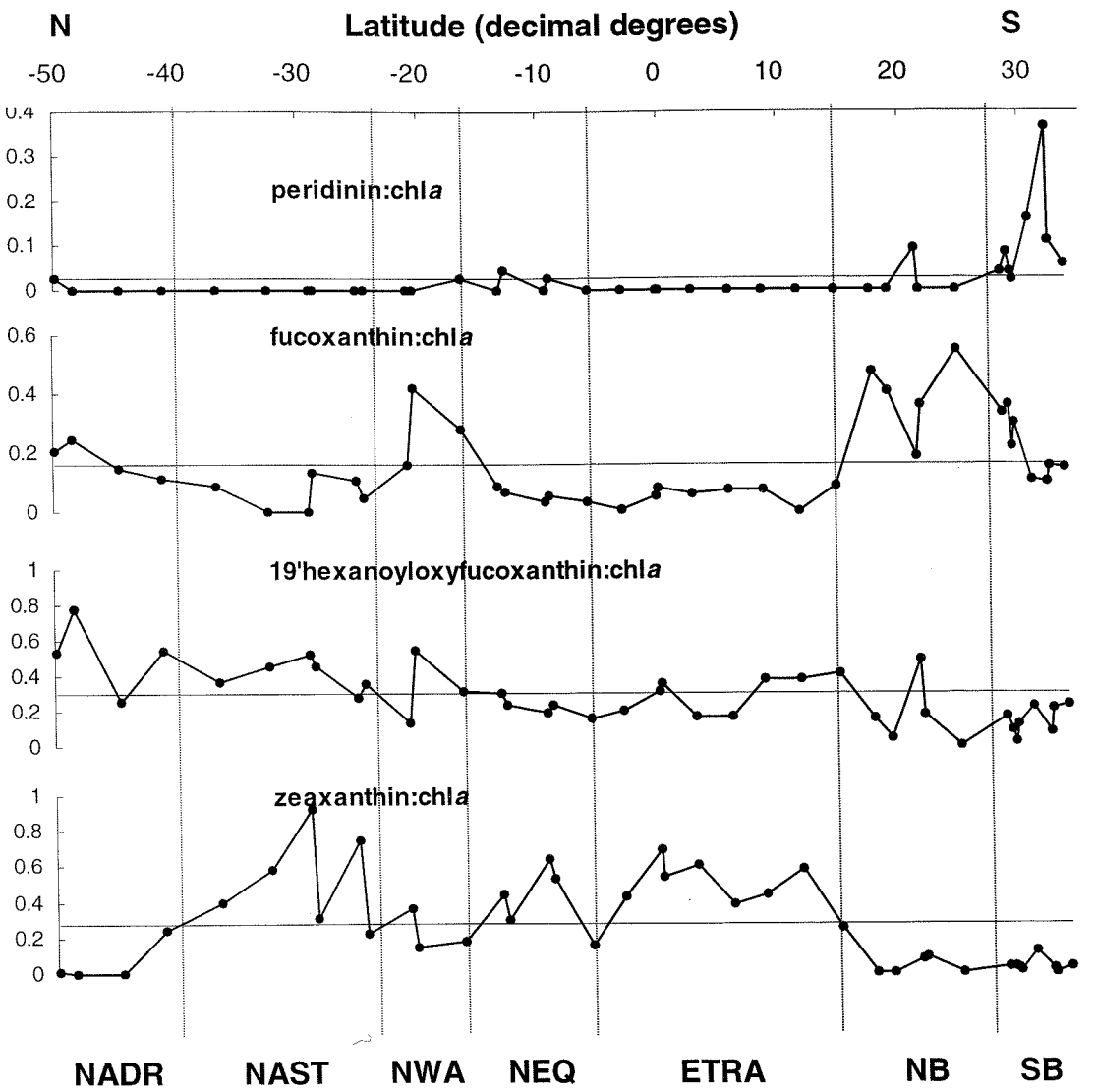

Figure 5.4.— Pigment to chlorophyll *a* ratios from CTD surface water samples (7m) throughout the AMT 6 transect. All pigments were measured by HPLC (see *Chapter 2*). Only main biomarker pigments (see main text) are shown: peridinin (per:chl *a*), fucoxanthin (fucox:chl *a*), 19'hexanoyloxyfucoxanthin (hex:chl *a*) and zeaxanthin (zeax:chl *a*). The horizontal line through each pigment:chl*a* series represents the mean of all measurements. Therefore, variations in pigment:chl *a* indicate above- and below-average values.

Numbers of picophytoplankton were highest in ETRA and NEQ and were largely composed of *Prochlorococcus*; *Synechococcus* were most abundant in the surface waters of NAST and NWA (M. Zubkov, pers.comm). These differences are reflected by the concentrations of dvchl *a* (relative to total chl *a*, *fig 5.5*) and zeaxanthinn (*fig 5.4.*),

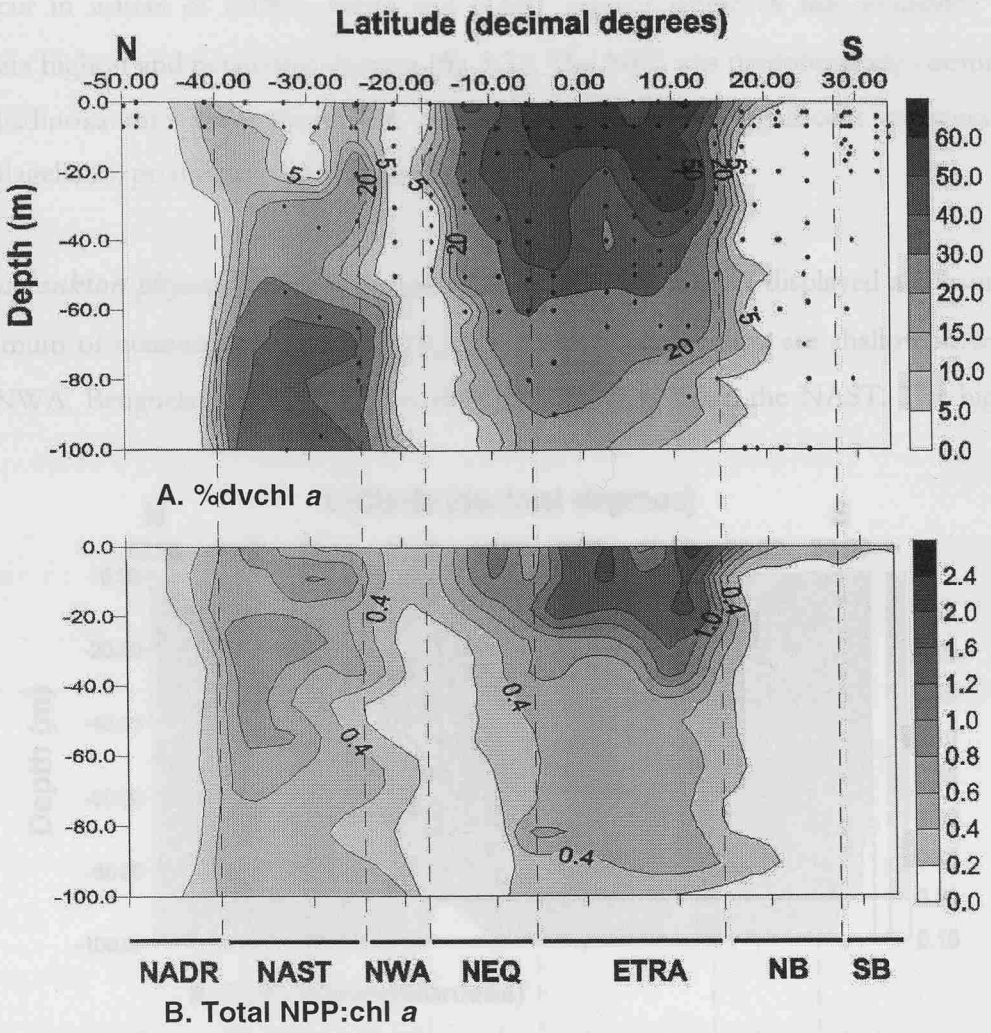

Figure 5.5.— Changes in parameters within the upper 100m of the water column throughout the AMT 6 transect collected from CTD casts. Panels (A) %dvchl *a* (of total chl *a* = dvchl *a*/dvchl *a* + chl *a*) and (B) total NPP:chl *a* (the ratio of the sum of all non-photosynthetic pigments to chlorophyll *a*). Non-photosynthetic pigments assigned according to Bidigare *et al.* (1990): zeaxanthin, antheraxanthin, violaxanthin, diatoxanthin and diadinoxanthin. Zeaxanthin is also found in Cyanophyceae (*Synechococcus*) and may indicate the relative abundance of this taxa. Time of each CTD cast was approximately 10:00-11:00 local time.

respectively. The chl *a*, F_v and %dvchl *a* maximum occur at similar depths (80-100m) in the NAST region. Conversely, the surface maximum of %dvchl *a* does not coincide with the maximum of chl *a* and F_v (40-50m) within ETRA and NEQ regions. The subsurface biomass maximum in these regions appears to coincide with increases in per:chl *a* and 19'hex:chl *a* (data not shown). As such, these trends imply a stratification of the phytoplankton community comprising surface prokaryote and subsurface eukaryotic dominated populations. The sum of non-photosynthetic pigments (NPP:chl *a*) (see figure text) is also plotted for each data point from above 100m (*fig 5.5.*). The highest NPP:chl

a occur in waters of ETRA, NEQ and NAST regions where *in situ* irradiance also appears highest and penetrates deepest (*fig 5.3.*). The NPP was predominately comprised of diadinoxanthin throughout the transect reflecting the significant presence of dinoflagellates, prymnesiophytes and/or diatoms.

Phytoplankton physiology— All stations throughout the transect displayed a subsurface maximum of quantum efficiency (F_v/F_m: *fig. 5.6.*). These maxima are shallowest within the NWA, Benguela and NADR provinces, and deepest within the NAST. The highest

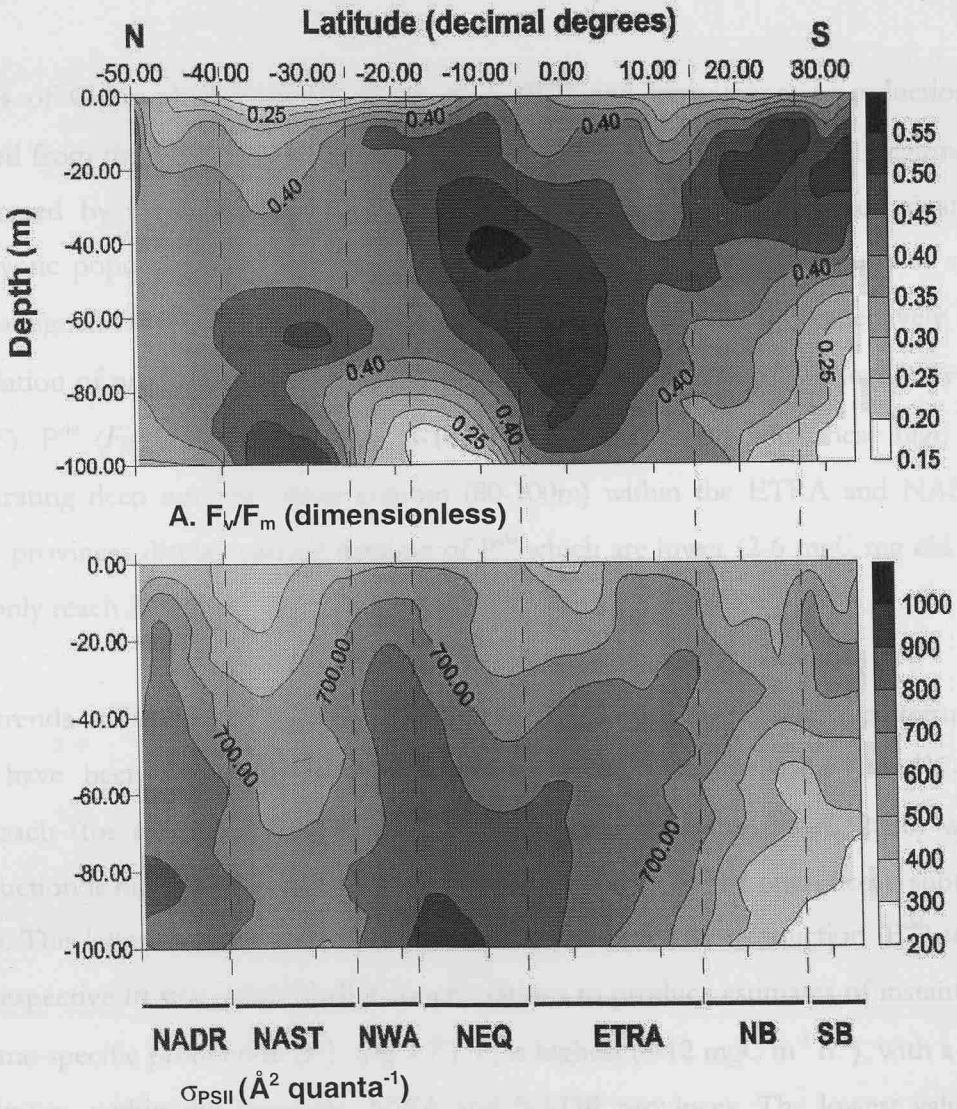

Figure 5.6.— Changes in parameters within the upper 100m of the water column, as measured using the FRRF throughout the AMT 6 transect: (A) Quantum efficiency of photochemistry (F_v/F_m, dimensionless) (B) Functional absorption cross section (σ_{PSII}, Å^2 quanta^{-1}). Sampling points for both data are the same as those given for F_v (*fig. 5.3.b.*). Transect has been divided into respective biogeochemical provinces as in *figure 5.2.*

values of F_v/F_m (0.5-0.6) were observed within ETRA, Benguela and NAST provinces, whilst lowest values (0.4-0.5) were in the NWA and NADR and were uniform throughout most of the water column. The functional absorption cross section (σ_{PSII}: *fig. 5.6*) increased with depth in all provinces, except for the Benguela where there was a near-surface (20-40m) maximum. σ_{PSII} was highest (900-1000 $Å^2$ $quanta^{-1}$) in the NWA, NEQ and NADR regions, whilst lower values (700-800 $Å^2$ $quanta^{-1}$) were observed for the NAST and ETRA. Increases in PAR were reflected in a reduction in surface values of both F_v/F_m and σ_{PSII} at the equator and NAST, but not the surface reduction of F_v/F_m in the southern ETRA or the surface reduction of σ_{PSII} in the northern NB.

Values of Chlorophyll *a*-specific production (P^{chl}) and instantaneous production (P_C) derived from the FRRF are given in *fig. 5.7.* The ETRA, NEQ and NAST regions were dominated by prokaryotic populations, whilst all other regions were dominated by eukaryotic populations (R. Barlow, pers.comm.). Therefore, these 2 groups of regions were assigned values for n_{PSII} of 1/300 and 1/500 molchl *a* $molRCII^{-1}$ respectively for the calculation of production (see *sections 1.3* and *1.4.* for derivation of production with the FRRF). P^{chl} (*Fig. 5.7.*) was highest (6-16 mgC mg chl a^{-1} h^{-1}) with these high values penetrating deep into the water column (80-100m) within the ETRA and NAST. All other provinces display surface maxima of P^{chl} which are lower (2-6 mgC mg chl a^{-1} h^{-1}) and only reach 20-30m.

The trends of P^{chl} derived from the FRRF in *fig 5.7.* do not conform with patterns of P^{chl} that have been previously observed throughout the Atlantic using the ^{14}C-uptake approach (for example, Marañón and Holligan 1999, Marañón *et al.* 2000) whereby production is highest towards coastal provinces and lowest in the open ocean subtropical gyres. This latter distribution is only observed when the FRRF production (P^{chl}) accounts the respective *in situ* chlorophyll *a* concentrations to produce estimates of instantaneous volume-specific production (P_c) (*fig 5.7.*). P_c is highest (8-12 mgC m^{-3} h^{-1}), with a surface maximum, within the Benguela, NWA and NADR provinces. The lowest values (2-4 mgC m^{-3} h^{-1}) of P_c are found in the ETRA, NEQ and NAST where production is observed to penetrate deeper into the water column (80-90m). Very high surface (0-20m) production rates (> 20 mgC m^{-3} h^{-1}) were observed at the station at 48.3°N and correspond with the elevated levels of chl *a* associated with the *Phaeocystis* bloom.

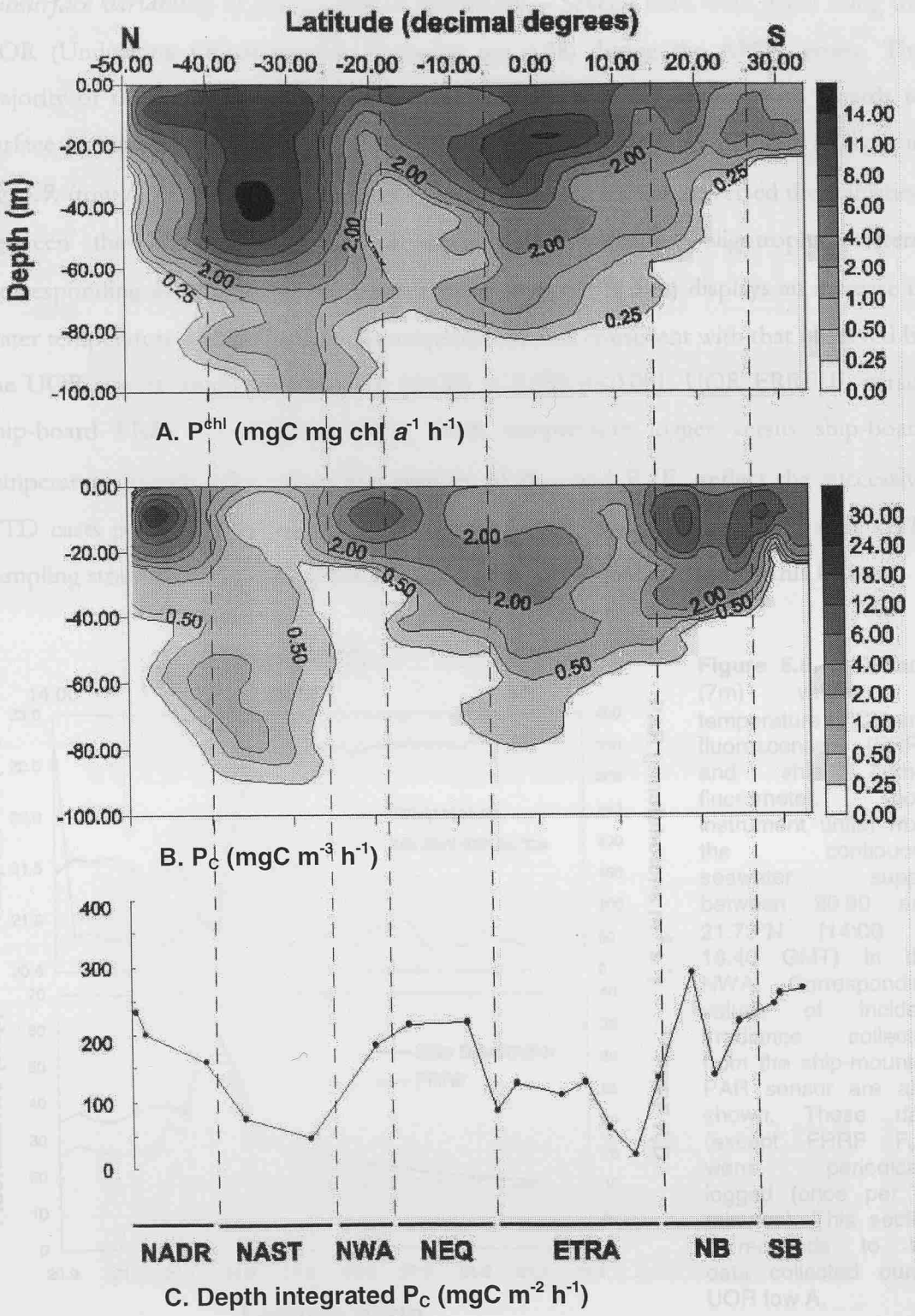

Figure 5.7.— Changes in parameters within the upper 100m of the water column, as derived through FRRF measurements taken throughout the AMT 6 transect: (A) P^{chl} (chlorophyll *a*-specific production: mg C mg chl a^{-1} h^{-1}), (B) P_C (instantaneous production accounting for chlorophyll *a* concentration: mg C m^{-3} h^{-1}). Sampling points for data are the same as those given for F_v (*fig. 5.3.b.*). (C) Values of P_C integrated to 200 meters for each CTD cast. Time of each CTD cast was approximately 10:00-11:00 local time. Transect has been divided into respective biogeochemical provinces as in *figure 5.2.*

Subsurface variability of phytoplankton physiology— Several tows were made using the UOR (Undulating Oceanographic Recorder, see p.38) during the AMT6 cruise. The majority of these describe a general homogeneity of the water column with regards to surface features or a continuum between successive CTD casts; an example is given in *fig. 5.9.* (tow A: 20.89°N 20.00°W - 21.73°N 20.00°W). This tow traversed the transition between the NWA upwelling and more deeply stratified oligotrophic waters. Corresponding surface sample data taken during tow A (*fig 5.8.*) displays an increase in water temperature and decrease in fluorescence which is consistent with that observed by the UOR tow (r^2 of values from 7m (n=32) = 0.553 $p<0.001$, UOR FRRF F_v versus ship-board FRRF F_v; 0.686 $p<0.001$, UOR temperature logger versus ship-board temperature logger). The subsurface changes of σ_{PSII} and F_v/F_m reflect the successive CTD casts performed between the NWA and NAST. As such, the broad scale CTD sampling strategy and surface water analysis appear to adequately describe this feature.

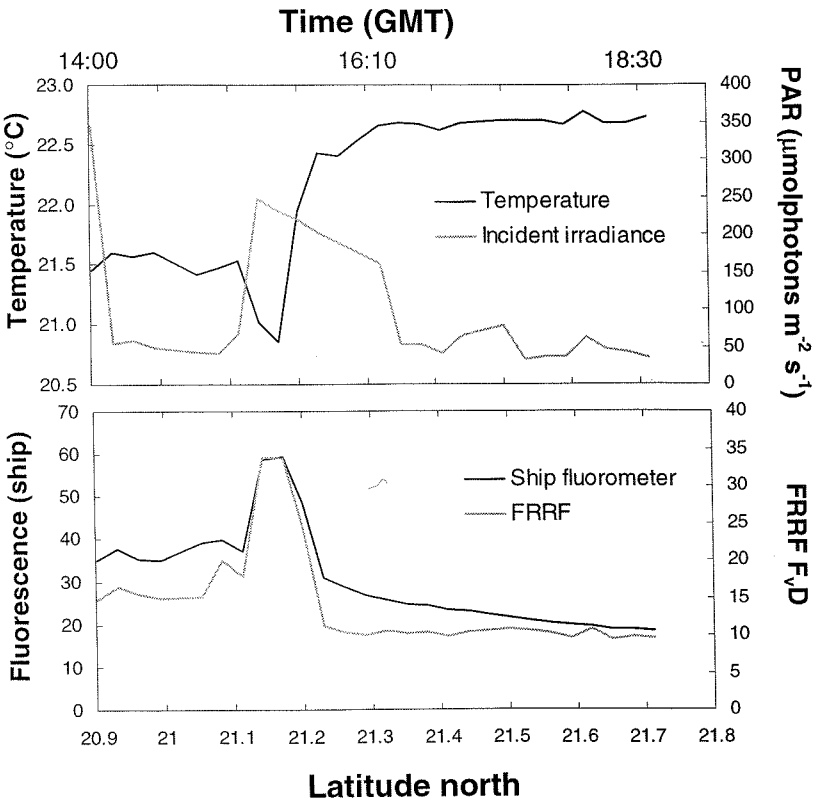

Figure 5.8.— Surface (7m) values of temperature (°C) and fluorescence (FRRF and ship Turner fluorometer, both instrument units) from the continuous seawater supply between 20.90 and 21.73°N (14:00 to 18:40 GMT) in the NWA. Corresponding values of incident irradiance collected from the ship-mounted PAR sensor are also shown. These data (except FRRF F_vD) were periodically logged (once per 10 minutes). This section corresponds to the data collected during UOR tow A.

The most interesting tow (B) was performed in the region of increased fluorescence around the equator (1.10°S 7.43°W to 0.26°S 8.05°W) at night (21:00-02:40 GMT), *fig 5.10.* A shallowing and intensification of the thermocline occurs in the first half of the

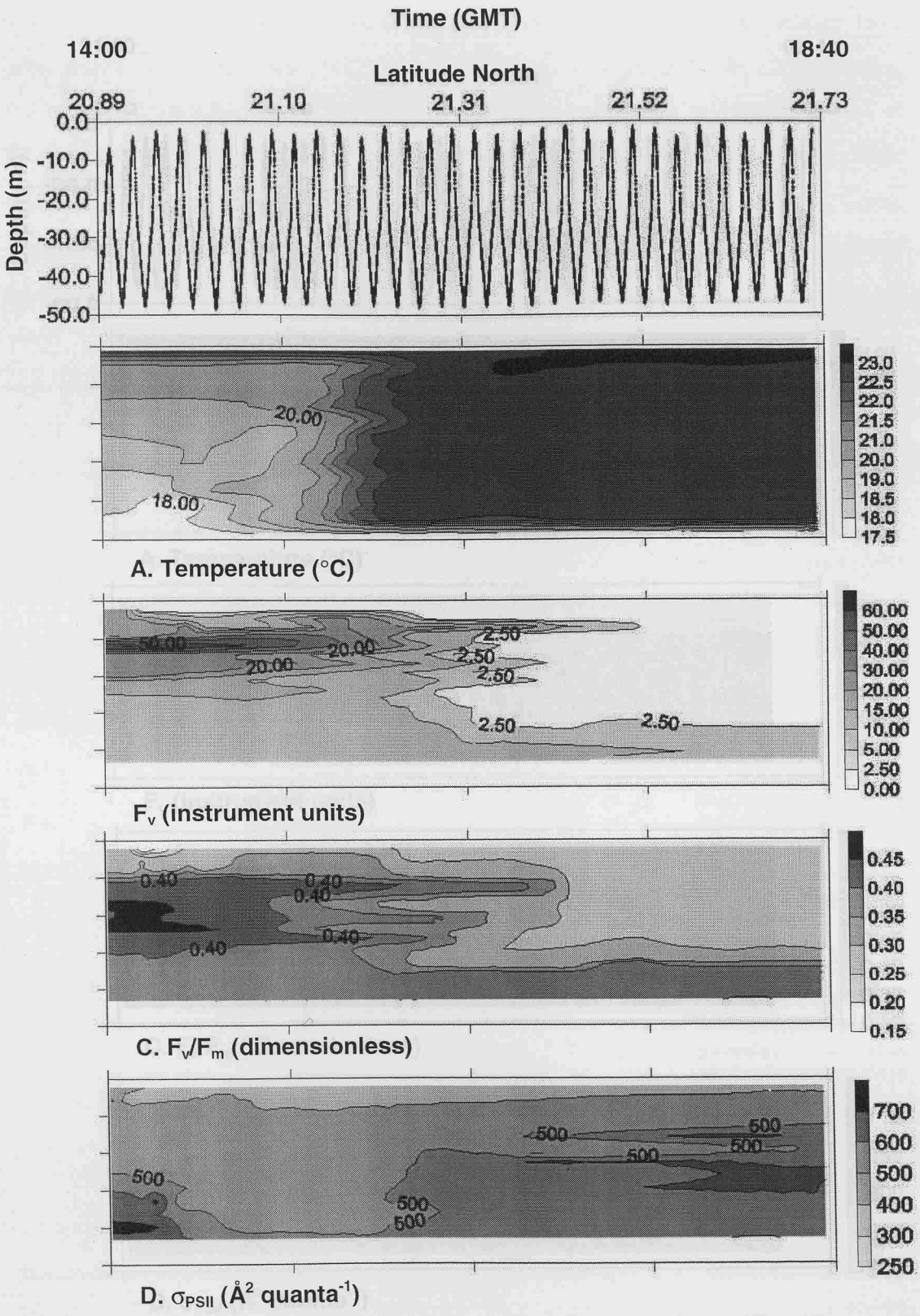

Figure 5.9.— Changes in parameters between 0 and 50 metres from UOR tow (A), AMT 6, between 20.89°N and 21.73°N (14:00 – 18:40 GMT), in the north-west African (NWA) upwelling region. Filled circles in upper panel represent sample points for all data shown in panels (A) Temperature (°C) from data logger and (B) Variable fluorescence yield, F_v, (C) Quantum efficiency of photochemistry, F_v/F_m and (D) Functional absorption cross section of PSII, σ_{PSII} measured with the FRRF. Corresponding surface data are given in *fig. 5.8.*

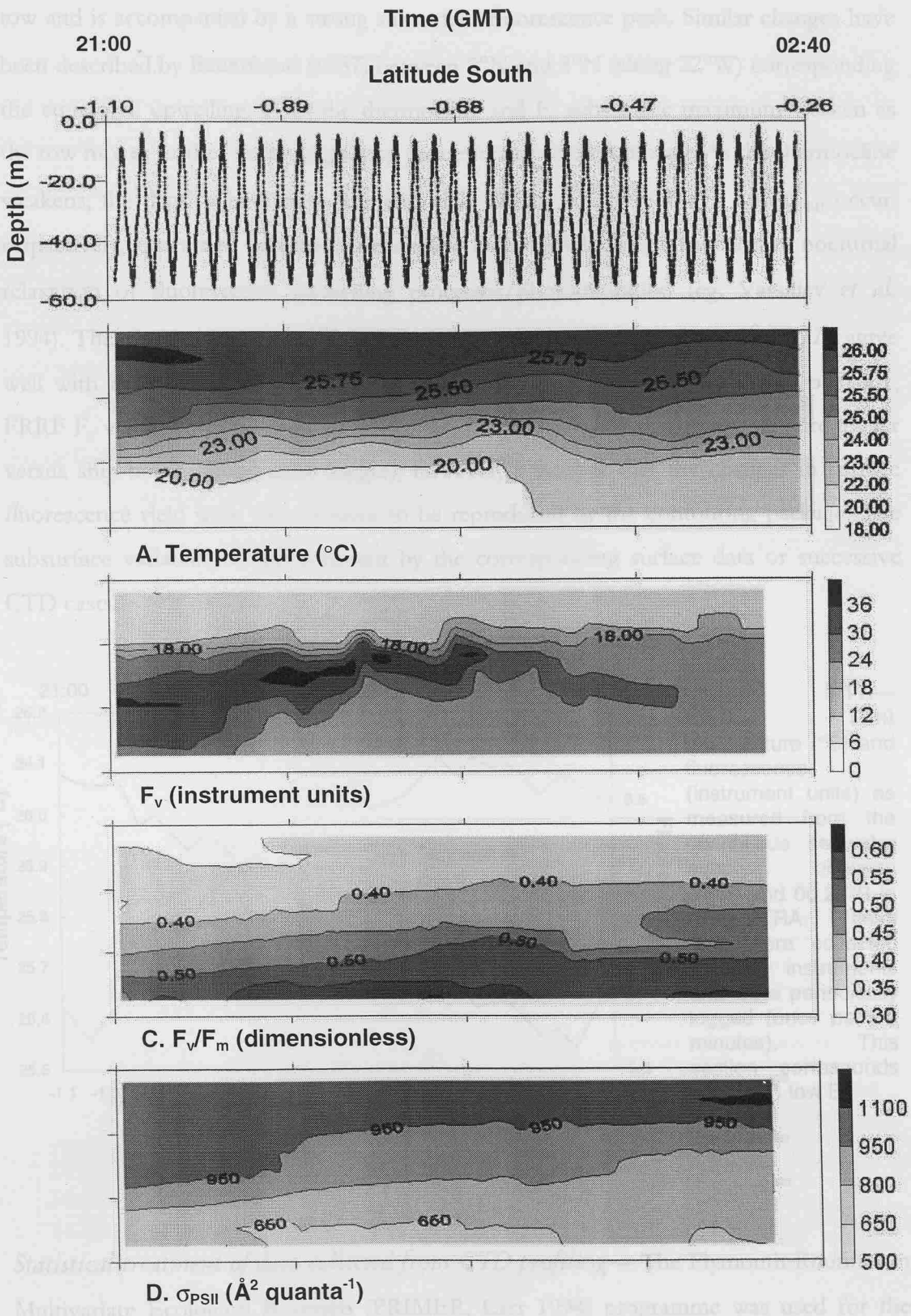

Figure 5.10.— Changes in parameters between 0 and 60 metres from UOR tow (B), AMT 6, between 01.10°S and 00.26°S (21:00 – 02:40 GMT), in the ETRA region. Filled circles in upper panel represent sample points for all data shown in panels (A) Temperature (°C) from data logger and (B) Variable fluorescence yield, F_v, (C) Quantum efficiency of photochemistry, F_v/F_m and (D) Functional absorption cross section of PSII, σ_{PSII} measured with the FRRF. Corresponding surface data are given in *fig. 5.11.*

tow and is accompanied by a strong subsurface fluorescence peak. Similar changes have been described by Bauerfeind (1987) between 2°N and 3°N (along 22°W) corresponding the equatorial upwelling. Both the thermocline and F_v subsurface maximum weaken as the tow moves further north suggesting greater water column mixing. As the thermocline weakens, the depth where both low and high surface values of F_v/F_m and σ_{PSII} occur, respectively, appears to become more shallow and may be partly a function of nocturnal relaxation of fluorescence quenching processes/photoinhibition (eg. Vassiliev *et al.* 1994). The changes in both surface fluorescence yield and temperature (*fig 5.11.*) agree well with those from the UOR tow (r^2 of values from 7m (n=33) = 0.591 $p<0.001$, FRRF F_v versus ship-board fluorescence yield; 0.726 $p<0.001$, UOR temperature logger versus ship-board temperature logger); however, it is clear that the changes in surface fluorescence yield were too sensitive to be reproduced by the contouring package. The subsurface variability is not reflected by the corresponding surface data or successive CTD casts.

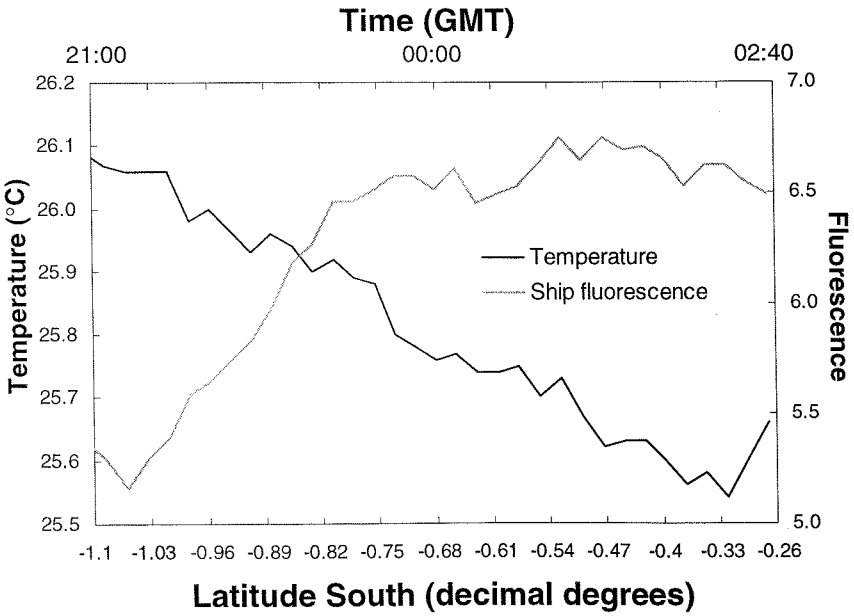

Figure 5.11.— Surface (7m) temperature (°C) and fluorescence (instrument units) as measured from the continuous seawater supply between 01.00 and 00.26°S in the ETRA. These data were collected by ship instruments and were periodically logged (once per 10 minutes). This section corresponds with UOR tow B.

Statistical treatment of data collected from CTD profiling— The Plymouth Routines in Multivariate Ecological Research (PRIMER, Carr 1994) programme was used for the calculation of the following statistics. A more complete description of these statistics (Clarke and Warwick 1994), and of the results generated from this AMT6 data, can be found in *Appendix 3*. A (Bray-Curtis) similarity matrix was generated between pairs of CTD stations using the following data: depths of the nitrate (NO_3) and phosphate (PO_4)

nutriclines, the nitrite (NO_2) maxima, the thermocline and the 1% of the surface PAR; integrated water column values for NO_3, PO_4 and NO_2 (from above the nutricline/NO_2 maximum); surface values of temperature and salinity. The approximate depths of the thermocline and nutricline were interpreted as the zone of maximum change between surface and deeper waters in temperature and nutrients respectively. The data were subsequently presented as a hierarchical dendrogram (see *Appendix 3*) to identify clusters of similar stations based on these characteristics. The analyses reveal that nutrients account for 50.71-54.16 % of the similarity between groups whilst all other hydrographic parameters compose the remaining 45.84-49.29 %.

An ordination technique provides a 2 or 3 dimensional map that reflects similarities of samples (Clarke and Warwick 1994). Ordination by non-metric multidimensional scaling (MDS, Kruskal and Wish 1978) was chosen to represent the clusters from the similarity matrix since it is a very flexible technique and lacks assumptions. A principal components analysis was originally performed on the data but was abandoned since it is limited and contains poor distance preservation when projecting samples onto a 2D plane. The MDS from the respective similarity matrix of the above data is given in *fig 5.12*

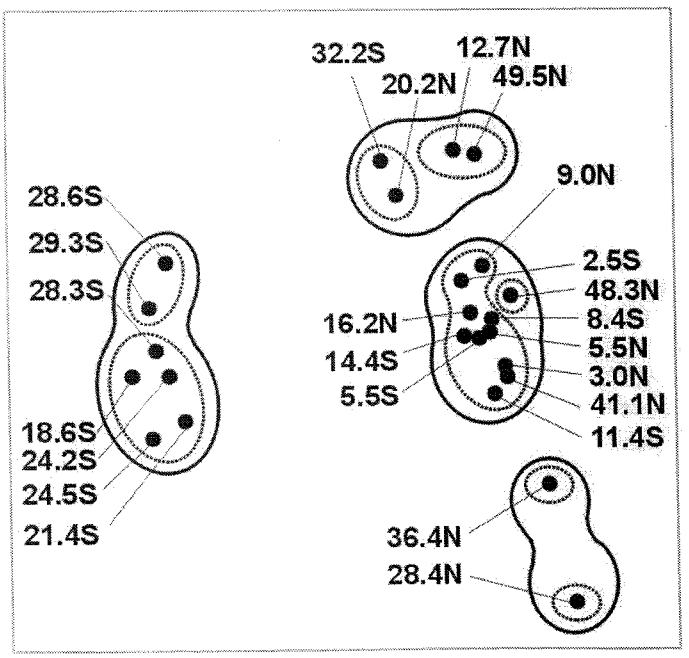

Figure 5.12.— MDS plot from Bray-Curtis similarity matrix of hydrographic (temperature, salinity and nutrient) characteristics, see main text, of CTD stations throughout AMT6. Clusters are derived from arbitrary levels of similarity chosen between stations in Bray-Curtis dendrogram (see appendix 3): solid line = 75% similarity; dashed (inner) line = 85% similarity between stations. Stations within clusters are described by decimal latitude. Minimum stress level of MDS = 0.05.

The clustering of similar stations is dependent upon the arbitrary level of similarity that is determined from the corresponding dendrogram (*Appendix 3*). At a relatively low level of similarity (eg. 75%) between samples, groups of stations can be easily identified and

correspond to the NAST (28-36°N), the NB and northern SB (29-18°S) and all stations from the southern NADR, NEQ and ETRA. This suggests that the boundaries of the different biogeographic boundaries are reasonably well defined. Stations at 20°N, 32°S, 12°N and 49°N appear to form another distinct group. If a higher level of similarity is used, eg. 85%, then more clusters of stations are identified since the conditions of similarity become more discriminative. This analysis had little trouble, or a low stress level, in reducing the data into a 2D plot and is reflected by the distinct nature of the clusters.

A second similarity matrix and MDS was constructed to include information concerning the nature of phytoplankton biomass and production throughout the water column as derived from the FRRF, in addition to the hydrographic variables contained in the first analysis. The respective depths of the maximum variable fluorescence (F_v), chlorophyll *a* concentration, chlorophyll specific production (P^{chl}) and production (P_C), in addition to absolute values of these parameters both at the maximum and at the surface (7m), were used to further describe conditions at each station. The resulting MDS (*fig 5.13.*) generates clusters of stations that are very similar to those found from the first MDS at the 75% similarity level, and again, was produced with a relatively low level of stress (see fig. legend). However, station 48.3N has become isolated and reflects the distinctive phytoplankton photosynthetic conditions observed. The consideration of more variables in the second MDS appears to result in a greater degree of discrimination (ie. more

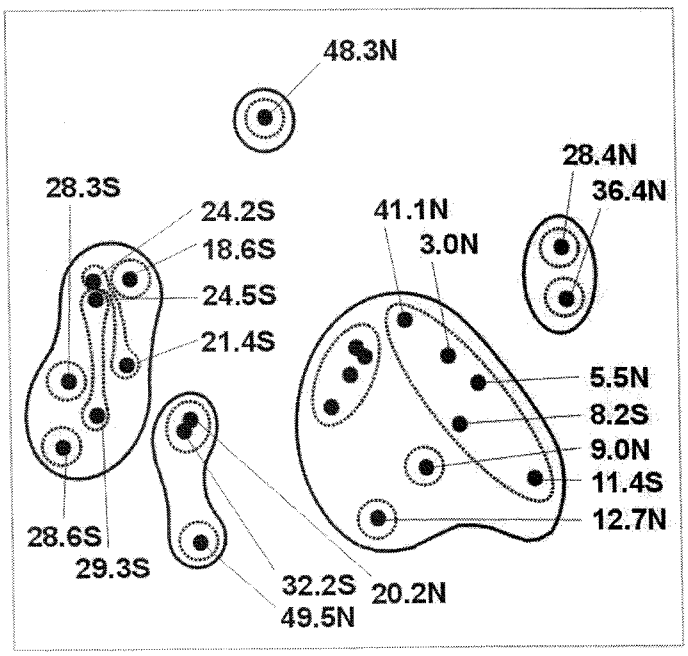

Figure 5.13.— MDS plot from Bray-Curtis similarity matrix of hydrographic (temperature, salinity and nutrient) and FRRF characteristics (see main text) of CTD stations throughout AMT6. Clusters are derived from arbitrary levels of similarity chosen between stations in Bray-Curtis dendrogram (see appendix 3): solid line = 75% similarity; dashed line = 85% similarity between stations. Stations within clusters are described by decimal latitude. Minimum stress level of MDS = 0.08.

clusters) when attempting to group stations at higher levels (eg. 85%) of similarity. A more detailed description of these analyses can again be found in *Appendix 3.*

The strong hydrographic differences are, therefore, mirrored by clear differences that exist in phytoplankton physiology and production between the provinces at the sampling scale employed. As such, the clusters produced above can be subjectively classified in terms of their trophic status: the NAST group is considered to represent a strongly oligotrophic regime, the NB and northern SB group as representative of strongly eutrophic, the group comprised of 20°N, 32°S and 49°N as representative of weak eutrophic, and the remaining stations (southern NADR, ETRA and NEQ) as representative of meso-oligotrophic conditions. The station at 48.3°N is exceptional but will be classified as strongly eutrophic since this station was under intense bloom conditions (see above).

Stations comprising environmental group	Trophic status	MSR relationships with hydrography	
18-29°S (NB) 48.3°N (NADR)	Strongly eutrophic	**Fv/Fm**	Temperature (44.6%) PAR (16.2%)
		σ_{PSII}	Nutrients (59.0%) PAR (11.4%)
		P^{chl}	PAR (44.6%)
		P_C	PAR (35.4%) Nutrients (15.7%)
32°S (SB) 20°N (NWA) 49°N (NADR)	weakly eutrophic	**Fv/Fm**	PAR (47.1%) Nutrients(36.0%)
		σ_{PSII}	Nutrients (66.6%) PAR (13.5%)
		P^{chl}	PAR (39.9%) Nutrients (31.2%)
		P_C	PAR (51.6%) Nutrients (37.0%)
14°S-16°N (NATR & NEQ)	Meso- to oligotrophic	**Fv/Fm**	Nutrients (46.3%)
		σ_{PSII}	Nutrients (14.1%) PAR (22.3%)
		P^{chl}	Nutrients (54.2%) PAR (10.1%)
		P_C	Nutrients (44.7%)
28-36°N (NAST)	Strongly oligotrophic	**Fv/Fm**	Nutrients (61.8%)
		σ_{PSII}	Nutrients (54.1%)
		P^{chl}	Nutrients (91.7%)
		P_C	Nutrients (85.0%)

Table 5.1.— Summary of data derived through MDS (non-metric multi-dimensional scaling) and MSR (Multiple Stepwise Regressions) statistics performed on all FRRF data obtained from CTD casts. Each environmental group is determined from MDS and is assigned an arbitrary trophic status based on common production, biomass and hydrographic conditions. The variables which explain the % of variance greater than 10% are displayed for the MSR between each respective physiological parameter and hydrographic conditions (temperature, nutrients and PAR). Full results from the MSR are given in *Appendix 3.*

Multiple Stepwise Regressions (using MINITAB) were subsequently performed to determine the degree to which each of F_v/F_m, σ_{PSII}, P^{chl} and P_C (as derived through the FRRF) were dependent upon corresponding measurements of temperature, nutrients and PAR within each of the 4 identified trophic regimes (*table 5.1.*). Full details of these analyses can be found in *Appendix 3.* F_v/F_m and σ_{PSII} generally display highest covariance with nutrients throughout all regimes, except within the strong eutrophic where temperature appears the predominant variable, and within the weak eutrophic where a similar covariance is exhibited for both nutrients and PAR. P^{chl} and P_C display a more distinct relationship, whereby the highest covariance occurs with PAR throughout the strong and weak eutrophic and with nutrients throughout the meso- and strong oligotrophic regimes.

5.3. Province characteristics based on continuous surface FRRF data

The variable fluorescence (F_v), quantum efficiency (F_v/F_m) and the functional absorption cross section (σ_{PSII}) observed in the surface water across the entire transect are presented in *fig. 5.14.* In general, F_v is high throughout the Benguela, NWA/NEQ and NADR but remains very low throughout the ETRA and NAST provinces. FRRF data from the equator is absent because the signal was saturated where the gain setting was too high but does indicate that the fluorescence yield increased significantly. The corresponding fluorescence trace from the ship-board fluorometer shows a slight increase in fluorescence yield between 3°S and 2°N. There was a significant agreement between these 2 sets of fluorescence data from the entire transect: FRRF fluorescence yield = 0.734 Ship-board F_v + 7.54, $r^2 = 0.592$ ($n = 3185$, $p<0.001$).

Both F_v/F_m and σ_{PSII} display obvious diel variability in their respective signals throughout the transect, as a decrease in parameter value during the day. A discrete state transition (see *section 1.4.*) of these signals also occurs at dawn and dusk (Behrenfeld and Kolber 1999) and dampens the night fluorescence signals. This phenomenon was observed throughout the more oligotrophic regions (see also *fig. 5.15.*) but is less easily distinguished from the signals within the dynamic upwelling regions. Differences between provinces can still be observed against this background pattern of diel variability

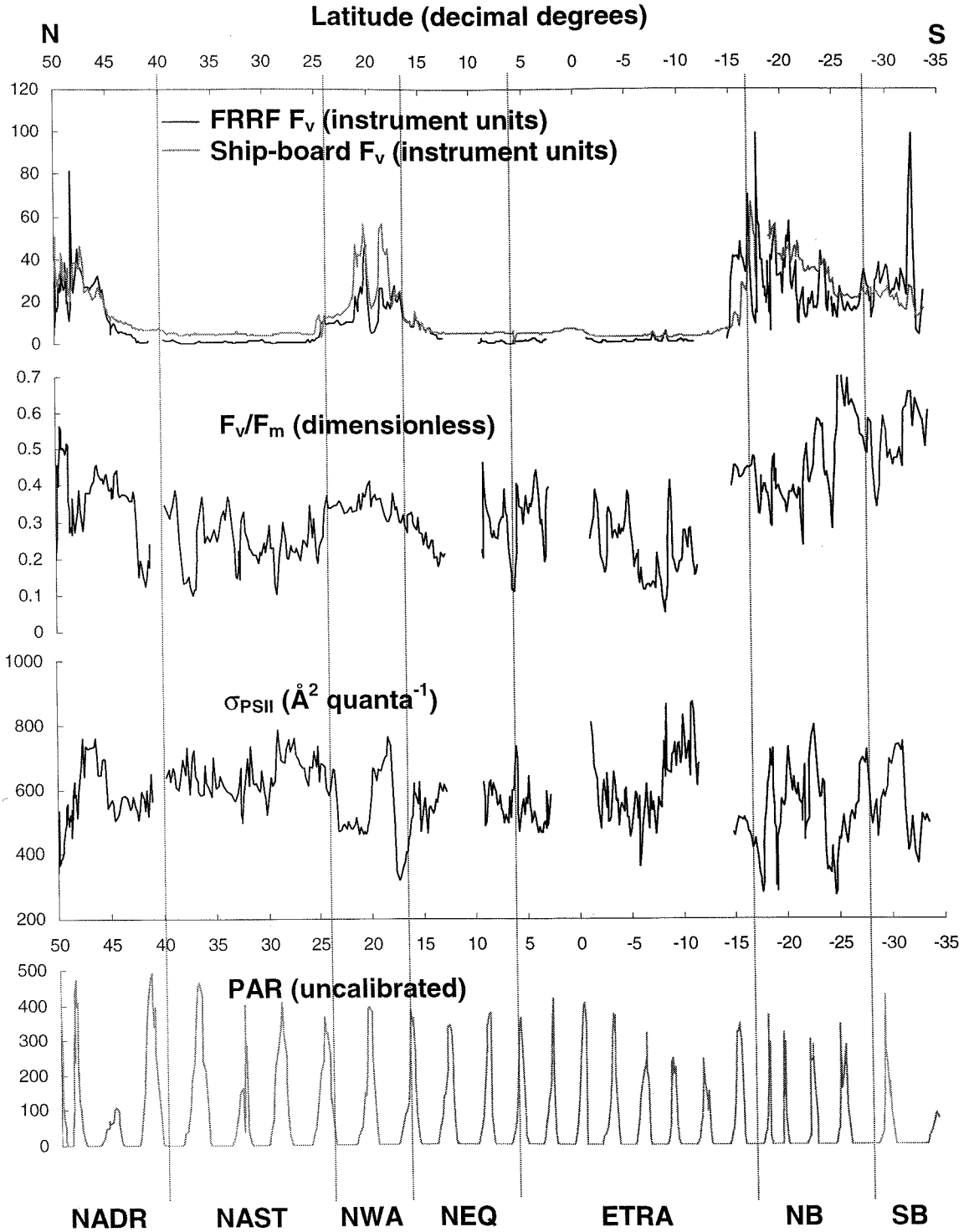

Figure 5.14.— Changes in surface (7m) FRRF variables as measured from the continuous non-toxic seawater supply throughout AMT6. Latitude and biogeochemical provinces (see *fig. 5.2.*) are indicated. Variables shown are variable fluorescence yield (F_v: instrument units), photochemical efficiency (F_v/F_m: dimensionless) and the functional absorption cross section (σ_{PSII}: Å^2 quanta^{-1}). The fluorescence yield (instrument units) and incident PAR (ship mounted, uncalibrated) collected by the ship logger are also shown as a means of comparison. All these data presented here are 'binned' into hourly averages. Full records (at the actual data collection resolution) are given in *Appendix 4.*

(see *Appendix 4*). F_v/F_m is high (0.4-0.5) within NWA and NADR regions but also appears to increase north of the equator. F_v/F_m is highest, and is close to its theoretical maximum, throughout the BENG region (0.6-0.65). The greater variability exhibited by the σ_{PSII} (*Appendix 4*) trace appears partly as a function of noise. However, the mean value of σ_{PSII} is relatively higher within NAST (634Å^2 quanta^{-1}) and relatively lower within ETRA, NEQ and NADR (538, 535 and 515 Å^2 quanta^{-1}) when compared to the mean σ_{PSII} from the entire BENG region (586 Å^2 quanta^{-1}).

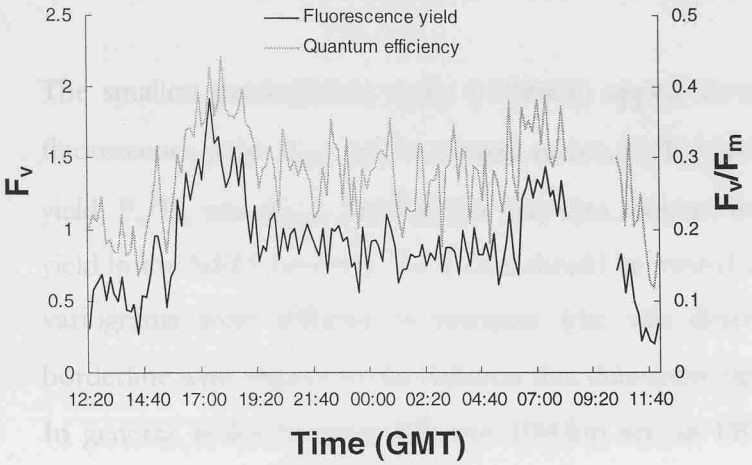

Figure 5.15.— Example of state transition of surface FRRF fluorescence yield (F_v) and quantum efficiency (F_v/F_m) occurring at dawn (approx. 07:00) and dusk (approx. 18:00). This diel track is taken between serial day (SD) 149 and SD 150, 5.59 and 2.65 °S, AMT 6. The process of the diel state transition is given in more detail in *section 1.4.*

Scales of variability of surface data throughout the Atlantic — Several techniques are commonly employed to assess the spatial scale, variability or patchiness of hydrographic parameters. The most popular of these techniques employed in oceanographic analyses are variance (power) spectra (eg. Denman and Platt 1976, Weber *et al.* 1986), semi-variograms (eg. Yoder *et al.* 1987, Seuront and Lagadeuc 1997, 1998), and correlograms (eg. Jumars 1978, Mackas 1984). These techniques are all closely related (Yoder *et al.* 1987) and are applications of the stochastic point process. A stochastic point process is essentially the difference in parameter values between all points separated by distance (dx) in a series of data, eg. Fasham (1978), and is assessed over a range of length scales.

Underway hydrographic and FRRF data were collected via continuous surface water sampling (see *Chapter 2*) throughout the cruise transect and are analysed using the variogram technique. A full account of this technique, and of all variograms produced from the AMT6 data, is given in *Appendix 3*. This technique was chosen because,

compared to other techniques, it is flexible, filtering of the data is not necessary, and it can operate where there are gaps in the data series (Yoder *et al.* 1987). Conversely, spectral analysis is favoured when transfer functions or filtering of the data is involved (Fasham 1978). However, the major limitation of variograms is that they only resolve the predominant scales and do not detail less obvious patterns. Using this approach, we can obtain information concerning the variability of physical and biological variability in each system The ease of the variogram technique eliminated the need to manipulate or extrapolate the transect data (shown fully in *Appendix 4*). *Table 5.2.* provides a summary of the dominant scales of variability determined from the variograms in *Appendix 3*.

The smallest predominant scales (<100km) appear to operate in the SB (temperature, fluorescence yield σ_{PSII}, and to a lesser extent, F_v/F_m) and the NWA (FRRF fluorescence yield, F_v/F_m and σ_{PSII}). Small scales may also account for the variability in fluorescence yield in the NEQ; however, these data should be treated with caution since the respective variograms were difficult to interpret (the sills describing the smaller scales were borderline with respect to the criterion that determine significant scales, see *Appendix 3*). In general, scales between 100 and 1000km act on FRRF parameters in all provinces except SB and NWA, and on hydrographic parameters in all provinces except ETRA and NAST. The hydrography of these last 2 provinces are governed by scales greater than 1000km. Indeed, the linear variogram produced for the hydrography of NAST (*Appendix 3*) indicates a scale with a period of at least twice that of the longest sample distance ie. 2 x 908km. Similarly, this also implies that the linear variograms produced for the temperature of NEQ and salinity of NB could also exceed scales greater than 1000 km. The temporal scales determined for PAR agree well ($r^2 = 0.92$, n=7, $p<0.001$) with the (mean) diurnal period within each province in the underway record (data not shown) and provides confidence in the technique for determining the predominant scales.

Fractal dimensional analysis can be subsequently employed on the variogram plots to further describe the nature of the inherent variability. This is a simple procedure and is described in detail in *Appendix 3*. To summarise (following Seuront and Lagadeuc 1997, 1998), the gradient of a log-log plot (m) of the variogram is used to provide a value for the fractal dimension, D. A high value of D (eg. = 2) is characteristic of a complex system where local variability is highly developed and is dominated by short range, such

as biological, processes. A relatively low value of D (tending towards zero) characterises larger scale variability as a result of long range (ie. physical) processes. This analysis has been applied to the variograms produced for the hydrographic and FRRF variables from each province.

Province	PAR	T	S	F	F_v	F_v/F_m	σ_{PSII}
SB	12.7	3.3	36.0	3.9	3.1 ± 0.6	5.5	3.8 ± 0.3
NB	11.5 ± 4.0	28.6	Linear	13.1	7.6 ± 0.8	10.4 ± 0.9	10.7
ETRA	11.9 ± 2.0	57.8	54.2	27.0	10.3 ± 0.9	11.7 ± 0.9	None
NEQ	13.0	Linear	9.0 ± 1.6	2.2	2.3	9.7	None
				10.6 *	11.7 *		
NWA	13.0	14.6	16.0	10.7	4.0	3.3 ± 0.8	3.3
NAST	15.0 ± 1.8	Linear	Linear	15.5	19.4	12.1 ± 1.2	13.4 ± 1.8
NADR	15.8 ± 0.4	27.5	10.5 ± 0.5	15.6	24.9	15.2	10.5 ± 0.9

Province	PAR	T	S	F	F_v	F_v/F_m	σ_{PSII}
SB	282	73	801	87	69	122	85
NB	256	636	Linear	291	169	231	238
ETRA	265	1285	1205	600	229	260	None
NEQ	289	Linear	200	49	51	185	None
				236 *	260 *		
NWA	289	325	356	238	89	73	73
NAST	333	Linear	Linear	345	431	269	298
NADR	333	612	234	347	554	338	191

Table 5.2.— Summary of dominant temporal and spatial scales of FRRF and hydrographic parameters within each province, as determined by variogram analysis (see *Appendix 3*). Top panel indicates scales in decimal hours, whilst bottom panel indicates scales in kilometres (whereby 1km/hr = 0.5396 knots, assuming ship speed at an average of 12 knots). *Linear* indicates that a variogram which did not exhibit a sill and, therefore, could not determine a dominant spatial scale from the largest between-sample distance; *None* indicates a high nugget value (the result of noise) hence any sills are unlikely to be significant; * indicates a possible alternate dominant scale where the initial sill is difficult to interpret.

Values of *D*, *fig. 5.16.*, typically appear higher for 'biological' data (see figure legend) than for the corresponding hydrographic data. A Wilcoxen's test for matched pairs confirms that the mean of all hydrographic fractal dimensions is significantly different from the mean of F, F_v F_v/F_m and σ_{PSII} (T=3, P<0.1) throughout the 7 provinces. In general, *D* remains between 1.3 and 1.5 for temperature, salinity and PAR in all regions except NWA and the Benguela where values of *D* that are typically 1.5 and 1.8. Using the above criteria, it appears that the variability of these parameters even in NWA, NB and SB provinces are predominantly influenced by large scale processes. The trend of *D* for PAR between provinces also emphasises that whilst the period of variability can remain constant, the scales of the forcing physical factors can vary. Fractal dimensions for the biological data appear to remain more consistent between provinces. A relatively large increase in the value of *D* for F_v/F_m is also observed between ETRA and NAST. Mean values of *D* for the physiology (F_v/F_m and σ_{PSII}) were significantly different (Wilcoxen's test for matched pairs: T=3, P<0.1) from those of fluorescence yield throughout the 7 provinces.

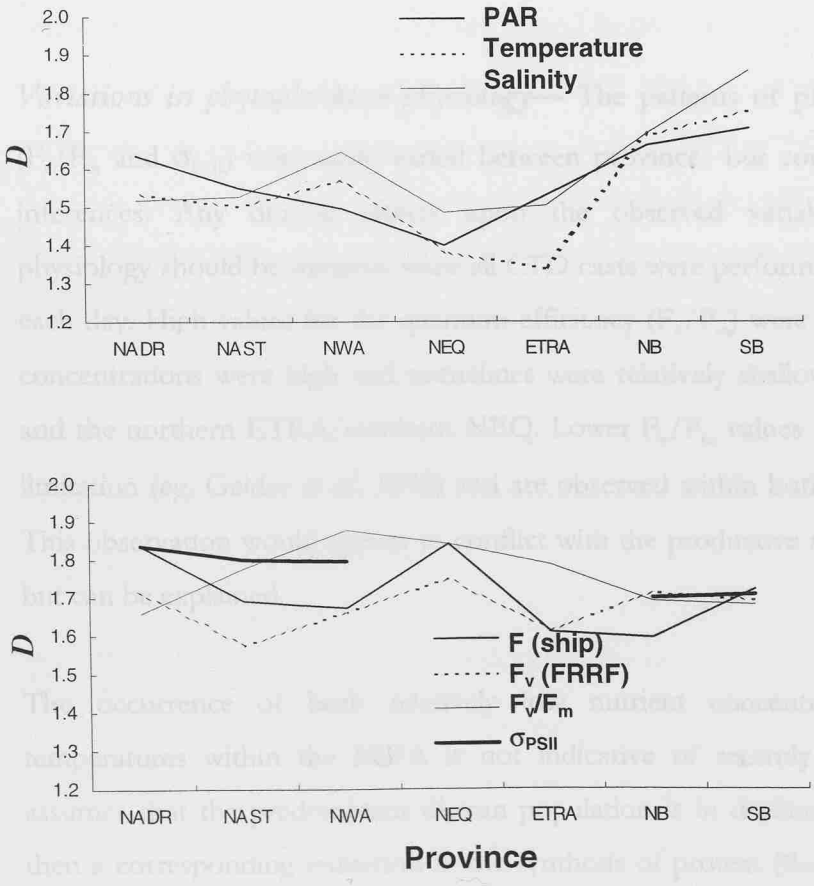

Figure 5.16— Values of the fractal dimension (*D*), as derived from the respective scales of variability using variogram analyses (see *appendix 3*), plotted for each province throughout AMT6. *D* is plotted for both hydrographic (PAR, temperature and salinity) and biological (fluorescence yields: F from the ship Turner fluorometer and F_v from the FRRF); quantum efficiency F_v/F_m and the functional absorption cross section of PSII (σ_{PSII}) parameters. More information regarding the calculation of *D* is given in *Appendix 3*. **Note:** A value of *D* could not be derived for σ_{PSII} in ETRA or NEQ as a result of the large amount of noise in the respective variograms

5.4. Discussion and conclusions

Province characteristics based on CTD profiling— The cruise transect was dominated by three areas of high productivity: the Benguela, the north-west African upwelling and the north-west continental shelf approaches (NADR). These systems contained taxonomic and physiological signatures which may be interpreted to indicate the biological age of the respective water-type. By definition, both the NB and NWA feature characteristics (eg. diatom dominance) of recently upwelled water (Barlow 1982a, Painting *et al.* 1993, 1994). The predominance of dinoflagellates in the more stratified SB is indicative of mature water types (Pitcher *et al.* 1992), and is well known for this region during the latter part of the upwelling season (Pitcher *et al.* 1998). Similarly, the especially strong bloom of the colonial (prymnesiophyte) flagellate *Phaeocystis* observed in NADR is not unusual, especially in late spring/early summer (Holligan 1987). Prymnesiophytes dominate post bloom waters whilst dinoflagellates develop as a later secondary component (Barlow *et al.* 1993, Lochte *et al.* 1993). Therefore, the high ratio of 19'hexanoyloxyfucoxanthin: fucoxanthin: peridinin would suggest developed but not mature bloom waters.

Variations in phytoplankton physiology— The patterns of phytoplankton physiology (F_v/F_m and σ_{PSII}) were quite varied between provinces but conformed with the above inferences. Any diurnal effects upon the observed variability of phytoplankton physiology should be minimal since all CTD casts were performed at the same local time each day. High values for the quantum efficiency (F_v/F_m) were observed where nutrient concentrations were high and nutriclines were relatively shallow, such as, the Benguela and the northern ETRA/southern NEQ. Lower F_v/F_m values are indicative of nutrient limitation (eg. Geider *et al.* 1993) and are observed within both the NWA and NADR. This observation would appear to conflict with the productive nature of these provinces but can be explained.

The occurrence of both relatively low nutrient concentrations and high water temperatures within the NWA is not indicative of recently upwelled water. If one assumes that the predominant diatom population is in decline from nutrient limitation then a corresponding reduction in the synthesis of protein (Barlow 1982b) and elevated

levels of storage products (carbohydrate and lipids, Falkowski and Raven 1997) would be expected. As such, there is typically a reduction in the amount of pigment associated with the PSII reaction centres (Falkowski 1992) available for photochemical energy conversion (Kolber *et al.* 1988) thereby reducing the efficiency of photochemistry. The low F_v/F_m (but relatively high nutrient concentrations below 20m) within the NADR cannot be explained by nutrient limitation but rather low light as a result of deep mixing (eg. Olaizola *et al.* 1996). Efficient photochemistry would not be maintained where the phytoplankton population is held at a mean light level which is below that of the compensation light intensity (*sensu* Kirk 1994: productive O_2 liberation relative to respiratory O_2 consumption, see *section 1.4*) and is, therefore, light limited. The depth of the 1% light depth was restricted to 20-25m in the NADR province (*fig. 5.3.*); however, the possibility of nutrient advection, or of taxonomic differences in yields of the quantum efficiency, cannot be accounted for and may confound the interpretation of phytoplankton physiology.

The functional absorption cross section (σ_{PSII}) can respond to the environment over both relatively short (photoacclimation) and long (photoacclimation and photoadaptation) scales. As such, the ability of σ_{PSII} to respond to the current light climate can also reflect the photo-history of a phytoplankton population. The lowest values of σ_{PSII} (at the σ_{PSII}-maximum) were observed within the region of the NB (23-27°S) which is located near to the upwelling centre of the Benguela. This observation is difficult to explain unless this phytoplankton community has acclimated or adapted to high light and therefore acquired a lower σ_{PSII} (eg. Dubinsky *et al.* 1986, see also *Chapter 4*). A taxonomic difference in absolute photon target size (eg. Berges *et al.* 1996) may serve to add confusion to this interpretation. Conversely, the higher chlorophyll *a* content and lower *in situ* irradiance penetration of the SB could explain the relatively higher values observed for σ_{PSII}.

Low values of σ_{PSII} were also seen within NAST where nutrients were severely depleted. The response of σ_{PSII} to increased light intensity becomes modified under conditions of nutrient limitation whereby σ_{PSII} further increases (Kolber *et al.* 1988, Greene *et al.* 1991, see *Chapter 4*). However, this was not observed. Higher values of σ_{PSII} coincided with high values of F_v/F_m deeper in the water column (60-100m) where phytoplankton approached the nutricline, instead suggesting low light acclimation. This may be

contrasted with the occurrence of high σ_{PSII} but low quantum efficiencies at depth in both the NWA and NADR. These values could reflect the declining physiological status of sinking-out or deeply mixed populations and perhaps an increase in noise to the FRRF signal.

Further evidence suggests that phytoplankton in the NAST are acclimated to low light: Prochlorophytes are known to dominate oligotrophic areas of the Atlantic (Platt *et al.* 1983, Veldhuis and Kraay 1990, 1993), especially in summer (Olson *et al.* 1990a, b), where water column conditions are relatively stable. These authors explain that *Prochlorococcus*-type organisms are well adapted to growth at low light since they have a high affinity for nutrients and seek the deep nutriclines. *Prochlorococcus* dominated the NAST province but showed highest cell numbers in the surface 20-75m (M.Zubkov, pers.comm.). A calculation of total chlorophyll *a*/cell (chl *a* m^{-3} divided by cell number m^{-3}) shows that surface populations contain less chl *a*/cell (mean ± standard error, 0-7m: $2.53x10^{-7} \pm 1.09x10^{-7}$) than those from deeper in the water column (80-100m: $6.78x10^{-7} \pm 8.02x10^{-8}$) in this province, and reinforces the suggestion of low light acclimated (or adapted) phytoplankton at depth.

The multiple stepwise regressions generally displayed a significant relationship between F_v/F_m and σ_{PSII} and nutrients throughout the majority of trophic regimes. This close association suggests that most of the observed communities have a physiology which is driven by nutrient availability and variability. However, temperature and PAR appeared to dictate the relationship of F_v/F_m within the strong and weak eutrophic regimes, respectively. Stations within the strong eutrophic come from dynamic areas where water has been most recently nutrient enriched (NB upwelling and inferred deep water column mixing within southern NADR). Light and nutrient limitation only become significant limiting factors as upwelled water matures (Brown and Field 1986) and phytoplankton adapt which might explain why temperature exhibits a strong correlation with photophysiology within the strong eutrophic. The strong association between PAR and photophysiology in the weak eutrophic would suggest that changes in light most strongly influence the variability in phytoplankton physiology under stable hydrographic and nutrient replete conditions. This response must also be reasonably strong in order to dominate the nutrient limited relationship of the NWA, which was also present within this category.

Scales of variability of biology and hydrography in surface waters— The observed horizontal spatial scales of variability typically reflected the physical nature of each respective region. Both the physical and biological parameters of the dynamic Benguela, and to a lesser extent NWA and NADR, were characterised with the smallest scales of variability. The Benguela and NADR displayed relatively low fractal dimensions (D), however, the D[physical parameters] are generally $\geq$ D[biological parameters] indicating that the physical processes acting on the horizontal variability of these systems are relatively small but dictate the variability observed in biological processes (eg. Seuront and Lagadeuc 1998). Similar scales of biological variability within the Benguela province have been reported as a result of rapid changes in the intensity and frequency of the upwelling (eg. Shannon *et al.* 1984) giving rise to eddies. The open ocean provinces are characterised by horizontal scales [of physical parameters] of the order 100s-1000s km and correspond with larger scale physical processes such as rings, [baroclinic] eddies and Rossby waves (eg. Venrick 1990, Mann and Lazier 1996). As such, biological variability occurs at scales that are smaller than those for physical parameters, most notably within ETRA and NAST.

The horizontal scales of fluorescence yield variability, which are high when compared to previous estimates of the scale of phytoplankton patchiness throughout the open ocean (10-100km Steele 1976 *in* Okubo 1978; 5-10km Denman *et al.* 1977), correspond with the spatial scales of daylight as measured by the underway PAR sensor throughout the transect. This is perhaps not surprising since diel variations of fluorescence can coincidentally arise from several physiological sources (such as changes in pigment content, state transitions, and quenching, Falkowski 1984, Falkowski and Raven 1997) and would, therefore, represent a very strong signal. Such temporal variability may mask the actual scales of phytoplankton patchiness. The scales of PSII variability typically correspond with those of fluorescence yield; however, values of D remain higher for both F_v/F_m and σ_{PSII} throughout all regions. This difference is greatest in the ETRA, NEQ, NWA and NADR regions signifying the strong influence of small scale biological processes upon the scales of variability. The strong small scale biological influence within NWA conflicts with the apparent control by physical processes under dynamic conditions but may perhaps be explained since this phytoplankton community appears physiologically stressed and would be less likely to display an ability to regulate PSII variability with the continually changing environment.

Finally, despite the above observations, the scales of fluorescence yield variability determined from the ship Turner fluorometer are different (for some provinces) to those described using the FRRF. The Turner fluorometer only measures the maximum fluorescence yield (F_m) of a water sample whilst the FRRF measures the variable fluorescence yield F_v (=F_m-background fluorescence yield, F_o). Therefore, changes in non-biological fluorescence and chlorophyll breakdown products could account for changes in F_o (and thus in F_v) but not in open ocean samples where the occurrence of such products is likely to be low (Geider *et al.* 1993). It might be considered that the sensitivity of the variogram technique contributes to the differences observed, for example, the greater sampling resolution of the FRRF could illustrate significant smaller scales of variability (F_v) than in corresponding analyses using the ship's Turner fluorometer (F) data. In general, the confused correspondence between the two measurements cannot be wholly explained.

Conclusions— The broad scale assemblages of phytoplankton throughout the Atlantic display a variety of physiological and productivity signatures. This investigation has demonstrated that geographically separated populations can be grouped according to similar characteristics such as hydrographic habitat, standing stock and production. The resolution of broad-scale CTD sampling appears sufficient for characterising the boundaries of biogeographic provinces when compared with corresponding observations from the continuous underway and UOR records. The physiology of the phytoplankton groups are reflected by corresponding variations in nutrients, but also light and temperature where nutrients are present in abundance. The predominant scales of physiological variation are observed at the diel scale. Oligotrophic regions (ETRA, NEQ and NAST) are strongly characterised by the effect of small scale biological processes upon the scales of variability, hence phenomena such as daily state transitions are most obvious throughout these regions. Finally, the more dynamic upwelling regions are characterised by physical processes which appear to overshadow phytoplankton physiological signals and/or influence the ability of phytoplankton to respond to their environment.

6. A comparison of primary productivity derived through alternate methodologies

6.1. Introduction

To date, the majority of production estimates in the aquatic environment have been made using techniques that follow ^{14}C-uptake and O_2 evolution. Recent developments in fluorescence induction methodologies have led to alternative indirect 'measurements' of primary productivity. The FRRF is currently the most commonly used fluorescence induction technique in oceanography (see *section 1.3.*) and avoids the limitations associated with conventional techniques to quantify primary productivity (eg. Sakshaug *et al.* 1997), such as 'bottle effects' (*section 1.2.*). In addition, rates of production derived through the FRRF are based on oxygen evolution and should be expected to be more comparable with conventional estimates of O_2 evolution rather than ^{14}C-uptake.

Previous chapters in this thesis have shown that an estimate of production derived from the FRRF requires several assumptions. However, neither the weight of these assumptions, nor the ability by which the FRRF compares to conventional methods for estimating production, are well documented in the literature. It is currently believed (eg. Sakshaug *et al.* 1997) that the use of the FRRF lies more in understanding the properties influencing photosynthesis and not in the quantitative values of measurement. The aim of this final chapter is to examine the relationship between corresponding estimates of production from the FRRF and ^{14}C-uptake techniques, within their respective limitations. An alternative model is also presented for the calculation of production based on FRRF measurements and subsequently compared with changes in the oxygen content of the water column. This chapter predominantly draws on information collected during the RV *Pelagia* cruise (see *Chapter 2*) but also uses some information from RRS *Challenger* and AMT 6 cruises. The details and general hydrographies covered during these cruises are given in *sections 3.1*, *4.2.* and *5.2.*, respectively. The respective protocols and sampling strategies employed are described in *Chapter 2*, whilst a more detailed

explanation and derivation of terms used throughout is given in *Section 1.4.*

6.2. Comparing corresponding FRRF and ^{14}C-uptake production estimates.

Rates of production calculated using the FRRF correspond to the *in situ* light intensity at which they are measured and are, therefore, instantaneous (P(E)). The FRRF photosynthesis-irradiance (P-E) relationship is an accumulation of *in situ* P(E) measured at various irradiances throughout the water column and represents the entire phytoplankton population. ^{14}C P-E curves are generated from discrete water samples taken throughout the water column. Each sample is experimentally incubated (for example, in a 'photosynthetron' (see general methodology: *section 2.2.*) under artificial light, RV *Pelagia* and RRS *Challenger*) at incremental light levels to describe the photosynthetic response from a range of possible light exposures and, therefore, the physiological status of phytoplankton from different depths of the water column. This is illustrated in the introduction, *fig 1.7.*

FRRF estimates of production— All *in situ* derived chlorophyll *a*-specific instantaneous production (P^{chl}) data from the *RV Pelagia* cruise are plotted as P-E curves in *fig 6.1.* Only one FRRF P-E curve was obtained at each of the 3 diel sites since the limited sampling resolution precluded the estimation of E_k (and hence τ_p and ϕ_e) for each cast within the diel-series (see *Chapter 3*). The P-E curves for the 3 sites have reasonably similar light-limited initial slopes (α_{chl}) of 0.062, 0.081 and 0.073 (mgC mgchl a^{-1} h^{-1})(μmol photons^{-1} m^{-2} s^{-1})$^{-1}$ for sites 1, 2 and 3 respectively (see also *table 6.1.*). The light-saturated photosynthetic rates (P_{max}^{chl}) vary between 3.62 and 6.31 mgC mgchl a^{-1} h^{-1}, with the highest value at the southern-most site (site 3: 37N). The changes in P_{max}^{chl} and in the saturation irradiance at which P_{max}^{chl} is established (E_k) suggest differences in the photoacclimation status of the phytoplankton (ie. phytoplankton at the southernmost site are acclimated to a higher light intensity since they exhibit greater photosynthetic capacity at higher values of E) that are consistent with the observations discussed in *Chapter 3.*

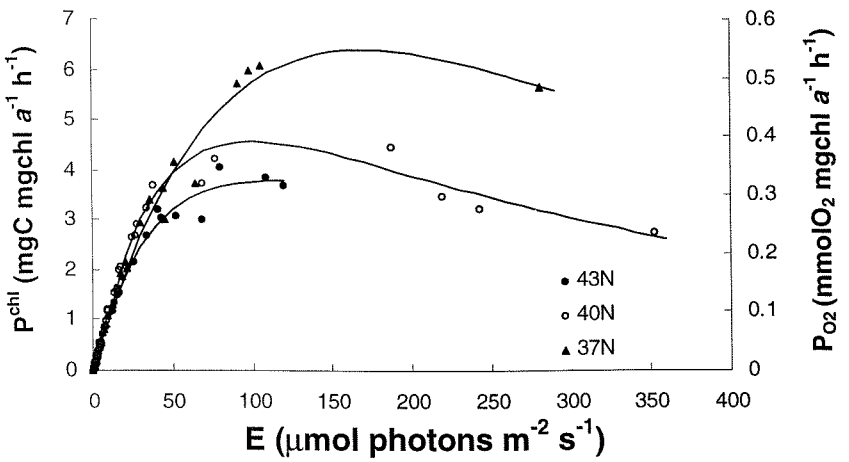

Figure 6.1.— Photosynthesis-Irradiance (P-E) curves reconstructed from data collected using the FRRF at the 3 diel sample sites (43°, 40°, and 37°N) from the RV *Pelagia* cruise (see *Chapter 3*). Instantaneous production (P(E)) is calculated from FRRF parameters measured at respective light levels *in situ*. Calculations of chlorophyll*a*-specific P(E) are given for both oxygen (mmol O_2 mg chla^{-1} h^{-1}) and carbon (mg C mg chla^{-1} h^{-1}), according to *equations 1.1.* and *1.2.* (*Chapter 1*), and assumes a photosynthetic quotient of 1. P-E curves are fitted by least squares non-linear regression according to *equation 2.1.*

The FRRF versus the ^{14}C-uptake approach— ^{14}C-uptake P-E experiments were performed on samples taken from between 5 and 40m at each of the three sites (*RV Pelagia*). The mean values of P_{max}^{chl} from all these experiments should represent the general response of the phytoplankton population and are 2.34, 2.57 and 2.41 mgC mgchl a^{-1} h^{-1} from sites 1 (43°N), 2 (40°N) and 3 (37°N), respectively (*table 6.1.*). These values are a factor of 2-3 lower than those determined by the FRRF (*fig 6.1.*). The initial slopes (α_{chl}) from the 3 sites average 0.0106 (mgC mgchl a^{-1} h^{-1})(µmol photons^{-1} m^{-2} s^{-1})$^{-1}$ and are approximately 1/8 of those calculated by the FRRF. A better means of assessing the rates of production determined from the two techniques is to compare the instantaneous production rate (P(E)).

To obtain instantaneous ^{14}C P(E), each P-E curve must be reconstructed using values of P_{max}^{chl}, α_{chl} and β (see *equation 2.1.*). The value of production corresponding to the *in situ* E from where the sample was originally taken is the instantaneous production. FRRF and ^{14}C P(E) are compared in *fig 6.2.* using an amalgamation of all data from the 3 diel

sites, RV *Pelagia* and signifies that the rate of chlorophyll *a*-specific production (P^{chl}) measured *in situ* by the FRRF is 5 times greater than that measured *in vitro* by ^{14}C uptake. However, one might consider that FRRF P^{chl} is not a meaningful estimate of production since biomass-specific variations are not strictly accounted for ($1/n_{PSII}$, molchl *a* molRCII^{-1}, is constant). Multiplication of P^{chl} with the chlorophyll *a* concentration of the sample (mgchl *a* m^{-3}) gives the rate of instantaneous production per unit volume of water (P_C: mgC m^{-3} h^{-1}). A comparison between FRRF and ^{14}C P_C reduces the difference between corresponding estimates of production but with a weakening of the (r^2) relationship, *fig 6.2.* A reasonably similar relationship is observed when comparing corresponding FRRF and reconstructed ^{14}C-uptake P_C from the RRS *Challenger* cruise (*fig 6.2.*, right panel, see fig. heading).

			Site 1 (43°N)	Site 2 (40°N)	Site 3 (37°N)
	a^*		0.056 ± 0.005	0.054 ± 0.002	0.064 ± 0.002
FRRF P-E curves	P_{max}^{chl}		3.62	4.35	6.31
	α^{chl}		0.061	0.081	0.073
	E_k		59.7	53.6	86.9
^{14}C P-E curves	P_{max}^{chl}	shallow	2.28 ± 0.05	1.89 ± 0.26	2.08 ± 0.19
		deep	1.66 ± 0.14	1.57 ± 0.11	1.52 ± 0.39
	α^{chl}	shallow	0.011 ± 0.001	0.010 ± 0.002	0.010 ± 0.001
		deep	0.011 ± 0.002	0.011 ± 0.002	0.009 ± 0.009
	E_k	shallow	207.2 ± 7.6	185.1 ± 8.2	205.9 ± 3.4
		deep	154.3 ± 2.9	146.2 ± 4.5	186.0 ± 12.2

Table 6.1.— Summary of P-E characteristics taken from FRRF P-E curves (*fig 6.1.*) and ^{14}C-uptake experiment P-E curves. ^{14}C data are shown as the mean (± standard error) P-E characteristics from all samples taken in relatively shallow water (10m, n=2, 4, 3 for sites 1-3 respectively) and in deeper water (30m n=3 and 5 for sites 1 and 2; 40m, n=2 for site 3). Data shown are light saturated rates of photosynthesis (P_{max}^{chl}, mgC mgchl a^{-1} h^{-1}) light limited initial slopes (α_{chl}, (mgC mgchl a^{-1} h^{-1})(µmol photons^{-1} m^{-2} s^{-1})$^{-1}$) and the light intensity of maximal photosynthesis (E_k, µmol photons m^{-2} s^{-1}). Also shown is the mean (± standard error) chlorophyll*a*-specific absorption from the 3 sites, a* (n=7, 14 and 12 for sites 1-3 respectively). All data are irrespective of time of day (a* is also irrespective of depth of sample).

An alternate method for estimating ^{14}C-uptake is to incubate the depth-specific water samples at an irradiance level corresponding to conditions from which they were taken for a longer period of time. Samples are typically maintained on-deck in flowing seawater

under a blue filter screening to approximate *in situ* spectral light quality (eg. Graziano *et al.* 1996). Hence, this approach attempts to simulate *in situ* conditions. AMT6 (*Chapter 5*) ^{14}C-uptake experiments were performed in such a manner for 6-7 hours and thus provide an estimate of time integrated production. AMT6 values of P(E) are compared with corresponding FRRF *in situ* instantaneous measurements, *fig 6.3.*, using all data collected along the transect.

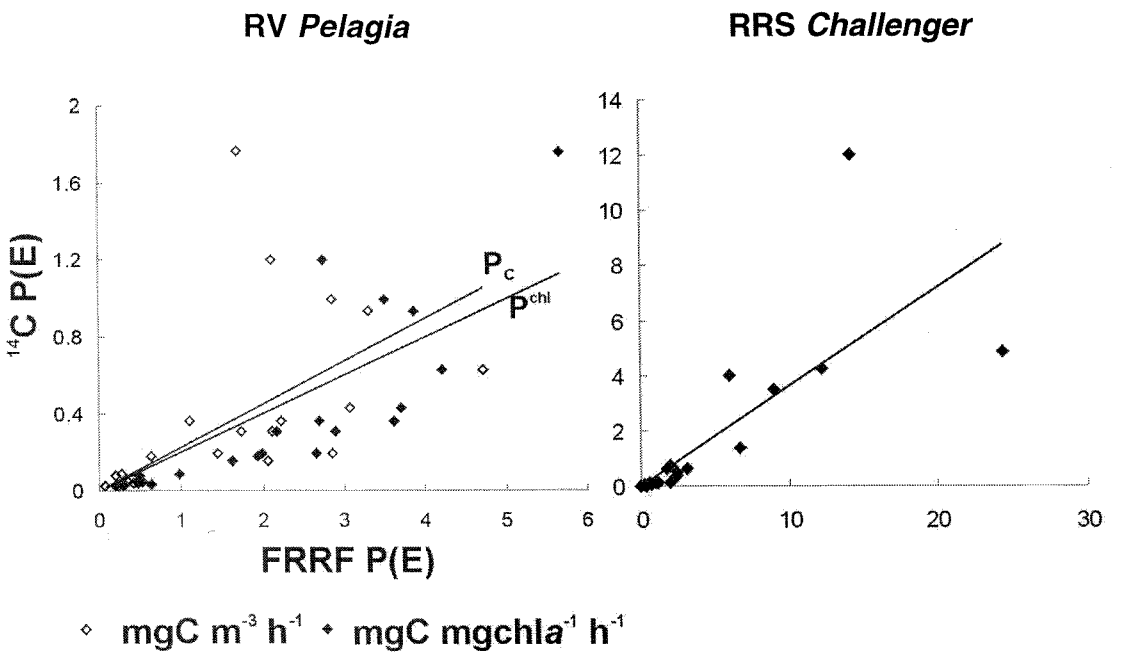

Figure 6.2.— Comparison of instantaneous estimates of production (P(E)) from *in situ* FRRF and *in vitro* ^{14}C-uptake measurements. P(E) is shown as chl*a*-specific production (P^{chl}, mgC mgchl a^{-1} h^{-1}) and production per unit volume of water, P_C (ie. P^{chl} * [chl *a*]: mgC m^{-3} h^{-1}). ^{14}C P(E) were derived from reconstructed P-E curves (P(E) using the *in situ* E from which the water sample was taken). FRRF P(E) was determined from *equation 1.2.* and assumes a photosynthetic quotient of 1. RV *Pelagia* relationships are ^{14}C P_C (mgC m^{-3} h^{-1}) = 0.224*FRRF P_C r^2 = 0.262, 0.02>p>0.01; ^{14}C P^{chl} (mgC mgchl a^{-1} h^{-1}) = 0.224*FRRF P^{Chl} r^2 = 0.639, p<0.001 (n=22); Only P_C data collected from *RRS Challenger* are given: ^{14}C P_C (mgC m^{-3} h^{-1}) = 0.361*FRRF P_C r^2 = 0.581, P<0.001 (n=21). All data collected throughout the RRS *Challenger* cruise are presented and not just sites M and U as described in *Chapter 4.*

A significant relationship is observed between corresponding estimates of instantaneous production per unit volume of water (P_C) from the 2 methods (*fig 6.3.*). This relationship is improved (^{14}C P_C = 0.410*FRRF P_C, r^2=0.596, n=107, p<0.001) upon the removal of data from the NWA upwelling (20.2°N) and from the *Phaeocystis* bloom at site 48.3°N (see *Chapter 5*). FRRF P_C remains approximately 2-3 times greater than that of ^{14}C-uptake. The AMT6 P_C data were further considered in terms of that collected from

eutrophic and meso-/oligotrophic waters (see *Chapter 5*). FRRF P_C from eutrophic waters remains approximately 2-3 times higher than ^{14}C P_C (see figure legend). However, a large proportion of AMT6 data were collected in meso-/oligotrophic waters where FRRF P_C rather exceeds that of ^{14}C by a factor of 5 (*fig. 6.3.*, left panel).

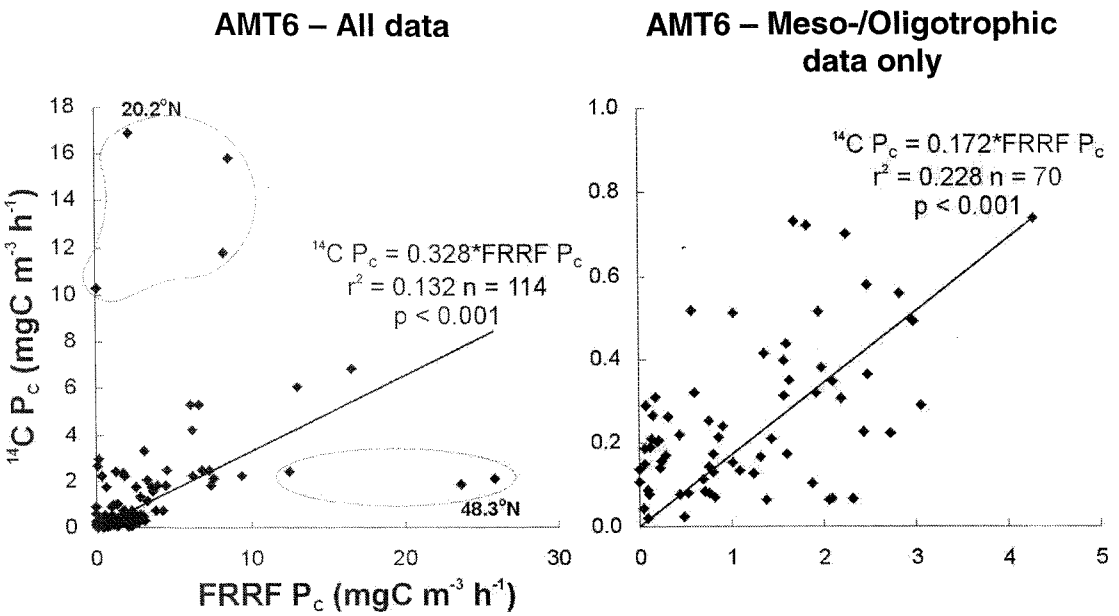

Figure 6.3.— Comparison between corresponding estimates of instantaneous production per unit volume of seawater (P_C: mgC m^{-3} h^{-1}) from *in situ* FRRF measurements and simulated *in situ* ^{14}C uptake incubations, collected during AMT6 (see *Chapter 5*). The data in the left panel were further treated by the removal of the extreme data points, and corresponded to those data collected from sites 20.2°N (NWA) and 48.3°N (NADR), which improved the relationship: ^{14}C P_C = 0.410*FRRF P_C, r^2=0.596, n=107, p<0.001). An analysis of data collected from the eutrophic waters (*Chapter 5*) revealed relationships of ^{14}C P_C = 0.337*FRRF P_C, r^2=0.021, n=54, not significant (all eutrophic data); ^{14}C P_C = 0.447*FRRF P_C, r^2=0.519, n=47, p<0.001 (upon removal of 20.2°N and 48.3°N data. The meso-/oligotrophic data are presented in the right panel.

Accounting for spectral differences in sources of light (^{14}C-uptake)

The ^{14}C-uptake incubations from AMT6 were performed on-deck in cylinders filled with seawater and exposed to the full spectrum of incident solar irradiation whereas those of the RV *Pelagia* and RRS *Challenger* cruises were made in a photosynthetron, illuminated by a light source of restricted waveband. As such, an adjustment to the data of the RV *Pelagia* cruise can be performed to account for the limited [incident] light field experienced by the photosynthesising phytoplankton:

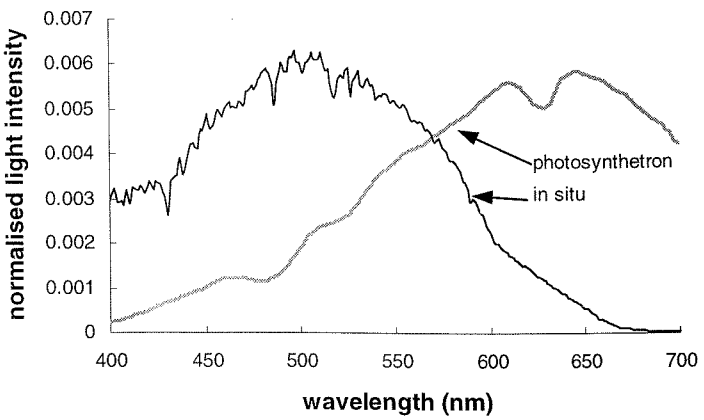

Figure 6.4.— Normalised spectra of photon flux density (400-700nm) measured in the photosynthetron and *in situ*, whereby the area under each spectra is equal to unity (=1) and is expressed in relative units (data interval = 1nm). *In situ* data from 7 wavelengths was interpolated following a global spectra (see text).

The photosynthetron spectra was measured at intervals of 1nm between 400 and 700nm whilst the *in situ* light was only recorded at 7 wavelengths relevant to the SeaWiFS satellite from optical profiles (see *Chapter 2*). A global spectrum was used to appropriately weight a non-linear interpolation (Gerald Moore, pers.comm.) between the (7) *in situ* wavelengths and give corresponding *in situ* light every nm between 400-700nm. These spectra were then normalized so that the total energy between 400 and 700nm was equal to unity as a means of comparison, *fig 6.4*. There is a clear difference between spectra at which most light occurs (~450-580 *in situ* and ~525-700 in the photosynthetron) and this will have a significant effect when considering the absorption properties by the photosynthetic pigments of the phytoplankton under consideration. The 'effective' rate of light absorption was calculated as the sum of chlorophyll *a*-specific absorption ($a^*_{(\lambda)}$) multiplied by the normalized irradiance ($E_{(\lambda)}$) from all values of λ between 400-700nm. The difference in the effective rate of light absorption between the 2 light spectra was obtained by dividing the rate of light absorption by the respective irradiance ($E_{400\text{-}700}$, which is equal to 1 since the spectra were normalized).

The mean effective absorption from the photosynthetron light source is 0.53 (site 1), 0.51 (site 2) and 0.41 (site 3) times lower than that for the *in situ* light field. Therefore, the irradiance (400-700nm) measured in the photosynthetron is only 0.41-0.53 as effective for photosynthesis as a corresponding value measured in the water column. Hence the rates at which light saturated photosynthesis are achieved (α_{chl}) in the photosynthetron will be underestimated. In order to compensate for these differences in spectral quality, the irradiances measured in the photosynthetron are multiplied by 0.53

(site 1), 0.51 (site 2) and 0.41 (site 3) when establishing the P-E curves for each water sample. These corrections result in lower values of E_k (mean E_k of 85.9, 76.1 and 82.7 µmolphotons m^{-2} s^{-1} from sites 43°N 40°N and 37°N, respectively) and higher values of α (mean $\alpha_{chl} = P_{max}{}^{chl}/E_k$ of 0.022, 0.020 and 0.023 (mgC mgchl a^{-1} h^{-1})(µmol photons^{-1} m^{-2} s^{-1})$^{-1}$ from sites 43°N 40°N and 37°N, respectively) since the irradiances at which light saturated photosynthesis occurs are lower. These changes to the characteristics of the ^{14}C P-E curves result in a more significant relationship (r^2) and higher values of instantaneous production (P(E)), *fig 6.5*. As such, the difference in corresponding estimates of P(E) from the FRRF and ^{14}C is reduced and is comparable to that observed from the AMT6 cruise.

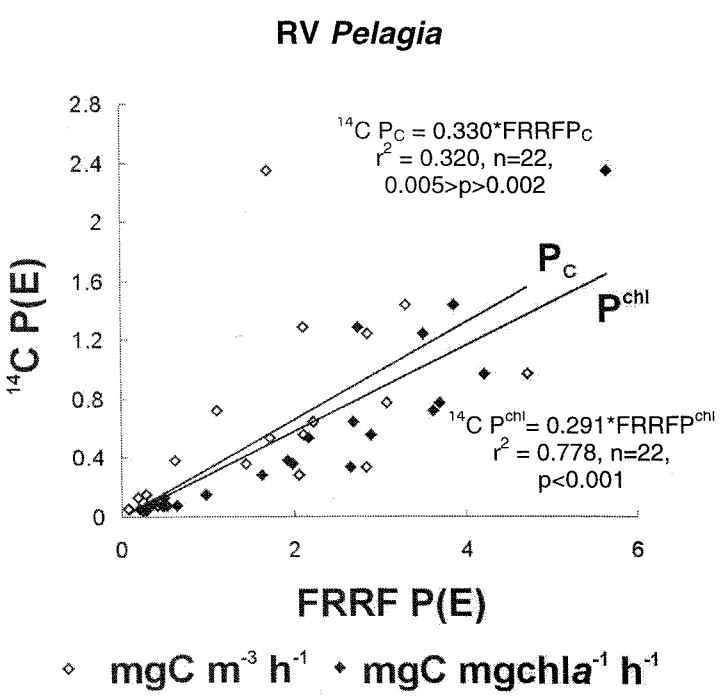

Figure 6.5.— Comparison of instantaneous estimates of production (P(E)) from *in situ* FRRF and *in vitro* ^{14}C-uptake measurements after accounting for the effects of spectral differences in the light source of the photosynthetron from that *in situ*. P(E) is shown as chl*a*-specific production (P^{chl}, mgC mgchl a^{-1} h^{-1}) and production per unit volume of water (ie. P^{chl} * [chl *a*]: mgC m^{-3} h^{-1}). ^{14}C P(E) were derived from reconstructed P-E curves (P(E) was extracted corresponding to the *in situ* E from which the water sample was taken). FRRF P(E) was determined from *equation 1.2.* and assumes a photosynthetic quotient of 1.

6.3. Modelling FRRF production

A basic model can be formulated to estimate FRRF instantaneous production where the actual FRRF temporal or spatial sampling resolution is less than desired. The model will be described using the data of site 2 (40°N) from the *RV Pelagia* cruise (see *Chapter 3*) and requires knowledge of the irradiance (E, µmol photons m^{-2} s^{-1}), light absorption (a*,

m^2 mgchl a^{-1}) and photosynthetic parameters determined from the FRRF. Calibrated light data were not available from the cruise. Therefore, the incident irradiance at the sea surface, which provides the energy for production, was estimated from the knowledge of time of year (Julian Day 76) and position (40°N 23°W), Kirk (1994). The diurnal variability of the incident irradiance was extracted from the uncalibrated ship-mounted PAR sensor and superimposed onto the estimated values (*fig. 6.6.*). The subsequent transition of the incident irradiance from air into water gives the required values of *in situ* irradiance which are used to calculate production. This model incorporates the effects of both reflection and refraction at the sea surface on the underwater light field. The estimates of reflection are dependent upon the solar elevation (β) and uses a refractive index (water:air) of 1.33 for seawater at ambient temperatures at any wavelength within the PAR spectrum (Kirk 1994). The water surface is assumed to be flat.

In situ irradiance (E) at each time (t) is calculated with respect to depth (z) as the product of E(t) and the vertical attenuation coefficient (K_d). Values of K_d were calculated at 10m intervals from light data collected by a PAR sensor mounted on the CTD frame (*fig. 6.6.*). A linear interpolation between these estimates provides a depth-dependent K_d ($K_{d(z)}$) and accounts for vertical differences in the spectral quality of PAR:

$$E_{(z,t)} = E_{(t)} \cdot K_{d\,(z)} \qquad \textbf{[6.1.]}$$

The rate of light absorption (*a*, μmol photons m^{-3} s^{-1}) is given by the product of the light intensity (E), the chlorophyll a-specific absorption (a^*) and the chlorophyll *a* concentration (mgchl *a* m^{-3}). Although a spectrum of absorption may be available, a single value of a^* is used for this model to correspond to the absorption at the peak wavelength of FRRF LED emission (475nm). This single value (0.054 m^2 mg chl a^{-1}) represents the mean of all measurements taken at site 2. In addition, *a* includes a characteristic estimate (the median) for the chl *a* concentration at this site, 0.8 mg chl *a* m^{-3}:

$$a_{(z,t)} = E_{(z,t)} \cdot a^*_{(z,t)} \cdot [\text{chl } a]_{(z,\,t)} \qquad \textbf{[6.2.]}$$

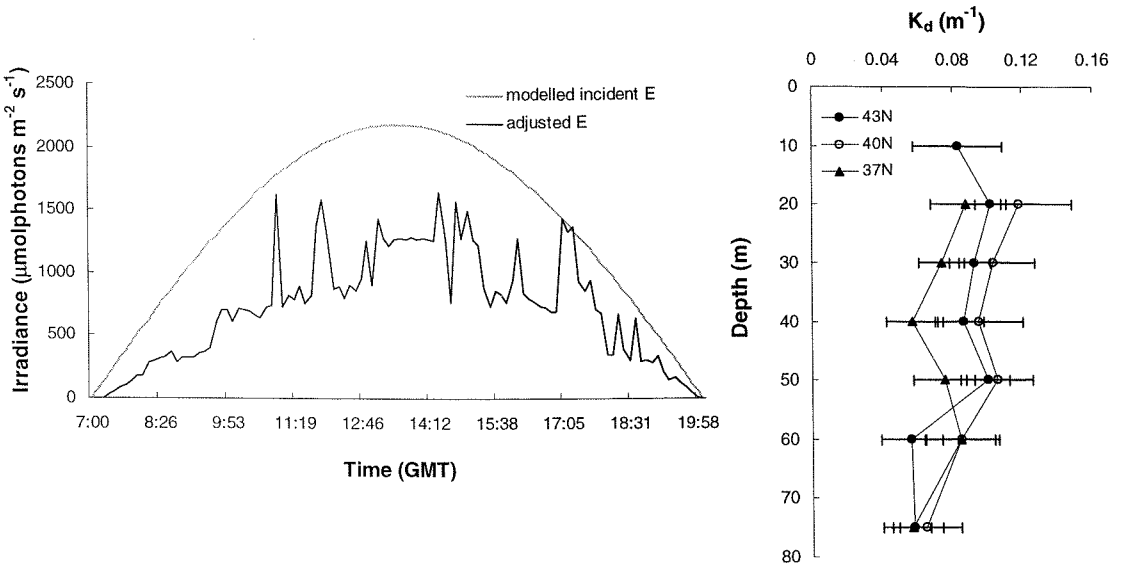

Figure 6.6.— (left panel) Modelled incident irradiance at the sea surface according to time of day and position (site 40°N). The uncalibrated surface PAR data were quantified assuming that the highest point at which the modelled and uncalibrated converged was a representative period of clear sky; (right panel) Vertical attenuation coefficients (K_d, m^{-1}) of PAR (400-700nm, measured from the FRRF PAR sensor) = $(\log E_{(Z1)}-\log E_{(Z2)})/(z_1-z_2)$ where light (E) is at depth (Z). Values at each depth are shown as the mean (± standard error) from all casts (n=4) performed during the day at the 3 sites.

Primary production is constructed from the product of the rate of light absorption (*a*) and the quantum yield of photosynthesis (ϕ_P, mol carbon mol photons^{-1}) (*equation 6.3.*). Values of ϕ_P were calculated from FRRF production divided by the product of chlorophyll *a*-specific absorption and light intensity ie. P(E)/(a* . E) at each depth and time where data was available. The relationships between discrete values of ϕ_P and E are given for each site occupied during the *RV Pelagia* cruise, *fig 6.7.* The relationship between ϕ_P and light at all sites is best described by an exponential equation. The equation from 40°N ($\phi_P = 0.0578e^{-0.0073*E}$, $r^2 = 0.887$, n=14 $p<0.001$) is applied throughout the model ($\phi_{P(E)}$) to account for variations in the quantum yield of photosynthesis throughout the day and with depth:

$$P_{(z,t)} = a_{(z,t)} \cdot \phi_{P(E)} \qquad \textbf{[6.3.]}$$

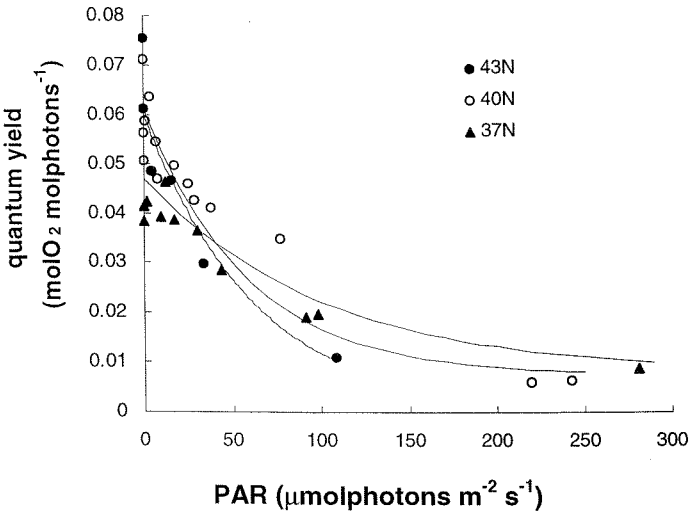

Figure 6.7.— Relationship between the quantum yield of photosynthesis (ϕ_p determined from P(E)/(a* . E)) from FRRF calculations of P(E), for each of the 3 sites. Data are taken from all casts performed throughout the diel period and is irrespective of time of day or depth.

Instantaneous model production was calculated throughout the diurnal period with a temporal resolution of 11 minutes and depth resolution of 2 metres (*fig 6.8.*). The model takes into account diel changes in incident solar radiation, vertical light attenuation within the water column, light absorption by phytoplankton, and the irradiance-dependence of the quantum efficiency of photosynthesis. It is clear from *fig 6.8.* that the underwater irradiance and absorption fields drive the spatial (vertical) and temporal pattern of modelled primary production.

The modelled production throughout the diurnal period reaches a maximum value of 0.12 μmolC m^{-3} s^{-1} (6.2 mgC m^{-3} h^{-1}). The depth and vertical extent of the zone exhibiting production values > 6.0 mgC m^{-3} h^{-1} increases with the increasing irradiance. Inhibition in the surface waters is established within the first 2 hours of the diurnal period and increases (in extent) with increasing irradiance. Values of modelled production have been integrated (0-60m) and further plotted in *fig. 6.8.* This trend indicates that a maximum value of integrated production (148-150 mgC m^{-2} h^{-1}) is reached by 09:15 (GMT), and is maintained throughout the diurnal period when photoinhibition becomes established in surface waters. Integrated production estimates based on arbitrarily assigned lower values of the incident irradiance (33%) show a similar pattern but with a lower maximum rate being maintained for a shorter period around midday. Confidence for this approach can be reinforced by comparing corresponding values of both *in situ* light and rates of production between the model and FRRF, *fig 6.9.* Both comparisons yield highly significant relationships with gradients close to 1.

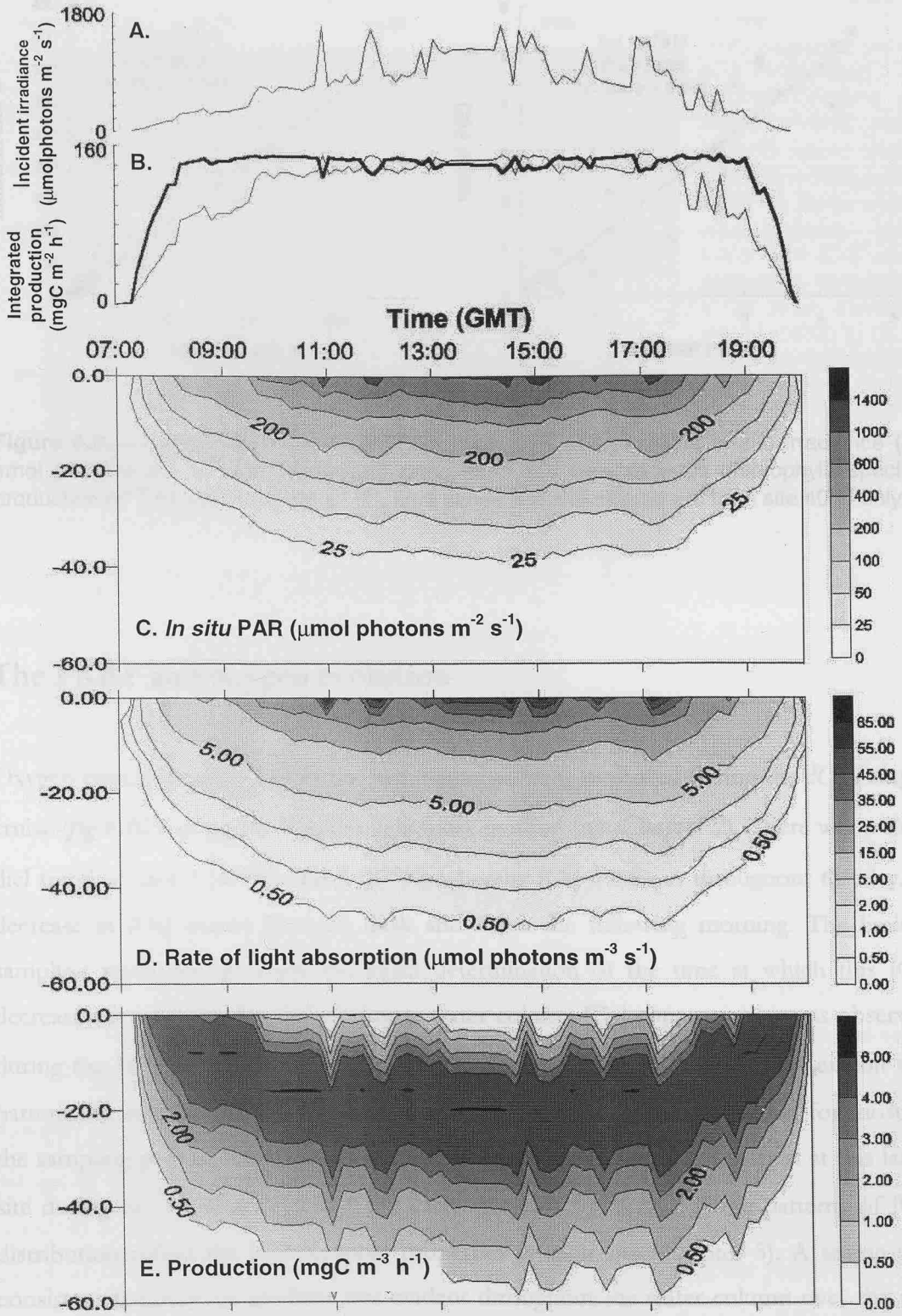

Figure 6.8.— Diurnal variability in parameters throughout the surface 0-60m at site 2 (40°N), RV *Pelagia* cruise following the model described in *equations 6.1-6.3*. All parameters are calculated according to modelled irradiance (panel C, µmol photons m^{-2} s^{-1}) following the incident irradiance (panel A), and to parameters measured using the FRRF. Depth integrated production (mg C m^{-2} h^{-1}) in panel B represents modelled production from 0-40m (panel E, mg C m^{-3} h^{-1}) using *in situ* irradiance (thick line) and 33% of *in situ* irradiance (thin line).

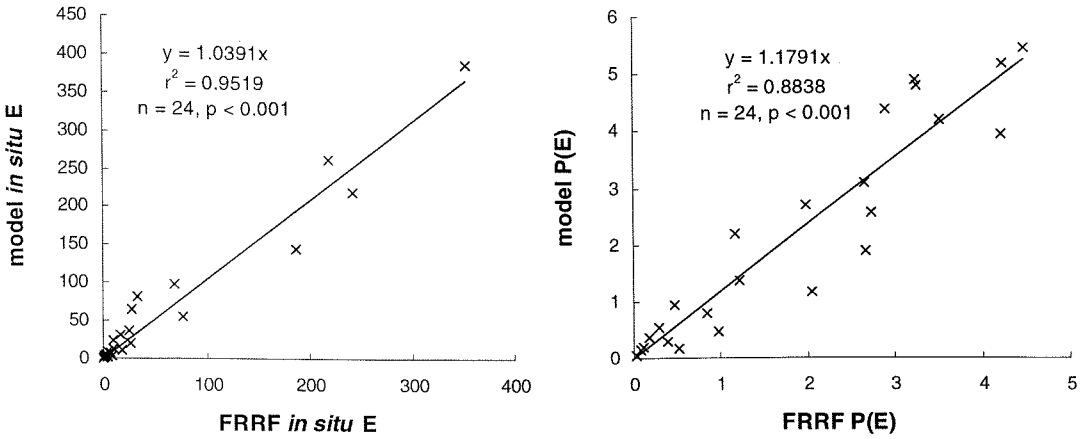

Figure 6.9.— Relationships between FRRF measured and modelled in situ irradiance (E, µmol photons m^{-2} s^{-1}, left panel) and rates of *in situ* instantaneous chlorophyll*a*-specific production ($P^{chl}(E)$, mg C mg chl a^{-1} h^{-1}, right panel). Data illustrated are from site 40°N only.

The FRRF and oxygen evolution

Oxygen concentrations [O_2] in the water column were measured during the *RV Pelagia* cruise (*fig 6.10.*), using the Winkler light/dark method (see *Chapter 2*). There was a clear diel trend at sites 2 (40°N) and 3 (37°N) whereby [O_2] increases throughout the day. A decrease in [O_2] occurs between dusk and dawn the following morning. The limited sampling resolution prevents the exact determination of the time at which this [O_2] decrease occurs; however the maximum water column [O_2] concentration was observed during the 16:30 and 21:00 GMT casts at both sites. Site 1 (43°N) does not exhibit this pattern but rather shows an increase in [O_2] throughout the water column for most of the sampling period. A decrease in the [O_2] of the water column is apparent at this latter site during the 13:30 and 16:30 CTD casts (see also *fig. 6.11.*). These patterns of [O_2] distribution reflect the hydrographic properties at each site (Chapter 3). A strong and consistent temperature gradient was evident throughout the water column over the diel period at site 3, and to a lesser extent sire 2. Conversely, the structure of the water column appeared less stable over the same period at site 1 (*figs. 3.2.* to *3.4.*)

The estimates of production provided by both the model and the FRRF are originally given in mmolO_2 (see *equation 1.1, section 1.4.*). Values of *in situ* [O_2] describe the

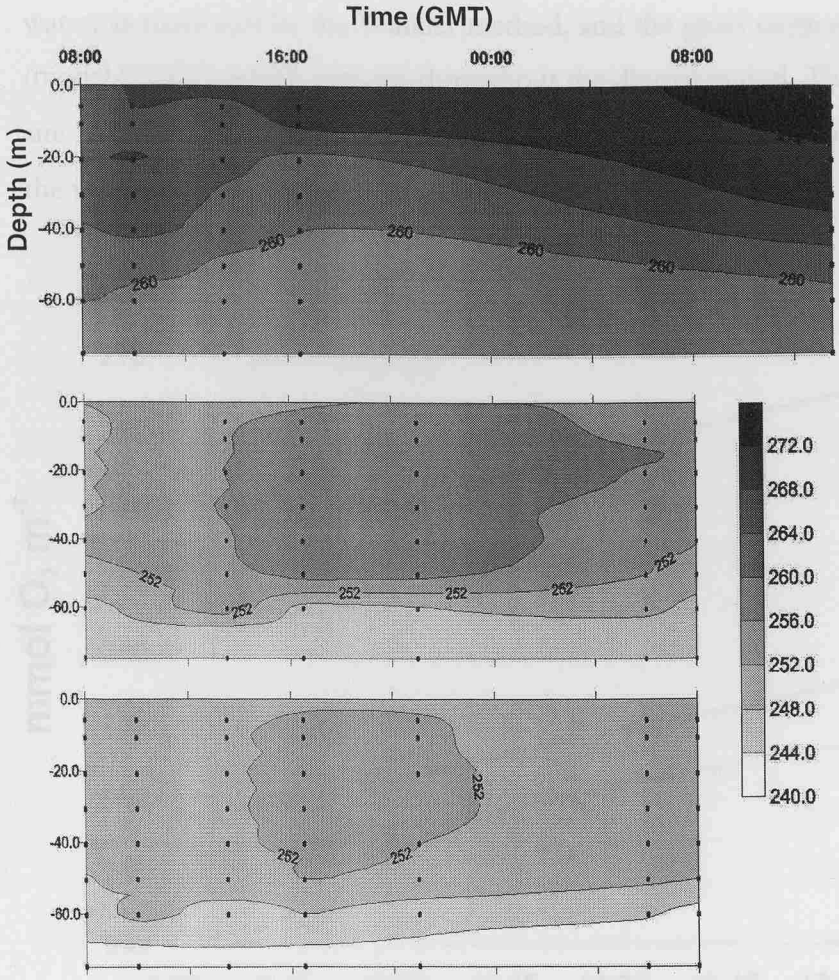

Figure 6.10.— Oxygen concentrations (mmol m^{-3}) measured by Winkler titrations for the 3 sample sites: 1(43°N) upper panel, 2 (40°N) middle panel, 3 (37°N) lower panel. Measurements were taken from CTD casts performed throughout a 24 hour sampling period (08:00 to 08:00 GMT) as represented by the filled circles. Sampling at site 1 (43°N) continued further until 13:30 the following day.

oxygen content of the water but are not analogous to production. As such, only the trends in oxygen production can be compared between corresponding data. The rate of gross oxygen production measured by the FRRF/model can be expressed cumulatively over time to express the contribution of photosynthetically produced oxygen to the water column throughout the day. The mean [O_2] throughout the mixed layer ie. 0-40m, (see *Chapter 3*) from both Winkler measurements and cumulative O_2 modelled production, are given for the 3 sample sites in *fig 6.11.* The initial background oxygen content is assumed to be close to that measured at 08:00 GMT by the Winkler method for the data point when FRRF/model production is equal to time 0 hours for the purposes of this comparison. Data from site 40°N show that the cumulative amount of O_2 calculated from the model is greater than the *in situ* increase in [O_2] throughout the day. When the modelled oxygen production is divided by 2 (and again expressed cumulatively), a regression with a slope close to 1 is established between the corresponding points (see figure heading). This difference reflects an offset between the net oxygen content of the

water, as measured by the Winkler method, and the gross oxygen production from PSII (model/FRRF), which remains throughout the diurnal period. This pattern is repeated at site 37°N but not at 43°N and presumably reflects the more physically variable nature of the water column throughout the diel period at the latter station.

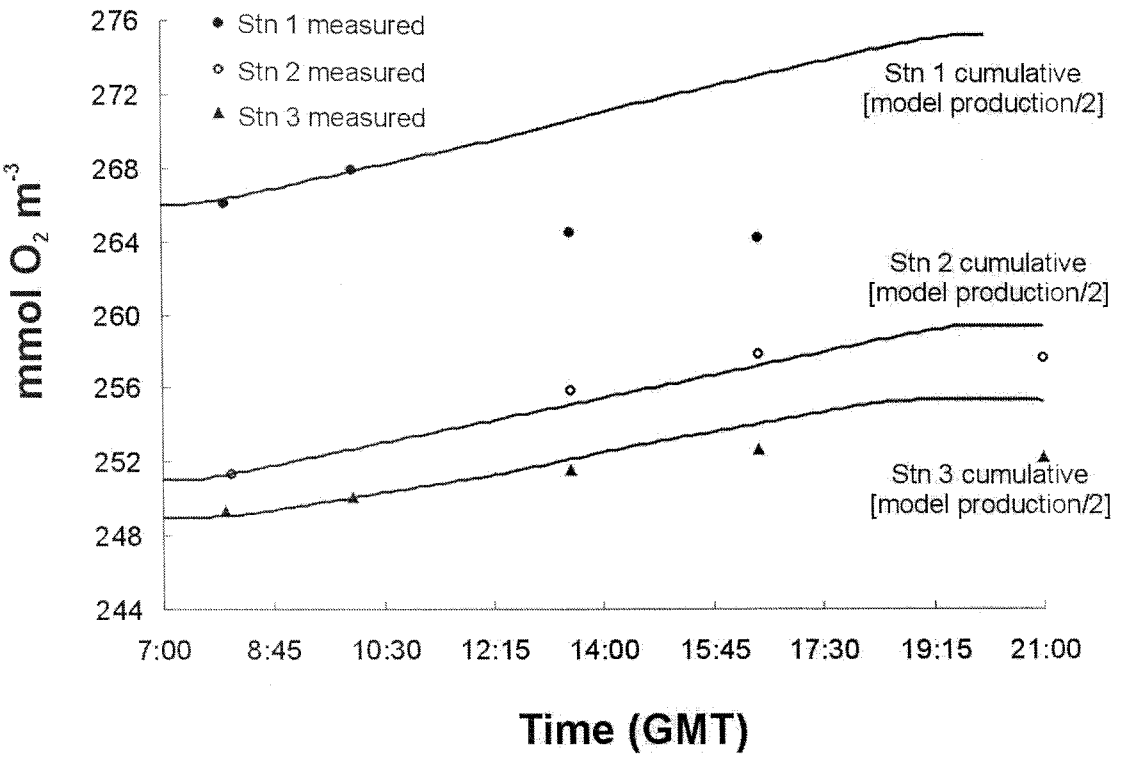

Figure 6.11.— Relationship between measured oxygen concentration (Winkler method, mmol O_2 m^{-3}) and modelled FRRF production (mmol O_2 m^{-3} h^{-1} * multiplied by time interval between estimates). Both measured and modelled data are the mean from 0-40m for each respective cast. The modelled data shows the cumulative (mean) O_2 production throughout the day assuming an initial [O_2] which approximated to the initial mean (measured) [O_2]. A significant regression is found between true modelled O_2 production and measured [O_2]: **40°N**: modelled [O_2] = 2.16*measured [O_2] – 291.66, r^2=0.888 n=4, 0.02 > p > 0.01. Significant relationships are also observed where modelled (O_2) production values (P(E)) are divided by 2 and again expressed cumulatively: **40°N**: modelled [O_2]/2 = 1.0003*measured [O_2], r^2=0..883 n=4, 0.02 > p > 0.01; **37°N**: modelled [O_2]/2 = 1.004*measured [O_2], r^2=0.744 n=5, 0.05 > p > 0.02. All other relationships were not significant.

6.4. Reconciliation of differences between FRRF, ^{14}C-uptake and O_2 estimates of production.

The photosynthesis-irradiance response curves for ^{14}C-uptake typically yield mean values of photosynthesis (P_{max}^{chl}, *table 6.1.*, P(E), *figs, 6.3* and *6.5.*) that are a factor of 2-3 lower than those determined by the FRRF. Several reasons could account for this discrepancy including a wrong assumption about the PSU size for FRRF calculations, an error in the estimation of E_k for the FRRF profiles, a failure to account for uncoupling of gross electron transfer (gross oxygen evolution) rates from net carbon-fixation rates in the FRRF calculations and/or errors in ^{14}C assimilation measurements associated with bottle effects. Although the last possibility cannot be ruled out, the P-E curves for RV *Pelagia* ^{14}C labeled samples incubated for periods of 30, 60 and 120 minutes were very similar indicating that photosynthesis was not time-dependent (at least between 30 and 120 minutes) and that the incubations were free from artefacts due to contamination (R.Geider, pers.comm.).

The number of PSII reaction centres, n_{PSII}— Estimation of P^{chl} using the FRRF is dependent on assuming an appropriate value for the photosynthetic unit size (PSU) of photosystem II ($1/n_{PSII}$: 500 and 300 molchl *a* molRCII^{-1} for eukaryotes and prokaryotes, respectively, Falkowski and Kolber 1995). However, observations on laboratory cultures indicate that $1/n_{PSII}$ can range from 133 to 384 molchl *a* molRCII^{-1} in *Synechococcus* spp. and 280 to 830 molchl *a* molRCII^{-1} in eukaryotic organisms (see *table 4.1., Chapter 4*). Furthermore, values of n_{PSII} appear to vary throughout the day and will alter corresponding estimates of photosynthesis. A comparison between production estimates (P^{chl}) using the constant $1/n_{PSII}$ (above) and those using the calculated $1/n_{PSII}$ (*Chapter 4*, data from RV *Pelagia* and RRS *Challenger* cruises), *fig 6.12.*, indicate that P^{chl} and, therefore, P_C, will be underestimated where a constant n_{PSII} is assumed. The greater spread of data around the regression line of the prokaryote populations (RV *Pelagia*) indicates that the relative changes of their naturally lower $1/n_{PSII}$ are greater than those seen for the eukaryote populations of the RRS *Challenger* cruise.

These calculations do not help to reconcile the ^{14}C results since they imply that the difference with corresponding FRRF estimates should be even greater. However, there are a number of uncertainties in the estimation of PSU_{RCII}, including the assumption of

equal distribution of excitation energy between RCI and RCII within the wavelength band of the FRRF light source, evaluation of the fraction of photochemically active RCIIs from $0.65/(F_v/F_m)$, and measurement of the absorption of light by photosynthetic pigments (see *Chapter 4*).

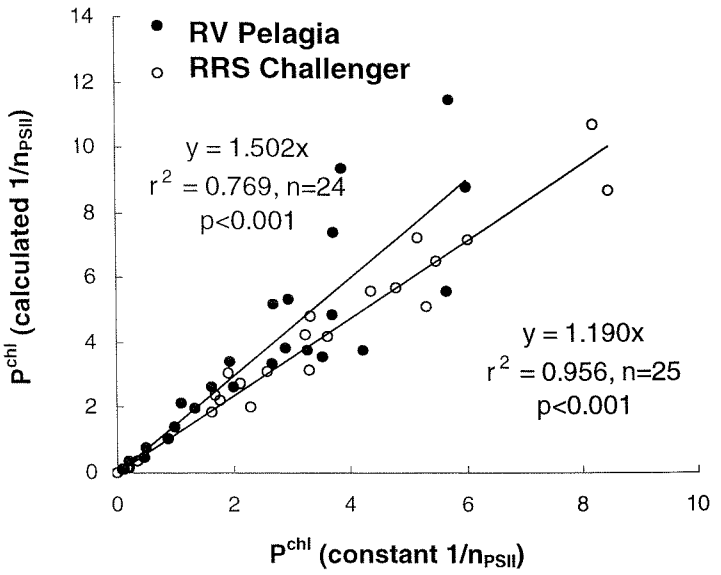

Figure 6.12.— Relationship between FRRF rates of instantaneous chlorophyll *a*-specific production (P^{chl}: mgC mg chl a^{-1} h^{-1}) calculated using a constant $1/n_{PSII}$ and corresponding derived values of $1/n_{PSII}$ (re. *Chapter 4*). Constant values of 300 and 500 molchl a $molRCII^{-1}$ were used throughout cruises RV *Pelagia* and RVS *Challenger* since the phytoplankton population were dominated by prokaryotes and eukaryotes, respectively. Corresponding calculations of $1/n_{PSII}$ were made following *equation 4.3., Chapter 4.*

Estimation of E_k— The light saturation parameter (E_k) is used to estimate the quantum yield of photosynthesis ($\phi_p = \phi_e * qP$) via the calculation of the minimum turnover time of electrons (τ_p) through the photosystem (following Falkowski 1992, Sakshaug *et al.* 1997: τ_p = 1/(light intensity of light saturated photosynthesis * functional absorption cross section) or $1/(E_k * \sigma_{PSII})$. Using the RV *Pelagia* data as an example, mean values of ^{14}C E_k (85.95, 76.11 and 82.71 µmolphotons m^{-2} s^{-1} for sites 1, 2 and 3 using the spectral correction) exceed those of the FRRF by a factor of 0-1.5. However, the FRRF determination of E_k comes from plots of qP versus E (see *Chapter 3*) and must, therefore, be considered as subjective and prone to error. If the FRRF E_k from site 2 (40°N) is assumed to be under-estimated by a factor of 1.5 then subsequent calculations of P(E) (above E_k) will be overestimated, *fig. 6.13.* Conversely, an over-estimation of FRRF E_k would result in higher values of [estimated] τ_p and subsequently lower values of P(E), thereby, accounting for some of the difference between the ^{14}C and FRRF techniques.

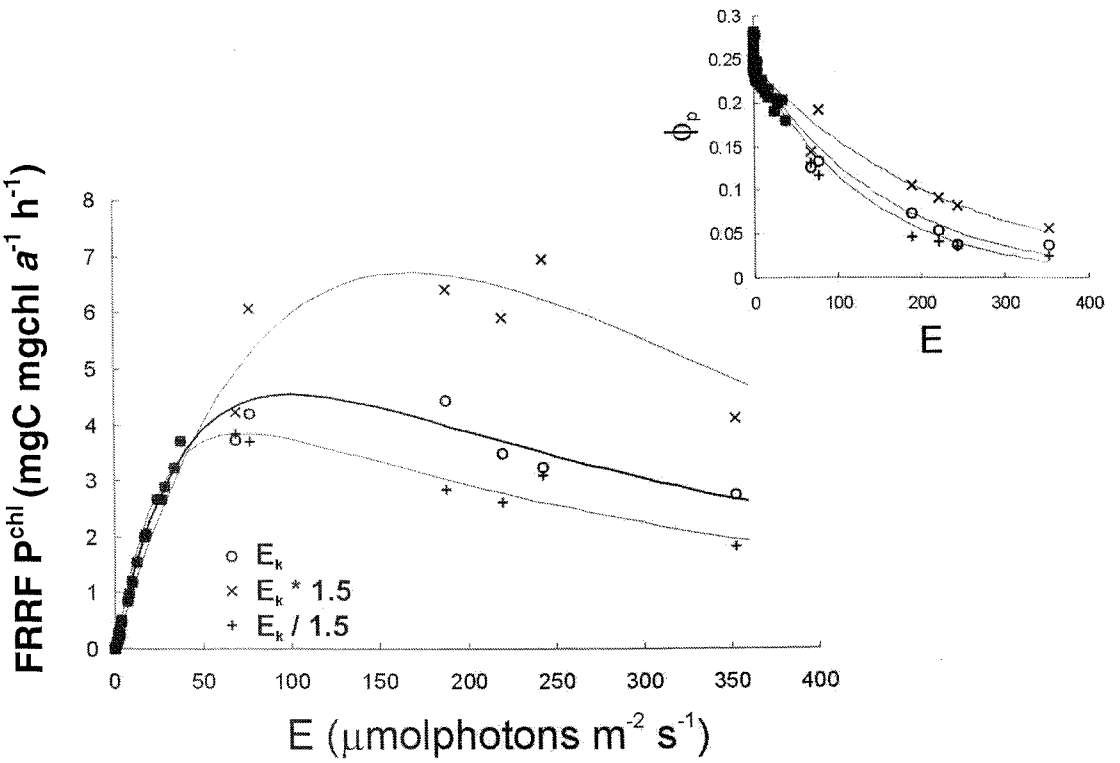

Figure 6.13.— Sensitivity analysis of variations in estimate of E_k (the light saturation parameter) to subsequent [FRRF] calculations of the quantum yield of photosynthesis (ϕ_p, $molO_2$ mol photons^{-1}, = ϕ_e, see *section 1.4.*, * qP) and instantaneous chlorophylla-specific photosynthesis (P^{chl}). Data is from site 2 (40°N), RV *Pelagia* cruise where E_k was estimated as 53.6 µmolphotons m^{-2} s^{-1} from a plot of qP versus irradiance (E). This values was then multiplied and divided by a factor of 1.5 for the purposes of this analysis.

This type of sensitivity analysis does not account for the differences between the chlorophyll *a*-specific initial slope of the P-E curve (α_{chl}) between the two techniques but does demonstrate that values of τ_p measured by the FRRF are insufficient to fully describe the actual electron transfer process (Kolber 1997). A comparison of values of τ_p measured by the FRRF (see *sections 1.3.*, *1.4.* and *2.1.*) with those estimated using $1/(E_k * \sigma_{PSII})$ for the *RV Pelagia* data is given in *fig. 6.14.* The measured values of τ_p are lower (by a factor of approximately 1.5-2.2) than those that are derived. τ_p measured during AMT6 and RRS *Challenger* cruises (data not shown) were 1.5-2.35 times lower than corresponding estimates from $1/(E_k * \sigma_{PSII})$. Although there appears a consistent difference between the two approaches there is no statistically significant relationship. Typical values of τ_p are reported to be between 2 and 15 ms and reflect the rates of the [PSI] dark reactions of photosynthesis (Kolber and Falkowski 1993). The values of α_{chl} and, therefore differences between FRRF and ^{14}C P(E) at irradiances below E_k, will be

sensitive to quantitative determinations of other parameters describing production ie. n_{PSII} and σ_{PSII}.

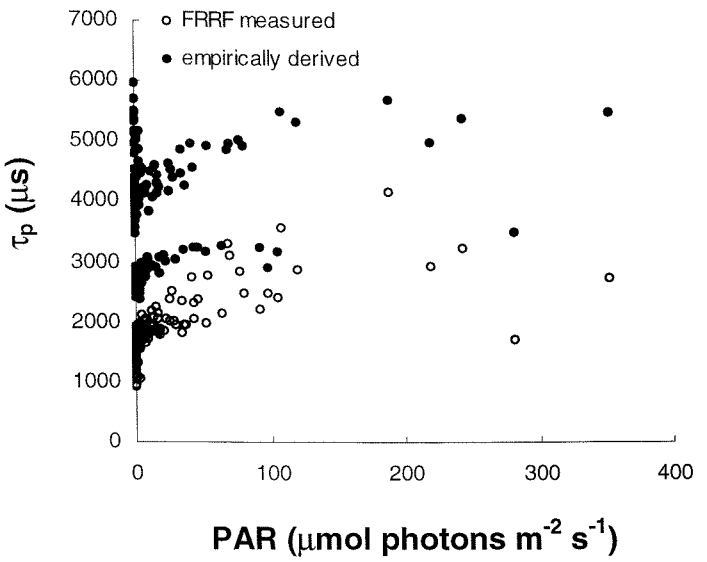

Figure 6.14.— Estimates of the minimum turnover time of electrons (τ_p) with corresponding measurements of light from all data collected at the 3 diel sites of the *RV Pelagia* cruise (*Chapter 3*). τ_p was determined from direct FRRF measurements and from empirical derivations ($1/(E_k * \sigma_{PSII})$ where E_k is obtained from plots of qP versus light and σ_{PSII} is obtained directly from the FRRF). No significant relationship was observed between corresponding measurements of τ_p.

It is possible to summarise the maximum error inherent to estimations of production using the FRRF (*table 6.2.*) where limits to the assumptions comprising *equation 1.1.* (p. 26) are known. The highest and lowest reported values of $1/n_{PSII}$ in the literature (*table 4.1.*) are significantly different from the values typically assumed and could lead to an error in the estimation of FRRF production by a factor of upto 2.25. The FRRF derivation of E_k (qP versus E) assumes that the water column is well mixed throughout (see *fig. 1.7.*); however, stratified water bodies contain distinct phytoplankton populations which display higher values of E_k (acclimated to high light) in surface waters when compared with corresponding values from deeper waters. The FRRF derivation of E_k in stratified waters will, therefore, represent some intermediary between the maximum and minimum present throughout the water column. The greatest difference between surface and deep water values of E_k are observed in open ocean waters (eg. Kirk 1994). A consideration of this difference could account for a further error in the FRRF estimation of production by a factor of +0.66, -10. (*table 6.2.*) Finally, the measurement of σ_{PSII}, following the excitation by blue light, is known to be overestimated in waters where spectral irradiance is narrower and shifted further into the red (Kolber and Falkowski 1993); for example, deep water and coastal waters. The extent of error in the subsequent calculation of production is more difficult to quantify and will be a function of the *in situ* spectral irradiance. The product of one or more of these factors represents

an extreme potential for error but does highlight the need for accurate assumptions when using the FRRF to estimate production.

Parameter	Limits of reported values	Effect on FRRF estimation of production
$1/n_{PSII}$ (mol chl *a* molRCII^{-1}) for eukaryotes	830 - assumed value of 500 underestimates by a factor of (830/500) 1.66	overestimated by a factor of 1.66 using assumed value
	280 – assumed value of 500 overestimates by a factor of 1.79	underestimated by a factor of 1.79 using assumed value
$1/n_{PSII}$ (mol chl *a* molRCII^{-1}) for prokaryotes	384 – assumed value of 300 underestimates by a factor of 1.28	overestimated by a factor of 1.28 using assumed value
	133 – assumed value of 300 overestimates by a factor of 2.25	underestimated by a factor of 2.25 using assumed value
E_k – stratified waters	Examples of the maximum factor of difference between open ocean surface and deep water measurements: 4.8 (Takahaski *et al.* 1988) 3 - 4.5 (Cullen *et al.* 1992) 2 - 10 (Marañón and Holligan 1999)	Using extreme values: overestimated by a factor of 0 – 10; underestimated by a factor of 0 – 6.57. Will depend on the *in situ* irradiance sample is measured at in relation to the E_k.
σ_{PSII}	Overestimated in waters where spectral irradiance is shifted further into the red	overestimated

Table 6.2.— Summary of factors of error upon the FRRF estimation of production using extreme reported values as the assumed parameters in the empirical equation (*equation 1.1.*, p.26). The number of reaction centres ($1/n_{PSII}$) are according to *table 4.1.* Example values of the light saturation parameter, E_k, are obtained from investigations in stratified open waters. The functional absorption cross section, σ_{PSII}, is measured by the FRRF (and not assumed in the empirical calculation) but remains subject to error. These factors are taken to be independent of any further operator error.

Relating O_2 evolution with CO_2 uptake— The FRRF provides a measure of the rate of electron transfer through RCII, which should be proportional to the gross rate of oxygen evolution. The assimilation of ^{14}C is commonly assumed to represent net carbon dioxide fixation even when incubation times are relatively short (≤1 hour), eg. Williams (1993). Therefore, the rate of gross oxygen evolution should not be expected to equal that of net carbon fixation. Amongst the processes that can account for the divergence of gross oxygen evolution from net carbon dioxide assimilation are the Mehler reaction, photorespiration (RuBP oxidase), both of which lead to photosynthetic oxygen consumption and are collectively termed 'light respiration' (eg. Grande *et al.* 1991), 'dark' respiration, and the utilisation of reductant generated by photosynthetic electron transfer for reactions other than carbon dioxide fixation. These processes are reviewed in *section 1.1.*

Typically, dark respiration can account for a 15% reduction in gross photosynthesis (Geider 1992). The utilisation of reductant for processes other than carbon assimilation is accounted for as the photosynthetic quotient (O_2/CO_2). This parameter can vary from 1.4 ± 0.1 when cells are growing with nitrate as the N source to 1.1 ± 0.1 when ammonium is the N source (Laws 1991), but has been reported as high as 2-3 for mixed assemblages of phytoplankton (Williams and Robertson 1991) and in cultures of *Synechoccocus* (Grande *et al.* 1991). These authors explain that this higher photosynthetic quotient is the result of nitrate metabolism, which involves hydrolysis of water and hence relatively more O_2 evolution, and light respiration. The Mehler reaction has been reported to account for 50% of gross oxygen evolution at light saturation in *Synechococcus* (Kana 1992). Therefore, a combination of processes of light respiration and a photosynthetic quotient of 1.4-2.0 could account for about a 3-4 fold difference between ^{14}C assimilation and gross oxygen evolution. This is consistent with the differences observed between the FRRF and ^{14}C estimates of production presented here.

The Mehler reaction is likely to account for uncoupling of gross oxygen evolution from net carbon dioxide fixation at irradiances that exceed E_K, but is not thought to be important at low irradiances corresponding to the initial slope region of the P-E curve (Kana 1992). The initial slopes (α^{chl}) from the FRRF P-E curves exceed those from the ^{14}C curves by a factor of 3-4 (*table 6.1.*). This difference is higher than can be explained relative to the importance of CO_2 and other compounds as electron acceptors through the photosynthetic quotient (Falkowski and Raven 1997) and to dark respiration. As such, it must be assumed that differences in α^{chl} reflect the respective abilities of the two techniques to accurately describe instantaneous photosynthesis.

6.5. Summarising the FRRF quantification of primary production

Despite the growing use of fluorescence techniques to provide estimates of production there are few comparisons amongst the literature with more classical techniques, such as ^{14}C-uptake (*table 6.3.*). Kolber and Falkowski (1993) obtain a coefficient of determination (r^2) of 0.74 and a slope of 1.06 between paired data of fluorescence (pump and probe) derived and ^{14}C (chl *a*-specific) instantaneous production. Boyd *et al.* (1997) observed a weaker relationship when comparing P_m^{chl} from vertical profiles (P-E) using

Reference	Relationship	Significance	Details
		FRRF versus ^{14}C	
This study	FRRF P^{chl} = ^{14}C P^{chl}*3.055	r^2 = 0.663 n=22	Using instantaneous P^{chl} from discrete measurements
Boyd *et al.* 1997	FRRF P^{chl} = ^{14}C P^{chl}*0.242	r^2 = 0.272 n=15	FRRF P_m^{chl} from water column profile compared with discrete ^{14}C P_m^{chl}
Kolber and Falkowski 1993	FRRF P^{chl} = ^{14}C P^{chl}*1.272	r^2 = 0.740 n=61	Using instantaneous P^{chl} from discrete measurements
		FRRF versus diel O_2	
This study	FRRF(†) PO_2= $[O_2]$*(2.16 to 2.45)	r^2 = 0.888 n=4 r^2 = 0.840 n=5	Discrete $[O_2]$ measurements compared with modelled O_2(†)
		$^{18}O_2$ versus ^{14}C	
Kiddon *et al.* 1995	Gross $^{18}O_2$ = 2.01*^{14}C assim	r^2 = 0.98 n=31	Discrete samples compared
Langdon *et al.* 1995 (††)	Gross $^{18}O_2$ = (1.16 to 2.55)* ^{14}C assim		Discrete samples integrated over 24 hrs compared
Grande *et al.* 1989 (††)	Gross $^{18}O_2$ = (1.74 to 2.75)* ^{14}C assim		Discrete samples compared
		O_2 light/dark bottle versus ^{14}C	
Davies and Williams 1984 (††)	Gross O_2 = (0 to 2.5)* ^{14}C assim		Discrete samples compared
Williams *et al.* 1979 (††)	Gross O_2 = 1.95*^{14}C	r^2 = 0.96 n=167	Discrete samples
Williams *et al.* 1983 (††)	Gross O_2 = (0.92 to 1.66)* ^{14}C assim		Discrete samples compared
Williams and Purdie 1991 (††)	Gross O_2 = (1.13 to 1.96)* ^{14}C assim		Discrete samples compared

Table 6.2.— Summary of reported relationships between corresponding estimates of production between alternate techniques. Note FRRF comparisons by Kolber and Falkowski (1993) and Boyd *et al.* (1997) used a pump and probe fluorometer which involves more assumptions to the underlying methodology/calculation of production than the FRRF; (†) indicates that model [FRRF] production is used rather than the direct *in situ* FRRF measurements; (††) indicates approximate differences between production estimates from alternate methods since corresponding data are given in the form of a tables or diagram. Values for the relationships shown here are adjusted (for comparative purposes) to those cited by removing any included photosynthetic quotient (s). This table does not represent a complete list of studies but aims to present the range of values reported throughout the literature.

the pump and probe with discretely measured ^{14}C samples. In addition, these latter authors observed FRRF values of P_m^{chl} that were markedly lower than those from ^{14}C-uptake experiments. However, both these comparisons are limited since pump and probe methodology involves more assumptions, for example σ_{PSII} must be assumed constant or measured on-deck, than the FRRF methodology. As such, any direct comparison between these studies should be treated with caution.

The FRRF appears to give *in situ* estimates of gross O_2 evolution which are significantly higher than equivalent estimates derived using the ^{14}C-uptake methodology. These differences may represent the contrasting mechanisms associated with the light and dark processes of photosynthesis, which can ultimately account for 2-3 times more gross O_2 evolution than corresponding ^{14}C-uptake, and is consistent with observations of gross O_2 production using more conventional methods (see *table 6.3.*). However, the stochiometry between O_2 evolution and ^{14}C uptake is known to be quite variable between taxa/trophic regimes, (Laws 1991, Williams *et al.* 1979, 1983, Williams and Robertson 1991) therefore, FRRF O_2 production is likely to relate differently to ^{14}C under alternate oceanographic conditions.

This investigation demonstrates that FRRF determined *in situ* production may closely follow that of the water column as determined by indirect Winkler methods, but is likely to be closer to 3-4 times higher than that estimated by ^{14}C uptake. This difference presumably accounts for discrepancies associated with the parameters comprising the FRRF production algorithm (for example n_{PSII} and the calculation of E_k, see above) and ^{14}C-uptake methodology (ie. confinement effects, such as, temperature and light). Longer-term incubations are described to affect the population characteristics of the water sample and typically lead to under-estimations of productivity based on isotopic uptake (eg. Lohrenz 1993). The AMT6 data demonstrates that longer incubations result in a greater discrepancy between FRRF and ^{14}C production. Data from eutrophic waters appear to produce a relationship that is similar to that observed from the short term P-E experiments of RV *Pelagia* and RRS *Challenger*. Conversely, samples from oligotrophic waters reveal a higher discrepancy between the two methods. Oligotrophic samples are predominantly composed of small prokaryotic phytoplankton under low concentrations of new nutrients (AMT6, *Chapter 5*) and suggests that the effects of confinement are most significant where a 'recycling' [of nutrients] community predominate. The

heightened difference between FRRF and ^{14}C P(E) estimates from the oligotrophic [longer term] incubations would further suggest that the ^{14}C techniques may underestimate CO_2 uptake by a factor as high as 2 (Williams *et al.* 1983) and is of considerable consequence to the carbon budget of a large proportion of the global marine system. However, such speculation is inconclusive given that there are still unexplained differences between both the processes and measurement of CO_2 uptake and O_2 evolution.

7. Summary and conclusions

7.1. General discussion of the variability of PSII and production as observed from FRRF measurements

Calculation of FRRF photosynthesis is achieved as the product of several measurable parameters, as defined in *equation 1.1.* Variability from the estimation of σ_{PSII}, the functional absorption cross section, F_v/F_m, the quantum efficiency of photochemistry, n_{PSII}, the number of reaction centres and E_k, the light saturation parameter, in addition to the amount of light (E), all contribute to the observed variability in oxygenic production estimates. The preceding chapters demonstrate that σ_{PSII} and F_v/F_m consistently respond to environmental variability.. Changes in σ_{PSII} and F_v/F_m have been previously documented to follow changes in light (eg. Vassiliev *et al.* 1994) or nutrients (eg. Kolber *et al.* 1988, 1990) relative to the background photoadapted state. However, the responses of PSII in nature are not controlled by mutually exclusive variables (Kolber *et al.* 1988, Falkowski 1992, Falkowski and Kolber 1995). The data presented in this study observes PSII variability over a wide range of co-varying environmental conditions. These observations can be summarised into a general schematic model for both σ_{PSII} and F_v/F_m throughout the Atlantic Ocean (*fig 7.1.*).

Changes in σ_{PSII} reflect alterations to the functional PSII antennae size and also changes in the number of functional reaction centres (RCIIs) and hence F_v/F_m. The product of these two parameters represents the rate of PSII light saturation and the ability of PSII to maintain high or light saturated levels of photosynthesis. The response of σ_{PSII} and F_v/F_m to variations in environmental parameters throughout this thesis appear consistent (summarised as *fig 7.1.* from trends observed in *Chapter 3* to *5*) and assumes that phytoplankton are acclimated to optimal conditions of light and nutrients available for growth. However, data from the Benguela upwelling (*Chapter 5*) have already illustrated that young phytoplankton populations in recently upwelled water lack a strong

acclimation status to light and/or nutrient regimes. Therefore, the schematic responses described by *fig 7.1.* may become altered under such dynamic conditions.

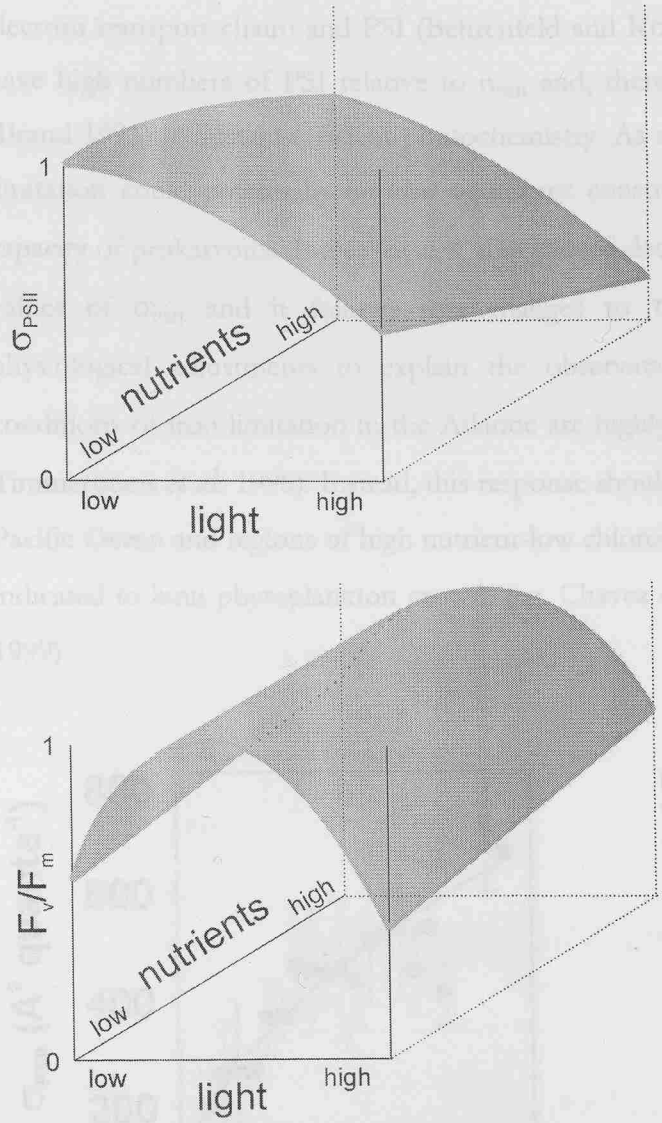

Figure 7.1.— Schematic summary of the *in situ* functional absorption cross section (σ_{PSII}) and quantum efficiency of photochemistry (F_v/F_m) following bivariate changes in light and nutrient conditions in the Atlantic Ocean. The bivariate response represents an interpolation between parameter-light and parameter-nutrient interactions. These relationships are non-linear and are characteristic responses from a variety of scales (within the life time of an organism) from Chapters 3-5. All axes consider relative changes to parameters. An initial photoadapted status of PSII must be assumed. Subsequent changes in light and nutrients will determine the described response over short (photoprotection) and long (acclimation) time scales. Exceptions to this model are stated in the main text.

The trends summarised in *fig. 7.1.* may require modification where conditions of physiological limitation, not investigated in *Chapters 3* to *5*, occur. An alternate response of σ_{PSII} by prokaryotic algae is apparent under conditions of iron limitation (Behrenfeld *et al.* 1996, see *fig 7.2.*) whereby σ_{PSII} rapidly increases upon the addition of iron to iron-depleted waters of the Pacific. Laboratory investigations of iron-limitation upon eukaryotic algae (Greene *et al.* 1991, 1992) observe elevated values of σ_{PSII}, τ_p, and n_{PSII} but a decrease in E_k. This is consistent with the response described in *fig. 7.1.* and, in terms of the equation $\sigma_{PSII} = 1/(\tau_p \, . \, E_k)$, Sakshaug *et al.* (1997), suggests that increases in

the minimum electron transfer time (τ_p) do not exceed the decrease to the light saturation parameter (E_k) in eukaryotic algae. Iron limitation leads to a decrease in cellular constituents with high iron requirements, such as cytochrome b_6f (part of the electron transport chain) and PSI (Behrenfeld and Kolber 1999). Prokaryotic organisms have high numbers of PSI relative to n_{PSII} and, therefore, a high requirement for iron (Brand 1991) to sustain efficient photochemistry. As such, one might consider that iron limitation could potentially impose significant constraints upon the electron transport capacity of prokaryotes. Increases in τ_p that exceed decreases in E_k would explain the low values of σ_{PSII} and it follows that changes to τ_p must predominate over other physiological adjustments to explain the observations in *fig 7.2*. It is noted that conditions of iron limitation in the Atlantic are highly debatable (eg. Martin *et al.* 1993, Timmermans *et al.* 1998). Instead, this response should be most readily observable in the Pacific Ocean and regions of high nutrient-low chlorophyll (HNLC) where iron has been indicated to limit phytoplankton growth (eg. Chavez *et al.* 1991, Pitchford and Brindley 1999)

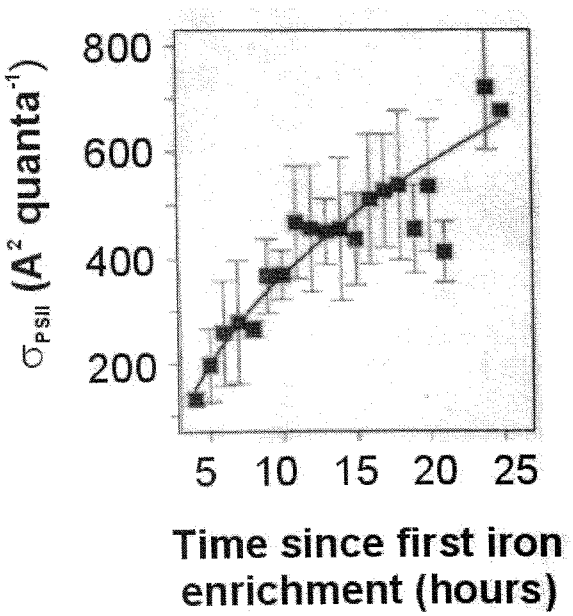

Figure 7.2.— Changes to the functional absorption cross section (σ_{PSII}) following iron additions, Ironex II (taken from **Behrenfeld *et al.* 1996**), Pacific Ocean. Mean σ_{PSII} ± s.d. are shown as measured on a flow-through of seawater from 3 metres, dark adapted for 3 minutes.

A need for the accurate knowledge of both the minimum turnover time of electrons (τ_p) and the number of reaction centres (n_{PSII}) is also required for calculating production using the FRRF (see *Chapter 6*). The FRRF does not appear to provide accurate quantitative estimates of τ_p; however, a subjective analysis of FRRF derived τ_p indicates

that this parameter is strongly affected by environmental change (*fig 7.3.*). Values of FRRF τ_p measured during the RRS *Challenger* cruise (*Chapter 4*), increase upon exposure to high light. Furthermore, this response is most obvious in data from the nutrient limited surface stratified waters of site U. These differences suggest that both high light and/or low nutrient concentrations increase the minimum turnover time of electrons presumably as a result of photoinhibition processes within PSII but also Calvin Cycle activity since the oxidation of the PQ pool is controlled by the dark reactions of photosynthesis (Kolber and Falkowski 1993). As such, this response of τ_p will also be strongly temperature dependent (Falkowski and Raven 1997). An ability to maintain low values of σ_{PSII}, through quenching and the prevention of damage to the reaction centres, and τ_p (fast photochemical turnover) will result in a high E_k (see Sakshaug equation above) and reflects acclimation to high light.

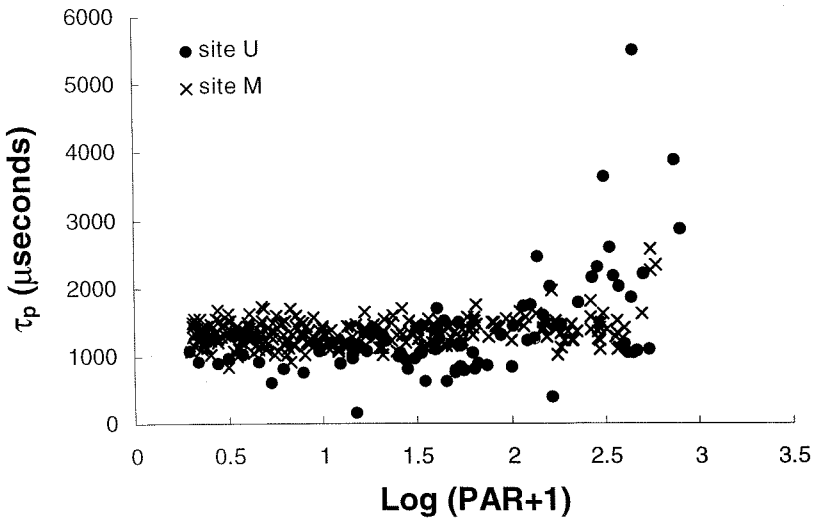

Figure 7.3.— Relationship between the minimum turnover time of electrons (τ_p, as measured from the FRRF dark chamber) and irradiance (log (PAR, μmolphotons m^{-2} s^{-1},+1)) from all data measured during the day at the mixed site (M) and [the surface 20m] of the stratified site (U), RRS *Challenger* cruise, *Chapter 4*. The mean of corresponding τ_p measurements taken at night (ie. dark acclimated) from the 2 sites (M = 1266.61 and U = 1280.96 μs) show no significant statistical difference (t-test: $t_{1,242} = 0.458$).

The characterisation of *in situ* n_{PSII} variability is difficult given the uncertainties associated with the method for calculating this parameter (see *Chapter 4*). However, changes in $1/n_{PSII}$ should, to some degree, reflect the changes of σ_{PSII}. Greater losses of

mol RCII than of mol chl *a* occur under nutrient limitation (Greene *et al.* 1991, Berges *et al.* 1996) and result in higher values of $1/n_{PSII}$ (mol chl *a*:mol RCII). An increase in σ_{PSII} will follow since saturation of the (lower) number of RCIIs can occur more quickly (eg. Kolber *et al.* 1988, Falkowski 1992). Similar corresponding changes to the two parameters might not be expected with variations in light since other factors, such as quenching and state transitions, serve to adjust σ_{PSII} at scales (minutes, eg. Falkowski *et al.* 1994) that are faster than the response of $1/n_{PSII}$ to light (10's minutes to hours, eg. Sukenik *et al.* 1990, Vassiliev *et al.* 1994). The additional lack of laboratory validation of n_{PSII} at time scales equivalent to *in situ* variability limits a conclusive description of *in situ* n_{PSII} in response to environmental change.

The photon flux density (E) intercepted by phytoplankton cells represents the final parameter from the [FRRF] production algorithm and contributes to the observed variability in production. It is the amount of light that drives the photosynthetic apparatus so phytoplankton acclimate and eventually adapt to make the most efficient use of the available light. However, light can vary on time scales as small as 10^{-1} s via fluctuations in sea surface waves (the flicker effect, see Falkowski 1984). Similarly, any particulate matter in the water column can scatter light and result in reduced light-quantity/-quality available to a cell (eg. Kirk 1994). Such small scale changes in E will only result in corresponding alterations to the instantaneous production P(E) and the amount of energy that is quenched (ie. qP and qN) since protective and acclimative mechanisms of PSII occur over longer time scales (see above). Above all, it is apparent that the variability of light, nutrients and temperature represent major factors responsible for the observed variability in primary production.

The FRRF has the ability to measure *in situ* photosynthesis and associated parameters at some of the smallest scales of physiological and ecological variability (measurements of $<450\mu s$ $100ms^{-1}$). Each of these instantaneous measurements of physiology and oxygenic production is the product of a complex web of interactions. Differences in the energy of the water column will dictate the encounter rate with light, nutrients, competitors and predators, and significantly influence both the photosynthetic capacity and the competitive ability of individual cells (Estrada and Berdalet 1997). Low energy environments are characterised by phytoplankton that are more stress tolerant (Margalef

1997) to variations in light ie. photoacclimation and nutrients (*Chapters 4* and *5*). Furthermore, morphological discrepancies will have an impact upon the ability of an individual cell to survive, for example, uptake of resources (Chisholm 1992) and predator 'attractiveness' (Reynolds 1999). Phenotypic variations may also discretely alter the internal composition of individual cells and add physiological variability at the micro-molecular scale (Falkowski and Raven 1997). As a result, the potential for small-scale ecological variability in photosynthetic capacity is immense and one should expect, given any operator and instrument error, that FRRF measurements will be correspondingly highly variable.

Larger scale variations in production are more difficult to characterise, primarily as a result of logistical constraints. Whilst the vertical water column can be easily documented with high resolution profiling instruments, horizontal spatial variability will be dictated by the passage of the sampling platform. The data from the AMT6 cruise, *Chapter 5*, reveals relatively few changes to the scale of horizontal variability (significant to instantaneous primary production) along the cruise track and reflects the lack of short-range physical processes operating throughout except within dynamic water bodies governed by upwelling and/or eddy field activity where smaller scales of variability were observed. The strong diel signal in fluorescence throughout the cruise track may have concealed the true horizontal variability (see below). The greatest spatial changes to photosynthetic capacity are seen at the biogeochemical province level as a result of changes between and adaptation within species. This conforms with observations from ^{14}C-uptake experiments (Marañón and Holligan 1999, Marañón *et al.* 2000) and reflects the stability of spatially defined light-nutrient fields. However, the most significant period of variability throughout the series of observations is the diel signature of phytoplankton activity. This is not surprising since the most consistent change experienced within the lifetime of all phytoplankton in any aquatic environment will be a difference in light between night and solar noon.

The consideration of temporal variability of phytoplankton fluorescence yield and physiology appears to be of more importance in terms of both sample resolution and ecosystem change. Transient perturbations to physical or biological forcing factors can shift the flow of energy in an environment, be it directional or steady state, to a different level. This is usually seen as a shift in species community composition/interaction

resulting from different scales of variability such as the passage of eddies (Falkowski *et al.* 1991), seasons (Barlow *et al.* 1993), years (Marañón *et al.* 2000) and of geological time (Berger *et al.* 1989). Indeed the degree of temporal change appears much greater than that of spatial change in the Atlantic Ocean (Kyewalyanga *et al.* 1988, Marañón *et al.* 2000). The consideration of temporal variability is, therefore, important for the prediction of larger-scale estimates of production; however, most current sampling strategies are of limited temporal resolution. A significant time series of data is available from the north Atlantic subtropical gyre (the Bermuda Atlantic Time Series (BATS) station) and indeed demonstrates that marine oligotrophic primary production varies significantly both within and between years (*fig 7.4.*). Although programmes such as AMT are spatially intensive they only operate twice yearly (Marañón and Holligan 1999, Marañón *et al.* 2000) and must typically assume the intra-annual pattern of

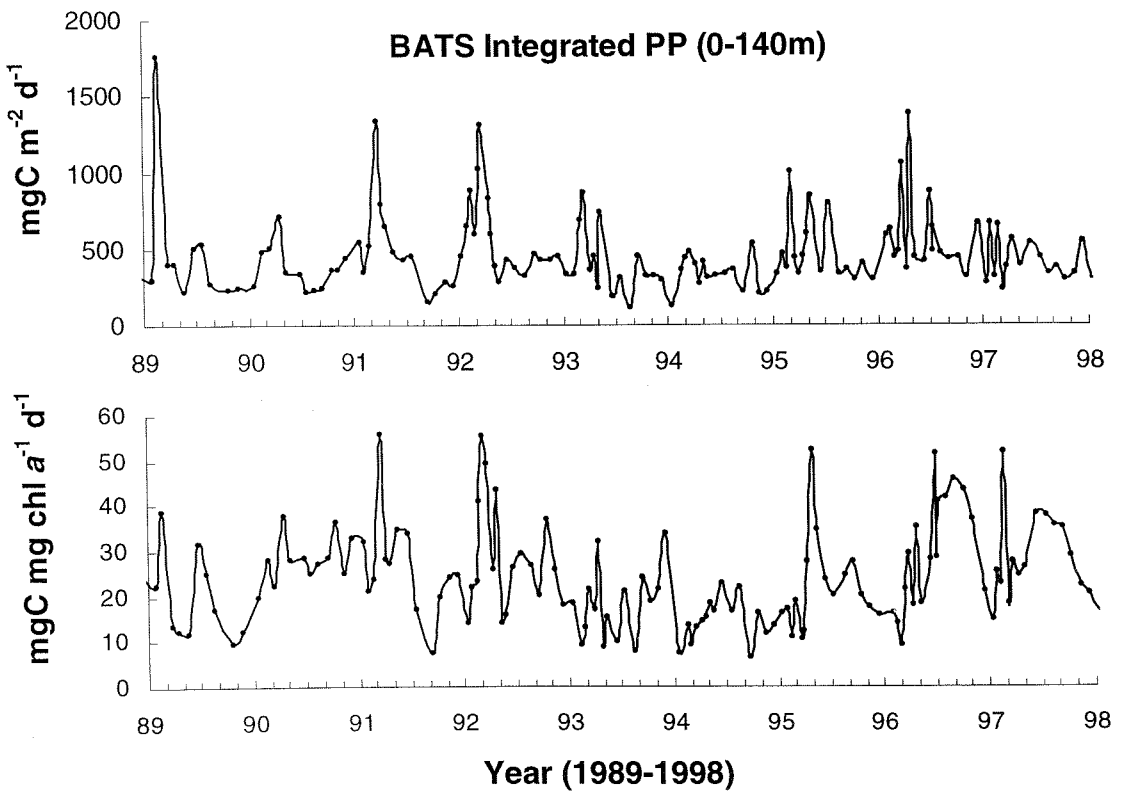

Figure 7.4.— Estimates of primary productivity (PP) collected at the BATS (Bermuda Atlantic Time Series) station, 31°N 64°W, in the north Atlantic subtropical gyre (eg. Longhurst *et al.* 1995) between 1989 and 1998. Data shown are estimates of daily integrated (between 0 and 140m) instantaneous primary production (upper panel) and chlorophyll *a*-specific production (lower panel) determined using ^{14}C-uptake PP methodology and fluorometric determination of chl *a* from discrete water samples taken throughout the water column (Lohrenz *et al.* 1992). Data was taken from the BATS data-base: **http://www.bbsr.edu/users/ctd** and represents 1-2 samples month^{-1}.

phytoplankton production within a given system to accurately quantify [larger-scale] estimates of marine primary production. Ultimately, such clarification is generated through a better understanding between phytoplankton and the environment they inhabit.

7.2. Conclusions and further work

In answer to the original aims concerning 'identifying factors and scales at which the variability of phytoplankton primary production operates within the Atlantic Ocean', it is clear that the both the nature and scale of environmental variability are fundamental determinants of PSII activity and production of Atlantic phytoplankton. This thesis has presented novel data to quantitatively describe the response of phytoplankton, relative to the conditions to which they are acclimated/adapted, to environmental variability. Daily alterations to the antennae pigments and quenching of excess energy appeared a consistent feature throughout the phytoplankton. Significant changes were also observed at high light as a result of RCII loss or damage (photoinhibition). This is seen in all parameters (F_v/F_m, σ_{PSII}, n_{PSII} and τ_p) relevant to the empirical calculation of production and becomes exaggerated where nutrients are limiting or temperatures are reduced. The product of these processes ensure that the diurnal scale of PSII variability appears the most consistent and significant feature relevant to phytoplankton production.

Phytoplankton show strong evidence of photoprotection strategies where waters become stratified and are, therefore, able to prevent the onset of photoinhibition and maintain higher levels of photosynthesis. Further environmental stress, within the boundaries of acclimation, will be tolerated as a temporary loss of high instantaneous production. As such, physical variability is an important factor responsible for changes in water column primary production and also for community succession where alternate phytoplankton can maintain efficient PSII photochemistry with the least amount of energy expenditure. Corresponding changes in PSI activity may also occur but have not been considered throughout this thesis. The ability to measure *in situ* variability of PSII using the FRRF indicates that phytoplankton oxygenic production can be highly dynamic throughout a given water column, presumably where physical processes operate at rates greater than those of PSII mechanisms employed to maintain maximal photosynthesis.

The FRRF estimates of production from these investigations appear to conform with the conventional understanding of (gross) O_2 photosynthesis. The agreement between corresponding FRRF and ^{14}C-uptake derived rates suggests that the FRRF can ultimately bridge the limited sampling resolution associated with the latter technique. However, a clear understanding of the stochiometry between O_2 evolution and carbon uptake, in addition to an intensive treatment of the limitations involved in the calculation of FRRF production (further work), will perhaps prove essential before any conclusive extrapolations are attempted. A discrepancy is also evident in ^{14}C-uptake incubations of confined water under different trophic environments. Data from this thesis suggest that 'classical' techniques for estimating production could underestimated CO_2 uptake (and hence gross O_2 evolution) from oligotrophic areas. This is of consequence to a large proportion of the marine environment, and the subsequent contribution to the global carbon budget, and must be further considered.

Finally, this thesis has demonstrated that the FRRF is a highly flexible instrument capable of characterising photosynthetic activity in the real phytoplanktonic environment. The collection of data of high temporal and spatial resolution is invaluable given that it can be subsequently averaged to the desired scale. Similarly, observations at high light levels are essential to the characterisation of PSII activity, in addition to the generation of qP versus E relationships which currently represents the most satisfactory quantification of τ_p. Simple manipulation to the FRRF 'boot protocol' has enabled this novel description of phytoplankton variability and provides a basis for future interpretation of FRRF data.

Further work

The FRRF has the capability to collect a phenomenal amount of information, however, the interpretation of these data represent the greatest limitation towards the use of this instrument as a widespread oceanographic tool. This should be considered, in part, as the lack of readily available information regarding the use of the instrument and subsequent treatment of data. An initial paper ('Assessment of photosynthesis in a spring cyanobacterial bloom using a Fast Repetition Rate Fluorometer', Suggett *et al.*, *subm.*) presents the calculation of production using the FRRF and a subsequent comparison with alternate (eg. ^{14}C-uptake) techniques, following *Chapter 6*. Other papers are intended for the interpretation of FRRF data from phytoplankton populations of

different physiological status. Further research is required to build or clarify the observations presented here:

1. Pursue improvements to estimate of parameters associated with the FRRF algorithm for primary production through (a) technological improvements are required for the accurate quantitative *in situ* estimation of PQ pool oxidation (τ_p) given the natural flushing rates of seawater samples across the optical windows; (b) validation of the method presented here, or the establishment of an alternative [model], for the calculation of n_{PSII} based on corresponding *in situ* measurements; (c) assess the accuracy by which σ_{PSII} measured using the FRRF (at 475nm, half band width 30nm) describes the functional absorption cross section given the different absorption characteristics (as a result of photosynthetic and non-photosynthetic pigment distributions) of contrasting phytoplankton taxa.

2. Provide a better understanding of the quantitative control by limiting environmental factors of light, nutrients and temperature upon phytoplankton production and physiology under controlled (laboratory or mesocosm) conditions; for example, does the heightened photoprotection response observed in the stratified waters of site U (RRS *Challenger* cruise, *Chapter 4*) represent a compensatory mechanism for the maintenance of efficient photochemistry where nutrients are limiting and/or temperatures are elevated, an ability to respond to the light field where time scales of water column mixing are lower, or a combination of factors ? In addition, these analyses should consider variability at scales equivalent to those experienced *in situ*. A consideration of the kinetics of cellular components, such as chlorophyll *a* and the number of reaction centres of photosystems I and II, will also aid the interpretation of these observations and lend to the validation of the method for calculating n_{PSII} (see above).

3. More specifically, implement the AMT6 basin-scale observations of PSII and production variability into a more detailed classification of the Atlantic. Several Atlantic transects of FRRF data now exist for a detailed temporal and spatial account. A critical assessment of the oligotrophic regions, in addition to a consideration of corresponding temporal variability through data sets such as BATS, will provide more accurate estimates of production. This will require further investigations to account for the differences between [AMT derived] ^{14}C-uptake and FRRF oligotrophic production rates (re. *Chapter*

6). However, it is clear that the identified limitations associated with the FRRF should be rectified before attempting a more detailed treatment with, for example, the ^{14}C technique.

8. References

Agawin NSR, Duarte CM, Agusti S. 2000. Nutrient and temperature control of the contribution of picoplankton to phytoplankton biomass and production. Limnol.Oceanogr. 45, pp.591-600.

Aiken J. 1985. The undulating oceanographic recorder: Mark 2 *In* Mapping strategies in chemical oceanography (Ed. Zinno A), pp.22-25.

Aiken J, Bellan I. 1990. Optical oceanography: an assessment of a towed method *In* Light and life in the sea (Ed. Herring PJ, Campbell AK, Whitfield M, Maddock L), pp. 39-57.

Aiken J, Rees N, Hooker S, Holligan P, Bale A, Robbins D, Moore G, Harris R, Pilgrim P. The Atlantic Meridional Transect: Overview and synthesis of data. Prog.Oceanog. (Special Issue). *Subm.*

Allali K, Bricaud A, Claustre H. 1997. Spatial variations in the chlorophyll-specific absorption coefficients of phytoplankton and photosynthetically active pigments in the equatorial Pacific. J.Geophy.Res. 102, pp. 12413-12423.

Aro EM, Virgin I, Anderson B. 1993. Photoinhibition of photosystem 2. Inactivation, protein damage and turnover. Biochim.Biophys.Acta. 1143, pp. 113-134.

Azam F, Fenchel T, Field JG, Gray JJ, Meyer-Reil LA, Thingstad F. 1983. The ecological role of water column microbes in the sea. Mar.Ecol.Prog.Ser. 10, pp.257.

Babin M, Morel A, Claustre H, Bricaud A, Kolber ZS, Falkowski PG. 1996. Nitrogen- and irradiance-dependent variations of the maximum quantum yield of carbon fixation in eutrophic, mesotrophic and oligotrophic marine systems. Deep Sea Res. 43, pp.1241-1272.

Banse K. 1993. On the dark bottle in the ^{14}C method for measuring marine phytoplankton production. ICES mar.Sci.Symp. 197, pp.132-140.

Barlow RG. 1982a. Phytoplankton ecology in the southern Benguela current. I. Biochemical composition. J.exp.mar.Biol.Ecol. 63, pp.209-227.

Barlow RG. 1982b. Phytoplankton ecology in the southern Benguela current. III. Dynamics of a bloom. J.exp.mar.Biol.Ecol. 63, pp.239-248.

Barlow RG, Alberte RS. 1985. Photosynthetic characteristics of phycoerythrin-containing marine *Synechococcus* spp. Mar.Biol. 86, pp.63-74.

Barlow RG, Cummings DG, Gibb SW. 1997. Improved resolution of mon- and divinyl chlorophylls a and b and zeaxanthin and lutein in phytoplankton extracts using reverse phase C-8 HPLC. Mar.Ecol.Prog.Ser. 161, pp.303-307.

Barlow RG, Mantoura RFC, Gough MA, Fileman FW. 1993. Pigment signatures of the phytoplankton composition in the northeast Atlantic during the 1990 spring bloom. Deep Sea Res. II 40, pp. 459-477.

Barber J, Malkin S, Telfer A. 1989. The origin of chlorophyll fluorescence in vivo and its quenching by the photosystem II reaction centres. Philos.Trans.R.Soc.London B 323, pp.227-239.

Baurfeind E. 1987. Primary production and phytoplankton biomass in the equatorial region of the Atlantic at 22 west. Oceanol.Acta.(Special Edition 1987), pp.131-136.

Behrenfeld MJ, Bale AJ, Kolber ZS, Aiken J, Falkowski PG. 1996. Conformation of iron limitation of

phytoplankton photosynthesis in the equatorial Pacific Ocean. Nature 383, pp. 508-511.

Behrenfeld MJ, Falkowski PG. 1997a. Photosynthetic rates derived from satellite-based chlorophyll concentrations. Limnol.Oceanogr. 42, pp.1-20.

Behrenfeld MJ, Falkowski PG. 1997b. A consumer's guide to phytoplankton primary productivity models. Limnol.Oceangr. 42, pp.1479-1491

Behrenfeld MJ, Kolber ZS. 1999. Widespread iron limitation of phytoplankton in the South Pacific Ocean. Science 283, pp.840-843.

Bender M, Grande K, Johnson K, Marra J, Williams PJ, Sieburth J, Pilson M, Langdon C, Hitchcock G, Orchardo J, Hunt C, Donaghay P. 1987. A comparison of 4 methods for determining planktonic community production. Limnol.Oceanogr. 32, pp.1085-1091.

Berger WH, Smetacek VS, Wefer G. 1989. Ocean productivity and paleoprodcutivity-an overview pp. 1-25 *in* Productivity of the oceans: Past and Present (eds. Berger WH, Smetacek VS, Wefer G.), John Wiley and Sons.

Berges JA, Charlebois DO, Mauzerall DC, Falkowski PG. 1996. Differential effects of nitrogen limitation on photosynthetic efficiency of photosystems I and II in microalgae. Plant Physiology 110, pp.689-696.

Berner T, Dubinsky Z, Wyman K, Falkowski PG. 1989. Photoadaptation and the 'package' effect in *Dunaliella tertiolecta* (Chlorophyceae). J.Phycology 25, pp.70-78.

Bidigare RR, Ondrusek ME, Morrow JH, Kiefer, DA. 1990. In vivo absorption properties of algal pigments. SPIE. 1302, pp.290-302.

Bisset WP, Patch JS, Carder KL, Lee ZP. 1997. Pigment packaging and Chl *a*-specific absorption in high-light oceanic waters. Limnol.Oceanogr. 42, pp.961-968.

Boyd PW, Aiken J, Kolber Z. 1997. Comparison of radiocarbon and fluorescence based (pump and probe) measurements of phytoplankton photosynthetic characteristics in the Northeast Atlantic Ocean. Mar.Ecol.Prog.Ser. 149, pp.215-226.

Brand LE. 1982. Persistent diel rhythms in the chlorophyll fluorescence of marine phytoplankton species. Mar.Biol. 69, pp.253-262.

Brand LE. 1991. Minimum iron requirements of marine phytoplankton and the implications for the biogeochemical control of new production. Limnol Oceanogr. 36, pp.1756-1771.

Bricaud A, Babin M, Morel A, Claustre H. 1995. Variability in the chlorophyll-specific absorption coefficients of natural phytoplankton: analysis and parameterisation. J.Geophy.Res. 100, pp. 13321-13332.

Brown PC, Field JG. 1986. Factors limiting phytoplankton production in a near-shore upwelling area. J.Plankton Res. 8, pp.55-68

Brunet C, Brylinski JM, Lemoine Y. 1993. In situ variations of the xanthophylls diatoxanthin and diadinoxanthin: photoadaptation and relationships with a hydrodynamical system in the eastern English Channel. Mar.Ecol.Prog.Ser. 102, pp. 69-77.

Bryan JR, Riley JP, Williams PJ. 1976. A Winkler procedure for making precise measurements of oxygen concentration for productivity and related studies. J.exp.mar.Biol.Ecol. 21, pp.191-197.

Burrough PA. 1981. Fractal dimensions of landscape and other environmental data. Nature 294, pp.240-242

Carr MR. 1994. Plymouth Routines in Multivariate Ecological Research (PRIMER) user manual. Plymouth, Plymouth Marine Laboratory. 48pp.

Cassoti R, Ribera M, D'Alcala D, Bowler C. 1997. A molecular approach to the study of photoadaptation in

phytoplankton. Genetic transformations of marine diatoms. Biologia Marina Mediterranea 4, pp. 24-29.

Charlson RJ, Lovelock JE, Meinrat DA, Stephen GW. 1987. Oceanic phytoplankton, atmospheric sulphur, cloud albedos and climate. Nature 326, pp.655-661

Chavez FP, Buck KR, Coale KH, Martin JH, DiTullio GR, Welschmeyer NA, Jacobson AC, Barber RT. 1991. Growth rates, grazing, sinking and iron limitation of Equatorial Pacific phytoplankton. Limnol.Oceanogr. 36, pp.1816-1833.

Chisholm SW. 1992. Phytoplankton size, pp.213-238 *In* Primary productivity and biogeochemical cycles in the sea (Ed. Falkowski PG, Woodhead AD), Plenum Press, 550pp.

Clark I. 1979. Practical geostatistics. Applied Science Publishers. 317pp.

Clarke KR, Warwick RM. 1994. Changes in marine communities: an approach to statistical analysis and interpretation. Plymouth, Plymouth Marine Laboratory. 110pp.

Claustre H, Marty JC. 1995. Specific phytoplankton biomassess and their relation to primary production in the tropical North Atlantic. Deep Sea Res. 42, pp.1475-1493.

Cullen JJ, Lewis MR. 1988. The kinetics of algal photoadaptation in the context of vertical mixing. J.Plankton Res. 10, pp.1039-1063.

Cullen JJ, Lewis MR., Davis CO, Barber RT. 1992. Photosynthetic characteristics and estimated growth rates indicate grazing is the proximate control of primary production in the Equatorial Pacific. J.Geophys. Res. 97, pp.639-654.

Davies JM, Williams PJ. 1984. Verification of ^{14}C and O_2 derived primary organic production measurements using an enclosed ecosystem. J.Plankton Res. 6, pp.457-474.

Demers S, Roy S, Gagnon R, Vignault C. 1991. Rapid light-induced changes in cell fluorescence and in xanthophyll-cycle pigments in *Alexandrium escavatum* (Dinophyceae) and *Thalassiosira pseudonoma* (Bacillariophyceae): a photoprotection mechanism. Mar.Ecol.Prog.Ser. 76, pp.185-193.

Demmig-Adams B. 1990. Carotenoids and photoprotection in plants: a role for the xanthophyll zeaxanthin. Biochim.Biophys.Acta 1020, pp. 1-24.

Denman KL, Okubo A, Platt T. 1977. The chlorophyll fluctuation spectrum in the sea. Limnol.Oceanogr. 22, pp. 1033-1038.

Denman KL, Platt T. 1977. Biological prediction in the sea. pp.251-260. *In* Modelling and prediction of the upper layers of the ocean. (Ed. Kraus EB). Pergamon. 428pp.

Doney SC., Najjar RG, Stewart S. 1995. Photochemistry, mixing and diurnal cycles in the upper ocean. J.Mar.Res. 53, pp.341-369.

Dubinsky Z, Falkowski PG, Wyman K. 1986. Light harvesting and utilisation by phytoplankton. Plant Cell Physiology 27, pp.1335-1349.

Ducklow HW, Harris RP. 1993. Introduction to the JGOFS (North Atlantic Bloom Experiment). Deep Sea Res. II 40, pp.1-8.

Dugdale RC, Wilkerson F. 1992. Nutrient limitation of new production in the sea, pp. 107-122 *In* Primary productivity and biogeochemical cycles in the sea (Ed. Falkowski PG, Woodhead AD), Plenum Press, 550pp.

Eppley, RW. 1972. Temperature and phytoplankton growth in the sea. Fish Bull. 70, pp. 1063-1085.

Eppley RW, Peterson BJ. 1979. Particulate organic matter flux and planktonic new production in the deep ocean. Nature 282, pp.677-680.

Eppley RW, Rogers JN, McCarthy JJ. 1969. Half stauration constants for uptake of nitrate and ammonium by marine phytoplankton. Limnol.Oceanogr. 14, pp.912-920.

Estrada M, Berdalet E. 1997. Phytoplankton in a turbulent world. Scientia Marina 61 (suppl 1), pp.109-123.

Falkowski PG. 1980. Light-shade adaptation in marine phytoplankton *In* Primary Productivity in the sea, pp.99-199. (Ed. Falkowski PG). Plenum Press, New York

Falkowski PG. 1981. Light-shade adaptation and assimilation numbers. J. Plankton Res. 3, pp. 203-216.

Falkowski PG. 1984. Physiological responses of phytoplankton to natural light regimes. J.Plankton Res. 6, pp.295-307.

Falkowski PG. 1992. Molecular ecology of phytoplankton photosynthesis. pp.47-67 *In* Primary Productivity and Biogeochemical Cycles in the Sea (Ed. Falkowski PG and Woodhead A). Plenum Press, New York. 550pp.

Falkowski PG, Fujita Y, Ley AC, Mauzerall D. Evidence for cyclic electron flow around photosystem II in *Chlorella pyrenoidosa*. Plant Physiology 81, pp. 310-312.

Falkowski PG, Greene RM, Kolber Z. 1994. Light utilization and photoinhibition of photosynthesis in marine phytoplankton *In* Photoinhibition of photosynthesis, pp407-432 (Ed. Baker NR and Bowyer JR). Bios Scientific Publishers.

Falkowski PG, Kolber ZS. 1990. Phytoplankton photosynthesis in the Atlantic ocean as measured from a submersible pump and probe fluorometer in situ, pp.923-926 *In* Current Research in Photosynthesis V.4, Kluwer.

Falkowski PG, Kolber ZS. 1993. Estimation of phytoplankton photosynthesis by active fluorescence. ICES mar.Sci. Symp. 197, pp.92-103.

Falkowski PG, Kolber ZS. 1995. Variations in chlorophyll fluorescence yields in phytoplankton in the worlds oceans. Aust.J.Plant Physiology 22, pp.341-355.

Falkowski PG, Kolber ZS, Fujita Y. 1988. Effect of redox state on the dynamics of photosystem II during steady-state photosynthesis in eucaryotic algae. Biochim.Biophys.Acta. 933, pp.432-443.

Falkowski PG, LaRoche J. 1991. Acclimation to spectral irradiance in algae. J.Phycology 27, pp.8-14.

Falkowski PG, Owens TG, Ley AC, Mauzerall DC. 1981. Effects of growth irradiance levels on the ration of reaction centres in two species of marine phytoplankton. Plant Physiology 68, pp.969-973.

Falkowski PG, Raven JA. 1997. Aquatic Photosynthesis. Blackwell Science, U.K. 375pp.

Falkowski PG, Wyman K, Mauzerall DC. 1984. Effects of continuous background irradiance on xenon-flash-induced fluorescence yields in marine microalgae *In* Advances in Photosynthesis Research (Ed. Sybesma C), pp.163-166. Martinus Nijhoff/Dr. Junk: The Hague.

Falkowski PG, Ziemann D, Kolber ZS, Bienfang PK. 1991. Role of eddy pumping in enhancing primary production in the ocean. Nature 352, pp.55-58.

Fasham MJR. 1978. The application of some stochastic processes to the study of plankton patchiness, pp.131-156 in Spatial pattern in plankton communities (ed. Steele JH). Plenum Press.

Fernández E, Pingree RD. 1996. Coupling between physical and biological fields in the north Atlantic subtropical front southeast of the Azores. Deep Sea Res. 43, pp.1369-1393.

Finenko ZZ. 1978. Production in plant populations, pp.3-88 *In* Marine Ecology IV: Dynamics (Ed. Kinne O), John Wiley & Sons, 746pp.

Flameling IA. 1998. Growth and photosynthesis of eukaryotic microalgae in fluctuating light conditions, induced by vertical mixing. Katholieke Universiteit Nijmegen, 135 pp.

Flameling IA, Kromkamp J. 1997. Photoacclimation of *Scenedesmus protuberans* (Chlorophyceae) to fluctuating PPFD simulating vertical mixing. J.Planton Res. 19, pp.1011-1024.

Flameling IA, Kromkamp J. 1998. Light dependence of quantum yields for PSII charge separation and oxygen evolution in eucaryotic algae. Limnol.Oceanogr, 43, pp.287-297.

Geider RJ. 1992. Respiration: Taxation without representation. pp. 333-360 *In* Primary Productivity and Biogeochemical Cycles in the Sea (Ed. Falkowski PG and Woodhead A). Plenum Press, New York. 550pp.

Geider RJ, Greene RM, Kolber ZS, MacIntyre HL, Falkowski PG.1993. Fluorescence assessment of the maximum quantum efficiency in the western North Atlantic. Deep Sea Res. 40, pp.1205-1224.

Goldman JC. 1988. Spatial and temporal discontinuities of biological processes in pelagic surface waters, pp. 273-296 *in* Towards a theory in biological-physical interactions in the World Ocean (Ed. Rothschild BJ).

Gould WJ. 1985. Physical oceanography of the Azores front. pp.167-190 *In* Essays on Oceanography: a tribute to John Swallow (Ed. Crease J, Gould WJ and Saunders PM). Pergamon Press.

Grande KD, Bender ML, Irwin B, Platt T. 1991. A comparison of net and gross rates of oxygen production on a function of high intensity in some natural plankton populations and in a *Synechococcus* culture. J. Plankton Res. 13, pp.1-16.

Grande KD, Kroopnick P, Burns D, Bender ML. 1982. ^{18}O as a tracer for measuring gross primary productivity in bottle experiments. EOS 63, pp.107.

Grande KD, Williams PJ, Marra J, Purdie DA, Heinemann K, Eppley RW, Bender ML. 1989. Primary production in the north Pacific gyre: a comparison of rates determined by the ^{14}C, oxygen concentration and ^{18}O methods. Deep Sea Res. 36, pp.1621-639.

Graziano LM, Geider RJ, Li WKW, Olaizola M. 1996. Nitrogen limitation of North Atlantic phytoplankton: analysis of physical condition in nutrient enrichment experiments. Aq.Microb.Ecol. 11, pp.53-64.

Greene RM, Geider RJ, Falkowski PG. 1991. Effect of iron limitation on photosynthesis in a marine diatom. Limnol.Oceanogr. 36, pp.1772-1782.

Greene RM, Geider RJ, Kolber Z, Falkowski PG. 1992. Iron-induced changes in light harvesting and photochemical energy conversion in eukaryotic marine algae. Plant Physiology 100, pp. 565-575.

Greene RM, Kolber ZS, Swift DG, Tindale NW, Falkowski PG. 1994. Physiological limitation of phytoplankton photosynthesis in the eastern equatorial Pacific determined from variability in the quantum yield of fluorescence. Limnol.Oceanogr. 39, pp.1061-1074.

Harding LW, Prézelin BB, Sweeney BM, Cox JL. 1982a. Diel oscillations in of the photosynthesis-irradiance (P-I) relationship in natural assemblages of phytoplankton. Mar.Biol. 67, pp.167-178.

Harding LW, Prézelin BB, Sweeney BM, Cox JL. 1982b. Primary production as influenced by diel periodicity of phytoplankton photosynthesis. Mar.Biol. 67, pp.179-186.

Herbland A, Voituriez B. 1979. Hydrological structure analysis for estimating the primary production in the tropical Atlantic Ocean. J.Mar.Res. 37, pp.87-101.

Holligan PM. 1981. Biological implications fronts of the north-west European continental shelf. Philos.Trans.R.Soc. London A 302, pp.547-562.

Holligan PM. 1987. The physical environment of exceptional phytoplankton blooms in the north-east Atlantic. Rapp. P-V. Réun. Cons. Int. Explor. Mer. 187, pp. 9-18.

Horton P, Ruban AV. 1992. Regulation of photosystem II. Photosyn.Res. 34, pp.375-385.

IPCC. 1995. Climate change 1994. Radioactive forcing of climate change. Cambridge University Press. 337pp.

Jeffrey SW, Vesk M. Introduction to marine phytoplankton and their signatures pp.37-84 in Phytoplankton pigments in oceanography: guidelines to modern methods (Ed. Jeffrey SW, Mantoura RFC, Wright SW), UNESCO Publishing.

Jeffrey SW, Welschmeyer NA. 1997. Spectrophotometric and fluorometric equations in common use in oceanography, pp.597-615 in Phytoplankton pigments in oceanography: guidelines to modern methods (Ed. Jeffrey SW, Mantoura RFC, Wright SW), UNESCO Publishing.

Jochem FJ, Zeitschel B. 1993. Productivity regime and phytoplankton size structure in the tropical and subtropical North Atlantic in spring 1989. Deep Sea Res. II. 40, pp.495-519.

Joint IR, Pomeroy AJ. 1986. Photosynthetic characteristics of nanoplankton and picoplankton from the surface mixed layer. Mar.Biol. 92, pp. 465-474.

Joint I, Pomroy A, Savidge G, Boyd P. 1993. Size fractionated primary productivity in the northeast Atlantic in May-June 1989. Deep Sea Res. II. 40, pp.423-440.

Jumars PA. 1978. Spatial autocorrelation with RUM (Remote Underwater Manipulator): vertical and horizontal structure of a bathyal benthic community. Deep Sea Res. 25, pp.589-604.

Kana, T.M. 1992. Relationship between photosynthetic oxygen cycling and carbon assimilation in *Synechoccocus* WH7803 (Cyanophyta). J.Phycology 28, pp. 304-308.

Kawamura M, Mimuro M, Fujita Y. 1979. Quantitative relationship between two reaction centres in the photosynthetic system of blue-green algae. Plant & Cell Physiology 20, pp.697-705.

Kiddon J, Bender ML, Marra J. 1995. Production and respiration in the 1989 north Atlantic spring bloom: an analysis of irradiance-dependent changes. Deep Sea Res. 42, pp.553-546.

Kirk JTO. 1994. Light and photosynthesis in aquatic ecosystems (2nd Edn). Blackwell Science, UK. 401pp.

Koblentz-Mishke OI, Volkovinsky VV, Kabanova Yu.G. 1970. Plankton primary production of the world ocean *in* Scientific exploration of the South Pacific (Ed. Wooster W), pp.183-193, National Academy of Sciences, Washington DC.

Kok B. 1960. Encyclopaedia of plant physiology (Ed. W. Ruhland) vol.1. Springer-Verlag, Berlin. 620pp.

Kolber ZS. 1997. Fast Repetition Rate Fluorometry – A method for assessing ocean photosynthesis 12pp. *in* FAST^{tracka} FRRF Handbook, Chelsea Instruments, U.K..

Kolber ZS, Falkowski PG. 1992. Fast Repetition Rate (FRR) Fluorometer for making in situ measurements of primary productivity. Proc.Ocean 1992 Conference, Newport, Rhode Island, pp.637-641.

Kolber ZS, Falkowski PG. 1993. Use of active fluorescence to estimate phytoplankton photosynthessis in situ. Limnol.Oceanogr. 38 (8), pp.1646-1665.

Kolber ZS, Prasil O, Falkowski PG. 1998. Measurements of variable chlorophyll fluorescence using fast repetition rate techniques: defining methodology and experimental protocols. Biochim.Biophys. Acta. 1367, pp.88-106.

Kolber ZS, Wyman KD, Falkowski PG. 1990. Natural variability in photosynthetic energy conversion efficiency: A field study in the Gulf of Maine. Limnol.Oceanogr. 35, pp.72-79.

Kolber ZS, Zehr J, Falkowski PG. 1988. Effects of growth irradiance and nitrogen limitation on photosynthetic energy conversion in photosystem II. Plant Physiology 88, pp.72-79.

Krause GH, Weis E. 1991. Chlorophyll fluorescence and photosynthesis: The basics. Ann.Rev. Plant Physiology Plant Mol.Biol. 42, pp.313-349.

Kremer BP. 1981. Dark reations of photosynthesis. pp. 44-64 *In* Physiological basis of phytoplankton ecology (Ed. Platt T). Can.Bull.Fish.Aquat.Sci. 210. 346pp.

Kroon 1994. Variability of photosystem II quantum yield and related processes in *Chlorella pyrenoidesa* (Chlorophyta) acclimated to an oscillating light regime simulating a mixed photic zone. J.Phycology 30, pp.841-852.

Kruskal JB, Wish M. 1978. Multidimensional scaling. Sage Publications, Beverley Hills, California. 462pp.

Kyewalyanga MN, Platt T, Sathyendranath S, Lutz VA, Stuart V. 1998. Seasonal variations in physiological parameters of phytoplankton across the North Atlantic. J. Plankton Res. 20, pp.17-42.

Langdon C, Marra J, Knudson C. 1995. Measurements of net and gross oxygen production, dark respiration and ^{14}C assimilation at the marine light-mixed layers site (59N 21W) in the north east Atlantic ocean. J.Geophys.Res. 100, pp.6645-6653.

Lewis MR, Smith CJ. 1983. A small-volume, short-incubation time method for the measurement of photosynthesis as a function of incident irradiance. Mar.Ecol.Prog.Ser. 13, pp.99-102.

Li WKW. 1980. Temperature adaptation in phytoplankton: cellular and photosynthetic characteristics. pp. 259-279 *In* Primary Productivity in the Sea (Ed. Falkowski PG). Plenum Press, New York.

Lizon F, Lagadeuc Y, Brunet C, Aelbrecht D, Bentley D. 1995. Primary production and photoadaptation of phytoplankton in relation with tidal mixing in coastal waters. J.Plankton Res. 17, pp. 1039-1055.

Lochte K, Ducklow HW, Fasham MJR, Stienen C. 1993. Plankton succession and carbon cycling at 47N 20W during the JGOFS North Atlantic Bloom Experiment. Deep Sea Res. II 40, pp. 91-114.

Lohrenz SE. 1993. Estimation of primary production by the simulated in situ method. ICES Mar.Sci. Symp. 197, pp. 159-171.

Lohrenz SE, Wiesenburg DA, Rein CR, Arnone RA, Taylor CD, Knauer GA, Knap AH. 1992. A comparison of *in situ* and simulated *in situ* methods for estimating oceanic primary production. J. Plankton Res. 14, pp.201-221.

Long SP, Humphries S, Falkowski PG. 1994. Photoinhibition of photosynthesis in nature. Ann. Rev. Plant Physiology Plant Mol.Biol. 45, pp.655-662.

Longhurst A. 1991. Role of the marine biosphere in the global carbon cycle. Limnol.Oceanogr. 36, pp.1507-1526.

Longhurst A. 1993. Seasonal cooling and blooming in tropical oceans. Deep Sea Res. 40, pp.2145-2165.

Longhurst A, Sathyendranath S, Platt T, Caverhill C. 1995. An estimation of global primary production in the ocean from satellite radiometer data. J.Plankton Res. 17, pp.1245-1271.

Lorenzen CJ. 1963. Diurnal variation in photosynthetic activity of natural phytoplankton populations. Limnol.Oceanogr. 8, pp.56-62.

Lorenzen CJ. 1966. A method for the continuous measurement of in vivo chlorophyll concentration. Deep Sea Res. 13, pp.223-227.

MacIntyre HL, Geider RJ, McKay RM. 1996. Photosynthesis and regulation of RUBISCO activity in net phytoplankton from Delaware Bay. J.Phycology 32, 718-732.

Mackas, DL. 1984. Spatial autocorrelation of plankton community composition in a continental shelf ecosystem. Limnol.Oceanogr. 29, pp.451-471.

Mandelbrot BB. 1983. The fractal geometry of nature. Freeman, San Francisco. 407pp.

Mann KH, Lazier JRN. 1996. Dynamics of marine ecosystems (2nd Edn), Blackwell Science, UK. 466pp.

Mantoura RFC, Jeffrey SW, Llewellyn CA, Claustre H, Morales CE. 1997. Comparison between spectrophotometric, flourometric and HPLC methods for chlorophyll analysis, pp.361-380 *In* Phytoplankton pigments in oceanography: guidelines to modern methods (Ed. Jeffrey SW, Mantoura RFC, Wright SW), UNESCO Publishing. 661pp.

Marañón E, Holligan PM. 1999. Photosynthetic parameters of phytoplankton 50°N to 50°S in the Atlantic Ocean. Mar.Ecol.Prog.Ser. 176, pp.191-203.

Marañón E, Holligan PM, Varela M, Mouriño B, Bale AJ. 2000. Basin-scale variability of phytoplankton biomass, production and growth in the Atlantic Ocean. Deep Sea Res. 47, pp.825-858.

Margalef R. 1997. Our Biosphere. Excellence in ecology (Ed. Kinne O). Ecology Institute Nordbünte 23, D-21385 Oldendorf/Luhe, Germany. 74pp.

Marra J. 1997. Analysis of diel variability in chlorophyll fluorescence. J.Mar.Res. 55, pp.767-784.

Martin JH, Fitzwater SE, Gordon M, Hunter CN, Tanner SJ. 1993. Iron, primary production and carbon-nitrogen flux studies during the JGOFS north Atlantic bloom experiment. Deep Sea Res. II 40, pp.115-134.

Mauzerall D. 1972. Light induced changes in *Chlorella* and the primary photo-reaction for the production of oxygen. Proc.Nat.Acad.Sci. 6, pp.1358-1362.

Mauzerall D, Greenbaum NL. 1989. The absolute size of a photosynthetic unit. Biochim.Biophys.Acta. 974, pp.119-140.

Morel A. 1978. Available, usable and stored radiant energy in relation to marine photosynthesis. Deep Sea Res. 25, pp.673-688.

Morel A, Antoine D, Babin M, Dandonneau Y. 1996. Measured and modelled primary production in the northeast Atlantic (EUMELI JGOFS program): the impact of natural variations in photosynthetic parameters on model predictive skill. Deep Sea Res. 43, pp.1273-1304.

Mulholland MR, Capone DG. 1999. Nitrogen fixation, uptake and metabolism in natural and cultured populations of *Trichodesmium* spp. Mar.Ecol.Prog.Ser. 188, pp.33-49.

Neale PJ, Richerson PJ. 1987. Photoinhibition and the diurnal variation of phytoplankton photosynthesis - I. Development of a photosynthesis-Irradiance model from studies of *in situ* responses. J.Plankton Res. 9, pp.167-193.

Neori A, Vernet M, Holm-Hansen O, Haxo FT. 1988. Comparison of chlorophyll far-red and red fluorescence excitation spectra with photosynthetic oxygen action spectra for photosystem II in algae. Mar.Ecol.Prog.Ser. 44, pp.297-302.

Olaizola M, Geider RJ, Harrison WG, Graziano LM, Ferrari GM, Schlittenhardt. 1996. Synoptic study of variations in the fluorescence-based maximum quantum efficiency of photosynthesis across the North Atlantic Ocean. Limnol.Oceanogr. 41, pp.755-765.

Olaizola M, Yamamoto HY. 1994. Short-term response of the diadinoxathin cycle and fluorescence yield to high irradiance in *Chaetoceros muelleri* (Bacillariophyceae). J.Phycology 30, pp. 606-612

Olson RJ, Chisholm SW, Zettler ER, Armbrust EV. 1990a. Pigments, size, and distribution of *Synechococcus* in the North Atlantic and Pacific Ocean. Limnol.Oceanogr. 35, pp.45-58.

Olson RJ, Chisholm SW, Zettler ER, Altabet MA, Dusenberry JA. 1990b. Spatial and temporal distributions of prochlorophyte picoplankton in the North Atlantic Ocean. Deep Sea Res. 37, pp.1033-1051.

Oschilles A, Garcon V. 1998. Eddy induced enhancement of primary production in a model of the North Atlantic Ocean. Nature 394, pp.266-269.

Owens TG, Falkowski PG, Whitledge TE. 1980. Diel periodicity in cellular chlorophyll content in marine diatoms, Mar.Biol. 59, pp.71-77.

Pai S-C, Gong G-C, Lui K-K. 1993. Determination of dissolved oxygen in seawater by direct spectrophotometry of total iodine. Mar.Chem. 41, pp.343-351.

Painting SJ, Lucas MI, Peterson WT, Brown PC, Hutchings L, Mitchell-Innes BA. 1993. Dynamics of bacterioplankton, phytoplankton and mesozooplankton communities during the development of an upwelling plume in the southen Benguela. Mar.Ecol.Prog.ser. 100, pp.35-53

Pauly D, Christensen V. 1995. Primary production required to sustain global fisheries. Nature 374 (6519), pp.255-257.

Pingree RD. 1980. Physical oceanography of the Celtic Sea and English Channel, pp.415-465 *In* The north-west European shelf seas: the sea bed and the sea in motion. II. Physical and chemical oceanography and physical resources (Ed. Banner FT, Collins MB and Massie KS). Pergamon. 588pp.

Pingree RD, Holligan PM, Mardell GT. 1978. The effects of vertical stability on phytoplankton distributions in the summer on the northwest European Shelf. Deep Sea Res. 25, pp. 1011-1028.

Pingree RD, Mardell GT, Reid PC, John AWG. 1986. The influence of tidal mixing on the timing of the spring phytoplankton development in the Southern Bight of the North Sea, the English Channel and on the northern Armorican Shelf, pp.164-192 *In* Tidal mixing and plankton dynamics (Ed. Bowman MJ, C.M.Yentsch & W.T.Peterson). Pergamon. 396pp.

Pitcher GC, Brown PC, Mitchell-Innes BA. 1992. Spatio-temporal variability of phytoplankton in the Southern Benguelan upwelling system. S.Afr.J.Mar.Sci. 12, pp.439-456.

Pitcher GC, Boyd AJ, Horstman DA, Mitchell-Innes BA. 1998. Subsurface dinoflagellate populations, frontal blooms and the formation of red tide in the southern Benguela upwelling system. Mar.Ecol. Prog.Ser. 172, pp.253-264.

Pitchford JW, Brindley J. 1999. Iron limitation, grazing pressure and oceanic high nutrient-low chlorophyll (HNLC) regions. J.Plankton Res. 21, pp. 525-547.

Platt T, Shubba-Rao RV, Irwin B. 1983. Photosynthesis of picoplankton in the oligotrophic ocean. Nature 310, pp.702-704.

Pomeroy LR. 1997. Primary production in the Arctic Ocean estimated from dissolved oxygen. J. Mar. Systems. 10, pp.1-8.

Pond S, Pickard G. 1983. Introductory Dynamical Oceanography (Second Edition). Butterworth-Heinemann, U.K. 329pp.

Prasil O, Kolber Z, Berry JA, Falkowski PG. 1996. Cyclic electron flow around photosystem II in vivo. Photosynth.Res. 48, pp.395-410.

Prézelin BB. 1981. Light reations of photosynthesis. pp. 1-43 *In* Physiological basis of phytoplankton ecology (Ed. Platt T). Can.Bull.Fish.Aquat.Sci. 210. 346pp.

Prézelin BB. 1992. Diel periodicity in phytoplankton productivity. Hydrobiologia 238, pp.1-35.

Prézelin BB, Bidigare RR, Matlick HA, Putt M, VerHoven BM. 1987. Diurnal patterns of size fractionated primary productivity across a front. Mar.Biol. 4, pp.563-574.

Prézelin BB, Ley AC. 1980. Photosynthesis and chlorophyll a fluorescence rhythms of marine phytoplankton. Mar.Biol. 55, pp.295-307.

Prézelin BB, Putt M, Glover HE. 1986. Diurnal patterns in photosynthetic capacity and depth-dependent photosynthesis-irradiance relationships in *Synechococcus* spp. and larger phytoplankton in three water masses in the Northwest Atlantic Ocean. Mar.Biol. 91, pp.205-217.

Raven JA, Geider RJ. 1988. Temperature and algal growth. New Phytologist 110, pp.441-461.

Rees AP, Joint I, Donald KM. 1999. Early spring bloom phytoplankton-nutrient dynamics at the Celtic shelf sea edge. Deep Sea Res. 46, pp.483-510.

Reynolds CS. 1999. With or against the grain: responses of phytoplankton to pelagic variability, pp. 15-44 in Aquatic life cycle strategies: survival in a variable environment (eds. Whitfield M, Matthews J., Reynolds C.). The Marine Biological Association, U.K.

Riebesell U, Wolf-Gladrow DA, Smetacek V. 1993. Carbon dioxide limitation of marine phytoplankton growth rates. Nature 361, pp.249-251.

Sakshaug E, Bricaud A, Dandonneau Y, Falkowski PG, Kiefer DA, Legendre L, Morel A, Parslow J, Takahashi M. 1997. Parameters of photosynthesis: definitions, theory and interpretation of results. J.Plank.Res. 19, pp.1637-1670.

Sathyendranath S, Longhurst A, Caverhill CM, Platt T. 1995. Regionally and seasonally differentiated primary production in the North Atlantic. Deep Sea Res. 42, pp.1773-1802.

Savidge G, Boyd P, Pomroy A, Harbour D, Joint I. 1995. Phytoplankton production and biomass estimates in the northeast Atlantic Ocean May-June 1990. Deep Sea Res. 42, pp.599-617.

Schatz GH, Brock H, Holtzwarth AR. 1988. A kinetic and energetic model for the primary processes in photosystem II. Biophys.J. 54, pp.397-405.

Seuront L, Lagadeuc Y. 1997. Characterisation of space-time variability in stratified and mixed coastal waters (Baie des Chaleurs, Quebec, Canada): application of fractal theory. Mar.Ecol.Prog.Ser. 259, pp.81-95.

Seuront L, Lagadeuc Y. 1998. Spatio-temporal structure of tidally mixed coastal waters: variability and heterogeneity. J.Plankton Res. 20, pp.1387-1401.

Shannon LV, Hutchings LH, Bailey GW, Shefin PA. 1984. Spatial and temporal distribution of chlorophyll in southern African waters as deduced from ship and satellite measurements and their implications to pelagic fisheries. S.Afr.J.mar.Sci 2, pp.109-130

Shannon LV, Nelson G. 1996. The Benguela: large scale fluctuations and processes and system variability, pp. 163-210 *in* The South Atlantic (Ed. Wefer G *et al.*). Berlin: Springer. 283pp.

Siefermann-Harms, D. Carotenoids in photosynthesis. I. Location in photosynthetic membranes and light harvesting function. Biochim.Biophys.Acta. 811, pp. 325-355

Simpson JH, Pingree RD. 1978. Shallow sea fronts produced by tidal stirring, pp. 29-42 *In* Oceanic fronts in coastal processes (Ed. Bowman MJ, Esaias WE). 133pp.

Sournia A. 1974. Circadian periodicities in natural populations of marine phytoplankton. Adv.Mar.Biol. 12, pp. 325-389.

Steeman Nielsen E. 1952. The use of radiocarbon (^{14}C) for measuring organic production in the sea. J.Cons.Expl.Mer. 18, pp. 117-140.

Suggett DJ, Kraay G, Holligan PM, Davey M, Aiken J, Geider RJ. Assessment of photosynthesis in a spring cyanobacterial bloom using a Fast Repetition Rate Fluorometer. Limnol.Oceanogr. *subm.*

Sukenik A, Bennett J, Mortain-Bertrand A, Falkowski, PG. 1990. Adaptation of the photosynthetic apparatus to irradiance in *Dunaliella tertiolecta.* Plant Physiology 92, pp.891-898.

Sverdrup HU. 1958. On the conditions for the vernal bloom of phytoplankton. J.Cons.Int.Explor.Mer. 18, pp. 287-295.

Takahashi M, Ichimura S, Kishino M, Okami N. 1989. Shade and chromatic adaptation of phytoplankton photosynthesis in a thermally stratified sea. Mar.Biol. 100, pp.401-409.

Tassan S, Ferrari GM. 1995. An alternative approach to absorption measurements of aquatic particles retained on filters. Limnol.Oceanogr. 40, pp.1358-1368.

Tett PB, Joint IR, Purdie DA, Baars H, Osterhuis SN, Daneri G, Hannah F, Mills DK, Plummer D, Pomeroy AJ, Walne AW, Whitte HJ. 1993. Biological consequences of tidal stirring gradients in the North Sea. Philos.Trans.R.Soc.London A 343(1669), pp. 493-508.

Timmermans KR, Gledhill M, Nolting RF, Veldhuis MJW, de Baar HJW, van den Berg CMG. 1998. Responses of marine phytoplankton in iron-enrichment experiments in the northern North Sea and the north-east Atlantic Ocean. Mar.Chem. 61, pp.229-242.

Tomczak M, Godfrey JS. 1994. Regional Oceanography: An Introduction. Elsevier Science Ltd., UK. 422pp.

Vassiliev IR, Prasil O, Wyman KD, Kolber Z, Hanson AK, Prentice JE, Falkowski PG. 1994. Inhibition of PSII photochemistry by PAR and UV radiation in natural phytoplankton communities. Photosynth.Res. 42, pp.51-64.

Veldhuis MJW, Kraay GW. 1990. Vertical distribution and pigment composition of a picoplanktonic prochlorophyte in the subtropical North Atlantic: a combined study of HPLC-analysis of pigments and flow cytometry. Mar.Ecol.Prog.Ser. 68, pp. 121-127.

Veldhuis MJW, Kraay GW. 1993. Cell abundance and fluorescence of picoplankton in relation to growth irradiance and nitrogen availability in the Red Sea. Neth.J.Sea.Res. 31, pp.135-145.

Venrick EL. 1990. Mesoscale patterns of chlorophyll a in the central North Pacific. Deep Sea Res. 37, pp. 1017-1031.

Vincent WF, Neale PJ, Richerson PJ. 1984. Photoinhibition: algal responses to bright light during diel stratification and mixing in a tropical alpine lake. J.Phycology 20, pp.201-211.

Wallace RA, Sanders GP, Ferl RJ. 1991. Biology: The science of life (3rd Edn.). Harper Collins Publishers, U.S. 1246pp.

Weber LH, El-Sayed SZ, Hampton I. 1986. The variance spectra of phytoplankton, krill and water temperature in the Antarctic Ocean south of Africa. Deep Sea Res. 33, pp.1327-1343.

Welschmeyer NA. 1994. Fluorometric analysis of chlorophyll a in the presence of chlorophyll b and phaeopigments. Limnol.Oceanogr. 39, pp.1985-1992.

Williams PJ. 1993. Chemical and tracer methods of measuring plankton production. ICES mar.Sci.Symp. 197, pp. 20-36.

Williams PJ, Heinemann KR, Marra J, Purdie DA. Comparison of ^{14}C and O_2 measurements of phytoplankton production in oligotrophic waters. Nature 305, pp.49-50.

Williams PJ, Jenkinson NW. 1982. A transportable microprocessor controlled Winkler titration suitable for field station and shipboard use. Limnol.Oceaonogr. 27, pp.576-584.

Williams PJ, Purdie DA. 1991. *In vitro* and *in situ* derived rates of gross production, net community production and respiration of O_2 in the oligotrophic subtropical gyre of the north Pacific Ocean. Deep Sea Res. 38, pp.891-910.

Williams PJ, Raine RCT, Bryan JR. 1979. Agreement between ^{14}C and O_2 methods of measuring phytoplankton production: reassessment of the photosynthetic quotient. Oceanol.Acta. 20, p.411-416.

Williams PJ, Robertson JE. 1991. Overall planktonic oxygen and carbon dioxide metabolisms: the problem of reconciling observations and calculations of photosynthetic quotients. J.Plankton Res. 13 (suppl.), pp.153-169.

Yoder JA, McClain CR, Blanton JO, Oey L. 1987. Spatial scales in CZCS-chlorophyll imagery of the southeastern U.S. continental shelf. Limnol.Oceanogr. 32, pp.929-941.

Appendix 1— Persons responsible for data sampling

The understanding, operation and manipulation of the Fast Repetition Rate Fluorometer (FRRF) was a lengthy and remains a continual process. As such, I could not become directly involved with a vast majority of the routine collection of additional data (see *Chapter 2*) useful for subsequent interpretation of the FRRF data. However, I have previously practised some of the methodologies listed below (†), otherwise I attempted to become familiar with those of which I had no previous experience (††). *Table A1.1.* lists and gratefully acknowledges those participants of the cruises (Methodology, *Table 2.1.*) whose data was used in this thesis.

Methodology	Cruise		
	RV *Pelagia*	AMT 6	RRS *Challenger*
Filtration for pigments†	M. Davey	P. Holligan	P. Holligan
Production (^{14}C-uptake) ††	R. Geider	G. Tilstone/ E. Tierra	M. Lucas
Production (O_2) †	G. Kraay	n/a	n/a
Optical profiling	D. Suggett	S. Hooker/J. Aiken	n/a
Chl *a*-specific absorption analysis	P. Shaw	n/a	D. Suggett
Nutrients analysis	U. Riebesell	M. Woodward	D. Hydes
HPLC††	S. Gibb	R. Barlow	C. Lucas
Underway hydrographic data	K. Timmermans	J. Aiken	J. Sharples
CTD operations and hydrographic data	K. Timmermans/ R. Groenewegen	D. Richmond/ V. Afanasyev	D. Teare/ J. Short

Table A1.1.— Summary of cruise participants who collected the data for the respective parameter methodologies. Operation of the FRRF is not included since I was responsible for the majority of the data collection, however, R.Geider, M.Davey, M.Moore and E. Abraham are gratefully acknowledged for aiding in the operation of the FRRF, most notably during watch periods. The person responsible for the underway hydrographic data collection also signifies the Principle Scientist of each respective cruise. Whilst I was not directly responsible for the majority of ancillary data collection, I have previous experience (†), or have observed the protocol at sea and am therefore familiar with (††), some of the above methodologies.

Appendix 2— Chlorophyll*a*-specific light absorption measurements from sites M and U, RRS *Challenger* (re. *Chapter 4*)

The following figure (*fig. A2.1.*) provides a summary of all chl *a*-specific absorption (a*) measurements of filtered seawater samples corresponding to the mixed and stratified sites, RRS *Challenger* cruise, described in *Chapter 4*. Samples were taken at 3-4 depths from 5 CTD samples during each of the 25 hour sampling periods. Measurements of absorption were made between 350 and 850 nm in a spectrophotometer and subsequently converted to chl *a*-specific absorption (see *section 2.2.*)

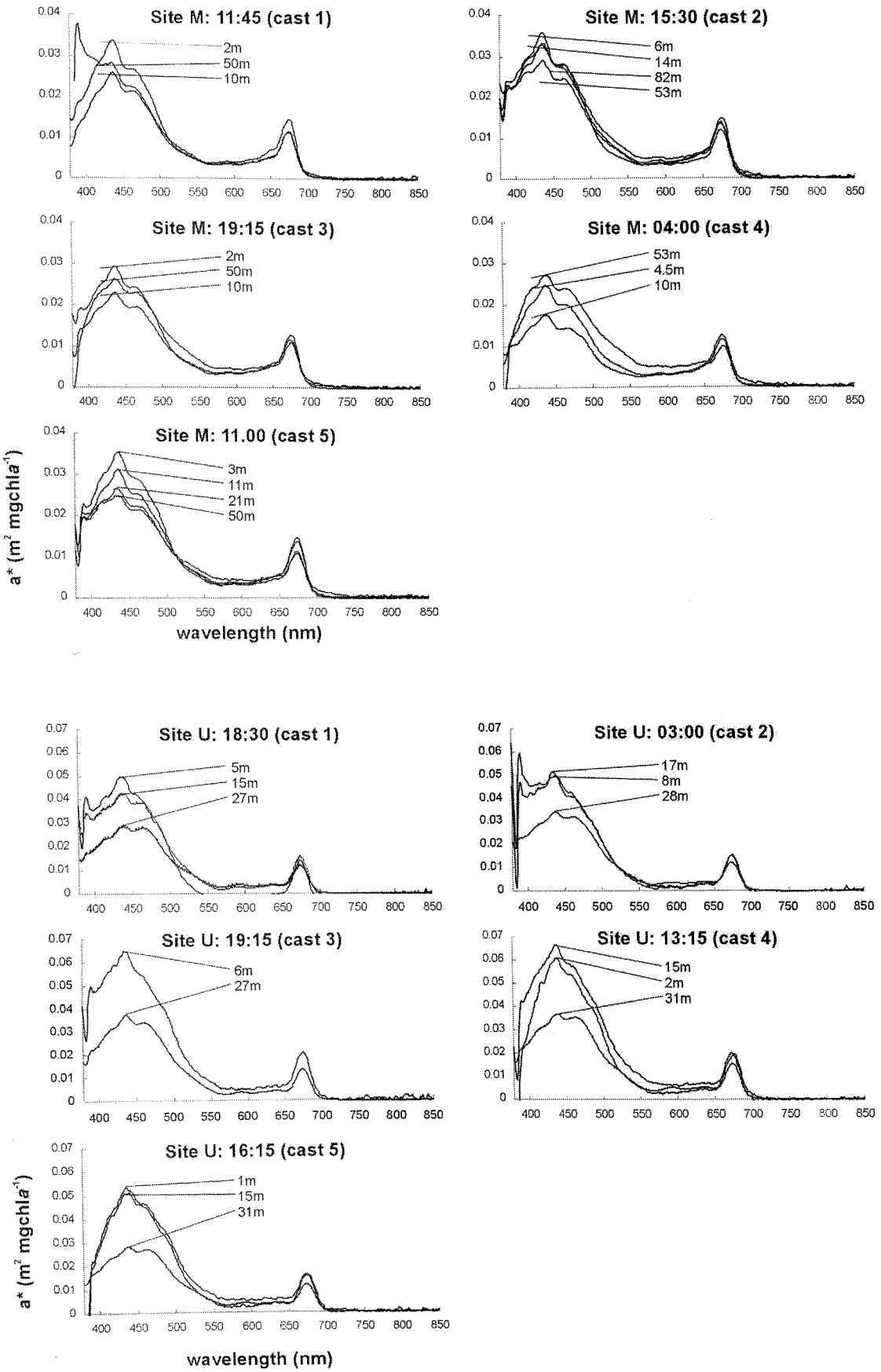

Figure A2.1.— Summary of all chlorophyll *a*-specfic absorption (a*) measurements from water samples collected at the mixed (M) and stratified (U) sites, *Chapter 4* (see main text).

Appendix 3— Statistics employed for AMT6 data analysis (*re.* Chapter 5)

The following calculations were performed using the Plymouth Routines in Multivariate Ecological Research (PRIMER, Carr 1994) programme. The information provided below is intended to support the calculation and results of the analyses presented in Chapter 5. Much of this understanding is drawn from Clarke and Warwick (1994) and readers are referred to this source for a more detailed explanation of these techniques.

Calculation of similarity matrices— Similarities were calculated between every pair of samples to give a lower triangular matrix. The Bray-Curtis coefficient was chosen since it is commonly applicable to environmental data. The data used were hydrographic and quantitative summaries of phytoplankton biomass/production (ie. environmental). I was interested in analysing the similarities for the absolute values of each parameter (eg. surface temperature, integrated nutrient concentrations) that were contributed to the samples (CTD stations). I also intended to subsequently subject the resultant matrix to an MDS analysis, which is very flexible (this technique ranks similarities in a matrix and then interprets their relative distances apart). As such, it did not appear necessary to transform the data. The Bray-Curtis similarity matrices that were derived for the hydrographic -/+ the biomass/production data are given below (*figs A3.1.* and *A3.2.*, respectively).

Hierarchical dendrograms (agglomerative clustering)— This technique provides a graphical display linking samples that, based on the degree of common characteristics/values, have mutual levels of similarity. A dendrogram successively fuses the samples into groups and then groups into large clusters. This method can provide a check (and the levels of similarity) for which the clusters are identified in subsequent ordination techniques. The Bray-Curtis similarity matrices are plotted as dendrograms for the hydrographic -/+ the biomass/production data are given below (*figs A3.3.* and *A3.4.*, respectively).

	28.4N	36.4N	11.4S	9.0N	12.7N	14.4S	5.5S	2.5S	16.2N	8.4S	5.5N	3.0N	41.1N	48.3N	29.3S	28.6S	28.3S	21.4S	24.5S	24.2S	18.6S	32.2S	20.2N	49.5N
28.4N																								
36.4N	79.70																							
11.4S	64.57	81.42																						
9.0N	50.52	66.15	80.53																					
12.7N	39.71	52.34	66.74	83.06																				
14.4S	58.79	73.56	90.68	85.76	71.41																			
5.5S	58.98	72.77	87.94	86.11	71.48	93.26																		
2.5S	53.35	66.17	82.44	89.93	78.53	90.12	91.07																	
16.2N	56.31	71.33	85.90	90.82	75.57	91.56	92.18	90.97																
8.4S	56.29	73.05	87.92	92.11	75.71	88.82	91.03	88.66	95.73															
5.5N	56.98	73.40	88.45	90.45	75.46	91.93	93.74	88.25	92.69	94.64														
3.0N	63.05	80.52	93.53	84.10	68.60	89.49	89.43	83.37	87.74	90.96	92.38													
41.1N	66.95	82.99	90.58	78.01	63.90	88.04	88.04	81.94	85.20	85.14	86.17	93.23												
48.3N	58.99	70.33	80.24	80.24	68.59	87.05	85.89	85.83	81.04	79.01	80.88	80.37	82.18											
29.3S	32.26	37.85	44.30	48.79	50.60	49.33	50.66	52.96	51.05	47.67	47.17	44.65	46.61	49.77										
28.6S	32.29	38.59	45.35	52.13	55.48	50.90	52.33	54.96	52.96	49.54	48.60	46.10	47.86	51.38	92.14									
28.3S	33.87	39.39	46.26	51.09	48.78	50.98	52.20	54.38	51.82	48.73	48.55	45.88	48.07	51.29	91.08	84.31								
21.4S	41.35	47.78	53.27	51.23	41.54	56.22	59.40	54.03	56.25	54.03	54.78	53.61	55.40	54.03	81.21	73.98	88.13							
24.5S	35.26	40.24	46.83	48.31	38.99	50.77	51.54	50.19	50.64	48.09	47.91	45.72	47.59	48.16	78.29	71.65	85.55	92.18						
24.2S	37.00	42.96	49.60	51.25	45.44	54.20	55.32	54.75	53.54	51.10	52.23	49.55	51.56	54.43	88.02	80.60	94.65	93.03	88.33					
18.6S	32.76	37.72	43.67	43.33	43.90	47.51	49.46	47.90	45.97	43.54	44.62	43.40	45.65	48.13	87.51	80.10	90.19	93.44	87.70	93.48				
32.2S	39.89	50.41	61.45	72.99	79.39	69.89	71.80	77.15	73.82	69.43	67.89	63.05	64.72	69.88	63.30	66.69	55.14	48.96	45.76	53.77	53.87			
20.2N	43.34	53.69	67.32	76.98	81.94	75.11	76.70	81.97	77.03	73.67	72.70	66.93	68.41	74.51	61.32	63.99	57.35	51.89	48.68	56.31	53.78	93.04		
49.5N	39.99	53.44	65.60	80.95	86.67	72.26	71.32	78.38	75.67	73.81	74.04	67.25	66.15	73.05	49.37	52.36	48.45	42.63	40.68	45.65	41.88	77.96	81.78	

	28.4N	36.4N	11.4S	9.0N	12.7N	14.4S	5.5S	2.5S	16.2N	8.4S	5.5N	3.0N	41.1N	48.3N	29.3S	28.6S	28.3S	21.4S	24.5S	24.2S	18.6S	32.2S	20.2N	49.5N
28.4N																								
36.4N	80.48																							
11.4S	64.95	77.23																						
9.0N	52.26	62.68	77.28																					
12.7N	43.47	52.29	66.77	81.60																				
14.4S	53.72	63.39	83.22	78.26	72.12																			
5.5S	56.00	65.50	83.71	81.39	70.47	91.16																		
2.5S	52.27	61.30	81.14	82.04	78.38	87.06	86.98																	
16.2N	52.02	61.55	79.54	84.90	81.38	87.98	87.17	87.49																
8.4S	57.84	69.76	89.21	85.20	73.11	84.70	88.89	86.04	88.10															
5.5N	61.26	75.28	85.03	82.31	71.57	80.69	84.64	81.62	79.90	88.61														
3.0N	63.40	75.79	92.75	80.11	68.32	84.30	87.31	82.33	82.11	92.72	87.54													
41.1N	64.55	75.37	87.76	74.45	63.22	83.24	87.36	78.30	80.16	86.08	80.29	91.83												
48.3N	38.72	41.44	48.59	54.41	49.86	55.92	54.48	53.10	55.84	48.98	46.93	49.98	52.58											
29.3S	28.14	31.39	40.41	50.40	53.86	47.55	45.48	48.30	52.54	43.88	40.20	41.38	41.58	57.05										
28.6S	24.62	27.56	36.10	48.46	50.93	45.46	43.63	43.94	49.16	39.67	35.85	37.27	39.69	53.86	85.24									
28.3S	25.22	27.48	35.24	44.93	44.42	42.87	41.38	41.57	45.45	37.54	34.76	35.64	38.04	60.52	81.08	82.36								
21.4S	36.76	41.37	51.04	53.54	53.01	59.54	59.28	54.76	61.86	53.16	50.00	51.95	54.48	48.22	75.44	68.39	73.00							
24.5S	35.86	39.96	49.10	53.70	52.48	54.45	52.42	53.19	56.70	50.81	48.96	48.57	48.14	49.52	78.57	70.81	74.44	86.95						
24.2S	33.49	36.94	45.81	52.38	49.23	50.73	49.34	48.74	53.04	47.89	45.00	46.46	47.03	63.98	86.23	75.08	85.29	79.44	82.11					
18.6S	39.89	42.71	49.02	47.73	52.04	52.51	51.17	51.69	51.27	49.56	46.99	49.14	48.38	46.14	78.55	69.96	71.91	83.11	85.84	81.73				
32.2S	32.62	37.62	50.35	62.12	69.54	62.12	59.40	61.77	67.45	55.79	50.17	51.87	53.53	60.15	76.02	70.11	62.39	58.60	59.72	64.65	59.44			
20.2N	33.55	37.82	50.71	62.81	65.96	60.23	57.72	60.36	64.74	54.62	49.87	51.02	51.91	64.68	76.76	75.56	67.18	56.54	60.44	70.28	58.79	87.23		
49.5N	29.65	35.34	48.02	56.08	64.95	59.32	55.48	57.15	61.94	52.94	48.25	49.42	50.91	62.47	68.77	61.97	56.20	51.91	55.56	62.05	52.36	80.80	82.26	

Figures A3.1. and A3.2.— Bray-Curtis similarity matrices determined from all hydrographic data (upper panel, A3.1.) and from all hydrography + all biomass/production characteristics as measured from the FRRF (lower panel, A3.2.). All CTD stations were used in the analyses and are signified in decimal degrees. All calculations were made using PRIMER.

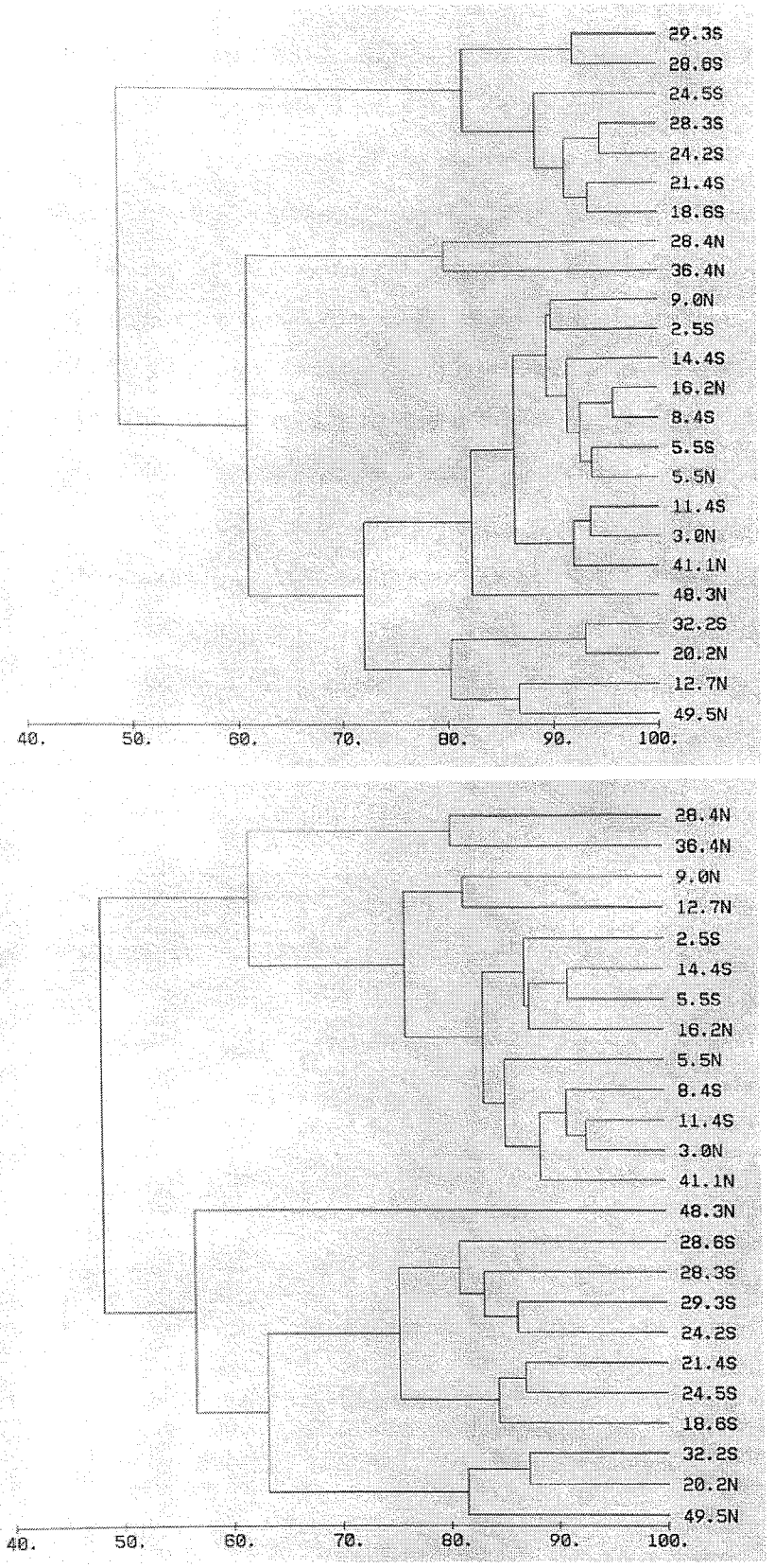

Figures A3.3. and A3.4.— Dendrogram plots using Bray-Curtis similarity matrices determined in *Figs. A3.1.* and *A3.2.*, respectively. All CTD stations were used in the analyses and are signified in decimal degrees. All calculations were made using PRIMER.

Non metric multidimensional scaling (MDS)— This ordination technique is relatively modern and very flexible. This method recognises the essential arbitrariness of absolute similarity values meaning that the *state of the source data* is more critical to how one interprets it than to the *outcome of the algorithm*. The reliability of this technique can be determined from the level of stress generated during each calculation (a value of stress is assigned to each iteration of the algorithm [to the data] as it attempts to reduce the multidimensional data into 2 or 3 dimensions). The technique works towards minimising the stress value and, as such, a minimum stress level is derived (with the appropriate data). Six iterations are recommended for this technique and were, therefore, applied (see *table A3.1.*). Re-calculation using more iterations did not yield a different result. Stress levels for the reduction of the AMT6 data remained below 0.1 thus providing "a good ordination with no real prospect of a misleading interpretation". This method was performed in favour of a Principle Components Analysis (see *Chapter 5*).

	Stress values of MDS			
	Hydrographic data		All data	
Iteration	3D	2D	3D	2D
1	0.03	0.05	0.04	0.08
2	0.03	0.05	0.04	0.08
3	0.03	0.05	0.04	0.09
4	0.03	0.05	0.04	0.09
5	0.03	0.05	0.04	0.08
6	0.03	0.05	0.04	0.08

Table A3.1.— Summary of stress values produced from MDS calculations using data from the Bray-Curtis similarity matrix. Calculations were repeated for 6 iterations on both the hydrographic data only and hydrography + all biomass/production characteristics as measured from the FRRF (all data).

Multiple Stepwise Regressions (MSR)— These analyses were performed for comparing the variance of each of the physiological [dependent] variables F_v/F_m, σ_{PSII} and production from the FRRF with the variance of hydrographic [independent] variables

(temperature, nutrients and PAR). All data was grouped according to the clusters produced from the MDS statistics and MSR analyses were subsequently performed using the *Minitab* statistics package. Each MSR analysis was re-calculated with only the 4 most significant variables to reduce the amount of error generated (from minor variables) in the calculation of the statistic. The following results provide the coefficient (of the independent variable in the regression equation), the t-statistic, the probability of significance, the r^2 (the proportion of variance accounted by each independent variable) and an ANOVA summary of the data for each MSR.

A. Strongly eutrophic stations:

regression eqn:	F_v/F_mD	=	-0.00023PAR	+0.127NO_2	-0.0325PO_4	+0.06Temp	+7.8
t-statistic:			-2.77	1.54	-3.03	7.18	5.12
probability (P):			0.01	0.134	0.005	0.000	0.000
r^2 (%):			16.20	2.0	6.72	44.64	

source	DF	SS	MS	F	P
regression	4	0.32	0.064	18.07	0.000
error	30	0.103	0.004		
total	34	0.422			

regression eqn:	σ_{PSII}	=	-0.423PAR	-7.91NO_3	-129PO_4	+852
t-statistic:			-2.55	-3.56	-6.45	18.31
probability (P):			0.015	0.001	0.000	0.000
r^2 (%):			11.44	12.55	46.45	

source	DF	SS	MS	F	P
regression	3	1142682	285671	16.59	0.000
error	36	602736	17221		
total	39	1745418			

regression eqn:	P^{chl}	=	0.0127PAR	-0.0725NO_3	-7.48NO_2	+0.473Temp	+22.0
t-statistic:			3.94	-1.34	-2.35	1.38	-0.34
probability (P):			0.001	0.192	0.027	0.178	0.740
r^2 (%):			44.61	6.47	2.95	6.88	

source	DF	SS	MS	F	P
regression	4	210.819	35.136	6.90	0.000
error	29	137.527	5.094		
total	33	348.345			

regression eqn:	P_C	=	0.373PAR	-0.349NO_3	-262NO_2	-26.8PO_4	+638
t-statistic:			2.71	-1.18	-1.76	-1.51	0.22
probability (P):			0.013	0.249	0.094	0.147	0.826
r^2 (%):			35.4	6.66	4.53	4.49	

source	DF	SS	MS	F	P
regression	4	211570	35262	3.97	0.008
error	23	186686	8890		
total	27	398256			

B. Weakly eutrophic stations:

regression eqn:	F_v/F_mD	=	0.016 NO_3	-0.381 PO_4	-0.1615PAR	+0.0145Temp	+6.001
t-statistic:			2.65	-3.98	-2.59	1.61	2.85
probability (P):			0.001	0.16	0.018	0.125	0.1
r^2 (%):			29.8	6.2	47.1	5.8	

source	DF	SS	MS	F	P
regression	4	0.281	0.0703	8.17	0.001
error	19	0.163	0.0086		
total	23	0.444			

regression eqn:	σ_{PSII}	=	-0.0624PAR	+4.18NO_3	+121 NO_2	-111 PO_4	-9464
t-statistic:			-1.06	1.26	1.63	-1.93	-10.63
probability (P):			0.156	6.084	0.122	0.071	0
r^2 (%):			13.5	27.3	16.7	22.6	

source	DF	SS	MS	F	P
regression	4	511681	102336	40.0	0.000
error	17	40939	2559		
total	21	552620			

regression eqn:	P^{chl}	=	0.0021PAR	-0.0489NO_3	-3.58NO_2	+0.173Temp	+36.8
t-statistic:			2.10	-2.26	-2.87	2.07	1.81
probability (P):			0.05	0.037	0.07	0.053	0.087
r^2 (%):			39.93	19.94	12.7	2.11	

source	DF	SS	MS	F	P
regression	4	32.238	6.4476	8.72	0.000
error	19	13.304	0.7391		
total	23	45.542			

regression eqn:	P_C	=	0.0443PAR	-17.9NO_3	-64.8NO_2	+182PO_4	-1140
t-statistic:			1.55	-3.88	-1.84	3.19	-1.82
probability (P):			0.143	0.002	0.087	0.007	0.09
r^2 (%):			51.63	17.12	14.08	5.8	

source	DF	SS	MS	F	P
regression	4	31634.7	6326.9	12.12	0.000
error	15	7309.7	522.1		
total	19	38944.4			

C. Meso-Weak oligotrophic stations:

regression eqn:	F_v/F_mD	=	0.359 NO_2	-0.083PO_4	+0.0083Temp	-1.65
t-statistic:			5.25	-2.33	2.01	-1.45
probability (P):			0.00	0.022	0.048	0.15
r^2 (%):			19.28	27	5.3	

source	DF	SS	MS	F	P
regression	3	0.93720	0.23430	19.9	0.00
error	82	0.95391	0.01178		
total	85	1.89111			

regression eqn:	σ_{PSII}	=	3155	-0.138PAR	-14.4NO_3	-58.8Temp

t-statistic:		1.46	-2.32	-2.65	-0.97
probability (P):		0.148	0.023	0.01	0.336
r^2 (%):			6.1	22.3	4.3

source	DF	SS	MS	F	P
regression	3	994939	331646	8.11	0.000
error	76	3109455	40914		
total	79	4104394			

regression eqn:	P^{chl} =	$-0.298NO_3$	-0.115Temp	-3.18PAR	+111	
t-statistic:		3.25	-2.40	-4.14	3.90	
probability (P):		0.002	0.019	0.000	0.000	
r^2 (%):		54.17	3.43	10.14		

source	DF	SS	MS	F	P
regression	3	476.62	158.85	39.31	0.000
error	68	274.80	4.04		
total	71	751.42			

regression eqn:	Pc =	1.15 NO_3	+10.6 PO_4	-1.01Temp	+0.0031PAR	-10.2
t-statistic:		2.23	1.20	-1.76	1.01	-0.84
probability (P):		0.029	0.236	0.084	0.318	0.403
r^2 (%):		42.68	2.06	1.93	0.98	

source	DF	SS	MS	F	P
regression	4	5574.5	1393.6	13.07	0.000
error	59	6293.0	106.7		
total	63	11867.5			

D. Strongly oligotrophic stations:

regression eqn:	F_v/F_mD =	0.696	-0.0032PAR	-0.00287 PO_4	-1.41 NO_2	-0.845 NO_3
t-statistic:		4.51	-0.73	-0.42	-0.74	-2.49
probability (P):		0.006	0.498	0.690	0.495	0.055
r^2 (%):			nd	nd	nd	61.82

source	DF	SS	MS	F	P
regression	4	0.17565	0.04414	2.58	0.164
error	5	0.08567	0.01713		
total	9	0.26223			

regression eqn:	σ_{PSII} =	649	+1.14PAR	+6.91NO_3	+811NO_2	-183 PO_4
t-statistic:		11.34	0.71	2.43	1.16	-0.97
probability (P):		0.00	0.575	0.072	0.31	0.382
r^2 (%):			nd	54.12	nd	nd

source	DF	SS	MS	F	P
regression	4	20989	1247	2.38	0.210
error	4	8808	2202		
total	8	29797			

regression eqn:	P^{chl} =	0.044 NO_3	-8.68PAR	-0.003NO_2	+0.75
t-statistic:		4.97	-2.22	-0.22	2.83
probability (P):		0.004	0.077	0.839	0.053
r^2 (%):		91.68	4.43	0.94	

source	DF	SS	MS	F	P

regression	3	8.9035	2.2259	31.33	0.001
error	6	0.3553	0.0711		
total	9	9.2587			

regression eqn:	Pc	=	-24.9 NO_3	-0.008NO_2	-4.94Temp	+0.045PAR	-89.7
t-statistic:			-4.62	-0.36	-2.18	2.25	-2.38
probability (P):			0.044	0.753	0.161	0.153	0.14
r^2 (%):			85.01	4.14	2.69	2.41	

source	DF	SS	MS	F	P
regression	4	12.9099	2.1517	22.38	0.043
error	4	0.1923	0.0962		
total	8	13.1022			

Semivariograms and fractal dimensions— These techniques were employed to characterise the predominant spatial scales of variability in continuous surface water measurements along the AMT6 transect, and were chosen because of their flexibility and ease of use (see *Chapter 5*). The following provides a summary of the semivariogram technique as described in detail by Clark (1979) and Yoder et al (1987): The variogram is a plot of the semivariance (S-V) against distance between samples (h). S-V is calculated as:

$$\text{S-V}\ (h) = [1/2n]^*[g_x - g_{x+h}]^2$$

$$\textbf{S-V} = \sum_{x=1}^{n(h)} [1/2n]\ ]^*[g_x - g_{x+h}]^2$$

Where h is the distance (lag) between samples; g_x is the sample value; and n is the number of observations between each lag. When applied to a continuous set of data, one or more patterns can be produced (*fig. A3.5.*). The predominant scales of variability can be extracted from analysing the sill(s) of a variogram. The initial sill signifies the maximum difference between values of a parameter comprising a patch and corresponds to **1/2** the wavelength at which the patch occurs (*fig. A3.5.*). The sill may be further represented throughout the variogram as a wave function where subsequent sills have a spatial scale equal to the distance between successive sills. In addition, more than one dominant spatial scale may be apparent and result in alternate sills and wave functions. However, not all sills are easy to distinguish, for example, where multiple sills of a wave function dampened with increased scale length. As such, a series of criteria can be employed to separate real (dominant) patches from noisy data or weak signals (Yoder *et*

al. 1987): 1. The decrease in slope must be 10% or less of the mean slope before the decrease; 2. Constant (±10%)/decreased S-V after a break in the slope for >20% of the resolved scale length; 3. A sill value at least twice that of the nuggett variance (see *fig. A3.5.* legend). These were applied throughout the analyses of the AMT6 transect given in *fig A.3.6.*

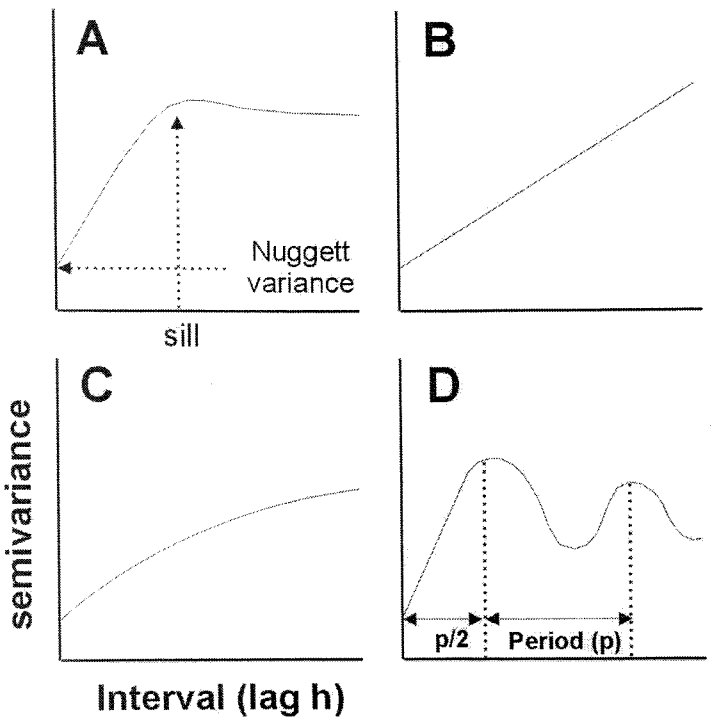

Figure A3.5: Example patterns of semi-variograms: (A) rational quadratic (or spherical) (B) linear (C) exponential (D) wave. The abbreviations in plots (A) and (D) show some of the features of a variogram. The peak (sill) indicates a dominant spatial scale and is equal to **1/2** the lag distance at which the peak occurs. Some variograms do not have an S-V value = 0 at the first (lag 1) distance. This non-zero is referred to as the nuggett variance and is the result of measurement error and/or variability at scales less than lag 1 and is equivalent to white noise in spectral analysis (Journel and Hujibregts 1978). Where a variogram remains at a constant value, following the S-V at lag 1, there will be no resolvable sills, and therefore, no dominant spatial scale. (B and C) A linear or curvilinear S-V indicates a trend that has a period at least twice that of the longest lag. (D) A periodic distribution of variability produces an S-V with regular sills where the distance between sills is equal to the wavelength.

Semivariograms are applied to assess spatial scales of variability, however, the technique can be taken a stage further to assess the hetero/homogenetic nature of the respective variability. This is achieved by calculating the Fractal Dimension, D, and is summarised below following Burrough (1981), Mandelbrot (1983) and Seuront and Lagadeuc (1997, 1998).

$D = 0.5^{*}(4\text{-m})$ [where m is derived from the gradient of a log-log plot of the semivariogram]

D describes the variability of a continuum of scales. Under this approach, the degree of hetero/homogeneity is associated with patterns remaining similar upon subdivision in time. Where m=0: *D*=2, indicating that variation within and between sampling units is the same (ie. no directional change in the value of the semivariogram following lag 1). As such, variability is evenly distributed and relatively unstructured in space. High values of *D* characterise short range (local) variability, such as biological processes, which obscure long range physical processes; lower values of *D* (m increases) describe processes which are not [as easily] repeated upon subdivision in time, ie. long range physical processes with larger periods of variability. Some semivariograms can exhibit greater than 1 gradient (m) and give multiple fractal-dimensions where different periods of variability are developed and dominant. These calculations are easy to perform but again require an objective criteria. Following Seuront and Lagadeuc (1997), the values of D presented in Chapter 5 were calculated as describe these criteria as: 1. Maximise the coefficient of determination (r^2) of the semivariogram; 2. Minimise the total sum of the squared residuals for the regression. An example is given in *fig. A3.6.*

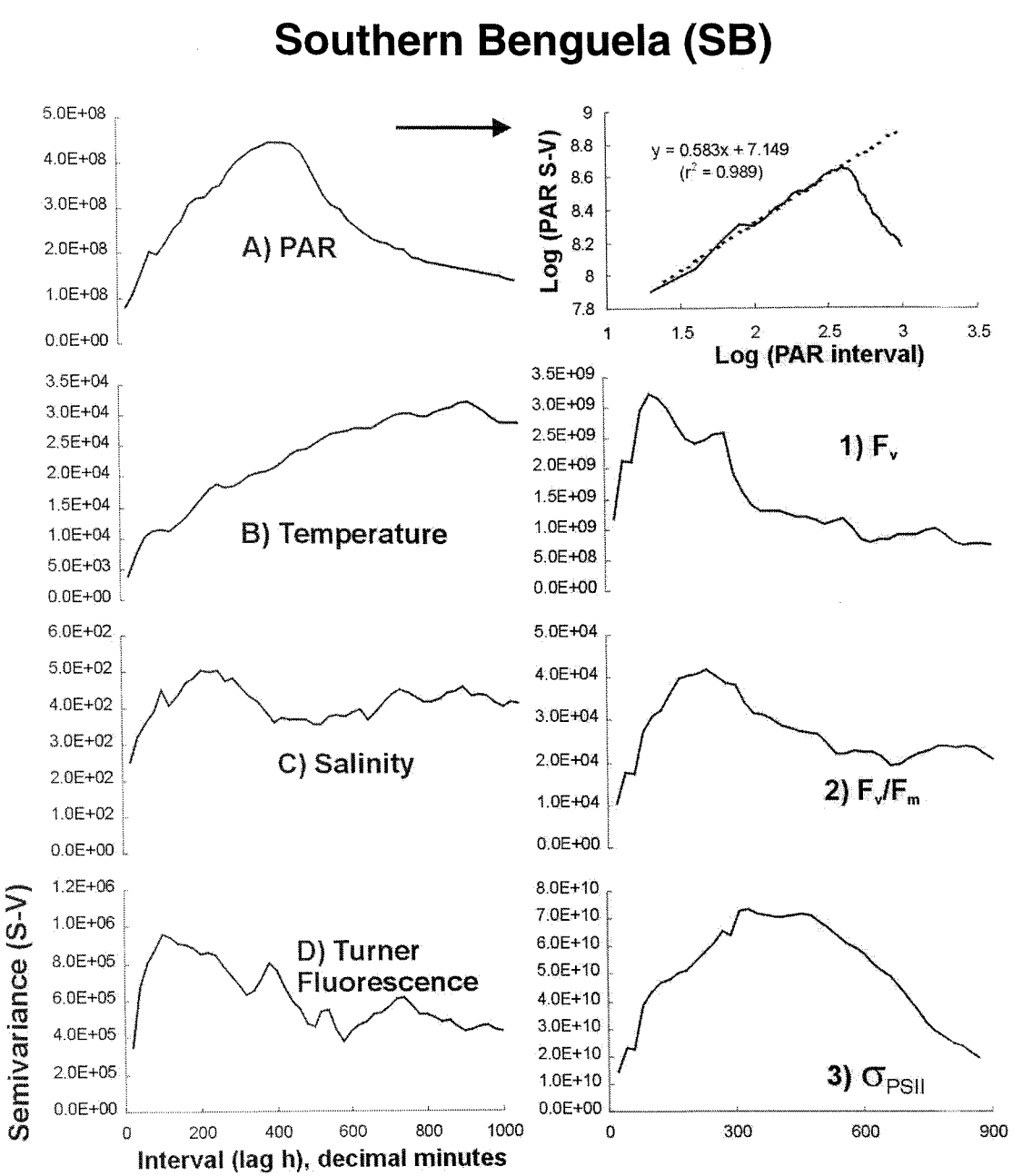

Figure A3.6.— Summary of semivariograms performed on along track surface (7m) data (see *Appendix 4*) of F_v, F_v/F_m and σ_{PSII} (FRRF) and PAR, temperature, salinity and fluorescence (ship data) collected throughout the **southern benguela (SB)** province, AMT6. Semivariograms (S-V) are in parameter units squared whilst lag h is in decimal minutes. Data used was from data points logged every 10 minutes. The upper most right hand figure also gives an example of the calculation of fractal dimension (*D*) whereby both axes of the S-V are logged. The gradient of a best-fit linear slope (m), see above) is established to calculate *D*.

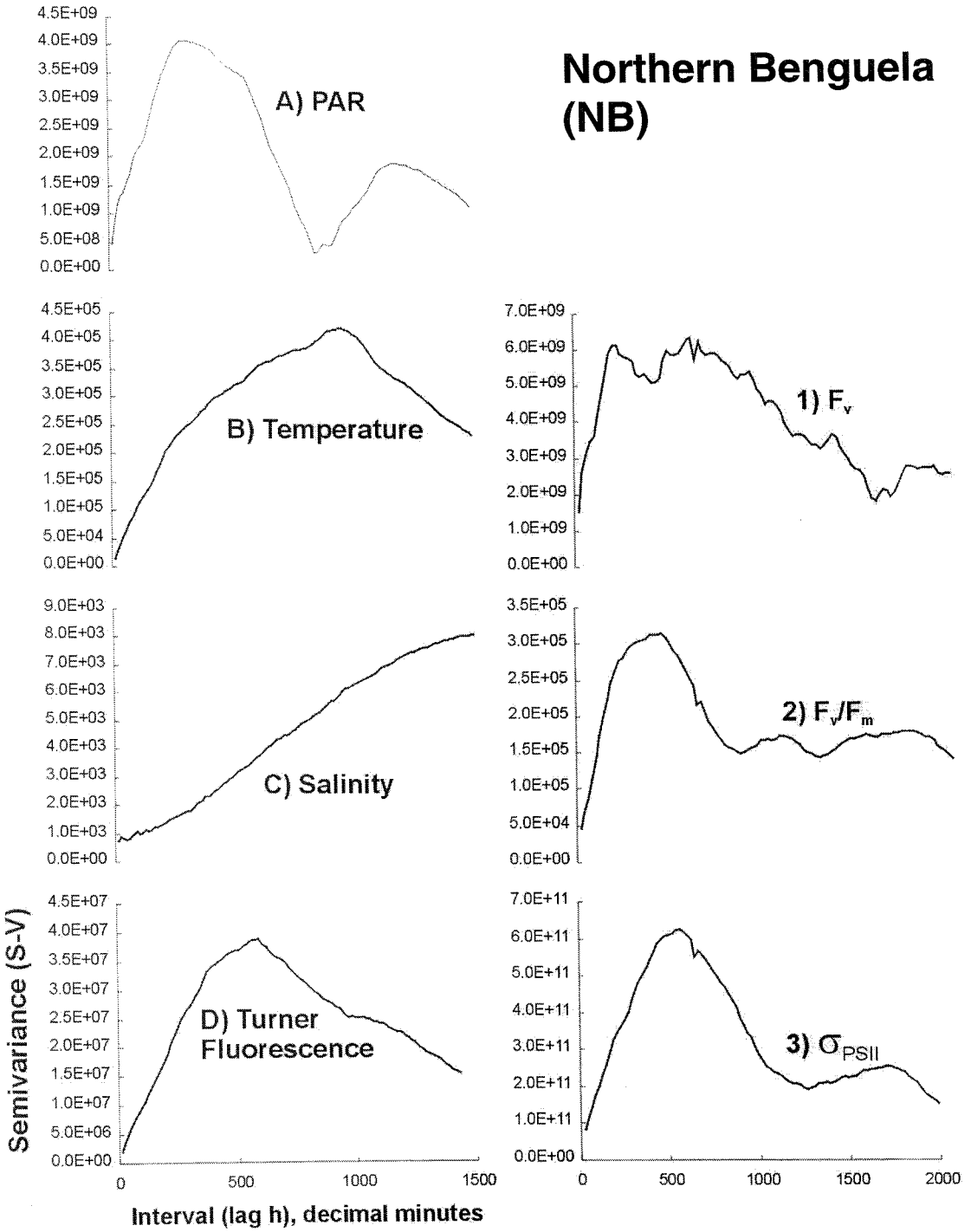

Figure A3.6. (contd.)— Summary of semivariograms performed on along track surface (7m) data (see *Appendix 4*) of F_v, F_v/F_m and σ_{PSII} (FRRF) and PAR, temperature, salinity and fluorescence (ship data) collected throughout the **northern benguela (NB)** province, AMT6. Semivariograms are in parameter units squared whilst lag h is in decimal minutes. Data used was from data points logged every 10 minutes.

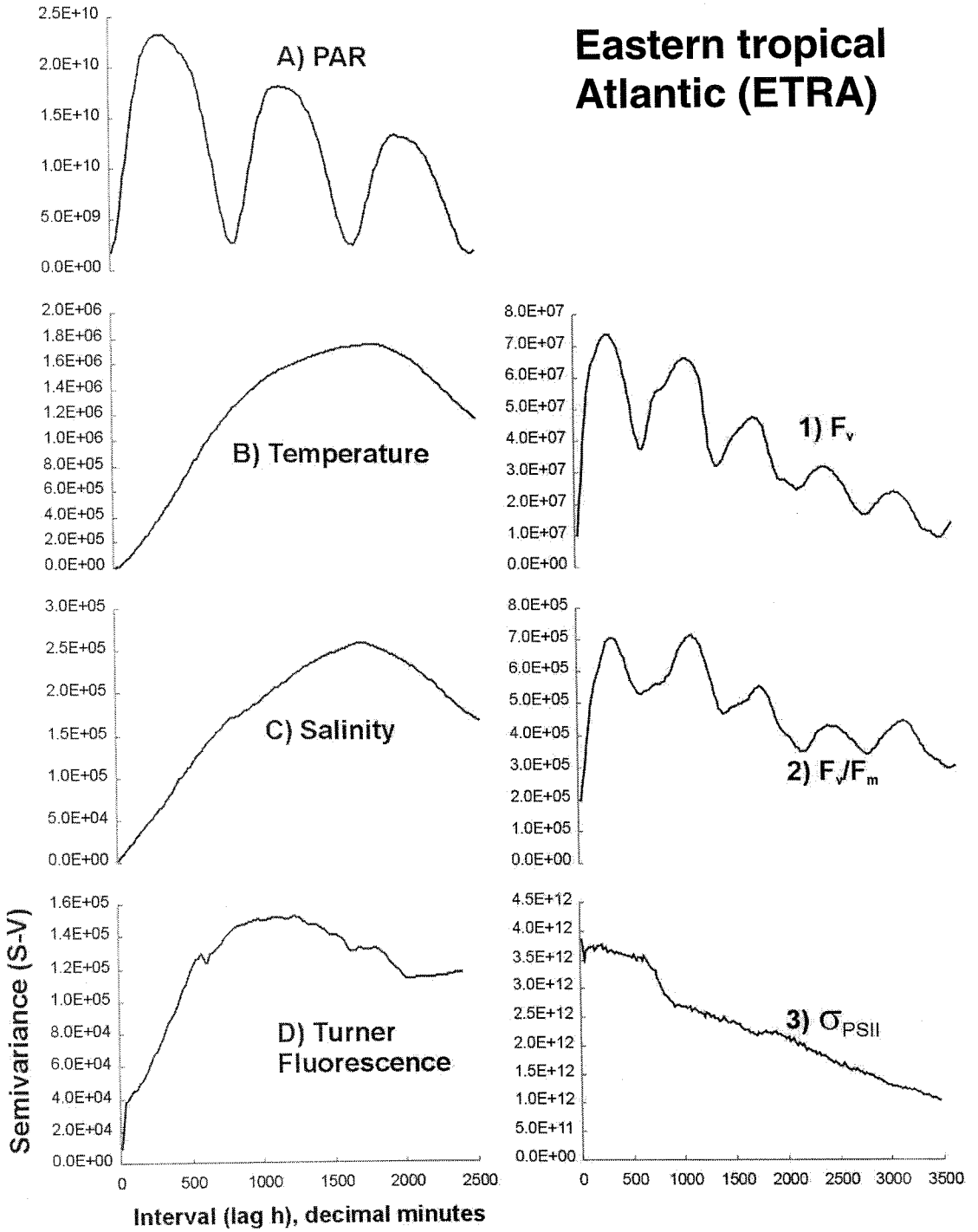

Figure A3.6. (contd.)— Summary of semivariograms performed on along track surface (7m) data (see *Appendix 4*) of F_v, F_v/F_m and σ_{PSII} (FRRF) and PAR, temperature, salinity and fluorescence (ship data) collected throughout the **eastern tropical Atlantic (ETRA)** province, AMT6. Semivariograms are in parameter units squared whilst lag h is in decimal minutes. Data used was from data points logged every 10 minutes.

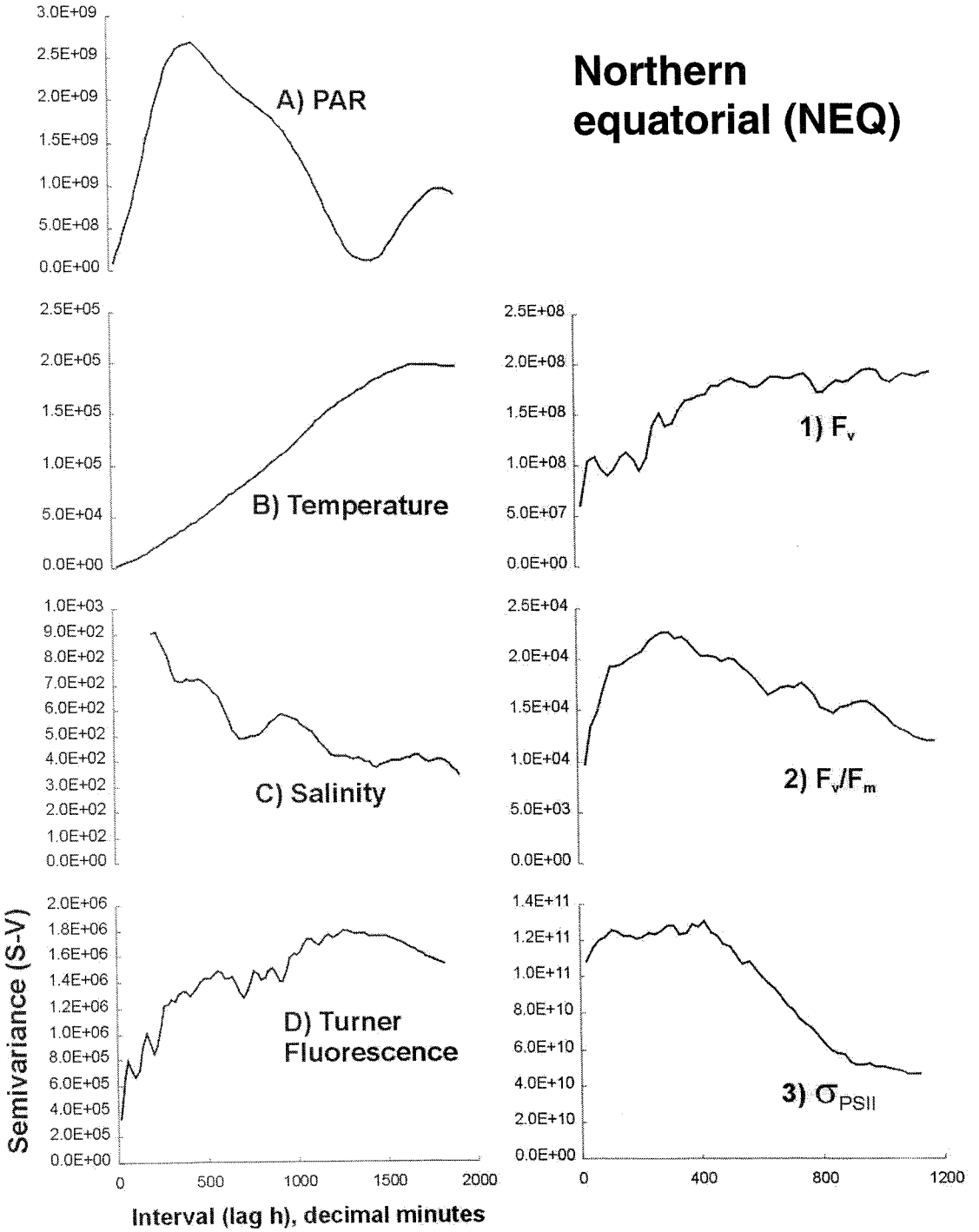

Figure A3.6. (contd.)— Summary of semivariograms performed on along track surface (7m) data (see *Appendix 4*) of F_v, F_v/F_m and σ_{PSII} (FRRF) and PAR, temperature, salinity and fluorescence (ship data) collected throughout the **northern equatorial (NEQ)** province, AMT6. Semivariograms are in parameter units squared whilst lag h is in decimal minutes. Data used was from data points logged every 10 minutes.

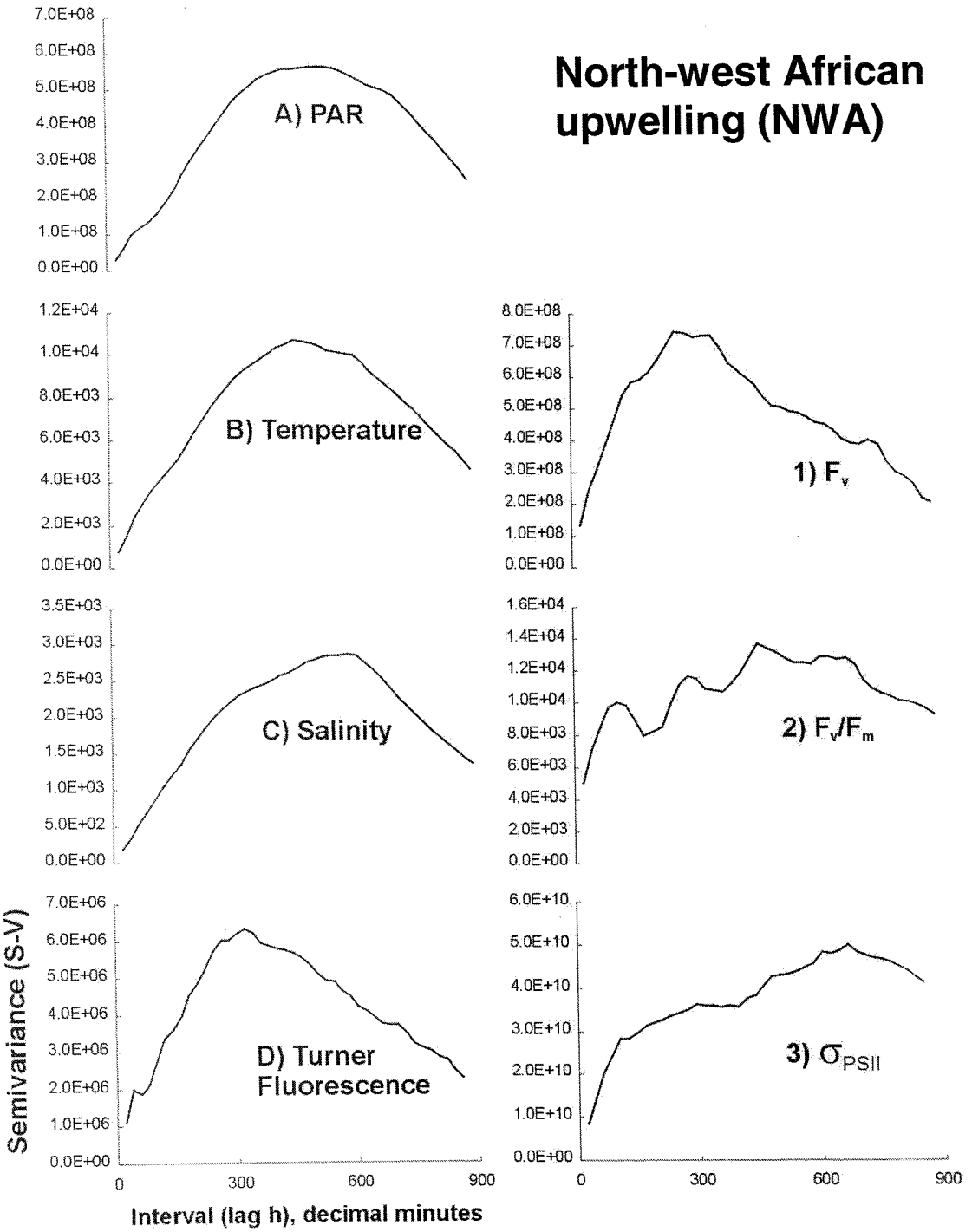

Figure A3.6. (contd.)— Summary of semivariograms performed on along track surface (7m) data (see *Appendix 4*) of F_v, F_v/F_m and σ_{PSII} (FRRF) and PAR, temperature, salinity and fluorescence (ship data) collected throughout the **northwest African upwelling (NWA)** province, AMT6. Semivariograms are in parameter units squared whilst lag h is in decimal minutes. Data used was from data points logged every 10 minutes.

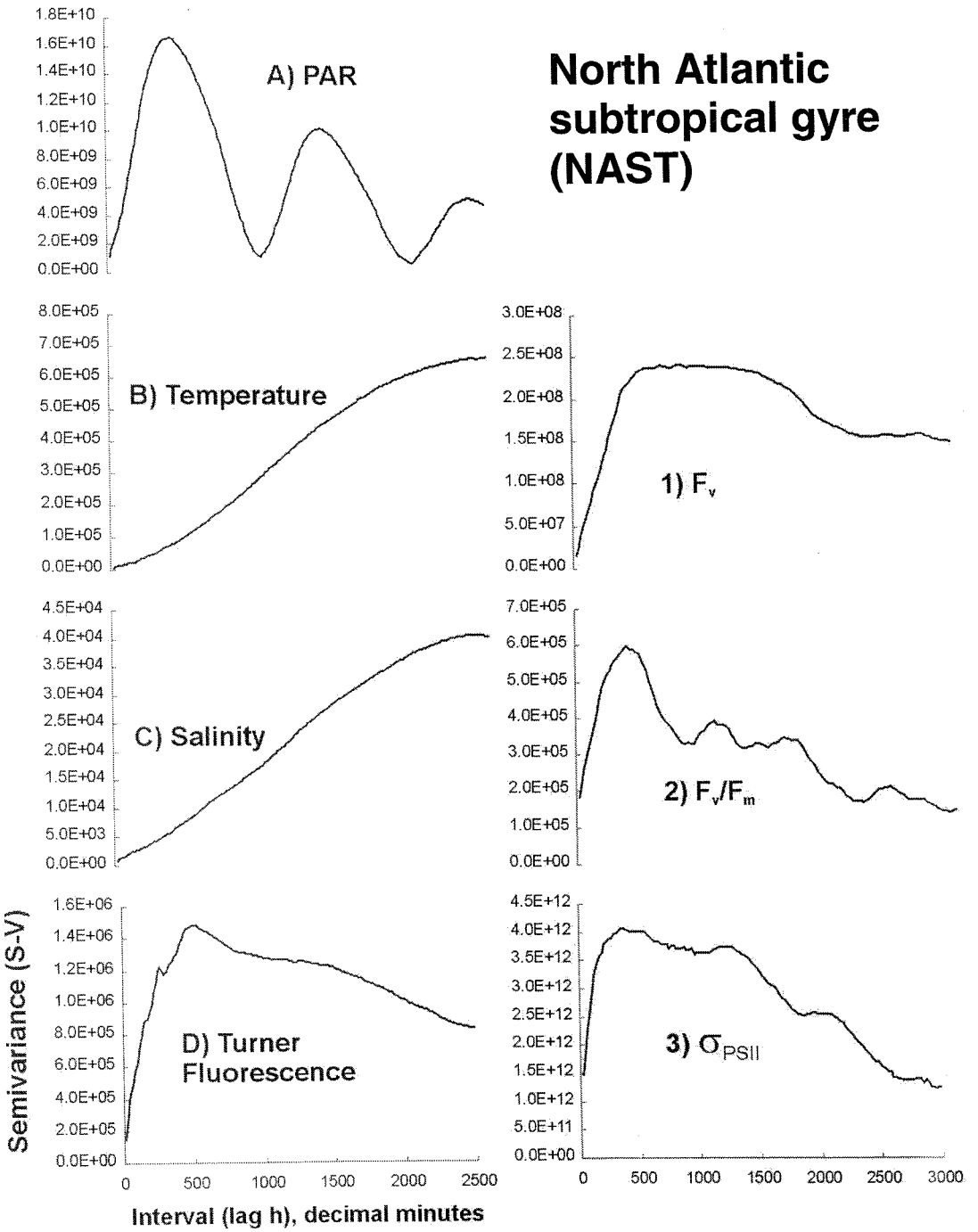

Figure A3.6. (contd.)— Summary of semivariograms performed on along track surface (7m) data (see *Appendix 4*) of F_v, F_v/F_m and σ_{PSII} (FRRF) and PAR, temperature, salinity and fluorescence (ship data) collected throughout the **north Atlantic subtropical gyre (NAST)** province, AMT6. Semivariograms are in parameter units squared whilst lag h is in decimal minutes. Data used was from data points logged every 10 minutes.

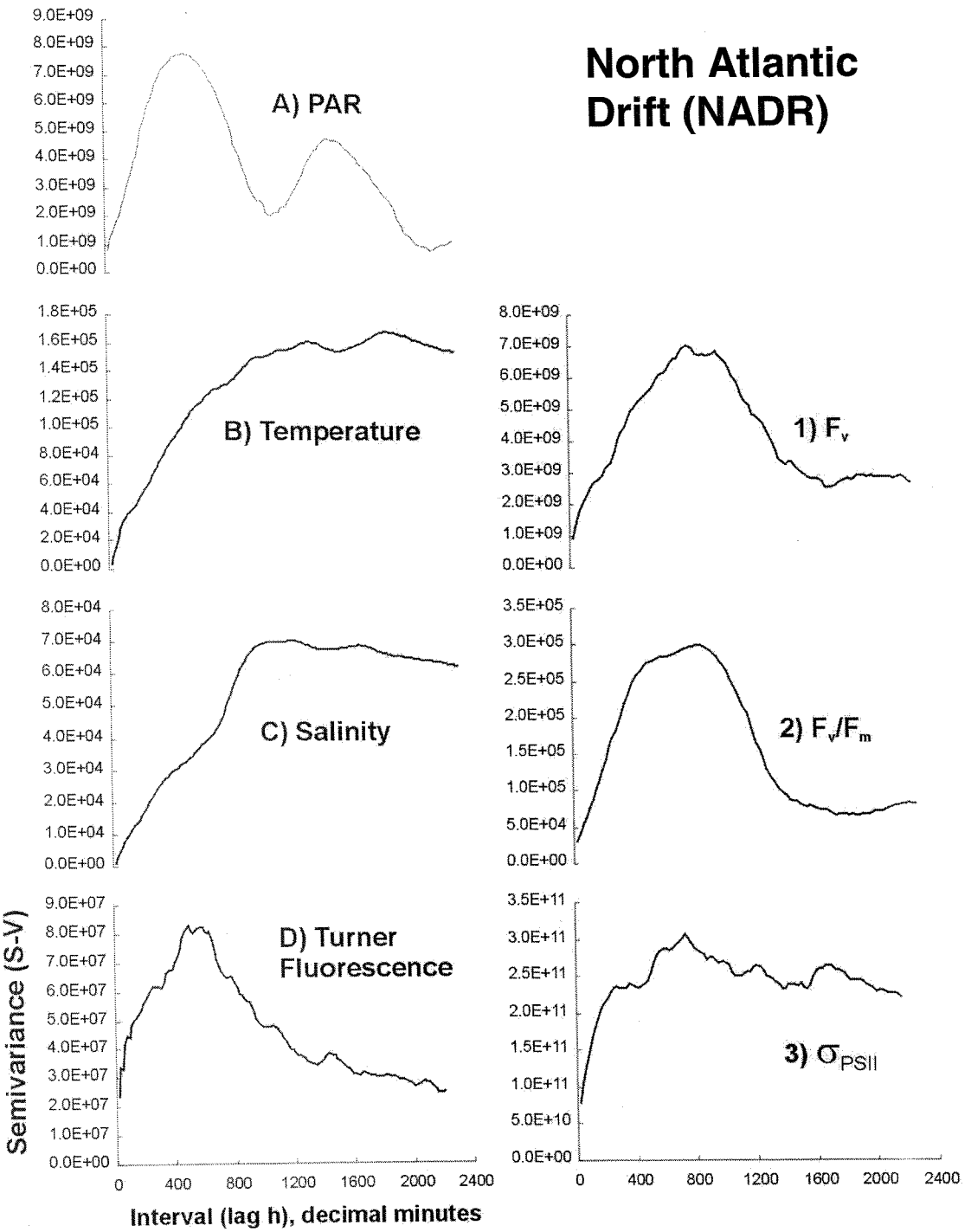

Figure A3.6. (contd.)— Summary of semivariograms performed on along track surface (7m) data (see *Appendix 4*) of F_v, F_v/F_m and σ_{PSII} (FRRF) and PAR, temperature, salinity and fluorescence (ship data) collected throughout the **north Atlantic drift (NADR)** province, AMT6. Semivariograms are in parameter units squared whilst lag h is in decimal minutes. Data used was from data points logged every 10 minutes.

Appendix 4— Along-track continuous measurement of phytoplankton physiology, AMT6.

FRRF data were measured from the surface (7m) seawater supply throughout the AMT6 transect. These data were binned into hourly averages and presented in *Chapter 5. Fig. A4.1.* presents the data at the full resolution of acquisition (FRRF dark chamber data logged approximately every 45 seconds) to give an idea of the noise/variability encountered. The corresponding along track measurements of seawater temperature are also shown as a means of comparison (hydrographic data logged once every 10 minutes). Conversely, the FRRF data are also binned into day (PAR<0) and night (PAR=0) averages, *fig. A4.2.* to further show the differences in mean parameter values between provinces.

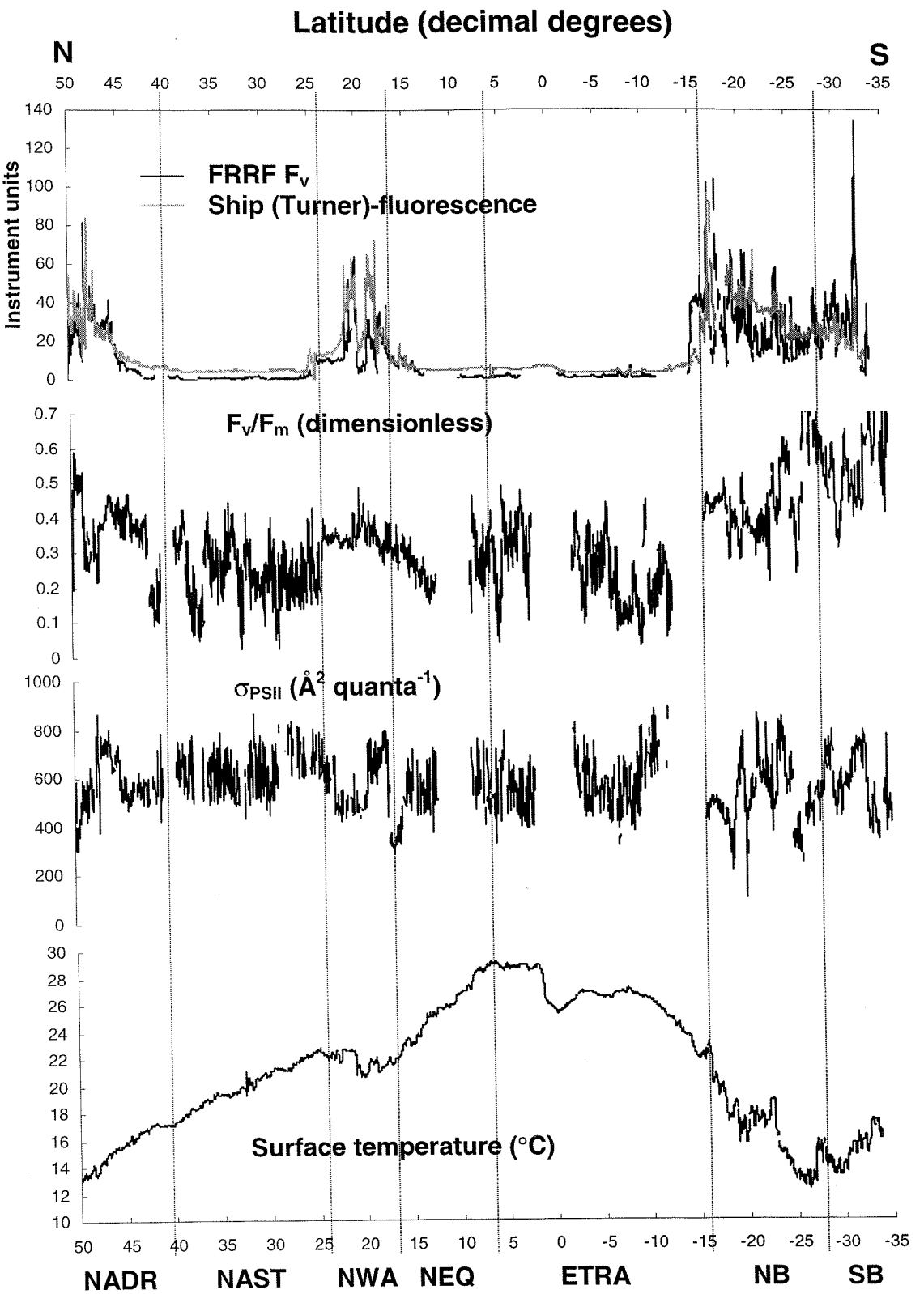

Figure A4.1.— Changes in surface (7m) FRRF variables as measured from the continuous non-toxic seawater supply throughout AMT 6. Latitude (decimal degrees) and biogeochemical provinces (see *section 5.2.*) are indicated. Data was collected every 45 seconds. Also shown is ship-measured fluorescence and surface seawater temperature (collected every 10 minutes).

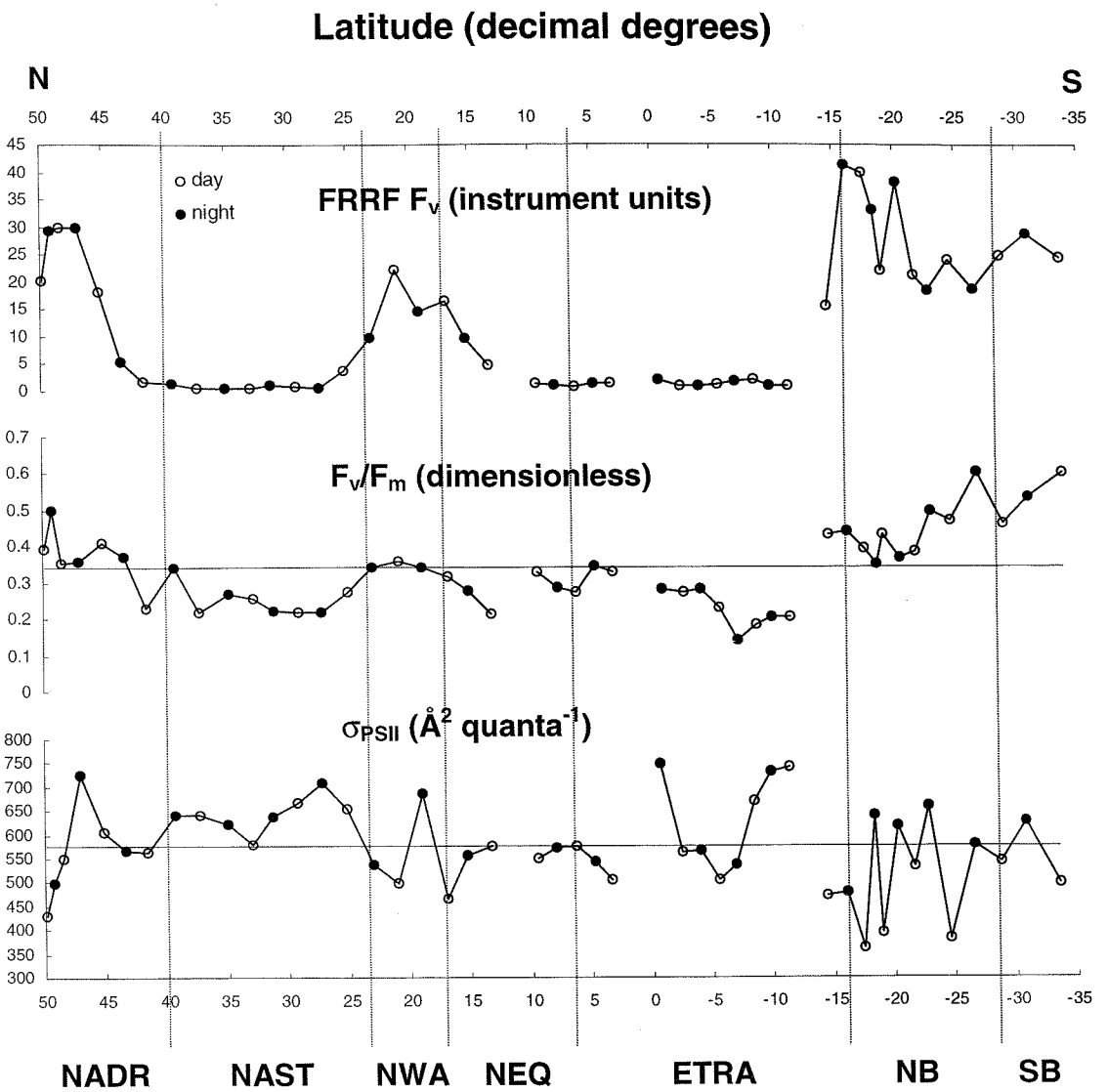

Figure A4.2.— Changes in surface (7m) FRRF variables as measured from the continuous non-toxic seawater supply throughout AMT 6. Latitude (decimal degrees) and biogeochemical provinces (see *section 5.2.*) are indicated. Data was collected every 45 seconds but has been binned into day and night averages. 'Day data' was determined from corresponding surface (ship-mounted) PAR, where PAR values (uncalibrated) were greater than 0.

SOUTHAMPTON UNIVERSITY LIBRARY

USER'S DECLARATION

AUTHOR: SUGGETT, DAVID JOHN TITLE: VARIABILITY OF PHYTOPLANKTON PRODUCTION RATES IN THE ATLANTIC OCEAN AS OBSERVED USING THE FAST REPETITION RATE FLUOROMETER DATE: 2000

To be signed by each user of this thesis

DATE	SIGNATURE	ADDRESS